COMPARISON OF PQCT & PMRI VOLUMETRIC BONE IMAGING TECHNIQUES

A TRI-MODALITY COMPARISON OF VOLUMETRIC BONE MEASURE QUANTIFICATION USING 1.0 TESLA PERIPHERAL MAGNETIC RESONANCE IMAGING, PERIPHERAL QUANTITATIVE COMPUTED TOMOGRAPHY AND HIGH-RESOLUTION-PERIPHERAL QUANTITATIVE COMPUTED TOMOGRAPHY IMAGES

By ANDY KIN ON WONG, B.SC.

A Thesis Submitted to the School of Graduate Studies in Partial Fulfillment of the Requirements for the Degree Doctor of Philosophy

McMaster University DOCTOR OF PHILOSOPHY (2013) Hamilton, Ontario (Medical Sciences, Physiology & Pharmacology)

TITLE: A Tri-modality comparison of bone structure quantified using 1.0 Tesla peripheral magnetic resonance imaging, peripheral quantitative computed tomography and high-resolution-peripheral quantitative computed tomography

AUTHOR: Andy Kin On Wong, B.SC. (McMaster University)

SUPERVISOR: Professor Jonathan D. Adachi

NUMBER OF PAGES: xxi, 298, Appendices 1-47

This text is dedicated to the CaMos study participants,
their friends and families

and to the memory of Dr. Colin E. Webber

ABSTRACT

This comparative study of peripheral (p) QCT, high-resolution pQCT (hr-pQCT) and 1.0 Tesla pMRI technologies focused on quantifying short-term test-retest reproducibility, validity, one-year detection limit and clinical sensitivity of each modality's derived bone measures. Select bone outcomes were evaluated from scans performed on Hamiltonian women above 50 years old and then externally validated in a population-based cohort of Canadian women 60-85 years old. In the local cohort (age: 74 ± 9 years and BMI 27.65 ± 5.74 kg/m^2), Tb.Sp measured on pMRI, Ct.Th and vBMD from pQCT showed significant correlations (r^2=0.52-0.85) with hr-pQCT and yielded slopes near unity. Bland-Altman analyses revealed significant relations between magnitude of pQCT and pMRI bone outcomes (Tb.Th(-), Tb.N(+), BV/TV(-)) and level of agreement with hr-pQCT. Except for hole geometry and connectivity, short-term reproducibility was < 5% for pQCT but only BV/TV was < 5% for pMRI. The more distal slice of pQCT scans at both sites showed superior reproducibility but slightly larger change than the proximal. Co-registering repeat images and excluding those on antiresorptive therapy mildly reduced precision error and one-year change. In the local cohort, only Ct.Th and cortical vBMD associated with fragility fractures (OR: 1.09-3.28) using hr-pQCT, which was externally validated in the national cohort. Certain trabecular measures on pMRI and pQCT erred towards increased odds for fractures locally. For pQCT, these became significant in the national cohort (OR:1.04-3.81). The national reference dataset for hr-pQCT showed larger Tb.Sp and smaller Tb.N compared to Americans but age-related rates of decline in Ct.Th and BV/TV were larger in Europeans. This study demonstrated validity of pMRI and pQCT image-derived volumetric bone outcomes and a reasonable degree of short- and long-term precision error for measures derived from pQCT images but not from 1.0T pMRI. For pMRI, a shorter scan was suggested to limit motion and to reduce precision error. Performing scans more distally was recommended, but a single CT slice from pQCT was comparable to 110 slices from hr-pQCT in associations with fractures.

ACKNOWLEDGEMENTS

I would like to thank my family for their patience when I'm too busy to come home; for their attempt at understanding the complexities of my academic life; for respecting my decisions for choosing a school so far away; and for not imposing restrictions on my academic interests.

I am indebted to my supervisor Rick Adachi for instilling in me the confidence I need to direct, manage and execute this study; for introducing me to our community of bone specialists and researchers, many of whom we have established strong ties to continue our string of collaborations; for constantly highlighting my work in front of key stakeholders; for offering me opportunities to train in various environments that have expanded my breadth of expertise; for his ongoing dedicated support and recognizing my potential since I was only an undergraduate student; for personally assisting me when I had mechanical troubles and for teaching me how to see the multi-use and flexibility of everyday tools; I am forever grateful for all the energy he has poured into making my career grow successfully.

I want to express my gratitude for Karen Beattie for training me to write and to become a scientist practicing the highest integrity; for telling me how academic life really is as a PhD and making me realize what I'm getting myself into; for giving me a reality check when I pressure myself too hard and lose focus of life and the people around me; for making scientific collaborations and discussions a highly social experience; for being a humble mentor and a good listener while challenging me with alternative possibilities and solutions; for constantly challenging me with new problems and challenging my knowledge of what I believed I already knew; for advocating for me when my weaknesses overshine my strengths; I appreciate Karen for sharing all her perspectives and experiences as a student, a post-doc and an assistant professor.

I am thankful for all the lessons I have learned from Colin Webber that have taught me how to become a scientist with an inquisitive and curious mind; for reminding me to always formulate hypotheses *a priori* the "McMaster way"; for always looking at my results in a positive light and finding the most peculiar quirks in my data that turn out to be worth publishing; for having the audacity to point out mistakes that everyone makes but blindly accept, making me more cautious with how I express ideas or use certain terms for caring about the technical details but recognizing when I do something right; I will always remember Colin Webber. His integrity, kindness and mentorship creates in many of us a legacy that forms part of a local McMaster culture of scientific rigour.

Alexandra Papaioannou has charged me with enthusiasm for performing research studies in an older adults population. I would like to specially thank her for her recognizing that my work crosses into the geriatrics field; for showing me a wealth of opportunities that led to my training in aging science and statistical analyses in longitudinal studies; for pushing me to enhance my capabilities of performing epidemiological research; for always reminding me to ensure my work bears clinical relevance and that it is communicated to my audience upfront; for introducing me to key stakeholders who have helped shapen my career; I appreciate the perspectives that Alex has given me, allowing me to think about the bigger picture and how my work will fit with the rest of the present knowledge.

Thank you Christopher Gordon for introducing me to the pQCT scanner and teaching me about all its capabilities; for sitting me down over coffee and explaining to me more difficult concepts in medical physics; for making me question and re-examine my study protocol until we were satisfied with a higher degree of precision in our measurements; for helping me recognize the inconsistencies in bone measurements across different platforms, motivating this very study; for introducing me to international investigators and giving me the opportunity to communicate my work to them; Chris has further

contributed to my career by introducing me to the manufacturer of the pQCT, further enabling my work to be recognized and disseminated widely.

Laura Pickard and Shannon Gale have to be graciously thanked for training me how to conduct a research study while maintaining ethical integrity with study participants; for showing me how to practice confidentiality at every level; for guiding me through writing cohesive, clear and transparent ethics applications that have helped improve the efficiency of this study; for teaching me how to think about the feasibility of study procedures and to conduct research studies by placing the betterment of participants first; for teaching me the inner workings of the CaMos research team to help streamline the national study component; for liaising with other study coordinators to understand the challenges that each site faces with conducting the multi-centre study; for playing multiple roles and helping the CaMos BQS become a success despite its financial limitations; Thank you for your patience with my initial naivety and especially Laura for her insight into making important cost-vs-benefit, scientific merit-vs-feasibility balances.

CaMos coordinators at the six CaMos BQS sites where the national study component was conducted must be thanked for their tremendous contribution so far in recruiting study participants, conducting all CaMos questionnaire interview and booking all other study procedures.

CaMos BQS technicians, my colleagues and friends, we share the same goal to examine bone structure using the scanners at your study centres – you operate them and give us the best quality of images. Our collaborations have proven successful and I wish to continue our collegial relationship for many years to come.

The BioPharm program led by Denis Crankshaw has foremost trained me to become the scientist I am today, equiped to handle the weight of a PhD project. I want to specially thank Denis and the program for training me with an undergraduate research experience

as rigorous as a Master's degree; for providing me with co-op work opportunities where I first met with my colleagues at Proctor & Gamble Pharmaceuticals and through them, met my current supervisor, Rick Adachi. Without this training and real-world work opportunities, I would not have been able to find my way through this rewarding career experience. Thank you, Denis.

My dearest friends have created for me a much needed distraction from all of this work. I want to thank them all for the continual support. Thanks Kevin, for getting me addicted to working at a coffee shop. This has become my second office and my focus couldn't have been better here than anywhere else. The coffee shop staff must be acknowledged for providing me with free coffee cakes throughout the late nights working on this thesis document. Their recognition of the importance of medical research is much appreciated.

Finally, I would like to acknowledge the Canadian Institutes of Health Research (CIHR) for funding the national component of this study (MOP-115094); Vanier Canada Graduate Scholarship (CGV-104858) for funding me in my ambitious goal to build a musculoskeletal capacity assessment tool using pQCT, hr-pQCT and pMRI technologies; Osteoporosis Canada for funding the pilot work that helped determine and refine the feasibility of this project; and all of CIHR, Canadian Arthritis Network, American Society for Bone and Mineral Research, and the European Research Association's Strategic Research Training opportunities that have allowed me to enhance my leadership capacity, knowledge of bone and muscle basic biology, advanced statistical methods, skills in grantsmanship, knowledge translation and for creating plenty of opportunities for team building with my peers from the United States, Europe and Asia.

TABLE OF CONTENTS

LIST OF FIGURES, TABLES AND EQUATIONS

LIST OF MOST COMMONLY USED ABBREVIATIONS AND SYMBOLS

pQCT	peripheral quantitative computed tomography
hr-pQCT	high-resolution peripheral quantitative computed tomography
pMRI	peripheral magnetic resonance imaging
DXA	dual-energy X-ray absorptiometry
µCT	micro computed tomography
T	Tesla
SPGR	Spoiled gradient echo
T_1	longitudinal relaxation
T_2	transverse relaxation
BV/TV	bone volume fraction (or bone volume to total volume)
Tb.Sp	trabecular separation
Tb.Th	trabecular thickness
Tb.N	trabecular number
Ct.Th	cortical thickness
aBMD	areal bone mineral density
vBMD	volumetric BMD, subscript i=integral, c=cortical, tr=trabecular
H_A	average hole size
H_M	mean hole size
Cx	connectivity index
CI	confidence interval
ROI	region of interest
SD	standard deviation
LSC	least significant change
RMSSD	root mean square standard deviation
RMSCV	root mean square coefficient of variation
ICC	intraclass correlation coefficient
ANOVA	analysis of variance
LOA	limit of agreement
SEE	standard error of the estimate
OR	odds ratio
HR	hazard ratio
ISCD	international society for clinical densitometry
Fx	fracture

DECLARATION OF ACADEMIC ACHIEVEMENT – LOCAL STUDY

Andy Kin On Wong	Study design, proposal, protocol development, ethics application, participant recruitment (80%), study appointment coordination (80%) 1.0T pMRI scans pMRI OsteoQ bone analyses (80%) National study streamlining (grant application, SOP, site visit, cross-calibration, sub-contract administration) Data entry (80%), data cleaning and analyses Publications and presentations Mentorship & student training
Aakash Bhargava *	participant recruitment (20%, for pQCT year 2) pQCT scans and image analyses Data entry (10%)
Dean Inglis	pQCT (proprietary) and MRI OsteoQ (freely available) software design pQCT OsteoQ analysis service Segmentation algorithm consultation
Zamir Merali *	pMRI OsteoQ bone data parsing pMRI OsteoQ bone data re-evaluation (year 2) Data entry (10%)
Kevin Min *	pMRI-hr-pQCT image co-registration pMRI test-retest image co-registration pMRI baseline-follow-up image co-registration Large hole size identification
Eva Szabo & Farah Ahmed	Hr-pQCT scans and image analyses

% contribution where noted. Otherwise, 100% contribution is implied.

* students trained by Andy Kin On Wong on all tasks completed

DECLARATION OF ACADEMIC ACHIEVEMENT – NATIONAL STUDY

Andy Kin On Wong	Study design, proposal, protocol development, ethics application (national, and site-specific templates) National study streamlining (grant application, SOP, site visit, cross-calibration, sub-contract administration) Data cleaning and analyses Publications and presentations
Shannon Gale & Laura Pickard	Annual national and site-specific ethics renewal Finances and payment Local participant recruitment, appointments, interviews, progress reporting, shipment management Transportation and parking management
Silvia Dumont & Suzanne Godmaire	CaMos national ethics application and renewals Interview and fracture data entry & data cleaning National study progress reporting

Vancouver Danmei Liu (A) Leigh Gabel (T) Nerkeza Andjelic (C)	**Administrative Assistant (A)** Managing study equipment, supplies and logistics Image file, scan data and study log shipments **Technicians (T)** Completing imaging procedures and image analyses Maintaining consistent local quality assurance efforts **Coordinators (C)** Study participant eligibility screening, participation history & background assessment Study participant recruitment Appointment booking, transportation and parking management Study compensation and financial statements Full interviews and short-interview administration Fracture questionnaire follow-up Study log and progress reporting Ethics applications and renewals Sub-contract agreements execution
Calgary Lauren Burt (A) Michelle Kan (T) Jane Allan (C)	
Saskatoon Andrew Frank (A,T) Chantal Kawalilak (T) Jola Thingvold (C)	
Hamilton Laura Pickard (A,C) Shannon Gale (A,C) Lesley Beaumont (T)	
Toronto Eva Szabo (A,T) Barbara Gardner-Bray (C)	
Kingston Carolyn Heymans (A) Margaret Bollen (T) Karen Rees-Milton (C)	

1 Introduction

1.1 Osteoporosis – epidemiology and clinical assessment

Osteoporosis is characterized by a loss of bone density, deteriorating architecture and a consequential loss of bone strength, manifesting in systemic skeletal fragility. The result of poor structural and material propagation is translated into an increased risk of fragility fractures. Fragility fractures, as operationally defined here, is considered as bones broken non-traumatically from standing height or less and excludes the toes, fingers, patella, tail bone, and skull (1). Although fractures are a hallmark of osteoporosis, the diagnostic criteria for osteoporosis vary internationally. Osteoporosis is recognized by the World Health Organization (WHO) as a disease defined by a low areal bone mineral density (aBMD) measured by single- or dual-energy X-ray absorptiometry (DXA) that is 2.5 standard deviations (SD) below a normative reference of young adult women between 20-29 years of age (2). Many member states of the WHO adopt a similar definition. However, the last two decades has seen a progression of osteoporosis management methods that has involved an increasing adoption of novel bone imaging technologies. The study reported here addresses the current technological limitations of DXA and describes the strengths and weaknesses of methods in development that aim to further estimate bone integrity.

1.1.1 Impact on Canadian healthcare

Considering just hip fractures alone, the annual health care costs of osteoporosis amounted to $650 million CAD in 2001 (3). By 2010, the overall annual cost of treating osteoporosis and fractures escalated to $2.3 billion, a figure that includes acute care

(accounting for about 50% of the total cost), outpatient care, indirect costs and prescription medications. When high and low trauma fractures were considered in this analysis, the upper bound of this figure could be as high as $4.1 billion (4). Incidentally, from 1993 to 2008, hospitalized hip fractures as determined from the Canadian Institute for Health Information (CIHI) increased from 21 302 to 28 867, in proportion to the 50% increase in the population above 50 years of age in Canada. During this period, healthcare costs due to osteoporosis just under doubled (4,5). In total, the number of hospitalizations due to osteoporosis (57 413), was higher than that due to stroke (29 874) and to myocardial infarction (49 220) in fiscal year 2007-2008 (4,6).Fractures are associated with decreased quality-adjusted life years (7,8). In fact, both vertebral and hip fractures have recently been shown to significantly increase mortality rates in Canadians with hazard ratios (HR) ranging from 2.7 to 3.7 (9).

1.1.2 Epidemiology

The incidence of fractures

The incidence of all fragility fractures in women above 50 years of age has been reported in Canadians through a large population-based cohort called the Canadian Multicentre Osteoporosis (CaMos) study as 15.3 (95% confidence interval (CI): 14.1, 16.7) per 1000 patient-years (10). This number is almost double the corresponding incidence in men of 7.2 (95% CI: 5.8, 8.7) per 1000 patient-years. A similar finding was previously observed in the Rochester study by Cooper et al for clinically diagnosed vertebral fractures (11). At age 50, the incidence of fractures in men and women are more similar to one another than later in life but the age-related increase in fracture incidence in women is more rapid than

that in men, leading to a disparity in fracture incidence for older age groups (12,13). Langsetmo showed significant geographical variation in the incidence of all fragility fractures which was similar to that of the incidence of hip fractures (r=0.46-0.76), but deviated from the pattern of geographical variation in the prevalence of low aBMD (r=0.00). Notably, Calgary displayed the highest region-specific incidence for fractures (18.5 (95% CI: 14.6, 23.3)) but only showed a prevalence of aBMD T-Score < -2.5 centred around the average across all sites (roughly 19%) compared to the highest prevalence of low aBMD found in Quebec and St. John's (22.5%) (10).

Age and sex-related differences in fracture risk

Age has been shown to be a well-established independent risk factor for fractures and has been supported by studies demonstrating significant age-related bone loss at the hip, spine and peripheral sites (14,15). In a population-based cross-sectional cohort study examining bone structure at the wrist from individuals 20-90 years of age, Khosla showed that over the life course, women lose bone by trabecular loss and an increase in the separation between trabeculae whereas men sustain intact trabeculae that thin without any net changes in the number of trabeculae per unit area (14). In both men and women, Lang quantified bone volumetric density and structure of the proximal femur using full body quantitative computed tomography (QCT) and measured significant loss of bone strength under different loading conditions in women (-8.3-12.8%) that were larger than in men (-4.2-7.0%) over a five year period (15). The ten-year risk for fractures of the hip, spine and shoulder has been shown to increase from 45 to 85 years of age for both men and women.

However, in men, forearm fractures showed the opposite trend (16). Because of its dramatic effect on fractures, bone structure and on density, adjustment for age is necessary in most statistical models examining the contribution of any of these outcomes.

Low aBMD as a risk for fractures

Low aBMD has been a well-established independent risk factor for hip, vertebral and non-vertebral fractures from a number of studies (17-22). Sornay-Rendu presented data from the Os des Femmes de Lyon (OFELY) study showing a 2.5 (95% CI: 1.3-4.6)-fold increased risk of fractures associated with aBMD T-scores between -2.0 and -2.5, independently of age (19). In the Rotterdam study, Schuit also demonstrated a similar association between one SD lower femoral neck aBMD and a 2.1 (95% CI: 1.7-2.5) -fold increased risk of hip fractures in women over 55, but noted that as much as 44% of fractures were not explained by aBMD T-scores below -2.5 (18). In the Dubbo Osteoporosis Epidemiology Study, low aBMD remained a significant independent risk factor for fractures even in non-osteoporotic men and women (aBMD T-score > -2.5) (20). One study showed, in a head-to-head comparison, that tibial epiphyseal aBMD (HR: 1.8) was just as strong as total hip aBMD (HR: 1.5) in estimating risk of clinical fragility fractures, after adjusting for age and prior fracture in Swiss women (22).

Falls and body mass as risk factors for fractures

Riggs suggested that falls may be an additional risk factor for those above 75 years of age, beyond aBMD (23). Van Helden further extended this proposition and showed that risk

factors for falls (odds ratio (OR) 4.0 95%CI: 2.7-5.9) and risk factors for fractures (OR: 2.9 95%CI: 2.0-4.1 for hip fractures), albeit partially overlapping, can be combined to predict hip fractures in women (24). Body mass also contributes to the maintenance of bone strength and modifies the risk of fractures. While obesity was once believed to be protective of fractures due to its weight-bearing effect on the skeleton (25,26), Beck dissected this population and demonstrated that in the obese, whose lean mass forms only a percentage of their overall body mass, aBMD, femoral cross sectional area and its resistance to bending are actually decreased with body mass in this group. Meanwhile lower extremity fractures, not protected from excess tissue padding, was more frequently observed in obese women with a higher body mass (27). These findings were supported by Travison et al in a similar study but which focused on men (28).

1.1.3 Clinical assessment and diagnosis

Since the establishment of the WHO definition of osteoporosis, there have been supportive literature regarding additional independent risk factors for fractures (29,30) culminating in a shift in attitude away from treating osteoporosis on the basis of just low aBMD alone. Population-based data and nomograms are now available, involving the use of a number of independent risk factors that enable the computation of absolute fracture risk information (16,31-33). However, depending on the threshold of fracture risk utilized, classification into a high risk category for fractures may differ, leading to variable treatment implications (34). In Canada, two absolute fracture risk assessment methods have been accepted by the 2010 Clinical Practice Guidelines for the management of

osteoporosis (35): the Canadian Association of Radiologists and Osteoporosis Canada (CAROC) tool (33) and the fracture risk assessment (FRAX) tool adapted to Canadians with CaMos cohort data (36). Although aBMD information is optional in the FRAX tool, the clinical practice guidelines provide grade A evidence for the use of at minimum the established risk factors: age, aBMD, prior history of fragility fractures and use of glucocorticoids for at least three months in the previous year at a prednisone-equivalent dose $\geq$ 7.5 mg daily (37). In addition, for the CAROC tool, prior fracture and use of glucocorticoids are major risk factors. When either is observed, the fracture risk is increased to the next level, and if both are observed, the patient is automatically considered at high-risk for fractures. The FRAX tool involves the use of these same risk factors but also includes BMI, parental history of a hip fracture, current smokers, rheumatoid arthritis, secondary causes of osteoporosis and having 3 or more units per day of alcohol (37). The FRAX tool utilizes each of these risk factors to compose a precise fracture risk value but CAROC outputs only one of three (low, medium or high) fracture risk categories. While the choice of either tool has been left open to physicians for convenience and personal preference (35), Beattie showed that when family physicians used the FRAX report, which provides information about treatment recommendations and a clearer statement of fracture risk, there was better agreement (κ =0.64) with osteoporosis specialists in terms of treatment recommendations compared to the CAROC tool (κ=0.32) (data not published). What is not taken into consideration in any of these fracture risk assessment tools is the treatment that patients are currently receiving that could modify their fracture risk.

1.2 Bone physiology

The underlying physiology of bone dictates its structure, density and strength. While the structure of the human skeleton defines its ability to support musculature, the interaction of the skeleton with the surrounding environment also alters its structure by modifying its physiology. Bones also serve as a storage and supply facility for calcium and phosphate. Long bones such as the femur are important homes for mesenchymal stem cells, important precursors for key defensive players of the immune system. Here, the focus of this section on bone physiology will be centred on structural maintenance of bone.

1.2.1 Composition of bone

Bone is a living organ that undergoes constant renewal. It consists of cortical and trabecular bone, with marrow space, cartilaginous articulations and calcified growth plates at the ends of long bones. Bones are constructed from of a series of collagen fibres, mostly type I, triple-helical strands composed of two α1 and one α2 strands, that form the scaffold for mineralization aided by nucleation proteins (38). The collagen matrix, acting as an extracellular matrix for cells, coexist with three major categories of bone cells: the osteocyte (the mature cells of bone, 90-95% of all bone), osteoblasts (bone builders, 4-6%) and osteoclasts (bone decomposers, 1-2%) that are known to interact with one another. These are the key players that regulate the composition and structure of bone. At the macromolecular level, hydroxyapatite [$Ca_{10}(PO_4)_6(OH)_2$] crystals are nucleated along type I collagen fibres and can be decomposed or deposited by the bone cells in concert using a series of proteins and enzymes (38). The degree of mineralization of bone is

therefore dependent on how densely packed the hydroxyapatite crystals are per unit volume as well as the conjugation of hydroxyapatite by a number of substituents such as carbonate, magnesium and acid phosphate (39). In addition to the series of non-collagenous proteins, water forms 10% of bone's weight found mostly in collagen matrices and serves to maintain nutrition and ion flux within bone (38). The degree of mineralization has been found to be inversely proportional to the relative amount of water in bone, leading to further improvement in mechanical strength with increased mineralization (40). Although accounting only for 2% of dry weight (38), lipids play an important, yet under-scrutinized role in the maintenance and construction of bone, as evidenced by dwarfism (41) and osteogenesis imperfecta (42) seen with sphingomyelinase deficiency and genetic mutation, respectively.

Anatomy of bone matrices and osteocytes

The three bone cell types interact with one another though dendritic processes that travel through the bone in microscopic tunnels called canaliculi. These canaliculi feed into the main Haversian canal system where nerves and blood vessels provide nutrients and afferent control over bone. Mature osteocytes are housed within spaces called lacunae scattered throughout the lacuna-canalicular network and communicate with bone surface cells, sensing changes in mechanical forces acting on bone (43). Single cylindrical units containing a lacuna-canaliculi network surrounding a Haversian canal, called osteons, are arranged parallel to the long axis of bone and exchange nutrients with its neighbours through blood vessels traveling through the transverse Volkmann's canals. Spread

throughout bone, osteocytes play distinct roles in regulating matrix mineralization through the pivotal role of fibroblast growth factor 23, which has shown to affect phosphate metabolism (44) and can be regulated by parathyroid hormone (PTH) through PTH receptors on its cell surface (45). Osteocytes are also important for bone remodeling. By undergoing apoptosis in the presence of pro-apoptotic factors, osteocyte death promotes osteoclast differentiation leading to a cascade of bone remodeling events (43).

Osteoclast function

Osteoclasts are characterized by a polarized morphology with a ruffled border and many vesicles containing degradation enzymes. They derive from the bone marrow macrophage lineage and function by creating an acidic environment with pH of 4.5 using a coupled proton-ATPase and Cl- channel pump, which breaks down the mineralized component of bone, leaving the collagen matrix that is then digested by the lysosomal enzyme cathepsin K and matrix metalloproteinases (46). The differentiation of osteoclasts requires the priming of precursors by receptor activator of NF-κβ ligand (RANKL), and macrophage-colony stimulating factor (M-CSF). These factors are required for proliferation plus continued survival of osteoclasts. RANKL activity on the RANK receptor is regulated by osteoprotegrin (OPG), which acts as a high affinity soluble inhibitor of RANKL, whose expression is negatively affected by pro-inflammatory cytokines (46).

Osteoblast function

Osteoblasts fill in resorption spaces created by osteoclasts as guided by chemoattractants. They mature by first proliferating, depositing extracellular matrix that then becomes mineralized (47). This process is initiated by activation of the transcription factor, Runt-related transcription factor 2 (Runx2), and is further fine-tuned by other signalling cascades including Wnt signalling – particularly the canonical pathway involving β-catenin (48). Activation of Runx2 enables the expression of proteins essential for bone growth and mineralization including type I collagen and alkaline phosphatase; the latter breaks down pyrophosphate, an inhibitor of osteoblastic mineralization (47). Both of these products are markers of a matured osteoblast. In maintenance of bone remodeling, osteoblasts also produce RANKL, necessary for osteoclastic differentiation while also releasing OPG to downplay RANKL's activity (49). Osteoblasts on bone surface have several fates. After mineralizing the bone matrix, they can undergo apoptosis, become a bone lining cell or mature into an osteocyte (43). Oxygen tension was previously shown to dictate the commitment of an osteoblast into an osteocyte (50,51).

1.2.2 Bone remodelling

Bone is a highly dynamic tissue that undergoes a constantly orchestrated cycle of bone resorption and bone formation. This process enables the bone to handle heavy loads and regenerate itself to overcome microdamage. Because the balance between these two opposing processes is necessary to maintain a net zero loss or gain in bone, bone remodelling is tightly regulated at both systemic and local levels. Harold Frost first

described the basic multicellular unit (BMU) through his investigations using tetracycline-labeled histomorphometry (52); a BMU involves the cooperation of osteoclasts, osteoblasts and osteocytes in bone remodelling cavities (53). In normal bone, a full cycle could last 150-200 days but with bisphosphonate therapy could be elongated to 1000 days when bone turnover is low. Bone resorption pits were measured at a mean depth of 40 μm in older adults with a median resorption activity duration of 30-40 days followed by bone formation over 150 days for trabecular bone and 120 days for cortical bone. However, in osteoporosis, the osteoblasts are unable to completely refill the resorptive pit and each subsequent remodelling event results in cumulative net bone loss (54).

Bone resorption and formation are coupled processes within a BMU and dictate the remodelling events. Although neither the proton pumping ability nor the ruffled border characteristics of osteoclasts are needed by osteoblasts to proceed with bone formation (55), the actual presence of osteoclasts and M-CSF is required for proper bone formation to occur (56). Cell-to-cell interaction between the transmembrane protein Ephrin on osteoblasts and the EPH receptor on osteoclasts was shown to promote osteoblastic differentiation and attenuate osteoclastic differentiation (57). Release of sphingosine 1-phosphate by osteoclasts further recruits osteoblast progenitors to the site of resorption (58). Remodelling serves the function of replacing damaged bone and maintaining adequate structural and mechanical integrity. The initiation of remodelling events from regulated mechanisms can be primed by hormones such as PTH, growth hormone,

estrogen and drugs such as bisphosphonates and [1-34]PTH. These factors target mainly osteoclasts. Remodelling can also be triggered by damage to osteocytes due to microcracks or fractures, resulting in recruitment of osteoclast precursors (59). The recruitment of precusor cells to the BMU is effectuated by vascularization of the damaged area by vascular endothelial growth factor. In addition, endothelial cells assist in the commitment of marrow stromal cells to the osteoblastic lineage (60). Evidence in remodelling is seen where primary osteons are positioned next to secondary osteons and boundaries called cement lines can be evidenced histologically (61).

1.2.3 Bone structure and mechanical support

Bones in the body can be represented by cortical (80% of the skeleton) and trabecular or cancellous-type constructions (20% of the skeleton). There are five major classifications of bones in the skeleton: 1) short bones (cuboidal with thin cortices surrounding trabeculae), 2) flat bones (curvilinear parallel cortices surrounding thin layer of trabeculae), 3) sesamoid bones (bones found in tendon), 4) irregular bones (same as short bones but could be larger and irregularly shaped), and 5) long bones which are characterized by two ends containing a larger amount of trabecular bone – the epiphyses, and the shaft where there is a larger proportion of cortical bone and bone marrow – the diaphysis (61). Both cortical and trabecular bone can begin as woven bone, a rapidly constructed type of bone with disorganized collagen arrangement, which is then replaced through bone remodelling with the more organized, parallel osteon structure called lamellar bone. The former, often produced after a fracture or during ontogeny, is weaker

whereas the latter is more resistant to bending due to the parallelism of mineralized collagen fibres (62).

Structure dictates function of bone

The above descriptions of bone composition and remodelling in sections 1.2.1 and 1.2.2 hold true for both cortical and trabecular bone. However, cortical bone has a higher density of osteons than trabecular bone (61). It is the difference in distribution of bone material as well as the architecture and density of bone that bestows a dramatic difference in mechanical properties for cortical versus trabecular bone. In the diaphysis of long bones, the thick cortices enable high loads to be applied axially while resisting bending and torsional forces to the shaft – this concept can be represented by the cross-sectional moment of inertia and the buckling ratio of a volume of bone. Meanwhile, the spongier trabecular bone enable shock absorption and resilience to compression forces such as the downward axial compression of body weight on the spine (61). While trabecular bone has more immediate access to the bone marrow where progenitors are present, it also bears a higher turnover rate compared to cortical bone, where osteons are buried deeper and access to progenitors necessitates capillary delivery (62).

Like a building, the structure of beams and struts of bone along with its material properties define its strength. A superficial understanding of its overall density may result in a misinterpretation of how strong the structure is. For example, a building constructed of steel but with few beams may be comparable in overall density to a building built of

wood with many beams. However, the latter may be much stronger due to the orientation and number of support structures. Likewise, an understanding of bone strength necessitates scrutiny of its geometry, architecture and material density. Cortical bone is compact and its strength is largely defined by its thickness and its porosity. Trabecular bone expands in an interconnected network where vertical beams aligning in the direction of mechanical forces (63) are supported by horizontal struts. The thickness of individual trabecula, the degree of interconnectivity among them, how separated they are from one another, as well as the degree of directionality, also known as anisotropy, dictate trabecular bone's strength (64). In the context of osteoporotic fractures, these elements of bone structure become highly relevant. However, current clinical practice only employs DXA to obtain a two-dimensional rendition (areal) of bone mineral density while dismissing any structural information about bone.

Effect of loading and unloading on bone

Structure defines bone's ability to support the body but feedback through the generation of mechanical strains is also important to define how bones construct themselves strong enough to resist loads applied unto it. Wolff's law (1892) (65) states that bone in a healthy individual will adapt by remodelling itself to resist loads under which it is placed. Frost also noted that there are thresholds for mechanical strains that will trigger bone's "mechanostat" to respond by increasing bone formation (65). Evidence for this proposition comes from studies of bed rest interventions where loading on the body is decreased. The effect of insulin-like growth factor 1 (IGF-1) on bone formation was

ablated when loading was removed due to its inability to elicit its signal transduction cascade (66,67). Lack of mechanical loading is also a primary reason for disuse osteoporosis as shown in patients with spinal cord injury, leading to rapid hyperbolic loss of bone volume within three months followed by slow decline over time due to uncoupled bone remodelling (68).

Despite the loss of external loads during immobilization, muscles appear to play a large role in maintaining bone integrity – namely by the force that it exerts on bone (69), as well as its electrical stimulation on bone cells (70,71). In fact, Vico demonstrated in rats that disuse bone loss was not identified in regions of the load-bearing bone where muscle insertion sites were identified (72). By virtue of the highly diffusible lacuna-canalicular network, mechanical signals can be transmitted throughout the entire bone using electrical potentials generated by ion transport machinery (73,74), leading to signal transduction cascades that help reinforce bone to adequately compensate for strains (75). The osteocyte has been shown to be at the centre of mechanosensing. As mechanical signals drop below a threshold, osteocytes apopcytose; whereas continued mechanical stimuli promote osteocyte survival through expression of the anti-apoptotic factor, Bcl-2 (76). Pulsatile fluid flow over osteocytes further induce a release of bone anabolic factors (76).

The structural maintenance of bones by mechanosensing machinery and the resultant structural resistance of bones against loads demonstrate the high degree of dynamic interplay between bones and the environment, as well as among key cellular and

molecular players within bone. Additional intrinsic and extrinsic factors further contribute to inter-individual variability in the quality of bone by altering bone remodelling.

1.3 Bone structure imaging

1.3.1 Limitations of DXA

While annual reporting of aBMD has contributed towards improved fracture prevention, aBMD only explains a small percentage of those who fracture. The majority of fractures have occurred in patients with aBMD T-scores above the WHO diagnostic threshold (77). The WHO has noted that aBMD bears high sensitivity but poor specificity for predicting fractures, leading to certain countries' decision to refrain from performing population screening for osteoporosis using DXA (78).The disadvantages of DXA also extend to its inability to distinguish between cortical from cancellous bone, a lack of knowledge of trabecular orientation, and the fact that aBMD values are often confounded by the presence of osteophytes, sclerosis, and aortic calcification in the case of scanning the lumbar spine (79,80). Bolotin also criticized the validity of DXA due to the unknown contribution of soft tissue, particularly at the lumbar spine site, in the final aBMD value (80). However, more recently, DXA scans have been scrutinized further to obtain bone textural information using fractal signature analysis, estimating trabecular orientation (81,82). In addition, total hip DXA scans can be analyzed for mechanical properties by assuming symmetry and a uniform cortical thickness, enabling prediction of hip fracture risk (17). The move towards quantifying more structural features of bone has led to a

rapid progression in the osteoporosis field, reinstating the importance of structural and mechanical properties of bone.

1.3.2 Histomorphometry and μCT

Histomorphometry

The development of histomorphometric techniques for examining bone began in the mid 1900s, progressing from simple plastic-embedding technology with undecalcified bone staining, to the eventual use of tetracycline to measure dynamic mineralization of organic matrices. Frost, Johnson and Arnold were able to observe osteoclast resorption cones leaving cement lines, described apoptosis of osteocytes within their lacunae and were able to describe load-induced bone formation supporting the mechanostat theory (83). Two-dimensional structural elements of bone were quantified from microtome sectioned and fluorochrome-stained slices by using a cytometer grid under the microscope. Total area, bone area, and bone perimeter were the base measures used to derive the series of bone structural elements including: bone volume fraction (BV/TV), trabecular thickness (Tb.Th), trabecular number (Tb.N) and trabecular separation (Tb.Sp), all of which, although measured in two-dimensions, were expressed with three-dimensional units (84). Specifically, width measurements were multiplied by an obliquity correction factor of $\pi/4$. With digitization of images, connectivity analysis was enabled by skeletonizing the image. More advanced textural analysis has also been performed using fractal signature analysis, measuring the degree of anisotropy of the trabecular network, and trabecular bone pattern factor, which quantifies the ratio of bone perimeter versus area expansion before and after applying a dilation procedure to the bone image (85).

One challenge with histomorphometry in individuals treated with antiresorptive therapy (a class of osteoporosis medication that prevents bone resoprtion and increases mineral accumulation) is the fact that fluorochromes require exposed apatite binding sites for stable visualization by fluorescence microscopy. The iminodiacetic acid groups of fluorochromes such as Calcein and tetracycline act as chelators for apatite (86). Because bisphosphonates reduce bone turnover, the exposure of apatite by osteoclasts becomes limited, resulting in poorly stained sections and reduced sensitivity of measurements to change over time. The reference values, expected effect sizes, ability to detect rare events and required sample sizes are consequently affected (87). These issues remain unanswered and alternative methods have been sought to quantify bone structure and turnover where available.

µCT and the basis of CT technologies

Micro-computed tomography (µCT) has become the standard for *ex vivo* non-destructive bone microstructure quantification. With resolutions down to as low as 4 µm isotropic, bone structure measures can be derived from true three-dimensional reconstructions. Analyses of a much larger volume of interest can be performed faster than histomorphometry, which could take up to a week for plastic embedding (88). However, unlike tetracycline-labelled histomorphometry, it is difficult to study mineralization dynamics using µCT ex vivo and cellular composition cannot be determined. In vivo small animal studies can benefit from studying changes in bone with the assistance of

image registration techniques (89). Although, due to the high ionizing radiation conferred by μCT, and the limited gantry size available for samples, it cannot be applied to humans.

Computed tomography technology is based on the attenuation of X-rays by the sample. X-ray beams are generated by a glass-encased electron gun surrounded in oil, where inside the vacuumed glass chamber, a heated cathode filament emits ions by the thermoionic effect, and a biased voltage (20-150 kV) between the cathode and anode accelerates electrons towards the anode. At the anode, electrons are slowed, releasing mostly heat and a small fraction of higher energy X-rays. Anode discs are often rotated to increase the focal spot where electrons hit, while enabling heat dissipation. Depending on the atomic number of the anode, the degree of heat dissipation, the voltage and tube current, different efficiencies of X-ray photon emission are achieved (90). The X-ray beams exit through a slit adjustable by a multi-leaf collimator, producing a narrow polychromatic (different energies) X-ray beam. This X-ray source rotates around the gantry in synchrony with an array of photomultipliers on the opposite end that detect information on the intensity of X-ray particles passing through the sample (90). In certain μCT models, the sample rotates while the source and detectors remain stationary. With a slower scan speed (longer integration time) and collimator adjustable to a more focused X-ray beam, the signal-to-noise ratio (SNR) or clarity of the image could be superior and effective resolution higher. Adjustment of X-ray tube current and voltage can change the energy of the X-ray beam and thus resolving power. A three-dimensional reconstruction of the sample's spatial distribution and material density is generated from μCT images

(88). Because the ability of X-ray photons to pass through the sample is dependent on the density of the material, there is a direct relationship between linear attenuation values and object density. By scanning a phantom along with the sample (usually containing air (-1000 HU), bone (+1000 HU) and water (0 HU)), the greyscale values of the image, often expressed as Hounsfield units (HU), can be converted into realistic density values (mg/cm^3) (90). Instead of having to apply an obliquity correction factor like in histomorphometry, μCT-derived bone microstructure do not require adjustments . However, the challenge comes in selecting the correct threshold to separate bone from marrow. While bone separation from air is clearer, depending on where on the linear attenuation profile a threshold is selected for bone-bone marrow separation, a different thickness of trabecular bone could result. A full discussion of bone segmentation techniques will be detailed in later sections. Earlier intervention studies using μCT have been performed in humans primarily at the iliac crest where paired biopsies were taken to study pre- and post-intervention changes in bone structure (91,92). Because measurements cannot be standardized to the same volume of interest, they must be compared to the contralateral side while making the assumption that both left and right sides of the body exhibit similar enough biomechanics that any observable changes are attributable to true intervention effects. Due to this major limitation, it was recognized that non-invasive methods of bone structure quantification was needed.

1.3.3 QCT technology

Like µCT, quantitative CT (QCT) technologies designed for human applications function under the same principles of X-ray attenuation and gantry construction. Both technologies benefit from the "quantitative" aspect whereby a computer system integrates all linear intensity information from each detector to reconstruct the full tomographic slice. Because of the need for X-ray beams to pass through a larger object farther away from the X-ray source and detectors, there must be a balance between peak X-ray energy and the amount of ionizing radiation. Full body QCT systems have been well established, yielding 300-500 µm in-plane resolution and 1-3 mm slice thickness for standard machines but as high as 150-180 µm in-plane resolution and 300-500 µm thickness for high-resolution multislice spiral CTs (93). Access to full body QCT systems is mostly limited to hospital settings where protected clinical time precludes sufficient access for research purposes.

pQCT technology

The development of the pQCT, a sequential QCT, aimed to provide a small footprint yet high resolution system for quantifying bone structure (94). The X-ray source and array of CdTe detectors translate and rotate 180^{o} around the gantry to obtain images at different angles, while a mechanical system on a track table allows axial displacements along the anatomy. A computer console system attached to the scanner integrates the image data into tomographic slices using backprojection with filtration and also controls the mechanical requirements for scan protocols (94). Linear attenuation (µ) of X-ray beams

by absorbing material can be represented by the exponential relationship between the intensity of the emitted radiation before (I_0) and after (I) passing through the object of interest of a given thickness (d):

$I = I_0 \cdot e^{-\mu d}$ which can be rearranged to: $\mu = (\text{Ln } I_0 - \text{Ln } I) / d$

Equation 1. Relationship between linear attenuation and emitted radiation (94).

The image is divided by a matrix of maximum 256 x 256 pixels and a linear attenuation value is assigned to each three-dimensional image voxel, which can be converted into appropriate density values by calibration against a hydroxyapatite European forearm phantom. However, unlike µCT, pQCT scans are not routinely performed concurrently with a phantom. Instead, all linear attenuation values are calibrated using the same equation specific to the scanner, by assuming that the phantom calibration remains stable over time and can be applied similarly from scan-to-scan (94). By default, fat has been assigned a density value of 0 mg/cm^3 and the densest compact bone estimable is assumed to have a specific density of 1920 mg/cm^3 (58% collagen matrix with density of water 1.0 g/cm^3 + 42% mineral with density of 3.2 g/cm^3). All density values computed by pQCT represent the measurable apparent or Archimedean bone density (94). The best resolution achievable with the clinical version of the pQCT scanner – XCT2000 and beyond – is 200 µm using a collimator, an X-ray voltage of 38-60 keV, spot size of 50 µm, acquiring 145 projections using a fan-beam X-ray in translate/rotate fashion and backprojecting images onto a 256 x 256 pixel matrix (94). The minimum slice thickness remains at 2.5 ± 0.3 mm and can present a problem for accurate determination of structure. At this resolution, partial volume artifact is apparent due to the smaller scale of structures being quantified –

for example trabeculae range between 50-300 µm (95) – resulting in the inclusion of unmineralized tissue in the computation of volumetric BMD (vBMD). Consequently vBMD can be underestimated and thickness measures overestimated. Thicker structures such as the cortical bone may suffer less dramatically from partial voluming. All densitometric and structural measures can only be considered "apparent" since they are estimations of the true density. Because the back of the scanner is open, there is an unlimited gantry depth. The maximum object length for an axial scan is 400 mm, based on the maximum travel distance, and the maximum object diameter is 140 mm based on the gantry opening. Ionizing radiation is but a minor concern for pQCT scans with an effective dose of approximately 1 µSv per tomographic slice obtained. As a reference, the Canadian Nuclear Safety Commission established a dose limit of 1000 µSv per calendar year for the general public and reported an annual effective dose received by Canadians ranging from 1-92 µSv based on monitoring activities across Canada (96).

Hr-pQCT technology

The hr-pQCT system yields a standard isotropic voxel size of 82 µm, although the manufacturer claims resolutions down to 41 µm isotropic is achievable. However, because no collimator is present, selection of a different slice thickness is not possible. The X-ray voltage is set at 60 kV with a spot size of 80 µm. Matrix sizes can range from 512 x 512 up to 3072 x 3072 pixels (97). Having full-frame fast readout charge-coupled device (CCD) detectors, signal integration is rapid and SNR is high. At this higher resolution, hr-pQCT fairs better in quantifying trabecular thickness compared to pQCT

but is still subject to significant partial volume effects. Although the manufacturer has not acknowledged the need to refer to bone structural outputs as "apparent" measures (97),

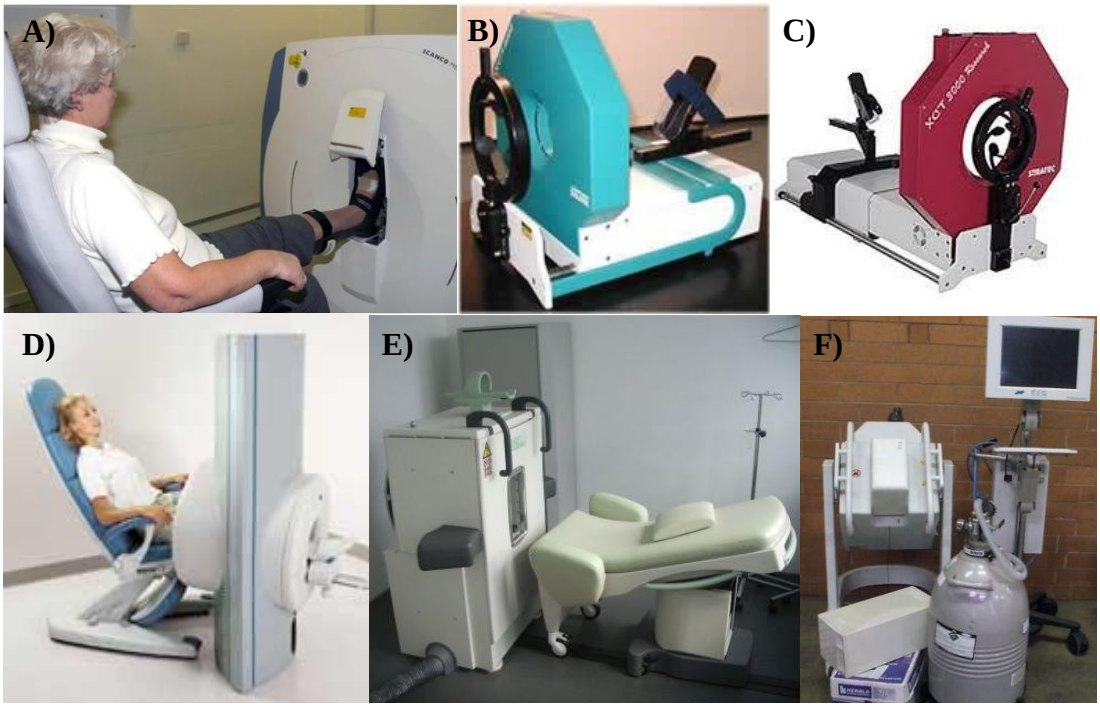

Figure 1. Illustration of different extremity QCT and MRI technologies.
A) Scanco Medical XtremeCT (hr-pQCT), B) Stratec Medizinteknik XCT2000 (pQCT), C) Stratec Medizinteknik XCT3000 (pQCT), D) General Electric ONI MSK Extreme 1.0T MRI, E) General Electric Lunar Artoscan M Extremity 0.2T MRI, F) General Electric MagneVu MV1000 0.2T MRI. Only A to D were examined in the present study.

the ability to accurately represent true structure remains limited when structures are thinner than 246 µm (less than three voxels across). In fact, even with a thickness of 246 µm, the probability that three voxels will span exactly across the width of a trabecula is slim – hence considering this condition, there is still substantial overestimation of thickness and underestimation of density measures. Hr-pQCT is equipped with a height-adjustable chair and custom limb fixation casts for both upper and lower extremities. Unlike pQCT, there is a limited scanner depth of 190 mm. The maximum object axial

scan length is 150 mm with a diameter of 126 mm. To achieve the higher resolution for hr-pQCT, an effective dose of 3 µSv per scan is conferred – though the volume of information (110 slices over a 9.02 mm region) is larger than pQCT for a standard scan protocol at the radius and tibia (97). Scan protocols for hr-pQCT have been standardized across most studies employing it using the same resolution at minimum (98).

1.3.4 MRI technology

Bone structure information can also be obtained with MRI. The basis of MRI technology is resonance of atomic spins using radiofrequency (RF) in the presence of a magnetic field. All atoms' nucleii bear a spin with an electronic charge, and this combination generates a magnetic moment. The magnetic moment of atoms have a transverse and a longitudinal vector component. In the body, the direction of magnetic moments of different atoms are scattered but when they are placed within an externally applied magnetic field (B_0), the spins start precessing and aligning with the magnetic field. The result is a net longitudinal magnetization of magnetic moments. The frequency at which the spin precesses towards B_0 is the Larmor frequency (ω_0) of the atom, which depends on the magnetic field strength (B_0) and the gyromagnetic ratio (γ), a property of the atom (99): $\omega_0 = \gamma \cdot B_0$

Equation 2. Larmor frequency of an atom in a given magnetic field (99).

When RF of a specific energy and amplitude matches closely with the Larmor frequency of an atom placed in B_0, the magnetic moment of the atom resonates towards the transverse plane away from the alignment of the magnetic field. Because of the electronic

property of the transverse spin precessing about the perpendicular magnetic field, an alternating voltage is generated (theory of induction), which can be detected by receiver coils (99). Spins eventually relax in the longitudinal direction due to spin-lattice (background) interaction and in the transverse direction due to spin-spin (phase incoherence) interactions. All atoms have the potential for its spin to be resonated but protons (H+) lack electronic shielding and their spins can be manipulated at low energetic costs – ie. with frequency in the radiowave range. Because protons exist in different chemical environments – for example, in fat are more shielded than in water – the longitudinal (T_1) and transverse (T_2) relaxation times vary by tissue type. While T_1 and T_2 occur simultaneously, T_1 times are longer (0.5-5 sec) than T_2 (100-300 msec), and dictate the length of signal acquisition steps for enhancing tissue contrast (100).

To distinguish tissues with different T_1 characteristics from one another, a short repetition time to the next excitation RF pulse is used. This method enables tissues with short T_1 to relax fully and provide a strong signal upon the next excitation versus tissues with long T_1 which would continue to relax when the next excitation pulse occurs, resulting in poorer signal. To distinguish tissues with different T_2 characteristics from one another, a longer time before signal collection (echo time (TE)) is allowed. This method enables tissues with shorter T_2 to decay and helps accentuate those tissues whose T_2 are longer (101). It is important to note that with short TRs, the remaining longitudinal excitation becomes smaller after each subsequent excitation, resulting in a saturation effect. This issue can be combated with use of a partial flip angle (smaller than a full 90^o RF pulse towards the

transverse axis), which preserves more longitudinal magnetization at the expense of minimizing transverse magnetization (99).

Once B_0 has aligned magnetic moments, three magnetic field gradients orthogonal to one another – each with opposite magnetic polarities and linearly increasing magnetic field strengths – can be used to modify Larmor frequencies in order to perform slice, frequency and phase selection. With the first field gradient (z direction), varying magnetic field strength correspondingly alters Larmor frequencies for atoms, specific to the location along the field to enable slice selection. If the gradient is marked by gradual magnetic field increase, a thicker slice results; and if the gradient is marked by a steeper magnetic field increase, a thinner slice results. A second gradient (y direction) is turned on for different durations and amplitudes after spin excitations so that different degrees of phase shift results along different positions in the y-axis. For example, in the higher end of the y-axis, field strength is larger and spins gain phase versus in the lower end of the y-axis where spins become dephased and slowed. Phase encoding enables marking of specific lines along slices (z) so as to separate them within the slice. A third gradient (x direction) enables frequency encoding, which works essentially the same way as slice encoding but is turned on at the time of MR signal collection. The combination of slice selection, phase and frequency encoding creates a unique Larmor frequency address that pinpoints voxel locations within the volume of interest (102). During MR signal collection, data fill a k-space where the phase (y) and frequency (x) domains are Fourier transformed in at least two dimensions to generate useful image data.

MR sequences appropriate for bone

Because basic MR imaging hinges on the precessional frequencies of protons, the quantification of bone structure in MRI is achieved by virtue of the surrounding soft tissue signals including the bone marrow, muscles and tendons contrasting with the lack of proton signal from bone (103). To benefit from bone tissue contrast and a shorter scan time, T_1-weighted imaging (short TE, short TR) is often used in combination with a 3D gradient echo sequence (104). In contrast to spin echo sequences, which require a 90^o pulse followed by 180^o RF pulse refocusing, gradient echo sequences begin with a 90^o RF pulse but use the frequency encoding gradient to induce dephasing by negative polarity fields followed by rephasing by applying a positive polarity field, effectively shortening the time to generate an echo. As such, TR can be shortened, reducing overall scan time. In addition, gradient echo sequences are less sensitive to motion artifact compared to spin echo sequences (105). However, static field inhomogeneities such as the contribution of iron from haemoglobin (which has its own magnetic field) can cause signals to decay more quickly and a short TR means tissues with shorter T_1 times may dephase too quickly and encounter saturation. Consequently, smaller flip angles must be used to counteract saturation effects. Another challenge is the fact that shorter TRs would result in left over signal from previous pulses that carry over to the next cycle – this carry over effect can be destroyed by turning on the slice select gradient again at the end of an echo before the next RF pulse to dephase remaining spins – a spoiled gradient echo sequence (106). Unlike QCT imaging, the greyscale values on MRI do not reflect the density or degree of mineralization of bone. Instead, a more complex relationship is represented between the

MR signal (S) and each of: T_1, amplitude of the gradient echo (A), flip angle (α) and TR, as described by the common Ernst's equation for nuclear magnetic resonance:

$$S = A\sin\alpha\frac{1-\exp(-T_1^{-1}TR)}{1-\cos\alpha\exp(-T_1^{-1}TR)}$$

Equation 3. Common Ernst's equation for signals in NMR (107).

Bone density information cannot be directly obtained by MRI, although some investigations have shown that the T_2 relaxation time affected by static field inhomogeneities (T_2^*) could be used to estimate bone density (108,109). Quantification of bone structure in the absence of density thresholds will be discussed in later sections.

Factors affecting MR image quality

Aside from the fact that MRI confers no ionizing radiation exposure, Wehrli proposed that the point spread function – or the impulse output representation from an object input signal – of MRI is only over 20% larger than the pixel size. In contrast, for QCT imaging, the point spread function is typically dependent on the focal spot size and larger than the size of a pixel (103). Regardless, the resolution achievable from MRI (between 150-300 μm in plane and 300 μm+ thickness) only enables apparent measurement of bone structure (93). In full body MRI, birdcage or peripheral coils can image similar peripheral sites as pQCT and hr-pQCT. Quantification of bone structure at the more clinically relevant proximal femur and lumbar spine locations remains a challenge due to the need for penetrating RF pulse deep within thicker layers of tissues. In some cases, surface coils

have been successful at imaging the proximal femur when soft tissue at the hip is minimal (103). However, peripheral MRI (pMRI) units available at 1.0T and 1.5T field strengths, although less prominent than either pQCT or hr-pQCT, can achieve high SNR images with peripheral coils fitted to the appendicular anatomy being imaged and occupies only a small footprint compared to full body MRI (110). Other imaging parameters also contribute to higher SNR: thicker slice, a smaller field of view, larger matrix, higher number of acquisitions, longer TR, lower RF bandwidth, and a higher field strength magnet (110). However, with a stronger magnet, certain artifacts such as chemical shift and geometric distortion become more apparent. Unlike pQCT and hr-pQCT, the application of pMRI is wider. A systematic review of dedicated extremity MRIs showed that it has been used to largely examine rheumatoid arthritis (15 studies), extremity injuries (5 studies), and osteoarthritis (4 studies). While one randomized controlled trial (N=500) has been performed, most other studies involved smaller sample sizes.

Dedicated extremity MRI systems

Among the available models of pMRI available, GE Healthcare has had an installed base of 175 ONI 1.0T MSK Extreme units worldwide since 2009, 150 1.0-1.5T MSK Extreme systems and acquired the 0.2T MagneVu 1000 from a previously bankrupt manufacturer which had 100 units installed (111). No total install base data was available for the 0.2T GE Lunar M Artoscan but it has been used in at least nine countries (111). So far, no standard MR imaging protocol has been established for examining bone structure at appendicular sites. One of the more widely available pMRI units, the GE OrthOne 1.0T

pMRI, consists of three receive and transit channels, a gantry that enables removable peripheral RF coil fittings of different sizes (80-180 mm diameter), field of view ranging from 40 to 160 mm, matrix size ranging from 64 to 512 for transverse directions and maximum 256 for the z direction. The manufacturer claims spatial resolution up to 50 μm can be achieved with slice thickness as thin as 0.5 mm. The unit is housed in a Faraday cage to prevent entry of external RF and a back-reclining strollable chair enables customized positioning of the peripheral anatomy into the bore of the gantry. However, no height adjustment is available. Wrist bone scans have been performed on this pMRI unit (112) but because of the limited size of the gantry and depth of the bore of the magnet, ankle scans cannot be performed without significant foot plantar flexion. The software installed on the GE OrthOne console is hard coded and does not permit custom programming for k-space image processing.

1.3.5 Bone-tissue segmentation and quantification

Image processing and tissue segmentation is one of the most important steps in extracting useful information from medical images. Segmentation involves the division of an image into discrete regions or labels that share similarities in gray level, texture, colour, brightness and contrast (113,114). The assistance of computer algorithms involving the application of image filters and processing image pixels can extract refined structures that can be subsequently quantified. However, the reliability and accuracy of the technique is dependent on the level of user intervention or automation, ability of the algorithm to converge with all iterations, and its ability to identify similar outputs each time. The

segmentation of bone from soft tissue in images derived from both pQCT and hr-pQCT rely primarily on threshold-based techniques in combination with edge detection algorithms that involve minimal user intervention. By contrast, MRI bone segmentation has involved mostly semi-automated methods capable of handling the blurred edges between bone and soft tissue including fuzzy clustering and cost-minimizing image foresting functions. The power of these tools is tempered by the trouble encountered with image artifacts including motion, which could result in a false representation of anatomical features.

Image segmentation algorithms

Thresholding or more generally amplitude-based segmentation involves defining one or more thresholds for separating an object from background, and is useful when the background has uniform brightness. Thresholds can be selected based on reference or biological standards, or by identifying local minima on histograms (114). Edge-based segmentation marks discontinuities in grey level and utilize detecting operators that rely on derivative gradient functions. Estimated edges are chained together by removing weak edges that contain low gradient amplitude by using thresholding. As such, performance is dependent on the clarity and gradient of the border between tissues, which could be affected by motion and resolution (114). Clustering segmentation alternate between segmenting an image and characterizing the properties of the labelled class to learn from itself without the need for training data (115). One such method is fuzzy c-means algorithm, which hinges on the idea that pixels bear a given probability of belonging to a

certain cluster with pixels on the edge sharing the lowest membership probability. This method overcomes the challenges of partial volume artifact and minimizes the influence of poorer SNR (116). The image foresting transform method begins with planted seeds within the image representing the roots, which expand outward at each subsequent pixel defined by three properties: the position of its predecessor, the cost function of the path drawn and its root. The image is partitioned into influence zones by virtue of how closely connected in cost-minimized function the pixels are (117). These above algorithms have been applied to QCT and MR images in the past. A more thorough discussion of specific algorithms and challenges will be addressed in Chapter 3.5.

Quantifying bone structure

After segmenting bone from soft tissue, quantifying the structural features can be achieved using direct measurement from 3D reconstructions or by applying model assumptions and measuring 2D slices using techniques derived from histomorphometry (118). The goal of structural quantification is to represent features of trabecular and cortical bone that most accurately reflect the pattern of bone loss observed in vivo veritas. For example, in women, the separations between trabeculae begin to grow larger after menopause and the number of intact trabecular bone units decreases over time. In men, trabeculae remain intact but thin more quickly than in women (14). Similarly, MacIntyre also showed that the size of the holes between trabeculae grow larger more quickly in women than in men (119). Cortical bone in women on the other hand thins more quickly than in men (120). Based on these biologically relevant observations, there is evidence to

support the measurement of Tb.Th, Tb.Sp, mean hole size (H_M), Tb.N and Ct.Th. By extension, total BV/TV and bone connectivity indices may also plausibly exhibit clinical relevance. However, there are many more bone structural outcomes than those listed here that can be computed. Evaluating hypotheses based on each one would inadvertently lead to type I errors being committed. Several studies have examined an exhaustive list of bone outcomes and employed principal components analysis to formulate major groups of variables that share the largest amount of variance with one another. Based on this type of analysis, component vectors representing groups of bone variables sharing commonalities demonstrated significant associations with fractures (121,122). However, using these component vectors to perform any clinical assessments would prove difficult. Details on the computation of individual bone structural measures will be described in section 3.5.4.

1.4 Developments in bone assessment

1.4.1 Evaluating the utility of a measurement

The utility of medical imaging technologies in the diagnosis and management of diseases is governed by the reliability of the instrument, the accuracy by which outcomes derived from it can represent disease pathology, their detection limit, clinical sensitivity, the prognostication (risk assessment) of clinical endpoints, their superiority over existing clinical standards for correct diagnosis and for correctly guiding treatment and management of the disease.

Reliability is quantified by the precision of the variable or the degree to which it yields the same value with each repetition. Precision is dependent on random error in the

observer operating the instrument, the instrument stability or biological variability in the sample examined. Standardizing the operation of the instrument and providing proper training to the operator can reduce observer variability. Automating the operation of the instrument can improve the variation due to any user intervention during the measurement process. Collecting data multiple times can reduce the uncertainty in the measurement while addressing each of these sources of random error (123). Accuracy of a measurement describes how well it represents characteristics that it is intended to reflect and can be measured by validation. Comparison against a reference standard or a well-accepted existent measure is termed criterion-related validity. Accuracy is threatened by systematic error derived from the same sources of error as precision, and can be reduced using similar approaches (123). The detection limit of an instrument describes its ability to detect and quantify finite differences in the characteristics of a sample (124). This measured quantity can be described by the least amount of change measurable or the long-term precision error. When the measured quantity (or stimulus) is described in terms of its association with a clinical outcome (or response), the clinical sensitivity can be described (124). Sensitivity and detection limits are intrinsic to the technology itself or in the way the raw data were processed to generate the outcome. These two measures are useful for informing end users of the degree of change one can expect to be able to quantify over time (123). Together, precision, accuracy, detection limit and sensitivity can inform on how to design a study with the appropriate length of follow-up periods, and with the sample size required given the amount of change that can be expected.

Measuring the association between the medical outcome and established clinical endpoints such as fractures enables the estimation of risk for the disease. Though an association study can be performed in a cross-sectional study design, the actual prediction of future risk of a disease-related event is best performed in a prospective longitudinal study where the outcome is quantified at baseline. The plurality of research studies contribute to a larger body of evidence supporting conclusions related to each of these outcome evaluation characteristics. In the end, these studies are necessary for meta-analyses or systematic reviews, which can be used to guide changes in policy. The International Society for Clinical Densitometry (ISCD) has made recommendations regarding the use of pQCT in adult and paediatric populations based on a systematic review of studies describing some of the above outcome characteristics (125,126). Further data detailing these items will contribute towards better informed recommendations guiding research and clinical decision making for pQCT, hr-pQCT and pMRI.

1.4.2 Short comings and challenges to progression of bone imaging technologies

As pQCT and hr-pQCT technologies have already been developed and utilized in many research studies over the last decade, their utility in examining various conditions and epidemiological questions is unquestionably relevant. However, there have been a lack of large epidemiological studies describing population-based reference data in different cohorts. Meanwhile the development of pMRI technology for imaging bone has only recently progressed, with the major limitation being the lack of global uptake and thus limited number of research groups examining its research and clinical utility. Even with

full body MRI, the limited access due to protected clinical dedication and high costs prevent more studies from being performed to further evaluate clinical outcomes with MRI-derived bone variables. Aside from these access-related hurdles, there is currently a lack data reporting one-year detection limits and clinical sensitivity – for example by reporting standard errors of the estimate (SEE), least significant change (LSC) or OR / HR for fractures– for bone volumetric outcomes on each of these modalities. Without an adequate population reference and without knowing how much change one must expect to observe before considering an observation to be clinically meaningful, there is a lack of guidance on 1) whether a measured degree of change is larger than what is expected for a given age group, 2) the effect size of change, 3) the sample size required to demonstrate adequate change with sufficient statistical power and 4) the best surrogate endpoint to use to benefit from observing larger changes sooner.

1.5 Study goal – addition to current state of knowledge

The overall encompassing goal of the current investigation was to compare and evaluate the analyses derived from images obtained by three bone structure-imaging technologies: hr-pQCT, pQCT and 1.0T pMRI in terms of their validity, reliability, detection limit and clinical sensitivity. A reference dataset was also generated with which future investigations could compare. This step towards assessing these technologies primes the application of the imaging modalities to large-scale epidemiological studies and to clinical trials.

2 Objectives and Hypotheses

2.1 Objective 1. Validating volumetric bone outcomes across modalities

2.1.1 Current state of knowledge (at the time of hypothesis, 2010)

To date, hr-pQCT-derived bone structural variables have been validated against µCT (R^2 = 0.59-0.96) at 19 µm resolution (127). Cortical area and bone mineral content from pQCT have been compared to histomorphometry (R^2=0.50) and ashing (R^2=0.55) , respectively (128). In one study by Laib, bone outcomes derived from pQCT at a non-clinical in-plane resolution of 158 µm were validated against µCT (28 µm) using bone biopsies (R^2 = 0.81-0.96) (129). There have not been studies demonstrating bone structural validity for pQCT in vivo. One study by Liu et al. defined the accuracy of 7.0T (160 µm) full-body MRI-derived bone structural variables using cadaveric tibiae (R^2 =0.79 (BV/TV), 0.97 (Tb.Sp), 0.92 (Tb.N)) as compared to µCT (25 µm) (130). While these specimens lacked the ability to reconstitute magnetic susceptibility differences between tissues, Kazakia correlated hr-pQCT-derived bone structural measures with those obtained on 3.0T MRI (156 x 156 µm x 2 mm) in human volunteers and identified modest coefficients (R^2 =0.52-0.60). However, absolute values of these measurements differed between the two modalities with Ct.Th and Tb.N being larger on MRI, albeit the latter differed only by an amount within the short-term precision error (131). Krug similarly demonstrated validity of 3.0T MRI-derived (156 x 156 x 500 µm) bone structure by comparison against µCT (18 µm) of cadaveric specimens (132). There have not been any studies validating bone structural outcomes acquired from a 1.0T magnet. Due to the

smaller RF coils available on the pMRI system, improved SNR could contribute towards superior bone structure measurement accuracy.

2.1.2 Objective and specific aims

Objective 1: *To validate pQCT and 1.0T pMRI-derived volumetric bone measures by comparison against the same variables obtained from analyses of hr-pQCT scans*

Specific aims: To address this objective, study volunteers completed a scan of their ultradistal radius at the same region of interest on hr-pQCT, pQCT and 1.0T pMRI. Bone structural outcomes were computed using modality-specific segmentation software and compared using a linear regression analysis. A Pearson correlation coefficient informed on the degree of variance in hr-pQCT explained by pQCT- and pMRI-derived volumetric bone outcomes. The slope and intercept reported from linear regression models quantified the degree of systematic deviation from hr-pQCT-derived variables. Intraclass correlation coefficients (ICC) determined the degree of agreement in bone structural outcomes between modalities. Bland-Altman analyses determined any patterns of biased agreement between modalities.

Study outputs: intermodality R^2, intermodality ICC, slopes and x-intercept, Bland-Altman limits of agreement (LOA) and linear equations where relevant

2.2 Objective 2. Reliability of volumetric bone outcome quantification

2.2.1 Current state of knowledge (2010)

Hr-pQCT short-term precision for all bone microstructural outcomes has been reported previously (RMSCV: 2.5-4.4%) (98). Swinford showed that increases in participants'

body size contributed towards reduced precision for bone structure on pQCT (133). In vivo test-retest precision for pQCT-derived cortical and trabecular areas were found to be between 4.9-7.6% for tibia and radius (134). Another study quantified the test-retest precision for trabecular, cortical and integral density (0.8-1.6%) (135), but in vivo apparent microstructural pQCT measurements' reproducibilities have not been described. In one study, short-term precision errors of BV/TV, Tb.Sp and Tb.Th derived from 1.5T MRI of the calcaneus were between 1-2% in vivo (136). Using an automated co-registration algorithm, Blumenfeld was able to achieve test-retest precision values between 2-4.5% for tibial trabecular bone structural outcomes from MRI scans (137).

2.2.2 Objective and specific aims

Objective 2: To determine s*hort-term test-retest precision of volumetric bone outcomes for acquisitions on pQCT and 1.0T pMRI**

**Since short-term precision for all volumetric bone outcomes have already been quantified for the specific hr-pQCT used here, this analysis was not repeated.*

Specific aims: To address this objective, study volunteers who already completed a single scan on pQCT and 1.0T pMRI as per **Objective 1** were re-scanned immediately after the first scan, but with complete removal and repositioning in the scanner's gantry. Volumetric bone measures were computed using modality-specific segmentation software. Test-retest precision of bone outcomes was evaluated using root-mean square (RMS) coefficients of variation (CV) and standard deviations (RMSSD).

Study outputs: RMSCV, RMSSD

2.3 Objective 3. Detection limits and clinical sensitivity of volumetric bone measures

2.3.1 Current state of knowledge – detection limits and long-term precision (2010)

Few studies have reported detection limits of hr-pQCT, pQCT or MRI-derived bone structure. However, long-term precision data have been converted to LSC values, which putatively inform on the minimum change required to be considered clinically meaningful. Long-term precision of volumetric bone outcomes has been quantified from hr-pQCT scans repeated over an intermediate period (5 months) to longer durations (28 months) (2.2-3.4%) (138). Long-term precision for 1.5T MRI-derived BV/TV, Tb.Sp and Tb.Th were between 3-6% (136). No reports on the long-term precision of pQCT-derived bone structural outcomes have been identified to date.

2.3.2 Current state of knowledge – clinical sensitivity (2010)

A more useful way to describe clinically meaningful change of volumetric bone outcomes is by quantifying the association between change in the measure and an appropriate response such as fractures since fracturing a bone is a clinically important endpoint. Although most studies measuring odds and risks for fractures do not actually measure change in bone outcomes, the notion of change is represented by the associated increased odds or risks per unit difference in the outcome (interpreted as a hypothetical "increase" or "decrease") . Laib demonstrated that each SD increase in hr-pQCT-derived Tb.Sp and decrease in Tb.N was associated with an age-adjusted increase by 1.85-2.03 fold in the odds for fractures (139). However, in a similar cross-sectional analysis, Melton did not see any association between volumetric bone outcomes and prevalent fractures at the

distal radius on hr-pQCT (140). Although not examined in terms of changes in SDs, MacIntyre showed that a mean inter-trabecular pQCT-derived hole area greater than two SDs from the mean translated to a 5.4 fold increase in the odds for fractures (141). One investigation by Boutry reported a significantly increased odds for fractures per SD difference in 11 out of 13 volumetric bone outcomes obtained from calcaneous scans on MRI (142). All the above studies so far have only been examined cross-sectionally.

2.3.3 Objective and specific aims

Objective 3: *To determine the long-term detection limits, and clinical sensitivity of volumetric bone outcomes for acquisitions on hr-pQCT, pQCT and 1.0T pMRI*

Specific aims: To address this objective, study volunteers who already completed a single scan on hr-pQCT, pQCT and 1.0T pMRI as per **Objective 1**, were scanned a year later at the same region of interest. Volumetric bone outcomes were computed using modality-specific segmentation software. Long-term test-retest precision of bone outcomes was evaluated using RMSSD, which was then converted to a one-year LSC according to recommendations from the ISCD (143). Binary logistic regression analysis using prevalent fracture data from the last 15 years was used to determine unadjusted and age-adjusted odds for fractures based on each bone outcome.

Study outputs: Long-term RMSSD, LSC, OR (95% CI)

2.4 Objective 4. Population reference for volumetric bone outcomes

2.4.1 Current state of knowledge (2010)

In a population-based cohort study, Khosla described volumetric bone outcomes derived from hr-pQCT scans of 324 women and 278 men between 21-91 years of age (14). Riggs similarly examined 373 women and 323 men 20-90 years of age but only quantified integral, cortical and trabecular vBMD using central QCT (144). In the Study of Osteoporotic Fractures (SOF) in women and in the Osteoporotic Fractures Study in Men (MrOS), pQCT-derived bone structural outcomes were described in over 1000 participants (122). However, these studies only examined participants at a maximum of two city locations. No population-based cohort studies have been performed on MRI modalities for quantifying bone structure. The largest cohort that examined volumetric bone measures using MRI comprised of just under 150 participants (139).

2.4.2 Objective and specific aims

Objective 4: *To construct a reference dataset consisting of bone structural outcomes derived from hr-pQCT, pQCT and 1.0T pMRI for women above 50 years of age*

Specific aims: Participants over 50 years of age at six study centres were scanned at the same region of interest on pQCT and/or hr-pQCT. Because 1.0T pMRI was only available at one location, scans were completed in a local cohort to establish the pMRI-derived bone structural outcome reference dataset. All bone structural data were evaluated for fit to a normal distribution and descriptive statistics computed according to age groups by half decades.

Study outputs: Mean (median), standard deviation (interquartile range), p-value Kolmogorov-Smirnov test, kurtosis, skewness, min, max

3 Methods

3.1 General Study Design

Objectives 1-3 above were addressed using a local cohort of study participants. To formulate a dataset that sufficiently represented the Canadian population, objective 4 was targeted with a national population-based cohort comprising six Canadian cities where pQCT and/or hr-pQCT were available. 1.0T pMRI was performed only at one study centre since no other pMRI units were available for access. Study designs for the local and national scale studies are separately described in detail below. All study activities were coordinated centrally at the Charlton Medical Centre (Hamilton, ON) by a local and national study coordinator (AKOW).

3.1.1 Effect of grant funding on study design

This study was funded by a Canadian Institutes of Heath Research (CIHR) Operating Grant (MOP-115094) and Vanier Canada Graduate Scholarship Award (CGV-104858). Because the original study budget was reduced by 20%, funding was available to study only half the anticipated cohort. Consequently, all foregoing objectives of the local study were focused on women above 50 years of age and the national component focused on recruiting women 60-85 years of age.

3.2 Local study design

The local study situated in Hamilton/Toronto, ON, Canada was conducted as a cross-sectional and a one-year prospective cohort study examining volumetric bone outcomes

from hr-pQCT, pQCT and 1.0T pMR images obtained from Canadian women over 50 years of age. No interventions were applied to study participants in this study.

3.2.1 Overview of study procedures

Participants had the opportunity to partake in the completion of all imaging procedures (1-3) in all repetition formats (A-B) or in only a component of these:

1) **pQCT** imaging was conducted at the McMaster University Medical Centre (Hamilton, ON).
2) **1.0T pMRI** scans were acquired at the Charlton Medical Centre (Hamilton, ON).
3) Imaging procedures for **hr-pQCT** were executed at the Toronto General Hospital (Toronto, ON – 70 km from the Charlton Medical Centre).

A. One set of scans on each modality was repeated once during the same study visit.
B. A baseline scan on each imaging modality was followed by a follow-up scan timed approximately one-year later.

All participants completing any procedure also consented to providing information about their medical history and medication use in addition to releasing information regarding their history of fragility fractures over the last 15 years.

3.2.2 Study procedure timeline and time allowance

All scans were performed on different imaging modalities within, at most, three months of one another. For one-year follow-up scans, a similar three-month allowance window

was used as a guide. However, because of unpredictable availability over a one-year trajectory (due to holidays, medical appointments ,etc.), and the difficulty of retaining a sufficient sample size of individuals able to complete scans within a three-month window of the anticipated one-year anniversary, this three-month period was relaxed to a maximum of 6-months when necessary. The final long-term precision and LSC computed were qualified but not statistically-adjusted by the mean follow-up period.

3.2.3 Sample selection

All study participants were recruited from a local cohort belonging to the Canadian Multicentre Osteoporosis (CaMos) study, leveraging over 15 years of study data. This cohort was selected because there was already a rich dataset of detailed fracture information and a long history of study coordinator and participant relationships enabling a high level of interest and dedication to the principal (CaMos) and ancillary studies.

Women from CaMos were recruited between 1995 to 1997 and were followed for the subsequent 15 years. Over 200 women were recruited to each of nine study centres using a scientific random selection process, with contact information derived from residential telephone books. This population-based cohort is unique because participants have contributed many years of data including the incidence of fragility fractures, aBMD of the total hip and lumbar spine, spinal X-rays and clinical risk factors for osteoporosis (145).

Inclusion/Exclusion criteria: Women over 50 years of age were invited to participate in all components of the local study. Women with valid contraindications to MR imaging were excluded from all 1.0T pMRI procedures (Form 1). Those participants weighing

above 250 lbs were excluded from hr-pQCT and 1.0T pMRI procedures due to the weight limit of the designated positioning chair. Women with self-reported tremors were also excluded to avoid yielding unusable scans due to significant motion artifact.

3.2.4 Study questionnaires and case reporting

A complete list of current medications (prescription, over-the-counter, vitamins, minerals and natural health products) including dose, duration and frequency was obtained from all participants (Form 2). Information on medical conditions from the last ten years was obtained from the CaMos database. Detailed fragility fracture information including cause and anatomical location of fracture were also obtained from the CaMos database from the last 15 years. Fragility fractures were defined as non-traumatic fractures occurring as the result of a fall from standing height or less, excluding any fractures of the skull, fingers and toes. Additional information on imaging procedure completion and scanned-limb sidedness was also recorded.

3.2.5 Local ethics approval

All study procedures were designed in accordance to the Tri-Council Policy Statement 2 (2012) and adhered to Good Clinical Practice guidelines. Procedures completed in Hamilton were overseen and approved by the St. Joseph's Healthcare Research Ethics Board (08-3072 and 08-3073). Procedures completed in Toronto were overseen and approved by the University Health Network (08-0826-AE and 10-0439-AE).

3.3 National study design

The national study attending to objective 4 was conducted in Vancouver (hr-pQCT and pQCT), Calgary (hr-pQCT), Saskatoon (hr-pQCT and pQCT), Hamilton (pQCT and access to hr-pQCT through Toronto), Toronto (hr-pQCT and pQCT) as well as Kingston (pQCT). In addition, a single site collected the reference dataset for 1.0T pMRI measures (Hamilton). This national reference data collection effort was designed as a cross-sectional population-based cohort study evaluating descriptive statistics of volumetric bone outcomes derived from hr-pQCT, pQCT and 1.0T pMRI in women over 50 years of age. There was no overlap in participants examined in the local versus national studies.

3.3.1 Overview of study procedures

Participants volunteered in the completion of one or more imaging procedures available at their local sites including:

1) **hr-pQCT** scans of the ultradistal radius and ultradistal tibia
2) **pQCT** scans of the ultradistal radius and ultradistal tibia
3) **1.0T pMRI** acquisitions of the ultradistal radius*

*** Note:** Due to limitations in the gantry diameter, ultadistal tibia scans were not completed, as this would have required participants to sustain an extensive plantar flexion position for the duration of the MRI scan (>15 minutes). While discomfort was a concern, the major challenge was maintaining minimal motion.

All participants completing any of the above procedures also consented to have medical history and medication use information collected, in addition to having information regarding their history of fractures released to the study. **Note:** Although participants had the opportunity to also complete a total hip and lumbar spine DXA scan, these data were centrally analyzed in Quebec City and were not available at the time of analyses.

3.3.2 Sample selection and biases

All study participants were recruited from local cohorts of the CaMos study, which benefited from a high study interest level maintained by the strong relationship between coordinators and existing study participants. Study retention for the CaMos study from inception to year 16 for women above 50 years of age has been just over 44% with 46% of those lost to follow-up due to refusal, 38% due to death and 16% to lost contact.

Inclusion/Exclusion criteria: Women over 60-85* years of age were invited to all components of the national study to the extent that an imaging modality involved was available. The same exclusion criteria from the local study applied to the national study as well (Section 3.2.3). * **Note:** Due to funding limitations, a decision to restrict the studied cohort to women 60-85 years of age was made on the premise that costs would be saved by leveraging from the concurrently running, principal CaMos study.

3.3.3 Study questionnaires and case reporting

A full year-16 CaMos questionnaire (Form 3) was completed by all consenting study participants. This form contained detailed medical history of a range of conditions including its diagnosis and treatment (Form 3 Section 2.1), medication use (Form 3 Section 3.1-3.2) including frequency, dose and duration of use; as well as detailed incident fragility fracture information (Form 4**)** including cause of fracture and anatomical location of fracture. Additional information on imaging procedure completion and scanned-limb sidedness was also recorded on hr-pQCT and pQCT tracking forms (Form 5 and 6, respectively**)**.

3.3.4 National and site-specific ethics approval

All national study procedures were streamlined by standard operating protocols coordinated by a national coordinating centre. The study was designed in accordance to the Tri-Council Policy Statement 2 . All procedures were approved by local institutional research ethics boards (Vancouver: #H94-70123, Calgary: #E-23839, Saskatoon: #12-209, Toronto: #10-0439AE, Kingston: #DMED-266-97). Nationally encompassing ethics review was completed at the St. Joseph's Healthcare Hamilton Research Ethics Board (#11-3618) and at the McGill University Research Ethics Board (#12-081).

3.4 Volumetric bone imaging procedures

All volumetric bone images acquired for the three modalities examined the same region of interest at the ultradistal radius. In addition, for the two QCT modalities, the same ultradistal tibia region of interest was examined. The region of interest selection was most

rigid for the hr-pQCT protocol due to limitations in the ability of the manufacturer software to analyze structural measures beyond this predefined region. Consequently, region of interest selection for all other modalities were centred according to that which was defined for hr-pQCT. Minor differences distinguished between the local and national study components are noted in each section below. For objectives 1 through 3, a slice map shown in Figure 2 illustrates relative co-localization of scans obtained across the three modalities. In general, the non-dominant arm and the leg on the same side was scanned. If the wrist or ankle of the non-dominant side had previously sustained a fracture within the last 5 years, or if any musculoskeletal abnormalities were present on the non-dominant limb preventing the participant from holding a still position for over 5 minutes, the contra-lateral side was scanned instead.

3.4.1 High-resolution peripheral quantitative computed tomography

Positioning and limb fixation

Technologists followed standard imaging protocols, established by the manufacturer (Scanco Medical) and previously reported by Boutroy et al (98), for correct positioning of the wrist and ankle for data acquisition. For ultradistal radius scans, participants' hand was immobilized in a fixation device commonly available at all study centres. Participants were asked to loosely grip onto the stationary handle bar and foam padding was inserted around the hand within the fixation cast. Seated in a height-adjustable chair, the cast was inserted into the scanner with the anterior aspect of participants' arm facing the sagittal direction. The height of the chair was adjusted so that the arm was parallel to the ground. Shoulder flexion was permitted to achieve a comfortable position for the study participant.

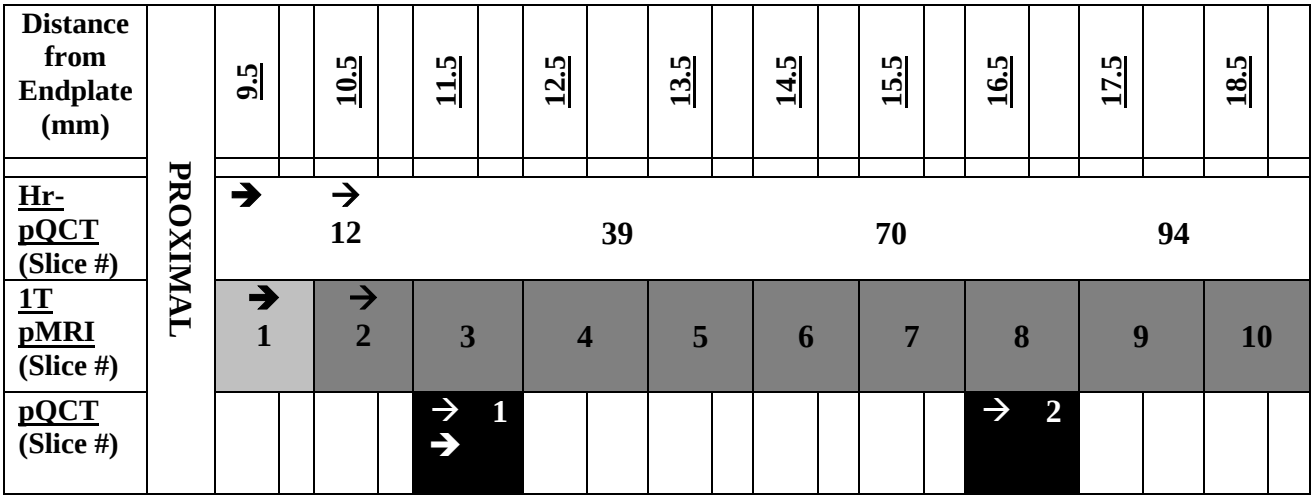

Figure 2. Slice and region of interest co-localization map.
Empirical co-localization of regions of interest examined using hr-pQCT, 1.0T pMRI and pQCT. Bolded arrows indicate beginning of image acquisition. Unbolded arrows indicate hypothetical beginning of co-registered analysis. Slice number from each imaging modality was approximately matched with the number on another modality. Hr-pQCT row contains 110 slices, not illustrated individually here.

For ultradistal tibia scans, participants' non-dominant leg, with shoes removed, was immobilized in a similar fixation device without a handle bar, also available at all study centres. Leg dominance was considered the same as hand dominance in this study. Those who required scans to be completed on the dominant hand for any reason but were still able to complete scans on the non-dominant leg proceeded with scans on the non-dominant leg. Foam padding was inserted around the heel and the toes were secured in a neutral non-flexed position against the cast either with foam padding or using adhesive tape to minimize motion during scans. Seated in a height-adjustable chair, the leg cast was secured into the scanner with the anterior aspect of participants' leg facing the coronal direction. The height of the chair was adjusted so that the leg was parallel to the ground and knees in a fully extended position. Hip flexion was permitted to achieve a comfortable position for the study participant.

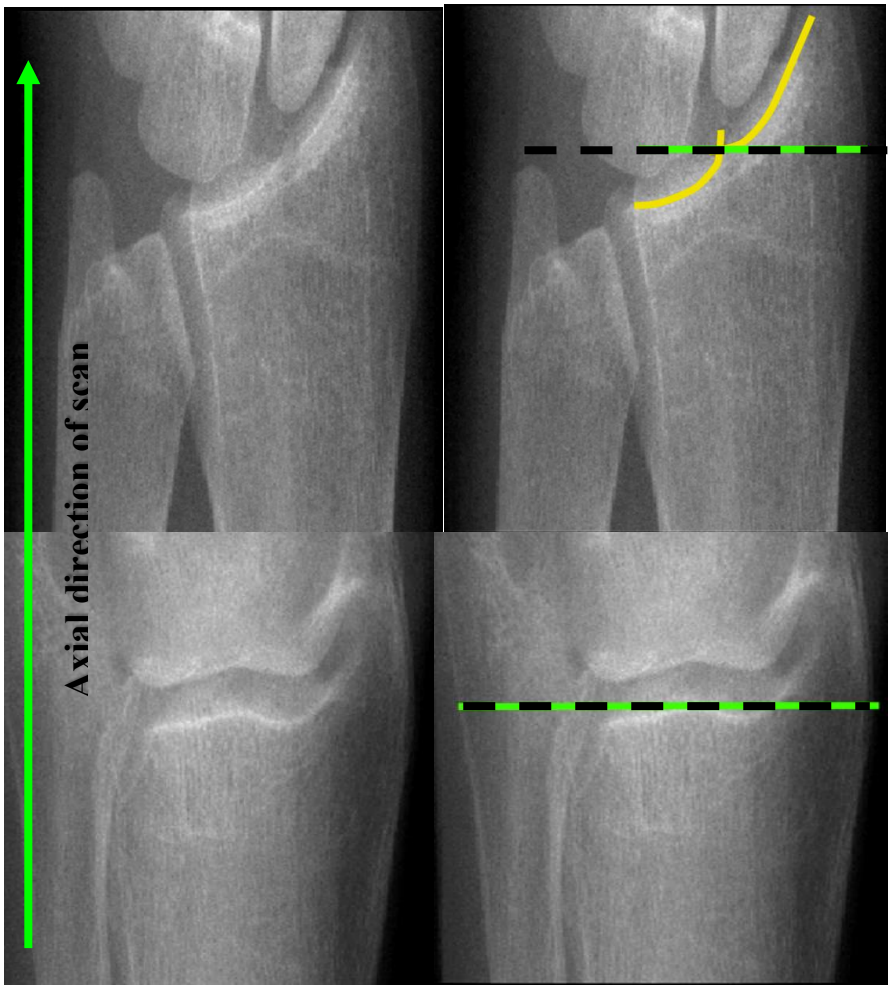

Figure 3. hr-pQCT reference line placement in sagittal scout views
Top: Reference line (dashed line) was placed at the intersection of two shallow concavities (smooth lines) along the radial tilt. Bottom: Reference line (dashed line) was placed tangential to the plateau portion of the tibial endplate.

Reference line placement and region of interest identification

Scans of the radius were completed at a site that was 9.5 mm proximal to a reference line located at the distal radius. This location at the distal radius was identified in a sagittal scout view and specified as a radial tuberosity visible along the radial inclination. This tuberosity was identified as a point converging from two shallow concavities along the radial inclination, located more than half way in distance proximal to the most distal point of the radius and more than one third distal to the base of the radial tilt. While this

tuberosity can be clearly identified ex vivo, its visibility on a scout view can be obscured by rotation of the wrist about the axial direction. The reference line was placed at this point of intersection perpendicular to the axial direction of scans (Figure 3). Tibial scans were completed at a site that was 22.5 mm proximal to a reference line located along the plateau portion of the distal tibial end plate, which was defined as the bright most horizontal feature of the cortical bone border identified in the sagittal scout view of the distal tibia (Figure 3). The reference line was superimposed on this cortical bone boundary, perpendicular to the axial direction of scans.

All technicians completing hr-pQCT have been trained to place reference lines consistently using a training scout image dataset provided by Boyd. A test-retest precision analysis had previously been performed on at least 7 participants to ensure adequate training and to minimize precision error.

Imaging technical parameters

All hr-pQCT scanners (XtremeCT, Scanco Medical AG, Bassersdorf, Switzerland) utilized were the same model and make. Images at the prescribed regions of interest indicated above were obtained using the following settings: 60 kVp, X-ray tube current of 95 mA, exposure time of 100 ms, and matrix size 1536 x 1536. 110 CT slices with 82 µm isotropic voxel resolution were acquired axially in the proximal direction beginning from the reference line, for a total coverage of 9.02 mm. For each site, scan time was approximately 5 minutes. Hydroxyapatite phantoms were scanned daily and weekly for

quality control purposes. All scans were processed on the hr-pQCT console using manufacturer's software (Scanco Medical AG, Bassersdorf, Switzerland). Outcomes of gross bone geometry (Ct.Th), microstructure (Tb.Sp, Tb.Sp SD, BV/TV, Tb.Th, Tb.N) and densitometry (integral, cortical and trabecular vBMD) were computed automatically.

3.4.2 Peripheral quantitative computed tomography

The XCT2000 system (Stratec Medizinteknik GmbH) was used to perform all pQCT scans in Hamilton. Except for Vancouver, with a XCT3000 system, all other national study centres also employed XCT2000. Because pQCT imaging protocols vary considerably across study centres, each section below describes procedures followed for the local study and alterations implemented in the national study. It was important to ensure the national study was both streamlined in scan procedures across study centres, but also that the data generated were comparable to previously reported data. Limb positioning, reference line and region of interest identification, as well as technical scan parameters were streamlined according to both consensus among local study centre directors and a method which most closely matched the positioning protocol utilized in the local Hamilton study for objectives 1-3. A single technician performed pQCT scans and preparations at each site.

Positioning and limb fixation

Prior to positioning and image acquisition, participants' radius and tibia lengths were obtained for the limb on which scans were completed. Limb sidedness decisions for pQCT imaging followed the same protocol as for hr-pQCT (section 3.4.1). Resting the

elbow on a desk, the radius was measured from the surface of the desk to the distal aspect of the ulnar styloid process to the nearest millimetre. While seated on a chair with feet flat on the ground and knees bent at a 90 degree angle, the tibia was measured from the distal malleolus of the tibia to the external border of the medial tibial plateau.

Local study: For distal radius scans, participants were seated in a height-adjustable chair facing the axial direction of the scanner with their non-dominant hand inserted into the gantry, anterior aspect of the arm facing down in the coronal direction and fingers resting on a convex hand rest while the proximal arm was clamped into a fixed position. The seat of the chair was adjusted so that the arm was parallel to the ground and the seat positioned as closely to the gantry as possible. Participants' shoulders were allowed to be flexed to maximize comfort during scans.

For distal tibia scans, the height-adjustable chair was lowered to enable participants to insert their leg into the gantry of the scanner, with the anterior aspect of their tibia facing up in the coronal position and their heel on a standard foot rest. A hook-and-loop fastener was used to secure the foot into place to prevent movement during scans. At the proximal end of the lower leg, a foam-padded fixation clamp was applied to secure the leg in the iso-centre of the gantry, centred about the ankle. The height of the chair was adjusted to ensure the tibia was parallel to the ground. Hip flexion was permitted to achieve a comfortable position for the study participant.

National study: The same positioning protocol was applied from the local study protocol. However, study centres were also allowed to position the participant facing perpendicular to the axial orientation of the scanner. In this position, the arm was extended and the shoulder was abducted to render the radius parallel to the ground.

Reference line placement and region of interest identification

Local study: Scans of the radius were completed at sites that were 11.5 mm and 16.5 mm proximal to a reference line located at the distal radius. This location coincided with scans obtained by hr-pQCT and was identified in a coronal scout view. Because the distal radius tuberosity previously described (section 3.4.1) cannot be viewed from this coronal scout view, an approximation was made to represent its putative location. The base of the radial tilt was identified as the most medial articulating aspect of the distal radius and the end of the radial tilt as the most lateral articulating aspect of the distal radius. The distance between these two landmarks was divided in half and added to the Z-distance of the radial tilt base landmark to determine the mid-point along the radial tilt (Figure 4).

Tibial scans were completed at sites that were 24.5 and 29.5 mm proximal to a reference line located along the distal tibial end plate. The distal tibial end plate was defined as the distal blue border identified in the coronal scout view of the distal tibia. The reference line was superimposed on this blue cortical bone boundary, perpendicular to the axial direction of scans (Figure 4).

A test-retest precision analysis was performed on a minimal group of 7 participants at each site to ascertain adequate training from a measurement error perspective.

National study: Reference line placement in the national study followed protocols that were most commonly shared across all study centres and with previously reported studies. The reference line was directly placed at the medial articulating aspect of the distal radius (Figure 4). For the tibia, the same protocol as the local study applied.

Rather than a fixed distance region of interest, scans were prescribed at the 4% site of the radius and tibia, proximal to the defined reference line. This percentage distance was quantified relative to the length of the ulna and tibia previously obtained. A second slice was similarly prescribed 5.0 mm proximal to the initial 4% site slice.

For objectives 1-3, it was important that the same region of interest be selected between pQCT and hr-pQCT. However, for objective 4 in establishing a reference dataset, consensus among study centre directors selected for a method that was most comparable to previous pQCT studies (ie. 4% of limb length, beginning from the medial articulating surface of radius and tibia) rather than for comparison to hr-pQCT.

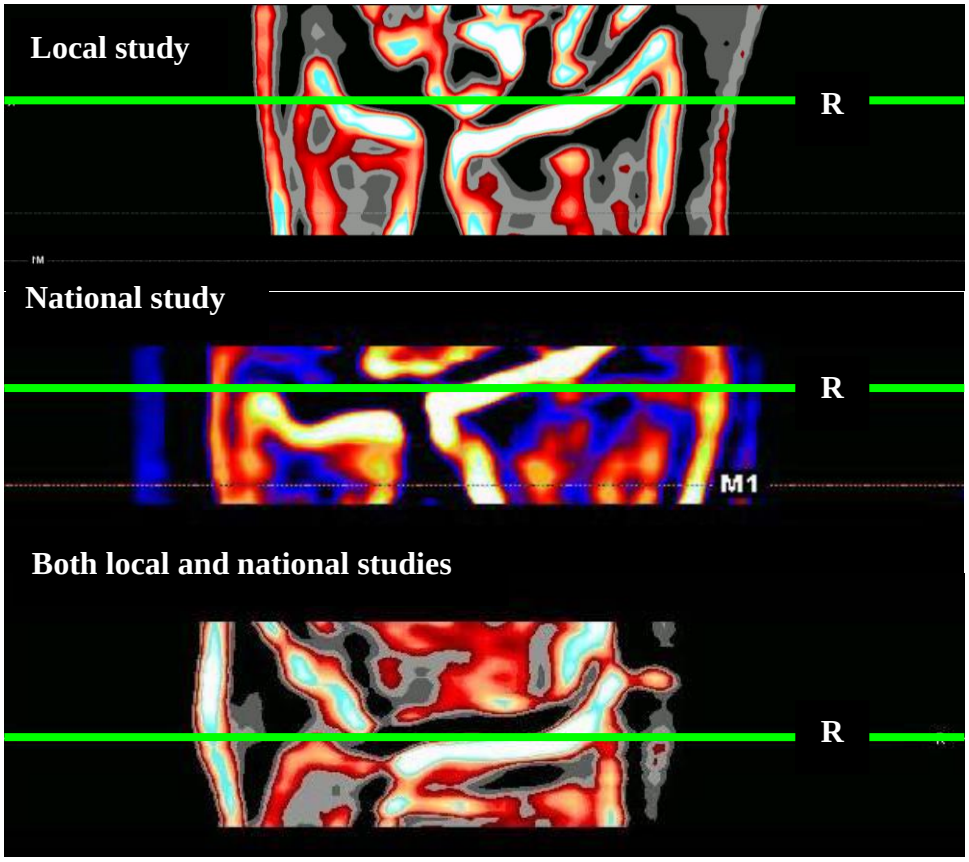

Figure 4. pQCT reference line placement.
Top: Reference line (R) was placed at the midpoint between the base and top of the radial tilt for the local study. Middle: Reference line was placed at the medial articulating aspect of the distal radius for the national study. Bottom: Reference line was placed tangential to the plateau portion of the tibial endplate.

Imaging technical parameters

At each region of interest for both radius and tibia scans, two slices 2.5 ± 0.3 mm thick separated by 5 mm was acquired with an in-plane resolution of 200 μm with the following acquisition parameters: CT scan speed of 10 mm/s, 38 kVp X-ray beam energy, a tube current of 0.3 mA, reconstructed by filtered back-projection on a matrix size of 256 x 256. Both slices obtained on each limb were acquired in sequence without interruption.

For each set of scans, a total acquisition time of 9 minutes was expected. Hydroxyapatite phantoms were scanned once on each day scans were to be obtained.

Previous pQCT studies have employed an in-plane resolution poorer than 200 μm (> 300 μm) and a scan speed at 15 mm/s or faster (119,128,146-148). These parameters would be appropriate for the computation of macrostructural and densitometric bone outcomes such as integral, cortical and trabecular vBMD. However, more accurate calculation of apparent microstructural measures can be limited by resolutions poorer than 200 μm and the penalty of a lower SNR imposed by a faster scan speed (≥ 15 mm/s).

Image analyses and outputs

Densitometric (integral, cortical and trabecular vBMD) and macrostructural (total cross-sectional area, cortical and trabecular areas) measures were obtained from Stratec v5.2.1 software after threshold-based segmentation. Primary measures of apparent cortical and trabecular microstructure (Ct.Th, Tb.Sp, BV/TV, Tb.N, Tb.Th) and connectivity (nodes (Nd), isolated points (Ip), free ends (FE), network length (NL) and connectivity index (Cx)) were computed with custom software package, pQCT OsteoQ (**Inglis Software Solutions Inc., Hamilton, ON**), which similarly required bone cropping.

3.4.3 1.0 Tesla peripheral magnetic resonance imaging

Positioning and limb fixation

Distal radius scans were performed on a 1.0T pMRI OrthOne scanner (GE Healthcare, USA) located at the Charlton Medical Centre (Hamilton, ON). The scanner was approved

for use by the Therapeutics Product Directorate of Health Canada. A 100 mm diameter transmit/receive RF coil obtained transaxial images of participants' ultradistal radius. Lying supine in a reclining chair, the wrist was positioned in the iso-centre of the bore of the magnet with the the forearm facing prone and the wrist slightly internally rotated to align the radius parallel to the coronal plane. Foam padding and a wrist brace were used to minimize the potential for motion during scans.

Reference line placement and region of interest identification

Both coronal and sagittal scout scans ensured correct alignment of the prescribed image slices with the longitudinal axis of the radius. In the sagittal scout view, coronal scout slices were prescribed, parallel to the long axis of the radius and centred about the middle of the radial inclination. On the coronal scout view, a reference line was placed at the midpoint between the base and top of the radial tilt as shown for pQCT reference line positioning. Scans began 9.5 mm proximal to this reference location. All slices were obliquely rotated so that slices were aligned perpendicular to the long axis of the radius, using the cortical shell of the radial shaft as an anatomical reference.

Imaging technical parameters

A T_1-weighted spoiled 3D gradient echo sequence (3D SPGR) was acquired in the axial plane with the following sequence parameters: number of excitations = 3, number of echoes = 1, flip angle = 40^o, bandwidth= 15 kHz, repetition/echo time (TR/TE) = 47ms/23.8ms, field of view = 100 x 100 mm, and a matrix size of 512 x 256 pixels (interpolated to 512 x 512) resulting in an in-plane resolution of 0.195 x 0.195 mm^2.

Scanned slices began at 9.5 mm proximal to the radial endplate, as defined using the method described in the pQCT protocol, in the coronal scout view. A slice thickness of 1.0 mm was used and 10 slices were obtained in tandem with 0 mm gap. The total scan time was 12:09 minutes. For each scan, total time including participant positioning, scout and final image acquisition was approximately 20 minutes. Quality control was performed on the pMRI scanner on a daily basis using a geometric phantom.

Image analyses and outputs

Bone structural measures were obtained from the central 8 slices since signal loss at end slices in 3D SPGR scans precludes sufficient image contrast between bone and marrow. Using a custom designed software package, MRI OsteoQ (**Inglis Software Solutions, Inc**), trabecular bone structural (Tb.Sp, Tb.Sp SD, BV/TV, Tb.N, Tb.Th) and connectivity (Nd, FE, Ip, NL, Cx) outcomes were computed on a per-slice basis and averaged to provide a final structural outcome for the image volume.

3.5 Image segmentation and processing

3.5.1 Hr-pQCT Scanco Medical software

Density: Hounsfield unit calibration

Physical absorption coefficient units (1/cm) are typically converted to Hounsfield units by calibrating scans on CT modalities using an air and water phantom. Pure water is assigned a value of 0 HU and air a value of -1000 HU. Bone is therefore considered to range between 2500 HU to 7000 HU. Because physical absorption of X-rays depends on

X-ray spectral properties such as its voltage, energy, collimator geometry (fan versus cone-beam), and detector type (scintillator, charged coupled device, photomultiplier, CdTe), the Hounsfield units output can vary somewhat. To circumvent comparability challenges, Hounsfield units on the hr-pQCT were standardized to hydroxyapatite (HA) density units (mg HA/cm^3) using calibration to four hydroxyapatite rod phantoms (149). This was a feasible option for rendering results comparable since air and water values change very little even after the Hounsfield unit scale was re-linearized according to a compact block of HA.

Cortical and trabecular masks - dual-threshold based segmentation

The entire bone region of 110 slices was manually cropped from the image and soft-tissue background prior to fully-automated dual-threshold-guided bone segmentation previously described by Buie et al (150). The foundation of dual-threshold segmentation lies in the separation of periosteal and endosteal surfaces, creating a trabecular and cortical bone mask that guides later bone quantification steps.

Briefly, the periosteal boundary of the cortical bone was identified within the manually cropped region by applying a global threshold (3000 HU), followed by a median filter to blur trabecular bone details. A connectivity rules algorithm was then applied to remove Volkmann's canals that penetrate the cortical bone. This step was achieved using a dilation followed by an erosion step as a morphological closing operation. In the final step, a second median filter was applied to reduce noise (150). The endosteal boundary

was found using a second global threshold density value (5000 HU), isolating the marrow region, which was then dilated and eroded using the same connectivity rules above, followed by Gaussian smoothing and thresholding to reduce noise (150). The total bone area and trabecular area masks constructed in 3D were combined to create a cortical and trabecular bone mask.

Trabecular bone segmentation

Trabecular bone was segmented from marrow by applying a Laplacian Hamming filter to sharpen image features with a cut-off frequency of 0.4 and epsilon of 0.5. Greyscale voxels within the image were normalized using a norm function followed by a threshold-based segmentation step. In an effort to smooth the image and remove noise, clusters smaller than 25 voxels in area were removed (151).

Bone structure computation

Trabecular number is the only trabecular parameter that was directly computed from hr-pQCT images. The Euclidean distance between trabecular bone ridges was determined across the full 3D structure and the inverse of the mean of Euclidean diameters gave the Tb.N value (129). Bone volume fraction was calculated as the apparent trabecular mineral density within the trabecular mask described above, divided by 1200 mg HA/cm^3, assuming that all trabecular bone bear a mean density of 1200 mg HA/cm^3 (129). All other trabecular outcomes were derived from a combination of Tb.N and BV/TV.

Tb.Th = (BV/TV) / Tb.N (mm)

Equation 4. hr-pQCT Trabecular thickness (Tb.Th) (129).

Tb.Sp = (1 – BV/TV) / Tb.N (mm)

Equation 5. hr-pQCT Trabcular separation (Tb.Sp) (129).

Ct.Th = Mean cortical area / Periosteal circumference (mm)

Equation 6. hr-pQCT Cortical thickness (Ct.Th) (150).

3.5.2 pQCT analysis software

Density: Hounsfield unit calibration

Linear attenuation values for each pixel within pQCT images were converted to HA-equivalent densities using a linear equation specifically calibrated to each site's pQCT scanner. Hydroxyapatite density measurements were calibrated to water (equivalent to 60 mg HA/cm^3) resulting in fat HA equivalents of 0 mg HA/cm^3 (152). Since the European forearm phantom used to cross-calibrate scanners was originally calibrated to water with 0 mg HA/cm^3, all density values acquired on pQCT using this phantom appeared increased by 60 mg/cm^3. This is also true when measures of density are compared to hr-pQCT values since water for the hr-pQCT calibration was zeroed at 0 mg HA/cm^3.

Stratec v6.20c Trabecular density, iterative contour detection and concentric peeling

Image processing for bone macro-structural and densitometric outcomes was achieved using manufacturer software (Stratec, Version 6.20a) by cropping a region surrounding

the cortical shell. Several segmentation algorithms were applied to differentially examine trabecular and cortical features. To examine purely trabecular features, Contour mode 2 iterative contour detection with automatic thresholding, and Peel mode 1 concentric peel with fixed percentage, were applied to segment bone from soft tissue as guided by a threshold of 480 mg/cm^3, and to isolate a purely trabecular region, respectively (94). For the iterative contour detection algorithm, the software automatically scanned the image for a voxel that best represented cortical bone using a bone density distribution graph. This seed voxel when identified with a second neighbouring voxel satisfying this condition then followed an iterative contour algorithm that proceeded in a clockwise direction to identify nearest neighbour voxels, using an eight-voxel pattern to identify potential candidates for the next neighbour. This iteration was repeated until the start voxel was met, closing a path of minimum curvature defining the periosteal bone contour. A 3x3 median filter was applied to this contour to eliminate noise along the cortical bone boundary (134).

Next, out of the total bone area confined by this boundary, 45% of the pixels from the outer edge were discarded to result in a region that consisted purely of trabecular bone and marrow. These discarded pixels represent cortical bone, an intermediate region containing trabecularized cortical bone, and a small medullary area containing trabecular bone. This assumption was shown to function optimally when the trabecular region was more regularly shaped (94). Since some of the truly trabecular region was also removed in this procedure, only trabecular bone density was computed from this mask.

Stratec v6.20c Cortical density, global thresholding

To compute cortical bone density, a global threshold of 710 mg/cm^3 was applied to the image using CortMode 1, removing all pixels below this value. This value was recommended by the manufacturer as it distinguishes between pixels that are completely filled by cortical bone from those partially filled by trabecular bone or soft tissue, two cases that would otherwise underestimate the true cortical density (153).

It was recommended previously that areal and density measurements cannot be concurrently obtained accurately using the same thresholds (Personal communication by Johannes Willnecker, Stratec Medizinteknik). In effect, areal and structural measures were computed using a separate software package as follows.

pQCT OsteoQ trabecular bone segmentation, region-growing algorithm

The pQCT OsteoQ Software (**Inglis Software Solutions Inc.**) employed a region-growing algorithm beginning with a seed equal to the highest linear attenuation value within cortical bone that was then expanded to one of eight nearest neighbour voxels. The lower bounds of the grown region was guided by a density value equal to two SDs above the mean soft-tissue signal computed from a minimum of 15 images within the image set examined (for wrist images: 187.95-189.62 mg/cc; for ankle images: 206.07-209.22 mg/cm^3) (154). Voxels located outside of the cortical bone were trimmed, and islands of unconnected bone were filled within the region. Bone regions were then binarized from non-bone by first applying a voxel-intensity histogram equalization procedure to increase

the contrast in bone signal dynamic range, followed by a high-pass spatial Laplacian (3x3 kernel) filter and a global threshold, derived using the Otsu (t) method from the bimodal histogram of the resultant image, to resharpen blurred voxels of bone (154). For connectivity measurements of the trabecular bone, binarized bone images were further skeletonized using the parallel thinning algorithm reported by Zhang and Suen (155).

Bone structure computation

Volumetric bone mineral density (vBMD) measurements for cortical and trabecular bone was obtained from Stratec software, which uses Equation 7:

$$\text{vBMD} = \sum_{i=1}^{n} \frac{BMC_i}{voxelvolume_i} \qquad (\text{mg/cm}^3)$$

Equation 7. pQCT volumetric bone mineral density (vBMD) (153)

where i represents each voxel within the volume of bone up to the total number of voxels, n. Bone structural outcomes were computed using binarized images achieved using the pQCT OsteoQ software.

Marrow hole geometry

For inter-trabecular spaces, the notion of marrow hole geometry was represented by growing the largest circle that could fit between trabeculae. For each voxel labelled as marrow, a region growing algorithm was used to expand the voxel seed following the eight-voxel neighbours method until a trabecular bone boundary was reached. This

procedure was repeated until all marrow-labelled voxels were assigned to a hole. The total number of holes to which individual marrow-voxels belonged was termed the hole number H_n; the mean of the area of each hole was termed mean (average (A)) hole size H_A; and the hole with the largest area was termed maximum (M) hole size H_M (154).

Connectivity

Compston and colleagues' Strut analysis (156) was applied to skeletonized images following the assumption that one-dimensional lines or "Struts" represented trabecular bone networks. The intersection among three struts formed a node (Nd). The end of a strut that was not connected to another network of struts was termed a free end (FE). An isolated point (Ip) was assumed to represent a strut that was run in the axial direction. Network length (NL), was therefore taken to represent the mean length of all interconnected struts. Ideally, a well-connected bone should contain a high number of Nd and few FE and Ip. The connectivity index (Cx) represented this notion, scaled by mean network length:

$$\mathrm{Cx} = \frac{Nd - FE - Ip}{NL} \times 100\%$$

Equation 8. pQCT connectivity index (Cx) (154)

Trabecular bone geometry

Binarized bone masks obtained from the pQCT OsteoQ software were used in the calculation of trabecular bone geometry. Their computation respected the natural

structural behaviour of trabecular bone by adhering to Parfitt's model of parallel plates. According to Parfitt, trabecular bone appears primarily as a network of interconnected plates (118). In the calculation of various trabecular bone geometric properties, it was assumed that: 1) bone tissue was isotropic, 2) each region of interest examined represented a randomly selected sample of uniform bone, and 3) trabeculae are parallel to one another. Parfitt emphasized the distinction between the thickness of trabecular plates (Tb.Th) and the density of trabecular plates, or number of trabeculae intersected per unit mm (Tb.N). Because trabeculae are formed from endochondral ossification from birth, it is not possible to create new trabeculae after epiphyseal fusion unless pathological formation of woven bone ensues. This observation implies that Tb.N should not increase. However, individual trabeculae can increase or decrease in thickness (118). Trabecular computations based on these model assumptions were validated against direct measurements of iliac crest trabecular bone quantified histomorphometrically using a Zeiss MOP 3 digitizing system (157). Equation 9 to Equation 13 represent trabecular bone features that were derived from three primarily two-dimensional quantities of the bone's stereology: the total perimeter length along the contour of bone (P_B); the total bone area (A_B); and the total area of the mask including bone and marrow (A_T).

$$BV/TV = A_B / A_T$$

Equation 9. pQCT Bone volume fraction (BV/TV) (118)

$BS/TV = P_B / A_T$

Equation 10. pQCT Bone surface fraction (BS/TV) (118)

$Tb.Th = 2\ A_B / P_B$ (mm)

Equation 11. pQCT Mean trabecular thickness (Tb.Th) (118)

Where 2 was a value experimentally determined.

Tb.Th in Equation 11 represented an indirect method of quantifying trabecular plate thickness that correlated well with and generated values that were not significantly different from direct measurement using histomorphometry (158). However, a disadvantage of this indirect estimation is that the variance in Tb.Th across the sample (Tb.Th SD) remains unknown.

$Tb.N = BV/TV / Tb.Th$ (#/mm)

Equation 12. pQCT Trabecular plate density, mean trabecular number (Tb.N) (118)

Similar to the way hr-pQCT computed Tb.N as the inverse of Euclidean distance means between trabecular bone ridges, Tb.N can be computed here by the original measurements, as: $Tb.N = P_B / 2A_T$.

$Tb.Sp = 1/Tb.N – Tb.Th$ (mm)

Equation 13. pQCT Mean trabecular separation (Tb.Sp) (118)

3.5.3 1.0T pMRI analysis with MRI OsteoQ software

Since MRI voxels cannot be calibrated to density equivalent units, densitometric measures are not typically reported. In addition, since cortical bone was subject to chemical shift artifact and magnetic susceptibility differences from surrounding tissue, causing geometric distortion, cortical bone measures were not computed here.

Trabecular region mask, endocortical envelope segmentation

In the MRI OsteoQ software, the region within the endocortical envelope in each axial slice was segmented from the cortical bone and surrounding tissue first using a semi-automated image foresting transform algorithm described previously by Falcao et al (117,159). This technique employed a path-cost-minimizing function that relied on colour, gradient and pixel relative position for separating the trabecular and marrow region from the cortical bone and surrounding tissues. In contrast to the region-growing algorithm employed in pQCT structural analyses, a seed was manually identified within the trabecular network and outside of the network to represent signal and noise, respectively.

Trabecular bone segmentation from marrow

To segment trabecular bone from marrow, the same image foresting transform was applied in a multi-scale dimension by combining information from three annotated images: 1) contour label images describe information about the number of bone-tissue boundaries; 2) pixel label images provide data on which pixels form the basis of each contour; and 3) Euclidean distance maps give information on the square distance away from the seed. The pixel and contour images were processed to analyze label transitions,

generating a difference image that was thresholded and applied to Euclidean distance maps. A trabecular bone binary image resulted from these series of steps, that enabled calculation of trabecular apparent microstructure (Tb.Sp, Tb.Sp SD, BV/TV, Tb.N, Tb.Th) connectivity (Nd, FE, Ip, NL, Cx) and hole geometry (H_A and H_M).

Bone structure computation

Marrow hole geometry, bone connectivity and trabecular bone geometry were computed using the trabecular bone binary image mask. The same computation equations from pQCT were used to derive all bone structural measures (See Section 3.5.2 pQCT Bone structure computation) in the MRI OsteoQ software.

3.5.4 Bone structural outcomes - overview

Although a large list of bone structural variables can be computed from all three imaging modalities, several have been identified previously to have demonstrated clinical relevance (98,139,160) and were supported by some reliability data (139,161). In the present study, focus was placed on Tb.Sp, BV/TV, Tb.N and Tb.Th since these variables can be computed on all modalities. In addition, Ct.Th and vBMD (integral, cortical and trabecular) were examined for the two QCT modalities and Cx was examined for pQCT and MRI. Cx was not computed from the manufacturer software for hr-pQCT. Parfitt's model-derived Tb.Sp and Tb.Th (computed using the pQCT equations) and model-independent versions of these (computed using the hr-pQCT equations) were examined for MRI and pQCT for ease of comparability to measures generated from hr-pQCT images.

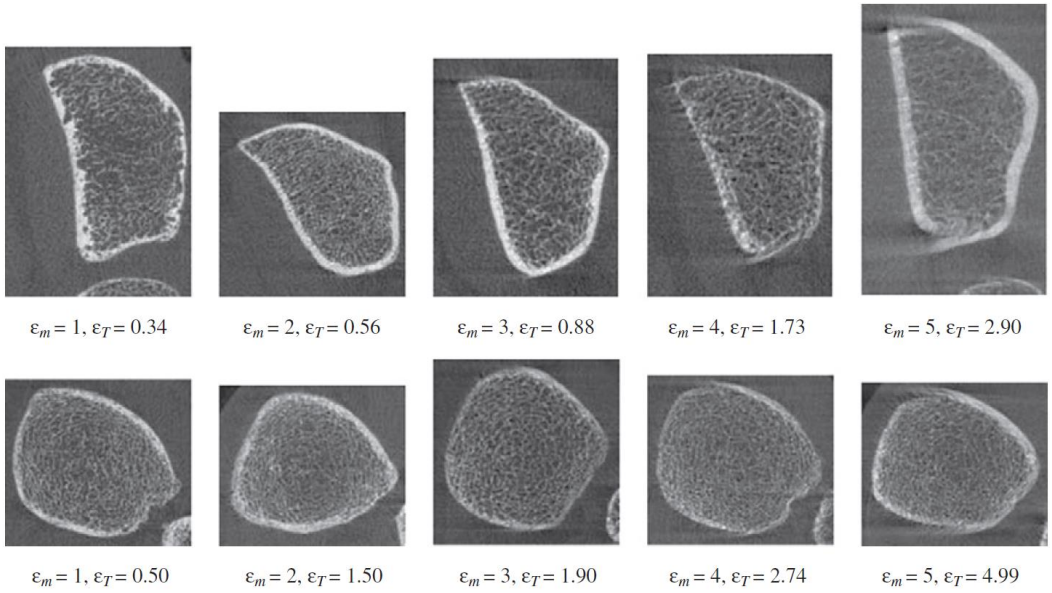

Figure 5. Motion artifact atlas for hr-pQCT scans of the radius and tibia.
Motion grades (ε_m) 1 through 5 (left to right) for radius (top) and tibia (bottom) were characterized by the degree of streaking and cortical bone discontinuity. Image reprinted with permission from Bone, Vol. 50, Y. Pauchard et al, Quality control for bone quality parameters affected by subject motion in high-resolution peripheral quantitative computed tomography, pp. 1304-1310. (162).

3.6 Bone structure image diagnostics

3.6.1 Image quality and motion assessment

Hr-pQCT motion atlas

Motion artifact on hr-pQCT scans was qualitatively assessed after reconstruction of images by the manufacturer software. Motion was graded on a scale of 1 to 5 with 1 representing the absence of motion artefact, through criteria that were recommended by the manufacturer (163). The evaluation of adequate quality remains subjective and a defined threshold for requiring repeat scanning is not currently recognized in the literature. However, Pauchard and colleagues from multiple study centres (Vancouver, Toronto and Calgary) rejected images with qualitative motion grades > 3 (163).

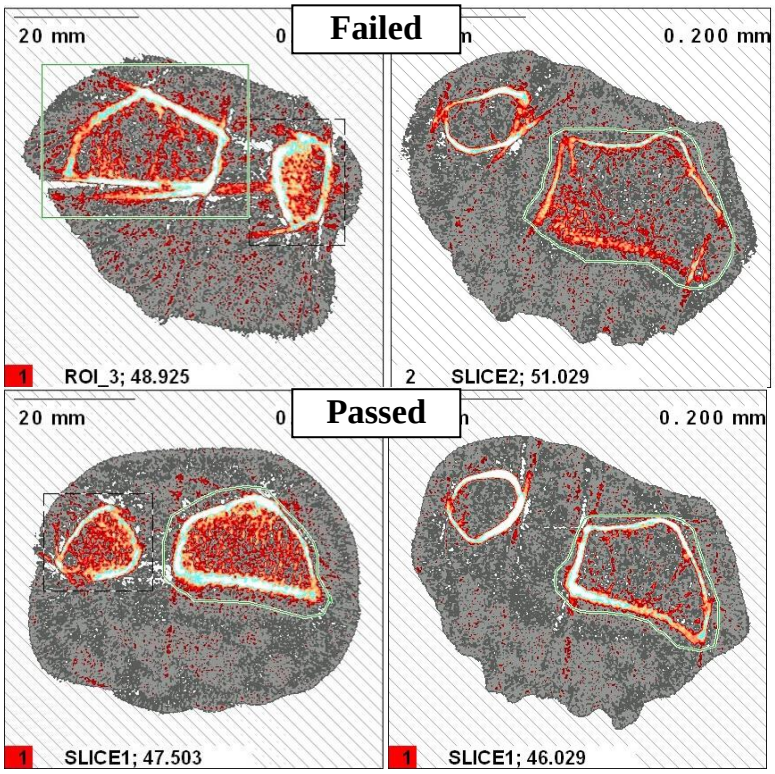

Figure 6. Assessing need for repetition based on motion on pQCT images.
Top: Images of radius that were rejected and required scan repetition due to breaks in cortical shell and significant streaking. Bottom: Two images that did not require repetition as breaks in the cortical bone were not present despite minor streaking.

In the local study, motion graded from the single hr-pQCT scanner was described by an atlas of hr-pQCT images. Examples of motion grades 1 through 5 are represented in Figure 5. In motion grade 1, neither motion streaks nor discontinuities in the cortical bone were present. In grade 2, only a small degree of streaking was observable. In grade 3, a moderate to large degree of streaking was notable. In grade 4 moderate to large streaks were visible and small breaks in the cortical bone were observed. Grade 5 similarly included images with moderate to large streaks but also had moderate to large discontinuities in the cortical shell (162).

In both local and national studies, a motion grade of 3 or below was considered acceptable and did not require repeated scanning. For those who were scanned a maximum of three times without any improvement in motion grades, the final scan was marked for exclusion from analyses. For all hr-QCT analyses, final scans that did not require any further repetition were analyzed for volumetric bone outcomes.

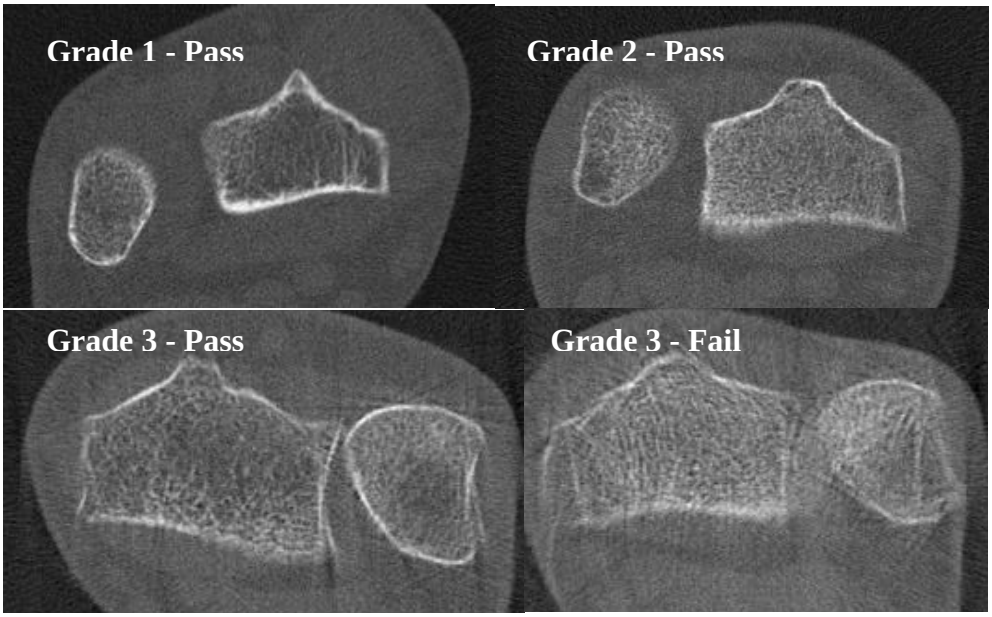

Figure 7. Motion artifact atlas for pQCT scans of the radius.
Motion grade 1 (top left), 2 (top right) and 3 (bottom row) were assessed semi-quantitatively based on the degree of streak formation and cortical bone discontinuity. Analysis was rejected for bottom right image due to obscured trabecular bone boundaries.

pQCT motion atlas

Rather than deciding on repetition based on an ordinal scale of 1 to 5, pQCT image quality check was represented as a binary grading of pass or fail. In general, any image with a notable discontinuity in the cortical bone was considered to have failed quality checks. This assessment is consistent with failing grades 4 and 5 in the motion grading

protocol for hr-pQCT. Images with significant streaking tangential to the cortical bone were also notable in images that did not bear any discontinuities in the cortical bone. In such cases, scans were not repeated (Figure 6).

For pQCT analyses, all final scans that did not require additional repetition were analyzed for bone density and macrostructural outcomes. However, due to the stringent demands for a superior SNR and contrast-to-noise ratio (CNR), separate rules for image quality guided bone apparent microstructural outcome computation. A semi-quantitative scale of 1-3 for motion artifact combined with a binary grade for overall image quality guided inclusion of images for analyses (Figure 7). Motion grade 3 represented images with definite artifacts present including discontinuities in cortical shell and streaking. Motion grade 2 indicated images displaying minor motion artifacts including streaking or blurring of the cortical shell but that did not involve discontinuous cortical bone boundaries. A motion grade of 1 represented an image that was void of streaking and cortical discontinuities. Motion grades 1 and 2 were all analyzable. Motion grade 3 images were further judged to pass or fail analysis based on the degree of disruption of trabecular bone within the endocortical envelope. A failed motion grade of 3 involved trabecular bone that was blurred or shifted. Overall image quality was graded as acceptable (1) or poor quality (0). This second quality assessment measure enabled the data analyst to identify potential outliers and suggest reasons for outlying data points despite an analyzable image with a motion grade of 2 or lower.

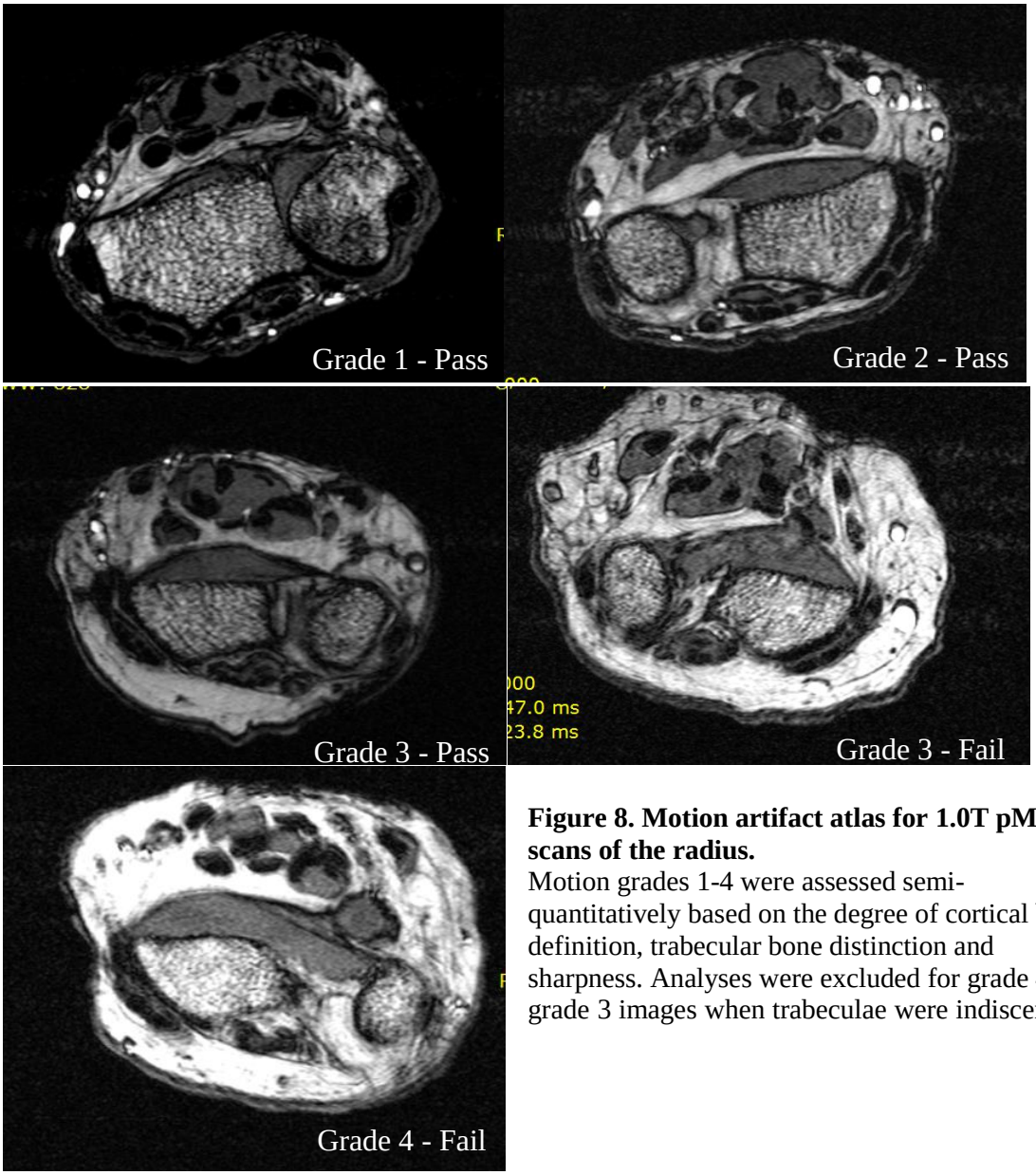

Figure 8. Motion artifact atlas for 1.0T pMRI scans of the radius.
Motion grades 1-4 were assessed semi-quantitatively based on the degree of cortical bone definition, trabecular bone distinction and sharpness. Analyses were excluded for grade 4 and grade 3 images when trabeculae were indiscernible.

1.0T pMRI motion atlas

There has been a lack of consensus on a recommended motion assessment method for MRI bone structure scans. One report of motion quantification and correction highlighted the use of the normalized gradient squared (NGS) metric, a statistical tool that quantifies

the degree of sharpness of an image (164). In this investigation, an artificially induced rotational motion applied to k-space was correlated with a decrease in NGS, indicative of poorer image sharpness in high-resolution MR images of trabecular bone. In addition, progressively increased motion reduced the difference in mean trabecular outcomes between younger and older age cohorts (164). The 1.0T pMRI system was not designed to enable extraction of k-space data. Consequently, NGS cannot be applied to quantify the sharpness metric in an effort to quantify motion artifact.

Similar to pQCT, a semi-quantitative scale of 1-4 for motion artifact and a binary grade for overall image quality guided inclusion of images for apparent microstructural analyses for pMRI (Figure 8). Grade 4 motion exhibited significant ghost image artifact, radius shape deformation or streaking around the cortical bone border concomitant to loss of trabecular details. All grade 4 motion images were noted to have failed quality assurance. Grade 3 motion showed noticeable blurring around the cortical bone edges at least on one side of the radius. Among grade 3 images, those that passed quality assurance checks maintain sufficient textural pattern in the trabeculae while failed images lacked discernible trabecular details. Grade 2 images show an intact cortical bone with sufficient trabecular details but lack sharpness. Grade 1 images are the most ideal images for analysis, with an intact cortical bone boundary and clear separation between marrow and trabecular bone, including a high degree of image sharpness.

3.6.2 Co-registration of multi-slice images

hr-pQCT automated co-registration and matching

Common volumes of interest in hr-pQCT images were automatically matched between baseline and follow-up acquisitions by assessing the percentage similarity in two-dimensional periosteal cross-sectional areas (165,166). This method has a limitation in failing to acknowledge the possibility of periosteal expansion resulting in longitudinal changes in area at the same region of interest. In addition, consideration of only the matched regions, which could be more proximally or distally situated for different individuals, would result in variation in the absolute region examined in the cohort. This limitation is precipitated by the fact that small shifts in region (± 0.5 mm) along the radius or tibia could result in significantly different volumetric bone outcomes of up to 6% (167).

pMRI manual co-registration of baseline-follow-up and test-retest images

Manual co-registration for test-retest pMR images was achieved using an open source software package, 3DSlicer (v4.2.1). The baseline/first image was set as the fixed image set and the follow-up/repeated image was set to be transformed. Each image was coloured in a contrasting colour scheme (ie. Inverted grey (bone = white; marrow: black) for baseline/first images, and iron (bone marrow = red; trabecular bone: yellow) for follow-up/repeated images). A visually-guided threshold was applied to the follow-up and repeated images such that the cortical bone was removed, and became transparent. Overlaid images generated an additive colour mixture that represented overlapped regions (maroon = marrow-marrow overlap; pink = non-overlapping marrow; bright yellow =

non-overlapping trabecular bone) when the follow-up/repeated image was set at 40% transparency. A successfully co-registered image provided a clear maroon coloured trabecular area with no pink borders, surrounded by a white cortical shell.

Rigid transformation involved medio-lateral, postero-anterior and proximal-distal axial translations as well as rotations within the axial image planes. No oblique rotations were performed to image sets to prevent multi-planar reformatting, which would result in inaccurate slice identification and reduced resolution. Matrix inversion was performed when images were flipped. Successful co-registration was decided by visually inspecting the degree of alignment in the endocortical perimeter for each slice.

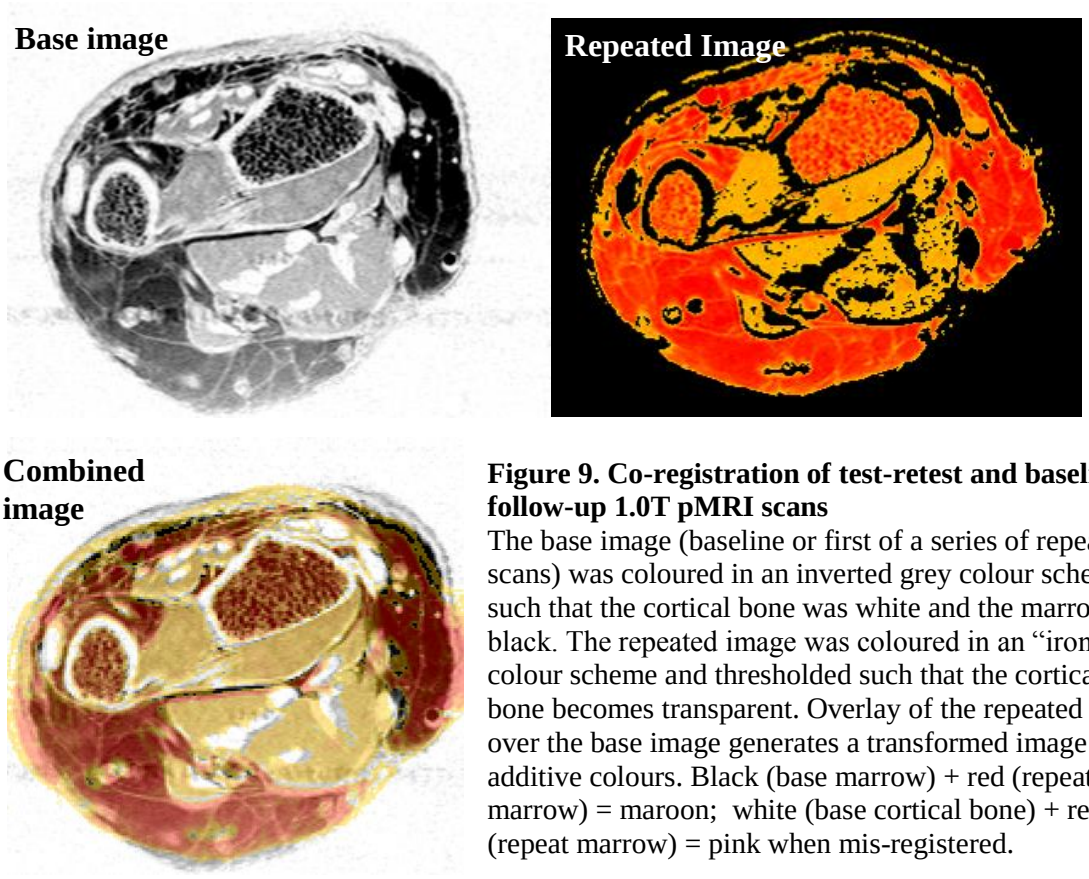

Figure 9. Co-registration of test-retest and baseline-follow-up 1.0T pMRI scans
The base image (baseline or first of a series of repeated scans) was coloured in an inverted grey colour scheme such that the cortical bone was white and the marrow black. The repeated image was coloured in an "iron" colour scheme and thresholded such that the cortical bone becomes transparent. Overlay of the repeated image over the base image generates a transformed image with additive colours. Black (base marrow) + red (repeat marrow) = maroon; white (base cortical bone) + red (repeat marrow) = pink when mis-registered.

Slices from one image set shown to align with the other set were identified for each participant's paired images. After identifying matching slices, a summary of matching slice numbers was compiled. Only the commonly matched slices across all participant images were used in the final computation of co-registered-volumetric bone outcomes. This procedure ensured that the region of interest examined in all study participants was the same. The means of volumetric bone outcomes obtained across all common slices were used in post-hoc analyses of objectives 2 and 3.

pMRI-hr-pQCT image co-registration

Co-registration of pMR images with hr-pQCT was similarly performed to identify the region of the radius on hr-pQCT images along which pMR images were matched. This cross-modality co-registration followed similar procedures as described for pMRI-pMRI co-registration. The pMR images were set as the fixed image set displayed in grey scale and the hr-pQCT as the transformed image set displayed in an iron colour scheme (Figure 10). Correct registration was decided on how well the yellow endocortical perimeter on hr-pQCT covered the black cortex on MRI. Because slice thickness was different between the two imaging modalities, a single slice on pMRI was matched to as many as 13 slices on hr-pQCT. Each pMRI slice therefore represented the collapsed volume summation of these slices identified on hr-pQCT. Only pMR image slices that were co-registered with hr-pQCT slices were included in pMRI-hr-pQCT validation analyses (Objective 1).

Since individual slice bone outcome computation cannot be achieved on hr-pQCT using manufacturer software, co-registration between pQCT and hr-pQCT was not performed.

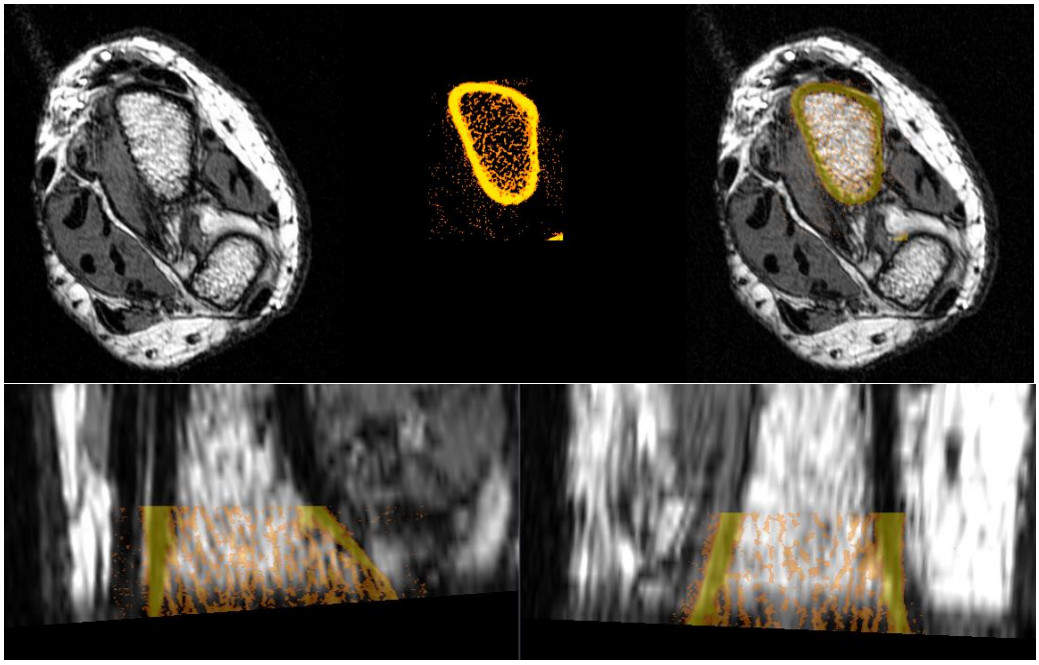

Figure 10. Co-registration of 1.0T pMRI with hr-pQCT scans
The base image was the pMRI scan, remaining in greyscale (top left). The hr-pQCT image set was coloured in an "iron" scheme and transparency set at 40% (top middle). Successful co-registrations showed endocortical boundary of the radius from both modalities aligning (top right). Cortical bone from sagittal and coronal views (bottom) was also used as guides for correct matching.

Co-registration challenges

Within-slice variation in matching

Multi-slice co-registration of inter-modality image sets with varying slice thickness and slice spacing is challenged by the fact that single slices on a thicker image set correspond to multiple slices on a thinner image set. This challenge is further complicated by the fact that angulation of one image set relative to the other results in the possibility that one slice on the thinner image set may also correspond with multiple slices on the thicker image set depending on the two-dimensional coordinate within the image slice. To overcome these challenges, a cursor was swept across each slice of the thicker image set

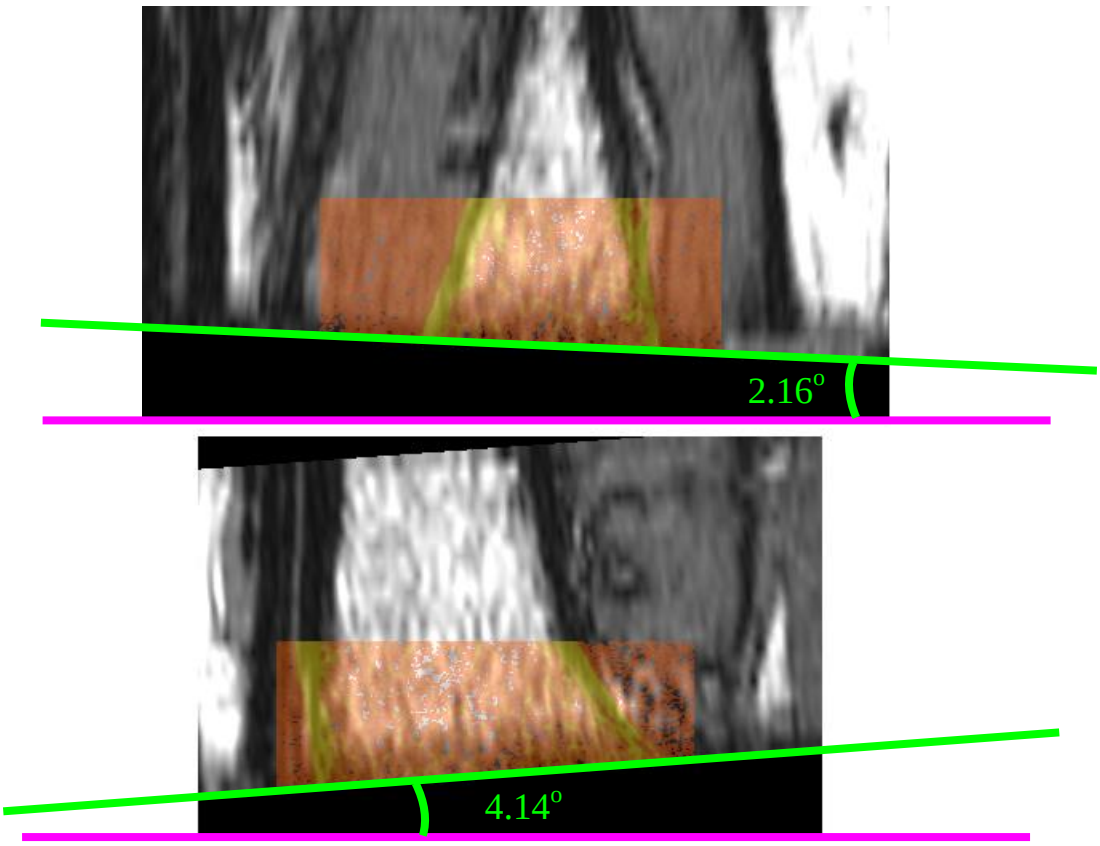

Figure 11. Axial angular deviation between pMRI and hr-pQCT image sets
The last slice location was identified and a screen shot was obtained. The angle subtended by the edge of the pMRI dataset (green) and the edge of the hr-pQCT dataset (pink) was quantified.

(pMRI) and each slice of the thinner image set (hr-pQCT) to record the slice number of the corresponding image set. The result was two lists of matching slice numbers that were then combined to provide the boundaries of the region of interest quantified.

Angulation between CT and MR image sets

It should be noted that the definition of axial imaging performed on each modality affected the ability to co-register CT and MR image sets. On hr-pQCT, imaging was performed in a transaxial orientation relative to the gantry (**Section 3.4.1**). Hence, if the

anatomy was angled when inserted into the gantry of the scanner, image slices would not be oriented perpendicular to the long-axis of the bone. Conversely, on pMRI, transaxial slices were obtained perpendicular to the long-axis of the radius as manually achievable by placing oblique slice selection widgets on scout views (**Section 3.4.3**). There was, therefore, an expected random angulation error between the actual imaged axis on hr-pQCT versus on pMRI. To measure the angulation error, the end slices of the already co-registered image sets were examined. At this slice location, a contrasting edge between the end of the slices of one image set forms an angle with the edge of the transaxial slice of the co-registered image set (Figure 11). An image capture of this geometry was obtained, and the angle quantified from both coronal and sagittal views using PixelStick (Plum Amazing, LLC).

3.7 National study streamlining

3.7.1 Overview of study logistics

An effort to streamline study imaging procedures was made due to existing inter-site differences in the way technicians prepare participants and complete pQCT and hr-pQCT scans. In addition, bone image and data transfers were standardized to enable comparison and data merge. Data quality assurance was implemented to ensure consistency of data variable structures and adherence to study protocols across all study centres. Because 1.0T pMRI modalities were not available at the other sites within the national study, only local Hamilton data were included as part of the pMRI bone outcome reference dataset.

3.7.2 Consensus on imaging parameters

pQCT differences in integration time (scan speed)

The rotation of X-ray source around the gantry at a slower speed results in a longer integration time, over which image data could be back-projected to produce an image with a higher SNR and CNR. Scans (330 μm in-plane resolution) completed on pQCT have been used previously to obtain marrow hole geometry, densitometric outcomes and macrostructural variables, at a scan speed of 15 mm/s (128,168). Although one previous study used a scan speed of 10 mm/s, bone apparent microstructural outcomes were not computed (169). Images obtained using the 10 mm/s scan speed have not been employed for apparent bone microstructural outcome computation thus far. By benefiting from a higher SNR and CNR, trabecular bone could be more accurately segmented with this slower scan speed. To demonstrate and ascertain this theory, a pilot scan of the wrist of a single volunteer was obtained to calculate the SNR and CNR of images obtained using 10

mm/s versus at 15 mm/s with all other imaging parameters kept constant. The SNR of each image was obtained by: mean bone signal / SD of noise. The CNR of each image was obtained by: (mean of bone – mean of soft tissue) / SD of noise.

Given a sizeable 17-25% increase in SNR and 18-26% increase in CNR from 15 mm/s to 10 mm/s scan speed (Table I), it was decided that all study centres would implement the 10 mm/s scan speed to obtain more accurate trabecular apparent bone microstructural outcomes. This implementation incurred a penalty of increased scan time from 3 to 5 minutes. Although it could be argued that additional motion incurred during the extra two minutes could contribute to worsened image quality, the fact that two image slices were obtained means at least that the first slice could benefit from a lower probability of motion.

Data analyses took into consideration the potential image quality differences between slice 1 and slice 2 of all pQCT images. Where analyses were verbose, only results for slice 1 (more distal slice) were displayed.

Table I. Comparison of SNR and CNR between faster and slower CT scan speeds.
The same volunteer obtained 4% ultradistal radius scans using a faster (15 mm/s) and slower (10 mm/s) CT scan speed.

		Slice1 (cm^{-1})				**Slice 2 (cm^{-1})**			
Scan Speed		**Mean**	**SD**	**SNR**	**CNR**	**Mean**	**SD**	**SNR**	**CNR**
10 mm/s	Noise	0.16	23.52			0.10	24.19		
	Bone	867.82	54.50	**36.90**	**27.25**	929.74	56.70	**38.43**	**28.95**
15 mm/s	Noise	0.11	28.26			0.10	27.43		
	Bone	837.15	78.92	**29.62**	**21.66**	899.07	74.00	**32.78**	**24.43**

pQCT & hr-pQCT differences in region of interest selection

As mentioned in section 3.4.2 on reference line placement for pQCT, the national protocol employed the 4% ultradistal radius and tibia region of interest rather than a fixed distance reference. The average discrepancy between the 4% site and the 9.5 mm site consequently became an issue of discussion. Depending on limb length, the 4% site could identify a different region of interest. As shown previously by Sun and colleagues (170), even a half millimetre shift in region of interest in the proximal direction could lead to significant decreases in trabecular bone density (-0.97 ± 0.55 mg/cm^3) and cross-sectional area (-21.17 ± 2.60 mm^2). A pilot study was performed to examine the difference between the 9.5 mm distance reference and the actual distance of the 4% ultradistal radius for a group of individuals. The same was repeated for the difference between 22.5 mm and the 4% ultradistal tibia.

The length of the radius and tibia were measured on 15 volunteers, following the limb length measurement procedures described in section 3.4.2 under limb positioning and fixation. A value equal to 4% of the radius and tibia lengths were compared to a fixed 9.5 mm and 22.5 mm distance value, respectively, using a one-sample, two-sided Student's T-test.

3.7.3 Between study centre and between scanner calibration

Phantom calibration

A European forearm phantom (EFP) consisting of four blocks of hydroxyapatite-mimicking material in decreasing diameters and density (Figure 12) was used to calibrate

both hr-pQCT and pQCT scanners across all study centres (171). This phantom was shown to be superior to an aluminum-based phantom, which was unable to predict density drifts in densitometers over time (172). Using this phantom, pQCT was shown to display the least amount of density drift from a previous study of 6.4 years in duration (172). Each block of the EFP was scanned three times on each pQCT and hr-pQCT scanner in the national study on a single occasion to obtain a total of 12 measurements on each modality. All phantom outcomes obtained from each study centre's pQCT or hr-pQCT were compared to a single pQCT scanner in Hamilton and to a single hr-pQCT scanner in Toronto. Linear regression analysis generated slopes and intercepts including 95% confidence intervals that were used to guide future calibration of bone density values across scanners.

Human calibration

Because the EFP does not provide microstructural outcomes, and a bone structural phantom was not available (only in design and production phase at the time of analyses), a single volunteer (AKOW) completed a standard pQCT and hr-pQCT scan twice with repositioning in between, on left and right ultradistal radius and tibia locations. The standard hr-pQCT and pQCT protocols indicated in the National components of sections 3.4.1 and 3.4.2, respectively were followed. Bone structural outcomes were computed as per the respective protocols in sections 3.5.1 and 3.5.2 and outcomes were compared across study centres using a linear regression analysis, reporting slope, intercepts and 95% confidence intervals. All scans were completed within one year. It was assumed that bone

structure and density in the single healthy volunteer (male, age: 27 years, BMI: 21.3 kg/m^2) did not significantly vary within a single year.

pQCT models XCT2000 and XCT3000 comparison

Except for the Vancouver site (XCT3000), all other study centres employed the XCT2000 model of pQCT. Bone density and bone structural measures obtained from the series of 12 phantom scans and the 8-slice human scan were compared between the XCT2000 and XCT3000 (both in Vancouver at the time of study) using a Bonferroni-corrected paired samples Student's t-test to ensure measurements were not significantly different. In addition, cross-calibration equations for structural and densitometric outcomes generated from linear regression analyses were used to adjust bone outcomes obtained on the XCT3000 model, should there be any sizeable differences between the models.

3.7.4 Technician test-retest precision

To ensure technicians for all scanners were interpreting and following the national study protocol correctly, a test-retest precision test was performed at each study centre on each of pQCT and hr-pQCT using a group of at least 7 study volunteers. Participants were imaged twice on the non-dominant ultradistal radius according to the standard national protocols on either or both scanners, where available, with complete removal and repositioning in between scans. Integral, trabecular and cortical vBMD were used as the primary guides for assessing adequacy of training.

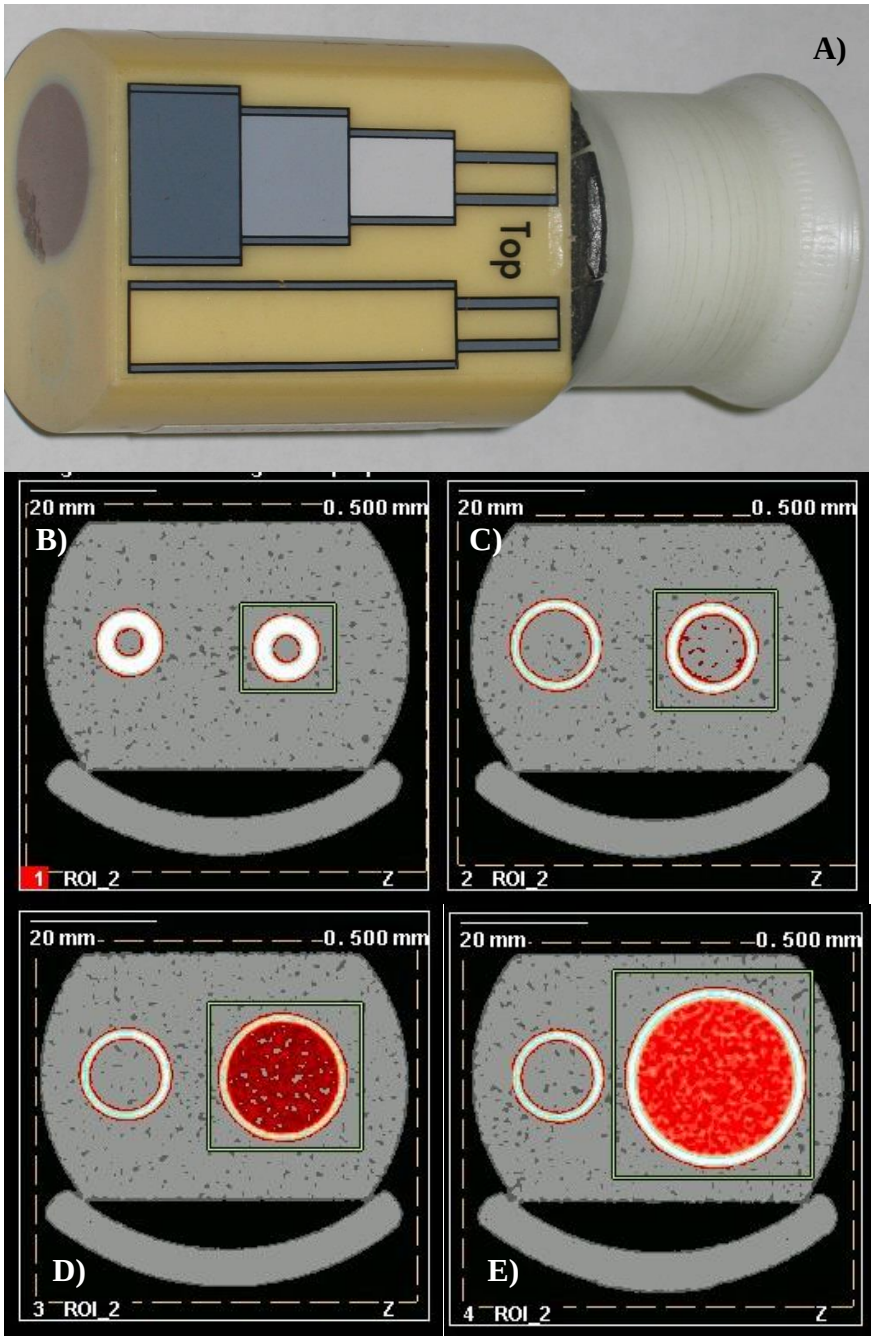

Figure 12. European Forearm Phantom.
Top (A): Phantom used for calibration of all pQCT scanners upon installation; and used for cross-calibration of pQCT and hr-pQCT scanners across study centres. Bottom: Phantom geometry, density and orientation of four sections (B-E) with respect to flanking mock ulna (left).

4 Data analyses

All data collected from the study were processed using Statistical Analysis Software (SAS v9.2 / 9.3, SAS Institute Inc, Cary, NC, USA). Data were cleaned by verifying variable length and content, with rules applied to applicable variables to ensure erroneous values were not incorrectly entered. All analyses were completed by a single investigator (AKOW) who was not blind to study participant data or images.

4.1 Descriptive statistics and diagnostics (Specific aim #4)

4.1.1 Measures of normality, distribution and central tendency

Volumetric bone outcome variables (continuous variables) computed from images obtained using each modality were statistically assessed for the degree of normality in their distributions. A Kolmogorov-Smirnov goodness-of-fit test, suitable for continuous outcomes, was executed to determine the probability that the variable belonged to a Gaussian distribution. All variables that violated the assumption of normality ($p < 0.05$) were considered for use in non-parametric statistical procedures. To further quantify the degree of deviation from normality, data distributions were described by skewness and kurtotic measures. Absolute values of highly skewed data were expected to deviate from 0. Large sample kurtosis values were indicative of data heavily weighted in the tails of non-normal distributions.

For all normal continuous variables, mean, standard deviation (SD), minimum and maximum values were reported. For continuous variables that violated the assumption of normality, median, Q1-Q3 interquartile range (IQR), minimum and maximum values

were reported. For binary or nominal outcomes, frequency and percentage values were reported. To address specific aim #4, for all volumetric bone outcomes on each modality, means were separated according to age group by half decade and according to those with and without a history of fragility fractures within the last 15 years, or on antiresorptives.

4.1.2 Identifying potential outliers

The classical method of using 1.96 or 2.00 times the SD from the mean as a threshold for identifying outliers is sensitive to far-outlying data. Consequently, Tukey's method of thresholding outliers using 1.5 times the IQR above and below the 75^{th} and 25^{th} percentiles, respectively, was employed. Since it is resistant to outlying data, Tukey's method was appropriate for application to non-parametric data as well as normally-distributed data. All suspicious variables were ascertained by cross-verifying the values against case report forms, imaging console database, image header information and/or images. If no notable characteristics were able to explain the occurrence of the outlier, the data point was included in the analyses. Otherwise, the data point was corrected in the case of erroneous entries or removed in the case of poor image quality or where values were not physiologically plausible.

4.2 Validation – linear regression and ICC (Specific aim #1)

4.2.1 Statistical reporting

To address the objective of validating bone structural outcomes obtained from 1.0T pMRI and pQCT against hr-pQCT as a reference, a linear regression model was fitted to each pair of imaging modalities' volumetric bone data collected from the during the same year

and on the same set of study participants. The Pearson correlation coefficients (r) were reported for parametric bone variables. Spearman rho's were reported for non-parametric bone outcomes. In either case, the slope and intercept from linear regression was reported along with 95% confidence intervals, as per the ISCD guidelines for slope-intercept calibration (173). Because body size was previously shown to affect intra-modality test-retest precision of bone density values on DXA (174), BMI was further explored as a covariate in linear regression analyses. Since linear regression models address systematic error between the variable pairs but do not inform on the degree of agreement between techniques, a type (2,1) intraclass correlation coefficient (ICC) was reported along with 95% confidence interval. The type (2,1)-ICC considered the proportion (ρ) of total error (between-modality target error (σ_T), within-modality error (σ_M) + measurement error (σ_E)) that is explained by the between-modality target error (σ_T) (Equation 14):

$$\rho = \sigma_T^2 / (\sigma_T^2 + \sigma_M^2 + \sigma_E^2)$$

Equation 14. Type (2,1) Intraclass correlation coefficient (175)

To better visualize conditions whereby validity may be poorer, Bland-Altman analyses were performed by plotting the mean of the two corresponding bone measure obtained from each modality against the difference of the same measure between the modalities. Linear regression models were fit to inter-modality mean values versus inter-modality difference values. Limits of agreement (LOA) for 95% CI were also reported.

4.2.2 Sample size / power calculation

Sample size for objective 1 was computed based on the highest priority statistical procedure, linear regression, which provided calibration slopes and intercepts.

The ISCD guidelines suggest the use of 30 degrees of freedom for determining the LSC within a modality. However, this is based on the random error of DXA measurements of aBMD (173). Sample size requirements for linear cross-calibration were assessed based on several studies. Kazakia and colleagues determined the correlations between 3.0T MRI and hr-pQCT Ct.Th and Tb.Sp of 0.59 and 0.54, respectively at the distal radius (n=46) (131). Similarly, Krug et al demonstrated correlations between 3.0T MRI and hr-pQCT for app. BV/TV (r=0.65), app. Tb.N (r=0.95), app. Tb.Sp (r=0.83) and app.Tb.Th (r=0.63) in a sample of 11 participants' distal radii (176). However, values derived from MRI were significantly different from hr-pQCT, except in the case of app. Tb.N. Correlations for volumetric bone outcomes between pQCT and hr-pQCT were not available in literature. Based on the above effect sizes for correlation analyses, a desired power of 0.80, at 0.05 significance level, an expected correlation coefficient of 0.80 able to explain 64% of the variance in bone structure outcomes from one modality to another, and a 95% confidence interval of 0.20, a sample size of 51 was obtained, with a primary focus on correlations of Tb.Sp between hr-pQCT and each of 1.0T pMRI and pQCT.

4.3 Reliability – RMSCV, RMSSD, Bland-Altman (Specific aim #2)

4.3.1 Statistical reporting

For the goal of quantifying the degree of short-term and long-term precision of bone structural outcomes obtained within each imaging modality, the absolute deviation between test- and retest image outcomes was quantified using the RMSSD (Equation 15) as described previously by Gluer et al (177). The corresponding measure of its relative percentage deviation, RMSCV (Equation 16) (177) was also determined to enable comparison across outcomes and modalities. Based on the ISCD guidelines for the minimum acceptable precision for individual technologists on DXA (maximum 5% error allowed for total hip BMD) (173), 5% was used as a guide for evaluating the acceptability of short-term precision error (RMSCV).

$$\text{RMSSD} = \sqrt{\frac{\sum_{i}^{n} \sigma_i^{\,2}}{n}} \qquad \text{(original units of measurement)}$$

Equation 15. Root mean square standard deviation (RMSSD) (177)

$$\text{RMSCV} = \sqrt{\frac{\sum_{i}^{n} \left(\frac{\sigma_i}{\mu_i} \right)^{2}}{n}} \qquad (\%)$$

Equation 16. Root mean square coefficient of variation (RMSCV) (177)

where i is each pair of observations and n is the total number of observation replicates. To visualize subject-to-subject variability in short-term test-retest deviations across the range of values for each volumetric bone outcome, a Bland-Altman analysis was also performed here.

4.3.2 Sample size / power calculation

Based on a 95% confidence level with power of 0.80, an expected standard deviation for mean trabecular hole size of (σ) = 1.5 mm^2, and a desired maximum mean one-year difference between test-retest evaluations (Δ) = 1.5 mm^2 adapted from MacIntyre's study (141), a sample size of n=17 provided sufficient power to determine RMSSD values for evaluating test-retest precision. According to the ISCD, however, a minimum of 30 degrees of freedom is required to provide RMSCV and RMSSD that accurately assess the short- and long-term precision of bone measurements (178).

4.4 Detection limits & clinical sensitivity (Specific aim #3)

4.4.1 Statistical reporting

<u>One-year detection limit</u>

The detection limit of change is characterized differently for varying fields of study. In the realm of radiology and bone densitometry, the long-term RMSCV and RMSSD have been informative measures (Section 4.3). Based on longitudinal changes, the standard error of the estimate (SEE) quantifies long-term precision while removing the expected biological variation (178). To derive this statistical measure, a linear regression analysis was performed between baseline (independent variable) and one-year follow-up (dependent variable) image outcomes. The predicted dependent variable ($\hat{y}$) was determined by applying the derived linear equation to independent variable values (x). Equation 17 was used to quantify SEE:

$$\text{SEE} = \sqrt{\frac{\sum_i^n (y_i - \hat{y}_i)^2}{n-2}}$$

Equation 17. Standard error of the estimate (SEE).
Where n-2 represents the estimated degrees of freedom.

Clinically meaningful detection limit

Despite being able to measure minute changes, the question remains how much of a change is considered to be clinically meaningful. The ISCD has accepted the LSC as a measure of how large a difference is required for qualifying an outcome as clinically significant. For long-term test-retest measurement, the longitudinal LSC was calculated using Equation 19 as a derivation from Equation 18.

$$\text{LSC} = Z\,(Pr)\,\sqrt{\frac{1}{n_1} + \frac{1}{n_2}} \qquad \text{(in units of Pr)}$$

Equation 18. Least significant change (LSC) original form (179)

where Z is the corresponding Z score based on the confidence level desired (95% confidence = 1.96), Pr is the precision value in either relative (RMSCV) or absolute (RMSSD) terms, n_1 is the number of baseline measurements expected clinically, and n_2 is the number of follow-up measurements expected clinically. Thus, for any clinical study examining change in a variable measured only once at baseline and once at follow-up, as would be expected for volumetric bone measurements, with a given confidence level of 95%, LSC can be calculated as:

$$\text{LSC} = 1.96\,(\text{RMSSD})\,\sqrt{2}$$

Equation 19. Least significant change (LSC) simplified for one baseline and follow-up measure (179).

Clinical sensitivity – odds for fractures

Statistically, the LSC represents a degree of change that is equal to 1.96 times the SD (at a 95% confidence level) of a one-year outcome change for a given reference population, assuming the measurement is normally distributed. Although statistical thresholds have shown useful in biological sampling, their meaning is only arbitrary and is often calibrated for its intended end product – for example, active threshold selection using *x* times SD in drug discovery defines how many actives are desired from a screen. There is no evidence supporting the notion that this detection limit translates to a discrete amount of clinical meaning in any outcome examined.

Instead, the idea of a clinical sensitivity can be useful because it relates the measured outcome to a clinical end point or response. This is the same classical slope definition of sensitivity (sensitivity = response/stimulus) recognized by the National Committee for Clinical Laboratory Standards (NCCLS) (124). In consideration of bone health, a fragility or osteoporotic fracture represents the clinical outcome bearing the most impact on patients. To further describe volumetric bone outcomes' clinical sensitivity, one can examine the amount of difference in the bone outcome required (stimulus) for an associated increase in the odds for fracture (response). Although a second question may be how large an increased odds would be impactful to the patient, the size of the stimulus or the change in bone outcome required can be easily fine-tuned to achieve a desired response, or odds for fractures, once the OR is determined.

To determine true fracture risk based on volumetric bone outcomes, a Cox proportional hazards model is indicated. However, this model requires the observation of prospective incident fragility fractures, data that were not available at the present time of analysis. Instead, ORs approximate the HR as sample size increases. A binary logistic regression model was fit to data to determine the odds for fragility fractures without adjustments. A second model was run to include age as a covariate. Odds ratios were reported along with 95% confidence intervals. Because the goal of quantifying ORs was to provide a reference clinical sensitivity for each modality, and not for attempting to estimate the true fracture risk of individuals, other covariates were not included. Inclusion of just age in the model serves as a base model which enables comparison to a wider range of studies that lack other covariates.

4.4.2 Sample size / power calculation

While there is a lack of sample size guidelines for determining an OR that sufficiently estimates HR, a general rule is that OR approximates HR when sample size is larger and the event rate is low, which in the case of fragility fractures, is true. A sizeable cohort obtained from the national CaMos study was available from addressing specific aim 4 and provides a larger sample than the local cohort. Sornay-Rendu previously demonstrated significant ORs for vertebral fractures based on bone structural outcomes on hr-pQCT (age- and aBMD-adjusted OR: 2.04 per SD decrease in Ct.Th) in a cohort of 462 women, with 100 fracture cases (180).

4.5 National study-centre calibration

4.5.1 Phantom calibration

The total of twelve density and geometry outcomes (four scans repeated three times) for phantom calibration were compared across all study centres using RMSCV and RMSSD. For pQCT, 12(scans) x 5(sites) – 5 = 55 degrees of freedom were provided. For hr-pQCT, 12(scans) x 4(sites) – 4 = 44 degrees of freedom were allowed. Both these figures were larger than the 30 degrees of freedom recommended by the ISCD (177). Absolute values of density and geometry obtained were also compared between each site and the Hamilton site as a reference for pQCT, and with Toronto as a reference for hr-pQCT using linear regression analysis to compute slope, intercepts and 95% confidence intervals for future calibration.

4.5.2 Human calibration

Similar to phantom calibration analyses, RMSCV and RMSSD statistics were computed for the two-slice scans performed on all four limbs once, at 5 study centres for pQCT (df = 2(scans) x 4(limbs) x 5(centres) – 5 = 35). For hr-pQCT, single acquisitions at all four limbs was performed at 4 sites (df = 1(scan) x 4(limbs) x 4(centres) – 4 = 12). Absolute values of bone volumetric measures from pQCT and hr-pQCT were compared with the same referent sites as indicated above (Section 4.5.1) using linear regression models to provide slope and intercepts for calibration, plus 95% confidence intervals.

Because 1.0 pMRI scans were performed only at one site in the local Hamilton cohort, no calibration efforts were required.

4.6 Post-hoc analyses

4.6.1 Sub-group analysis of those without fracture or not on antiresorptive therapy

One-year change in volumetric bone outcomes could be influenced by individuals who have a fragility fracture, as bone loss in these individuals with osteoporosis could occur at a more rapid rate. In addition, individuals on antiresorptive therapy experience a reduced bone turnover rate and consequently one could expect modified rate of bone loss. All one-year change analyses including one-year RMSCV, RMSSD, LSC, Bland-Altman analyses, were repeated with and without excluding those with a history of fragility fractures and/or were receiving antiresorptive therapy.

4.6.2 Re-analysis of slices that were co-registered

Test-retest precision analysis of the full region of interest described for each modality above encompasses errors in repositioning, image acquisition, image segmentation and computation. This error could be collectively called total repetition error. However, one may be interested in the error associated with only the image acquisition, segmentation and computation, by correcting for errors in positioning. This correction was achieved by first co-registering images from test-retest and from baseline to one-year follow-up. The manual co-registration step selected for only slices that were matched between repeated scans. Subsequently, only slices representing the same anatomical location were kept in analyses by selecting common slice numbers among individuals. Together, these steps led to the analysis of images that would yield an anatomical location-specific positioning-independent error. This error was again quantified using RMSCV and RMSSDs.

5 Results

LOCAL STUDY RESULTS:

5.1 Descriptive statistics and diagnostics

5.1.1 Imaging procedure completion

Sample requirements for all specific aims were met with a total of 98 study participants who completed various activities. The final number completing the various study procedures is illustrated in Figure 13. Among those participants in the local study, all but 2 participants completed the 1.0T pMRI radius scan. A smaller subset completed pQCT and hr-pQCT scans of the radius. One participant was excluded from pMRI and hr-pQCT scans due to weight over 250 lbs.

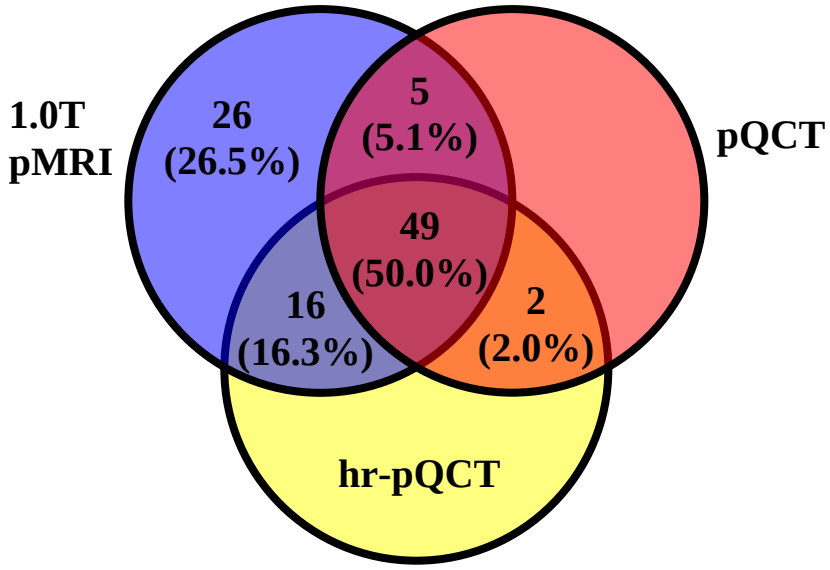

Figure 13. Completion Venn diagram of imaging procedures.
A total of 98 participants completed any imaging procedures. Each circle represents one modality and overlapped regions indicate number of participants completing a combination of scans. A total of 96 completed an MRI scan; 56 completed a pQCT scan and 67 completed an hr-pQCT scan.

5.1.2 Test-retest procedure completion

Among participants who completed an MRI scan of the radius, 53 (55.2%) completed a second scan during the same study visit to enable computation of short-term test-retest reproducibility. Of those who completed a pQCT scan, 54 (96.4%) also performed a repeated scan at the radius and tibia. Because a previous study already examined short-term test-retest reproducibility of the same hr-pQCT scanner utilized in this study, same unit retesting was not performed for participants scanned on the hr-pQCT.

5.1.3 Baseline-follow-up procedure completion

Among those who completed an MRI scan, 48 (50.0%) returned one year later for a follow-up scan. The mean duration of follow-up was 14.7 ± 1.7 months. Among those who completed a pQCT scan, 35 (62.5%) continued with a follow-up scan. The mean duration of follow-up for pQCT was 13.4 ± 1.4 months. Of the 67 participants who completed a hr-pQCT scan, 40 (59.7%) completed a follow-up scan. The mean duration of follow-up for hr-pQCT was 14.5 ± 1.9 months.

5.1.4 Study participant characteristics

Anthropometrics for all study participants were similar for all subgroups involved in different analyses including comparisons between hr-pQCT and each of pQCT and pMRI, baseline-follow-up for each modality, and test-retest for pQCT and pMRI. The recruited cohort of women represented a wide range of ages and from peri-menopause to late post-menopause. In total, 60 (61.2%) of the 98 participants have sustained a fragility fracture

within the last 15 years. Among those with a previous fragility fracture, only 5 (8.3%) were on osteoporosis medication, all of which were antiresorptive therapies. In addition, 10 (16.7%) were taking calcium and 49 (81.7%) were taking vitamin D_3 supplements.

Table II. Participant characteristics for all study procedures.
Anthropometrics and medication use descriptive statistics for study participants completing any of the local Hamilton study procedures. [a] indicates a parametric variable described using mean and standard deviations (Std Dev); [b] indicates a non-parametric variable characterized by median and first (Q1) and third (Q3) quartiles.

Variable	N	Mean[a]/ Median[b]	Std Dev[a]/ Q1-Q3[b]	Minimum	Maximum
Age (years) [a]	98	74	9	56	94
BMI (kg/m^2) [a]	98	27.65	5.74	18.73	48.28
Height (m) [a]	98	1.60	0.07	1.48	1.79
Weight (kg) [a]	98	70.46	13.86	45.00	119.00
Antiresorptive therapy (years) [b]	98	0.0	0-4.5	0.0	22.0
Vitamin D_3 (years) [b]	98	5.0	0.6-11.0	0.0	42.0
Calcium (years) [b]	98	5.5	0.0-12.0	0.0	42.0

5.1.5 Measures of normality, distribution and central tendency

The distribution of age groups across the local cohort did not appear biased towards any particular direction. In fact, there was a well balanced distribution of participants in all age groups by decade between 60 to 90 years. In contrast, weight and BMI both exhibited slightly right-skewed distributions with a greater proportion of women having lower BMI and weight. With over 60% of women not on antiresorptive therapy, and over 35% not on either calcium or vitamin D_3, all durations of these medications and supplements were

right skewed and highly kurtotic in the positive direction. However, at least 40% of participants have taken calcium, vitamin D_3 or both for at least 3 to 12 years.

Table III. Participant characteristics normality and measures of data distribution
Kolmogorov-Smirnov test of normality determined whether variables were suitable to be used in parametric or non-parametric statistical models.

Variable	Skewness	Kurtosis	Norm	P-value	Parametric
Age	0.074	-0.996	0.970	**0.023**	**No**
BMI	0.952	0.870	0.938	**<0.001**	**No**
Height	0.256	-0.368	0.984	0.253	Yes
Weight	0.789	0.952	0.959	**0.003**	**No**
Duration of					
Antiresorptive therapy	2.142	4.670	0.635	**<0.001**	**No**
Calcium supplement	1.336	2.085	0.851	**<0.001**	**No**
Vitamin D_3 supplement	1.737	4.092	0.822	**<0.001**	**No**

Table IV. MRI bone variables normality and measures of data distribution
Kolmogorov-Smirnov test of normality determined whether variables were suitable to be used in parametric or non-parametric statistical models.

MRI Bone Variable	Skewness	Kurtosis	Norm	P-value	Parametric
Tb.N	-1.095	1.395	0.927	**<0.001**	**No**
Tb.Sp MI	2.984	10.252	0.647	**<0.001**	**No**
Tb.Sp	2.602	7.544	0.703	**<0.001**	**No**
Tb.Th MI	0.777	1.547	0.967	**0.022**	**No**
Tb.Th	0.537	1.297	0.976	0.097	Yes
BV/TV	-2.073	4.460	0.770	**<0.001**	**No**
H_M	1.102	1.252	0.922	**<0.001**	**No**
H_A	3.145	10.981	0.604	**<0.001**	**No**
Cx	-0.334	-0.902	0.957	**0.004**	**No**

Table V. hr-pQCT radius bone variables normality and measures of data distribution
Kolmogorov-Smirnov test of normality determined whether variables were suitable to be used in parametric or non-parametric statistical models.

Hr-pQCT Bone Variable	Skewness	Kurtosis	Norm	P-value	Parametric
Tb.N	-0.955	0.708	0.935	**0.002**	**No**
Tb.Sp MI	2.992	12.831	0.716	**<0.001**	**No**
Tb.Th MI	0.672	3.846	0.944	**0.004**	**No**
BV/TV	-0.458	-0.035	0.975	0.193	Yes
Ct.Th	0.035	-0.366	0.988	0.786	Yes
$vBMD_i$	-0.133	0.057	0.983	0.462	Yes
$vBMD_c$	-0.462	0.118	0.974	0.157	Yes
$vBMD_{tr}$	-0.459	-0.029	0.975	0.197	Yes
Ct.Ar	0.035	-0.187	0.995	0.997	Yes
Tb.Ar	0.508	-0.005	0.974	0.164	Yes

Table VI. hr-pQCT tibia bone variables normality and measures of data distribution
Kolmogorov-Smirnov test of normality determined whether variables were suitable to be used in parametric or non-parametric statistical models.

Hr-pQCT Bone Variable	Skewness	Kurtosis	Norm	P-value	Parametric
Tb.N	-0.849	1.114	0.949	**0.008**	**No**
Tb.Sp MI	0.247	-0.503	0.981	0.382	Yes
Tb.Th MI	-0.541	0.362	0.973	0.140	Yes
BV/TV	-1.092	3.336	0.941	**0.003**	**No**
Ct.Th	-4.210	24.970	0.637	**<0.001**	**No**
$vBMD_i$	-1.034	2.830	0.942	**0.004**	**No**
$vBMD_c$	-1.022	2.786	0.943	**0.004**	**No**
$vBMD_{tr}$	-0.934	1.893	0.951	**0.009**	**No**
Ct.Ar	4.468	23.682	0.536	**<0.001**	**No**
Tb.Ar	-0.264	2.370	0.948	**0.007**	**No**

Table VII. pQCT radius bone variables normality and measures of data distribution
Kolmogorov-Smirnov test of normality determined whether variables were suitable to be used in parametric or non-parametric statistical models.

pQCT Bone Variable	Skewness	Kurtosis	Norm	P-value	Parametric
Tb.N	-1.035	0.283	0.891	**<0.001**	**No**
Tb.Sp MI	1.702	3.040	0.823	**<0.001**	**No**
Tb.Sp	1.767	3.079	0.806	**<0.001**	**No**
Tb.Th MI	0.521	0.181	0.971	0.224	Yes
Tb.Th	0.522	-0.228	0.967	0.219	Yes
BV/TV	-0.303	-0.457	0.985	0.722	Yes
Ct.Th	0.428	0.210	0.981	0.546	Yes
$vBMD_i$	0.121	-0.121	0.987	0.802	Yes
$vBMD_c$	-0.067	-0.656	0.985	0.738	Yes
$vBMD_{tr}$	-0.382	-0.558	0.973	0.265	Yes
H_M	0.437	-0.162	0.978	0.422	Yes
H_A	5.633	36.578	0.417	**<0.001**	**No**
Cx	-0.029	-0.964	0.970	0.198	Yes
Ct.Ar	-0.259	-0.221	0.986	0.794	Yes
Tb.Ar	0.107	0.760	0.984	0.662	Yes

Table VIII. pQCT tibia bone variables normality and measures of data distribution
Kolmogorov-Smirnov test of normality determined whether variables were suitable to be used in parametric or non-parametric statistical models.

pQCT Bone Variable	Skewness	Kurtosis	Norm	P-value	Parametric
Tb.N	-1.521	3.325	0.888	**<0.001**	**No**
Tb.Sp MI	2.848	10.524	0.722	**<0.001**	**No**
Tb.Sp	2.848	10.528	0.722	**<0.001**	**No**
Tb.Th MI	0.207	0.162	0.966	0.195	Yes
Tb.Th	0.207	0.162	0.966	0.195	Yes
BV/TV	-0.986	2.242	0.938	**0.017**	**No**
Ct.Th	-0.064	-0.402	0.986	0.846	Yes
$vBMD_i$	-0.468	0.538	0.978	0.406	Yes
$vBMD_c$	-0.666	0.378	0.950	**0.024**	**No**
$vBMD_{tr}$	-0.911	1.537	0.948	**0.021**	**No**
H_M	1.157	2.531	0.930	**0.008**	**No**
H_A	5.267	30.532	0.392	**<0.001**	**No**
Cx	-1.085	2.715	0.938	**0.017**	**No**
Ct.Ar	-0.157	-0.212	0.984	0.667	Yes
Tb.Ar	0.315	-0.297	0.982	0.569	Yes

Table IV through Table VIII display normality and data distribution characteristics for volumetric bone outcomes derived from images obtained by the three modalities. Measurements involving the quantification of hole geometry and trabecular bone separation were more likely to exhibit a non-Gaussian distribution. Significant Kolmogorov-Smirnov tests of normality suggest that these variables should be treated with caution when fitting parametric statistical models. While certain volumetric bone outcomes measured on one modality were found to be normally distributed but not on others (for example BV/TV measured on MRI versus on either pQCT or hr-pQCT), the normality conclusions were mostly consistent when observed at the same anatomical location (just radius or just tibia). Decision on whether to analyse volumetric bone outcomes using parametric or non-parametric statistical models was therefore guided by whichever normality conclusion was demonstrated by the majority (at least 2 of 3 modalities).

Table IX compares summary statistics using appropriate statistical models based on these normality conclusions. In general, the majority of volumetric bone outcomes acquired from either pQCT or pMR images were significantly different from those obtained using hr-pQCT. Model-dependent Tb.Sp and H_A were the only variables that did not exhibit significant differences across modalities after adjusting for the 20 pair wise comparisons performed. Notably, BV/TV and Tb.Th measured using hr-pQCT were both less than 30% of what was observed on either pQCT or pMRI. Despite these anomalies, all other variables range within a similar order of magnitude across all modalities.

Table IX. Summary statistics and comparison of volumetric bone outcomes across the three modalities.

Measures of central tendency (mean for parametric (P) and median for non-parametric (NP) variables) and error (standard deviations (SD) for parametric and interquartile range (Q1-Q3) for non-parametric variables). MI = variables not based on Parfitt's model of parallel plates. If at least 2 of the 3 modalities' bone outcome is non-parametric, a non-parametric Friedman comparison of medians was applied. Otherwise parametric repeated measures analysis of variances (ANOVA) compared means of volumetric bone outcomes. Post-hoc Tukey's HSD was applied to parametric data and a Wilcoxon signed ranks test applied to non-parametric pairwise comparisons. An adjustment for multiple comparison was performed using Bonferroni's correction. Bold = significantly different compared to corresponding variable from hr-pQCT. * Bold = significantly different compared to pQCT.

Variable	hr-pQCT-Mean ± SD	hr-pQCT Median (Q1-Q3)	pQCT-Mean ± SD	pQCT Median (Q1-Q3)	MRI-Mean ± SD	MRI Median (Q1-Q3)
BV/TV ^{P}	0.113 ± 0.034	0.116 (0.089-0.139)	**0.422 ± 0.113**	0.434 (0.340-0.500)	**0.471 ± 0.050**	0.486 (0.465-0.501)
Tb.Sp MI (mm) ^{NP}	0.527 ± 0.193	0.468 (0.420-0.558)	0.593 ± 0.275	0.479 (0.392-0.740)	0.622 ± 0.169	**0.573 (0.527-0.643)**
Tb.Sp (mm) ^{NP}			0.595 ± 0.276	0.479 (0.394-0.740)	0.641 ± 0.196	0.579 (0.532-0.657)
Tb.Th MI (mm) ^{P}	0.062 ± 0.012	0.062 (0.054-0.068)	**0.391 ± 0.056**	0.383 (0.347-0.430)	**0.535 ± 0.034**	0.529 (0.512-0.560)
Tb.Th (mm) ^{P}			0.391 ± 0.056	0.383 (0.347-0.430)	***0.539 ± 0.036**	0.533 (0.513-0.563)
Tb.N (#/mm^2) ^{NP}	1.8 ± 0.4	1.9 (1.6-2.1)	1.1 ± 0.2	**1.1 (0.9-1.2)**	0.9 ± 0.1	**0.9 (0.8-1.0)**
Ct.Th (mm) ^{P}	0.669 ± 0.178	0.670 (0.540-0.790)	**0.960 ± 0.126**	0.940 (0.864-1.050)		
vBMD$_i$ (mg/cm^3) ^{P}	277.43 ± 62.61	275.70 (242.50-325.40)	**337.54 ± 68.45**	332.80 (307.50-377.10)		
vBMD$_c$ (mg/cm^3) ^{P}	804.52 ± 63.16	804.00 (764.10-844.00)	**980.29 ± 64.31**	979.80 (931.70-1032.90)		
vBMD$_{tr}$ (mg/cm^3) ^{P}	136.14 ± 40.10	139.70 (106.60-167.20)	**162.43 ± 33.98**	173.00 (135.40-189.40)		
H$_M$ (mm^2) ^{NP}			94.19 ± 47.48	90.96 (56.16-127.52)	40.6 ± 14.11	***38.5 (28.86-50.83)**
H$_A$ (mm^2) ^{NP}			3.60 ± 6.64	1.83 (0.99-3.21)	3.22 ± 1.97	2.59 (2.10-3.12)
Cx (units) ^{NP}			-1.90 ± 12.22	-2.03 (-14.80-8.57)	6.67 ± 3.05	***7.31 (3.91-9.06)**
Ct.Ar (mm^2) ^{P}	45.63 ± 11.90	45.30 (38.60-54.50)	**40.07 ± 12.45**	39.56 (31.88-51.12)		
Tb.Ar (mm^2) ^{P}	204.71 ± 44.44	198.70 (175.60-227.00)	**189.55 ± 46.74**	182.28 (156.72-221.52)	**148.59 ± 35.05**	143.42 (124.78-171.69)

5.1.6 Identifying potential outliers

Outliers falling 1.5 times beyond the upper and lower quartiles were identified for a number of MRI, pQCT and hr-pQCT volumetric bone variables, including weight for one study participant. After cross-verification against study records, and after excluding images that did not pass quality assurance tests, only one outlier was excluded for pQCT-derived H_A at the tibia due to a poorer quality (0) motion grade 3 scan. Although one outlier was located over 3 times below (17 µm) the lower quartile (62 µm) for hr-pQCT-derived Tb.Th at the tibia, there was no visible motion and other bone structural measures were within an acceptable range. A comparison of this tibia (left) with one measuring Tb.Th at the mean value (right) is shown in Figure 14. While trabeculae towards the centre of the tibia may not be visibly different between the two participants, the outlying participant displayed thinner and less densely packed trabeculae in the cortical-trabecular bone transition zone.

5.1.7 Image quality assurance

Motion artifact

The motion grade ratings displayed in Table X-Table XIV represent the quality rating for the final image set obtained from participants. A larger number of images obtained by pMRI failed quality assurance followed by pQCT and then hr-pQCT, which had only one quality failure at the distal tibia. When image sets were separated according to motion grade, the majority of MR images exhibited at least some mild to moderate (grade 1-3) level of motion but were still acceptable for analyses. The same was true for pQCT of the

radius. However, at the same site for hr-pQCT, most images showed no motion to minor motion with only few exhibiting grades 3-5 motion. At the tibia, motion grades appeared to be lower than at the radius for both pQCT and hr-pQCT. For pQCT image sets, there did not appear to be any major differences in motion grade distribution between the more proximal and the more distal slice obtained. For the tibia, although the proximal slice was obtained last, there appeared to be less motion compared to the more distal slice.

Table X. Image sets failing quality assurance steps.
Comparison of pMRI, pQCT and hr-pQCT images with failed quality assurance for all baseline (BL), and repeated follow-up (FU R1, FU R2) protocols at the radius and tibia. Fractions indicate number of failures over total number of images with percent failing quality assurance in brackets.

Anatomy & ROI	MRI BL	MRI FU R1	MRI FU R2	pQCT BL	pQCT FU R1	pQCT FU R2	Hr-pQCT BL	Hr-pQCT FU
Radius (Prox)	11/94 (11.7%)	5/60 (8.3%)	8/56 (14.3%)	4/39 (10.3%)	1/57 (1.8%)	0/48 (0.0%)	0/68 (0.0%)	0/40 (0.0%)
Radius (Dist)				6/39 (15.4%)	0/57 (0.0%)	0/48 (0.0%)		
Tibia (Prox)				0/38 (0.0%)	2/57 (3.5%)	2/57 (3.5%)	1/68 (1.5%)	0/40 (0.0%)
Tibia (Dist)				0/38 (0.0%)	2/57 (3.5%)	2/57 (3.5%)		

Table XI. Motion grade breakdown for pMRI image sets.
Number (%) of hr-pQCT radius and tibia baseline (BL) and follow-up (FU) images exhibiting each motion grade.

Motion Grades	Radius BL	Radius FU R1	Radius FU R2
0	7 (7.4%)	6 (10.0%)	6 (10.7%)
1	38 (40.4%)	18 (30.0%)	14 (25.0%)
2	28 (29.8%)	24 (40.0%)	19 (33.9%)
3	16 (17.0%)	9 (15.0%)	13 (23.2%)
4	5 (5.3%)	3 (5.0%)	4 (7.1%)

Table XII. Motion grade breakdown for pQCT (more proximal) image sets.
Number (%) of pQCT radius and tibia baseline (BL) and follow-up (FU) images exhibiting each motion grade at the more proximal slice.

Motion Grades Proximal	Radius BL	Radius FU R1	Radius FU R2	Tibia BL	Tibia FU R1	Tibia FU R2
0	3 (7.7%)	5 (8.8%)	1 (2.1%)	17 (44.7%)	18 (31.6%)	16 (28.1%)
1	22 (56.4%)	32 (56.1%)	26 (54.2%)	17 (44.7%)	27 (47.4%)	25 (43.9%)
2	12 (30.8%)	17 (29.8%)	20 (41.7%)	4 (10.5%)	11 (19.3%)	12 (21.0%)
3	2 (5.1%)	3 (5.3%)	1 (2.1%)	0 (0.0%)	1 (1.8%)	4 (7.0%)

Table XIII. Motion grade breakdown for pQCT (more distal) image sets.
Number (%) of pQCT radius and tibia baseline (BL) and follow-up (FU) images exhibiting each motion grade at the more distal slice.

Motion Grades Distal	Radius BL	Radius FU R1	Radius FU R2	Tibia BL	Tibia FU R1	Tibia FU R2
0	5 (12.8%)	7 (14.6%)	5 (8.8%)	13 (34.2%)	23 (40.4%)	21 (36.8%)
1	18 (46.2%)	24 (50.0%)	33 (57.9%)	21 (55.3%)	16 (28.1%)	16 (28.1%)
2	15 (38.5%)	15 (31.2%)	16 (28.1%)	4 (10.5%)	16 (28.1%)	16 (28.1%)
3	1 (2.6%)	2 (4.2%)	3 (5.3%)	0 (0.0%)	2 (3.5%)	4 (7.0%)

Table XIV. Motion grade breakdown for hr-pQCT image sets.
Number (%) of hr-pQCT radius and tibia baseline (BL) and follow-up (FU) images exhibiting each motion grade.

Motion Grades	Radius BL	Radius FU	Tibia BL	Tibia FU
1	17 (25.0%)	3 (7.5%)	48 (70.6%)	27 (67.5%)
2	42 (61.8%)	23 (57.5%)	16 (23.5%)	12 (30.0%)
3	6 (8.8%)	10 (25.0%)	3 (4.4%)	1 (2.5%)
4	3 (4.4%)	4 (10.0%)	0 (0.0%)	0 (0.0%)
5	0 (0.0%)	0 (0.0%)	1 (1.5%)	0 (0.0%)

Other image artifacts

From MR images, all participants (63/63 co-registered pMRI-hr-pQCT scans) appeared to exhibit a loss of cortical bone void signal at the anterior aspect of the ultradistal radius. Although it was difficult to confirm this for 7 participants in whom CT and MR images were not co-registered well, this artifact was consistent across all scans. The apparently thinned cortex seemed to be caused by shifting of the marrow space into the cortical bone

region in the anterior direction. The effect was more dramatic at the proximal end as compared to the more distal end of the radius; and more severe for individuals with thicker compared to those with thinner cortices. For pQCT, aside from motion artifact, manifesting in diagonal lines of decreased signal intensity flanking the cortex, no other major artifacts were observable. For hr-pQCT, ring artifact can be observed in most images, situated at the bottom of the field of view. For certain images, it coincides with the centre of the tibia, and in others, the origin was outside of the anatomy (Figure 15). Like pQCT, hr-pQCT also demonstrated streaking artifacts as a consequence of motion.

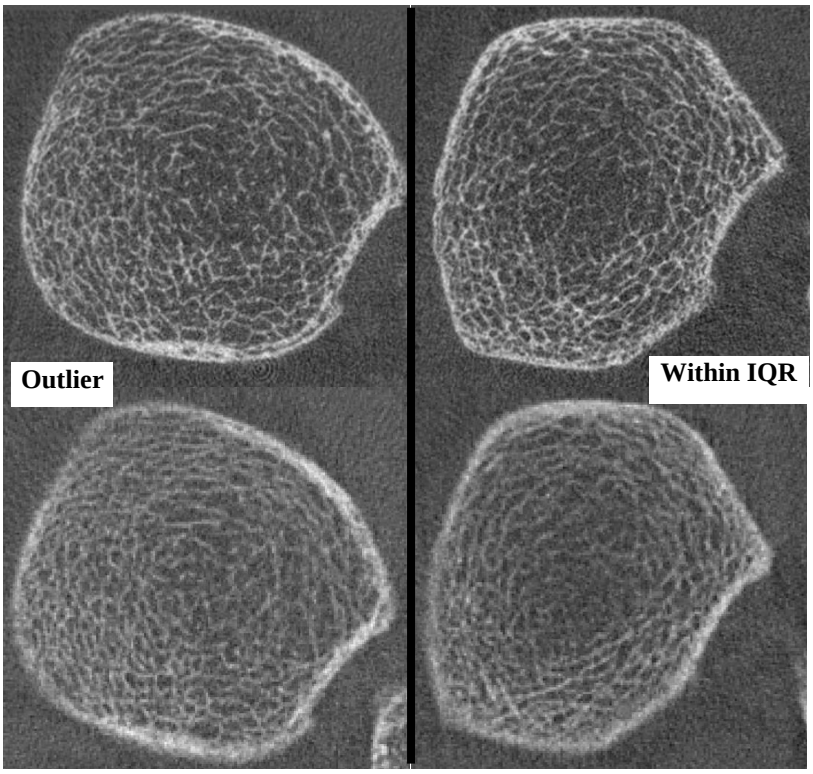

Figure 14. Comparison of trabecular bone between an identified outlier and a participant within the IQR.
Top row (hr-pQCT): Trabecular bone at the cortical-trabecular bone transition zone for the outlying participant (left, ID109) was shown to be less densely packed and thinner compared to the participant on the right (ID71). **Bottom row (pQCT):** For comparison, corresponding pQCT images are shown. Trabecular thickness even at the transition zone was not as evident due to partial voluming effects and a lower resolution for pQCT scans.

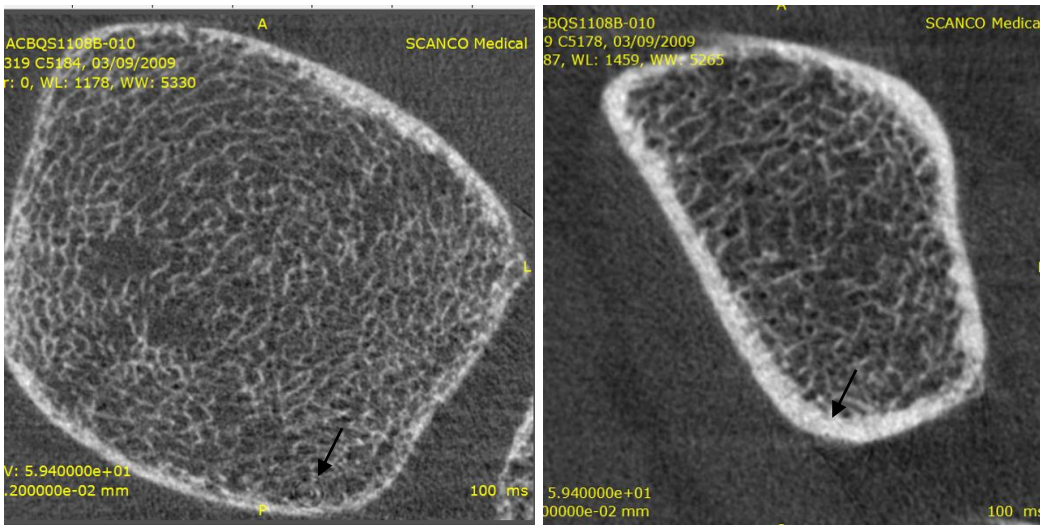

Figure 15. Ringing artifact observed on hr-pQCT scans.
Series of concentric circles with origin located at the bottom of the field of view, and coinciding within or outside of the anatomy. Above shows this artifact overlapping the tibia (left) and radius (right). Arrow points to centroid of ringing artifact.

5.2 Validation – linear regression and ICC (Specific aim #1)

5.2.1 Cross-calibration equations

Fitting parametric simple linear regression model to non-parametric data

Although non-parametric volumetric bone measures were identified among the three modalities, a simple linear regression, a parametric model, provided parameter estimates for slopes and intercepts for all variables under the assumption linearity. It was also assumed that extreme values would not considerably affect parameter estimates. To evaluate the validity of this assumption, parameter estimates from the simple linear model were compared to those obtained from an experimental generalized additive model (SAS 9.22) that relaxes the assumption of linearity by applying smoothing techniques to the non-parametric variables. To observe the maximal impact of the different models, model-

dependent Tb.Sp was selected since it exhibited the highest skewness and kurtosis compared to other bone measures. Aside from minor differences in standard error for each model, parameter estimates for both slope and intercepts were otherwise the same (Table XV). Thus, while one may be cautious with the margin of error estimated by simple linear regression confidence intervals for non-parametric bone measures, the slopes and intercepts are otherwise comparable to non-parametric model outputs.

Table XV. Comparison of model outputs for a simple linear regression versus a generalized additive model

The linear relationship between 1.0T pMRI and hr-pQCT-derived Tb.Sp was modeled using simple linear regression and generalized additive model employing spline smoothing. Slope and intercept parameter estimates were compared.

Variables / Model	Parameter Estimates	Standard Error	t value	P value
Simple linear model				
Intercept	-0.075	0.059	-1.28	0.208
Slope (Tb.Sp)	0.970	0.094	10.28	< 0.001
Generalized additive model with spline smoothing				
Intercept	-0.075	0.056	-1.34	0.186
Slope(Spline(Tb.Sp))	0.970	0.090	10.81	<0.001

Validation linear equations for pQCT and pMRI bone structure

Linear slopes and intercepts along with their respective 95% confidence intervals are reported in Table XVI for pMRI and Table XVII - Table XX for pQCT. For pMRI, only Tb.Th did not display a significant relationship with its counterpart on hr-pQCT. Model-independent Tb.Sp showed the highest correlation that was also closest to unity and had

Table XVI. Linear relationships between pMRI and hr-pQCT bone structure values
Hr-pQCT bone structural variables were used as the dependent variable and pMRI bone structure was treated as an independent variable. R^2 and R^2 BMI represented linear regression models with and without adjusting for BMI, respectively. All slopes and intercepts displayed have not included BMI in the model.

pMRI Bone Outcome	Slope 95% CI(Lower, Upper)	Intercept 95% CI(Lower, Upper)	R^2	R^2 BMI	P-value
BV/TV	0.484 (0.361, 0.607)	-0.119 (-0.179, -0.059)	0.526	0.552	<0.0001
Tb.Sp	0.744 (0.576, 0.911)	0.048 (-0.060, 0.157)	0.586	0.631	<0.0001
Tb.Sp MI	0.970 (0.781, 1.159)	-0.075 (-0.192, 0.043)	0.654	0.685	<0.0001
Tb.Th	0.016 (-0.039, 0.071)	0.053 (0.022, 0.084)	0.006	0.016	0.554
Tb.Th MI	0.016 (-0.04, 0.071)	0.054 (0.023, 0.085)	0.006	0.016	0.578
Tb.N	2.1 (1.4, 2.9)	0.0 (-0.7, 0.6)	0.376	0.403	<0.0001

Table XVII. Linear relationships between pQCT and hr-pQCT bone structure values at the more proximal ultradistal radius site (16.5 mm from end plate)
Hr-pQCT bone structural variables were used as the dependent variable and pQCT bone structure was treated as an independent variable. R^2 and R^2 BMI represented linear regression models with and without adjusting for BMI, respectively. All slopes and intercepts displayed have not included BMI in the model.

pQCT Bone Outcome	Slope 95% CI(Lower, Upper)	Intercept 95% CI(Lower, Upper)	R^2	R^2 BMI	P-value
BV/TV	0.291 (0.271, 0.31)	-0.01 (-0.018, -0.001)	0.949	0.950	<0.0001
Tb.Sp	0.567 (0.446, 0.688)	0.191 (0.112, 0.271)	0.653	0.653	<0.0001
Tb.Sp MI	0.576 (0.442, 0.71)	0.194 (0.107, 0.282)	0.653	0.653	<0.0001
Tb.Th	0.159 (0.116, 0.202)	0 (-0.017, 0.017)	0.542	0.571	<0.0001
Tb.Th MI	0.159 (0.116, 0.202)	0 (-0.017, 0.017)	0.542	0.571	<0.0001
Tb.N	1.5 (1.2, 1.9)	0.2 (-0.2, 0.5)	0.636	0.637	<0.0001
Ct.Th	1.032 (0.740, 1.324)	-0.32 (-0.61, -0.04)	0.518	0.518	<0.0001
$vBMD_i$	0.80 (0.67, 0.94)	4.26 (-41.89, 50.40)	0.756	0.769	<0.0001
$vBMD_c$	0.73 (0.53, 0.93)	89.89 (-105.33, 285.10)	0.537	0.538	<0.0001
$vBMD_{tr}$	1.09 (0.95, 1.22)	-40.79 (-63.31, -18.27)	0.846	0.851	<0.0001

Table XVIII. Linear relationships between pQCT and hr-pQCT bone structure values at the more distal ultradistal radius site (11.5 mm from end plate)

Hr-pQCT bone structural variables were used as the dependent variable and pQCT bone structure was treated as an independent variable. R^2 and R^2 BMI represented linear regression models with and without adjusting for BMI, respectively. All slopes and intercepts displayed have not included BMI in the model.

pQCT Bone Outcome	Slope 95% CI(Lower, Upper)	Intercept 95% CI(Lower, Upper)	R^2	R^2 BMI	P-value
BV/TV	0.293 (0.257, 0.33)	-0.011 (-0.026, 0.005)	0.849	0.850	<0.0001
Tb.Sp	0.696 (0.497, 0.895)	0.160 (0.047, 0.272)	0.514	0.514	<0.001
Tb.Sp MI	0.695 (0.471, 0.919)	0.167 (0.041, 0.294)	0.497	0.497	<0.001
Tb.Th	0.158 (0.114, 0.201)	0.005 (-0.011, 0.021)	0.531	0.543	<0.0001
Tb.Th MI	0.159 (0.116, 0.202)	0.000 (-0.017, 0.017)	0.542	0.571	<0.0001
Tb.N	1.7 (1.3, 2.2)	-0.2 (-0.7, 0.3)	0.583	0.584	<0.0001
Ct.Th	0.768 (0.255, 1.281)	-0.036 (-0.506, 0.435)	0.162	0.165	0.004
vBMDi	0.90 (0.72, 1.08)	45.26 (-1.70, 92.22)	0.685	0.694	<0.0001
vBMDc	0.59 (0.38, 0.80)	297.93 (115.48, 480.38)	0.400	0.401	<0.0001
vBMDtr	1.15 (1.00, 1.30)	-67.01 (-93.61, -40.40)	0.837	0.838	<0.0001

Table XIX. Linear relationships between pQCT and hr-pQCT bone structure values at the more proximal ultradistal tibia site (29.5 mm from end plate)

Hr-pQCT bone structural variables were used as the dependent variable and pQCT bone structure was treated as an independent variable. R^2 and R^2 BMI represented linear regression models with and without adjusting for BMI, respectively. All slopes and intercepts displayed have not included BMI in the model.

pQCT Bone Outcome	Slope 95% CI(Lower, Upper)	Intercept 95% CI(Lower, Upper)	R^2	R^2 BMI	P-value
BV/TV	0.353 (0.282, 0.423)	-0.034 (-0.065, -0.002)	0.685	0.713	<0.0001
Tb.Sp	0.872 (0.413, 1.331)	0.113 (-0.119, 0.344)	0.237	0.297	<0.001
Tb.Sp MI	0.874 (0.414, 1.333)	0.112 (-0.119, 0.343)	0.238	0.298	<0.001
Tb.Th	0.225 (0.142, 0.309)	-0.016 (-0.047, 0.015)	0.386	0.413	<0.0001
Tb.Th MI	0.225 (0.142, 0.309)	-0.016 (-0.047, 0.015)	0.386	0.413	<0.0001
Tb.N	2.0 (1.4, 2.6)	-0.5 (-1.2, 0.2)	0.492	0.528	<0.0001
Ct.Th	1.40 (1.05, 1.74)	-0.69 (-1.08, -0.30)	0.590	0.609	<0.0001
$vBMD_i$	1.03 (0.85, 1.22)	-62.70 (-118.55, -6.84)	0.728	0.742	<0.0001
$vBMD_c$	1.78 (1.14, 2.41)	-885.15 (-1471.70, -298.59)	0.402	0.436	<0.0001
$vBMD_{tr}$	1.20 (0.92, 1.48)	-72.13 (-124.40, -19.86)	0.607	0.623	<0.0001

Table XX. Linear relationships between pQCT and hr-pQCT bone structure values at the more distal ultradistal tibia site (24.5 mm from end plate)
Hr-pQCT bone structural variables were used as the dependent variable and pQCT bone structure was treated as an independent variable. R^2 and R^2 BMI represented linear regression models with and without adjusting for BMI, respectively. All slopes and intercepts displayed have not included BMI in the model.

pQCT Bone Outcome	Slope 95% CI(Lower, Upper)	Intercept 95% CI(Lower, Upper)	R^2	R^2 BMI	P-value
BV/TV	0.334 (0.267, 0.401)	-0.015 (-0.043, 0.013)	0.682	0.707	<0.0001
Tb.Sp	0.724 (0.386, 1.062)	0.124 (-0.078, 0.325)	0.283	0.342	<0.001
Tb.Sp MI	0.724 (0.386, 1.062)	0.124 (-0.078, 0.326)	0.283	0.342	<0.001
Tb.Th	0.217 (0.128, 0.307)	-0.014 (-0.048, 0.02)	0.337	0.365	<0.0001
Tb.Th MI	0.217 (0.128, 0.307)	-0.014 (-0.048, 0.02)	0.337	0.365	<0.0001
Tb.N	1.8 (1.3, 2.3)	-0.1 (-0.7, 0.4)	0.526	0.555	<0.0001
Ct.Th	1.249 (1.017, 1.481)	-0.726 (-1.029, -0.422)	0.714	0.730	<0.0001
$vBMD_i$	0.89 (0.73, 1.04)	-49.86 (-102.27, 2.56)	0.737	0.760	<0.0001
$vBMD_c$	1.33 (0.81, 1.86)	-545.70 (-1059.23, -32.16)	0.356	0.419	<0.0001
$vBMD_{tr}$	1.10 (0.83, 1.37)	-35.10 (-80.18, 9.98)	0.592	0.602	<0.0001

near zero intercept. Bone volume fraction, and to a lesser degree Tb.Sp, overestimated values on pMRI compared to hr-pQCT. On the other hand, Tb.N measured on pMRI was underestimated compared to hr-pQCT. BMI only conferred a mild increase in the amount of variance explained in the model when it was included.

pQCT proximal and distal slice volumetric bone outcomes' linear relationship with hr-pQCT at both the radius and at the tibia were similar to what was observed for pMRI, except the parameter estimates were smaller. Like pMRI, there was a lack of relationship between pQCT and hr-pQCT image-derived Tb.Th. At the radius, BMI did not further account for any additional unexplained variance in hr-pQCT by pQCT; and at the tibia, adjustment for BMI only modestly contributed to increased correlation between pQCT

and hr-pQCT bone outcomes. Although results were similar for both the proximal and distal pQCT slices, the more proximal slice at the ultradistal radius showed a linear relationship with hr-pQCT Ct.Th that was closer to unity than at the distal slice. The opposite was true at the ultradistal tibia. Both model-dependent and model-independent measures of Tb.Sp and Tb.Th yielded near identical results to one another for comparison of both pQCT and pMRI against hr-pQCT.

In separate analyses for bone outcomes common to only pQCT and hr-pQCT images, Ct.Th and $vBMD_{tr}$ both showed linear relationships near unity. Although, for $vBMD_{tr}$ the larger negative intercept value indicates that $vBMD_{tr}$ measured on pQCT is routinely larger than what is observed by examining hr-pQCT images. Integral and cortical vBMD were also overestimated by analysis of pQCT images. The large intercept for the pQCT-hr-pQCT relationship for $vBMD_c$ obtained at the radius further suggests that accuracy may be limited for this measurement. The even larger deviation observed for $vBMD_c$ at the tibia additionally corroborates this proposition. Meanwhile, Ct.Th, trabecular and integral vBMD were underestimated at the tibia compared to hr-pQCT.

Linear relationships are highlighted in Figure 16 for model-independent Tb.Sp and $vBMD_c$ to illustrate the superior correlation observed for the former and the large deviations identified with the latter.

POST-HOC: Effect of angular deviation on linear relations between pMRI and hr-pQCT

The maximum angular deviation measured from the combination of sagittal and coronal scout views of MR images axially co-registered to hr-pQCT images ranged from 0.14^{o} to 10.50^{o} with a mean centred at 4.46^{o}. None of the regression models examining the contribution of angular deviation to pMRI-hrpQCT bone structure deviations were found to be significant. Angular deviation explained less than 5% of the variance in the pMRI-hr-pQCT standard deviation observed for all bone structural measures. Notably, between-modality SD for both model-dependent and model-independent Tb.Th was explained up to only 3% by inter-modality angular deviation.

Because of the low degree of variance in inter-modality deviation explained by angular deviation, a cut-off value for maximum angular deviation at the third quartile was applied post-hoc. Image pairs exhibiting angular deviation above and below 5.91^{o} were compared in univariate analysis of variances. In this analysis, no significant differences in inter-modality SD between the high and low angular deviation groups were observed either.

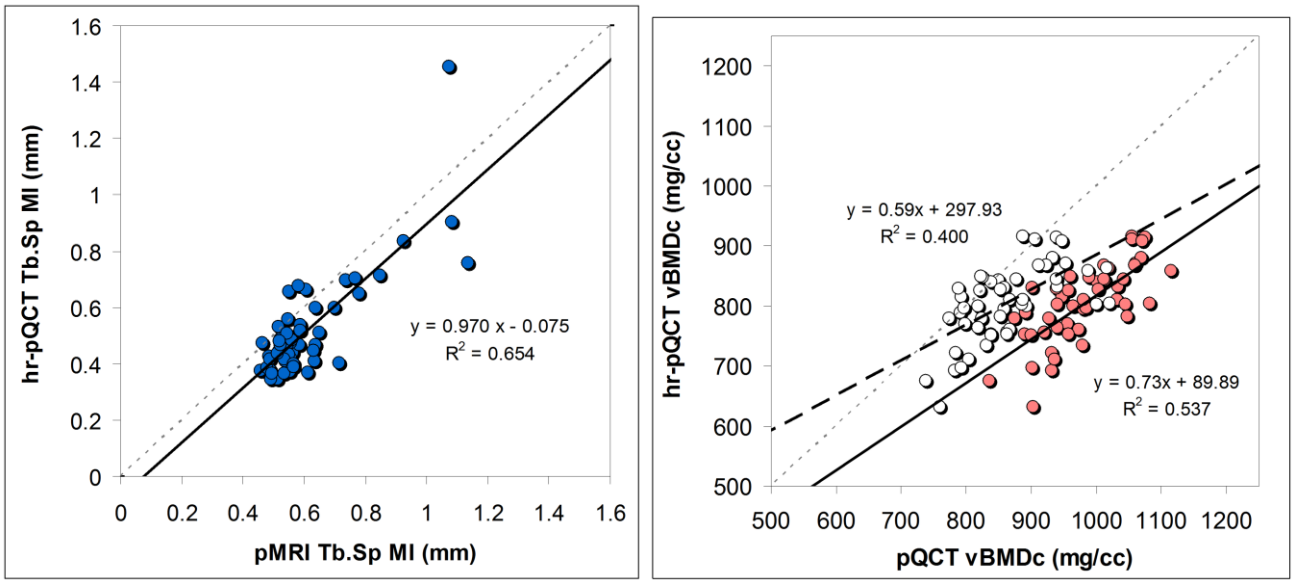

Figure 16. Illustration of the linear relationships for Tb.Sp and $vBMD_C$ between pMRI/PQCT and hr-pQCT.
Left: Linear relationship between pMRI model-independent (MI) Tb.Sp as independent variable and hr-pQCT MI Tb.Sp as dependent variable. **Right:** Comparison of linear relationship between hr-pQCT vBMD of the radial cortex at the more proximal slice (solid line filled circles) and at the more distal slice (dashed line open circles).

Table XXI. Linear relationships between co-registered pMRI and hr-pQCT bone outcomes
Hr-pQCT bone structural variables were used as the dependent variable and pMRI bone structure was treated as an independent variable. R^2 and R^2 BMI represented linear regression models with and without adjusting for BMI, respectively. All slopes and intercepts displayed have not included BMI in the model.

pMRI Bone Outcome	Slope 95% CI(Lower, Upper)	Intercept 95% CI(Lower, Upper)	R^2	R^2 BMI	P-value
BV/TV	0.767 (0.568, 0.967)	-0.263 (-0.362, -0.165)	0.514	0.541	<0.0001
Tb.Sp	1.640 (1.357, 1.924)	-0.414 (-0.575, -0.252)	0.706	0.712	<0.001
Tb.Sp MI	1.712 (1.419, 2.004)	-0.447 (-0.613, -0.282)	0.710	0.716	<0.001
Tb.Th	-0.010 (-0.064, 0.044)	0.068 (0.039, 0.097)	0.003	0.019	0.700
Tb.Th MI	-0.011 (-0.065, 0.044)	0.068 (0.038, 0.098)	0.003	0.019	0.700
Tb.N	2.2 (1.3, 3.0)	-0.1 (-0.9, 0.7)	0.296	0.310	<0.0001

POST-HOC: Effect of inter-modality co-registration on improving linear relationships

Co-registration increased the slope for BV/TV between pMRI and hr-pQCT without changing the regression coefficient. Neither Tb.N nor either of the Tb.Th measures' validities were affected by co-registering pMR images against hr-pQCT. However, values of both model-dependent and model-independent Tb.Sp were underestimated by pMRI after co-registration. This is to be compared with the near-unity slopes for Tb.Sp between pMRI and hr-pQCT without co-registration (Compare Table XXI with Table XVI).

5.2.2 Intra-class correlation coefficients

Agreement between hr-pQCT and each of pQCT and pMRI's volumetric bone variables

Agreement for all volumetric bone outcomes between hr-pQCT and each of pQCT and pMRI were above an ICC of 0.90 except for Tb.Sp (Table XXII-Table XXV). Confidence

Table XXII. Intraclass correlation coefficients for agreement between hr-pQCT and pQCT radius bone outcomes

Agreement in the computed volumetric bone variables between hr-pQCT and pQCT was evaluated using a type (2,1) intraclass correlation coefficient along with 95% confidence intervals (CI).

Volumetric Bone Variable	N	ICC	Lower 95% CI	Upper 95% CI
BV/TV	48	0.994	0.991	0.996
Tb.Sp	48	0.319	0.129	0.486
Tb.Sp MI	48	0.043	-0.173	0.254
Tb.Th	48	0.999	0.998	0.999
Tb.Th MI	48	0.999	0.998	0.999
Tb.N	48	0.986	0.979	0.991
Ct.Th	48	0.978	0.967	0.985
$vBMD_i$	48	0.916	0.877	0.943
$vBMD_C$	48	0.990	0.984	0.993
$vBMD_{tr}$	48	0.855	0.790	0.900

intervals for all of these measures were narrow. While the ICC for pMRI-derived model-dependent and model-independent Tb.Sp was above 0.80, pQCT-derived Tb.Sp measures suffered from poorer agreement. This observation aside, the Pearson correlation coefficient between pQCT and hr-pQCT Tb.Sp remained above 0.50.

Table XXIII. Intraclass correlation coefficients for agreement between hr-pQCT and pQCT tibia bone outcomes

Agreement in the computed volumetric bone variables between hr-pQCT and pQCT was evaluated using a type (2,1) intraclass correlation coefficient along with 95% confidence intervals (CI).

Bone Structural Variable	N	ICC	Lower 95% CI	Upper 95% CI
BV/TV	48	0.998	0.996	0.998
Tb.Sp	48	0.164	-0.036	0.350
Tb.Sp MI	48	0.170	-0.029	0.356
Tb.Th	48	0.999	0.999	1.000
Tb.Th MI	48	0.999	0.999	1.000
Tb.N	48	0.981	0.972	0.988
Ct.Th	48	0.916	0.878	0.943
$vBMD_i$	48	0.912	0.872	0.940
$vBMD_C$	48	0.975	0.962	0.983
$vBMD_{tr}$	48	0.936	0.907	0.957

Table XXIV. Intraclass correlation coefficients for agreement between hr-pQCT and pMRI radius bone outcomes

Agreement in the computed bone structural variables between hr-pQCT and pMRI was evaluated using a type (2,1) intraclass correlation coefficient along with 95% confidence intervals (CI).

Bone Structural Variable	N	ICC	Lower 95% CI	Upper 95% CI
BV/TV	57	0.999	0.999	0.999
Tb.Sp	57	0.834	0.769	0.882
Tb.Sp MI	57	0.807	0.733	0.862
Tb.Th	57	1.000	0.999	1.000
Tb.Th MI	57	1.000	0.999	1.000
Tb.N	57	0.995	0.992	0.996

POST-HOC: Effect of co-registration on hr-pQCT-pMRI bone structure agreement

By examining only pMRI slices that successfully co-registered with hr-pQCT slices, the degree of agreement between the two modalities' Tb.Sp was decreased. Meanwhile, other bone structural variables' agreement between pMRI and hr-pQCT was relatively unaffected. A contrast between Table XXIV and Table XXV illustrates this observation.

Table XXV. Intraclass correlation coefficients for agreement between hr-pQCT and co-registered pMRI radius bone outcomes

Agreement in the computed bone structural variables between hr-pQCT and co-registered pMRI image sets was evaluated using a type (2,1) intraclass correlation coefficient along with 95% confidence intervals (CI).

Bone Structural Variable	N	ICC	Lower 95% CI	Upper 95% CI
BV/TV	57	1.000	0.999	1.000
Tb.Sp	57	0.608	0.479	0.711
Tb.Sp MI	57	0.566	0.428	0.678
Tb.Th	57	1.000	0.999	1.000
Tb.Th MI	57	1.000	0.999	1.000
Tb.N	57	0.994	0.992	0.996

5.2.3 Bland-Altman analyses

Inter-modality limits of agreement and Bland-Altman plots

The limits of agreement between pMRI and hr-pQCT image-derived BV/TV and Tb.Sp measures were, on average, tighter than for comparisons between pQCT and hr-pQCT. However, Tb.Th and Tb.N measures obtained from pQCT images agreed slightly more closely with hr-pQCT counterparts than pMRI variables did (Table XXVI-Table XXVII). Bland-Altman plots showed that although a correlation existed between modalities, the degree of agreement was dependent, in many cases, on the mean value of the volumetric

bone measure. This was particularly true for pQCT, which displayed significant and large Pearson correlation coefficients between the mean of volumetric bone measures and the difference between pQCT and hr-pQCT measurements at both radius and tibia (Figure 17 & Figure 18). In particular, correlations and linear slopes between mean value and absolute differences were largest for BV/TV and Tb.Th. For pMRI, although a similar association was observed, only stronger correlations between means and absolute differences were identified for Tb.Th and Tb.N (Figure 19). A larger amount of bone in general seemed to be responsible for a larger inter-modality deviation. In contrast, larger Tb.Sp was modestly associated with a larger inter-modality difference for both pMRI and pQCT at the distal radius. However, this correlation may be largely influenced by outlying data.

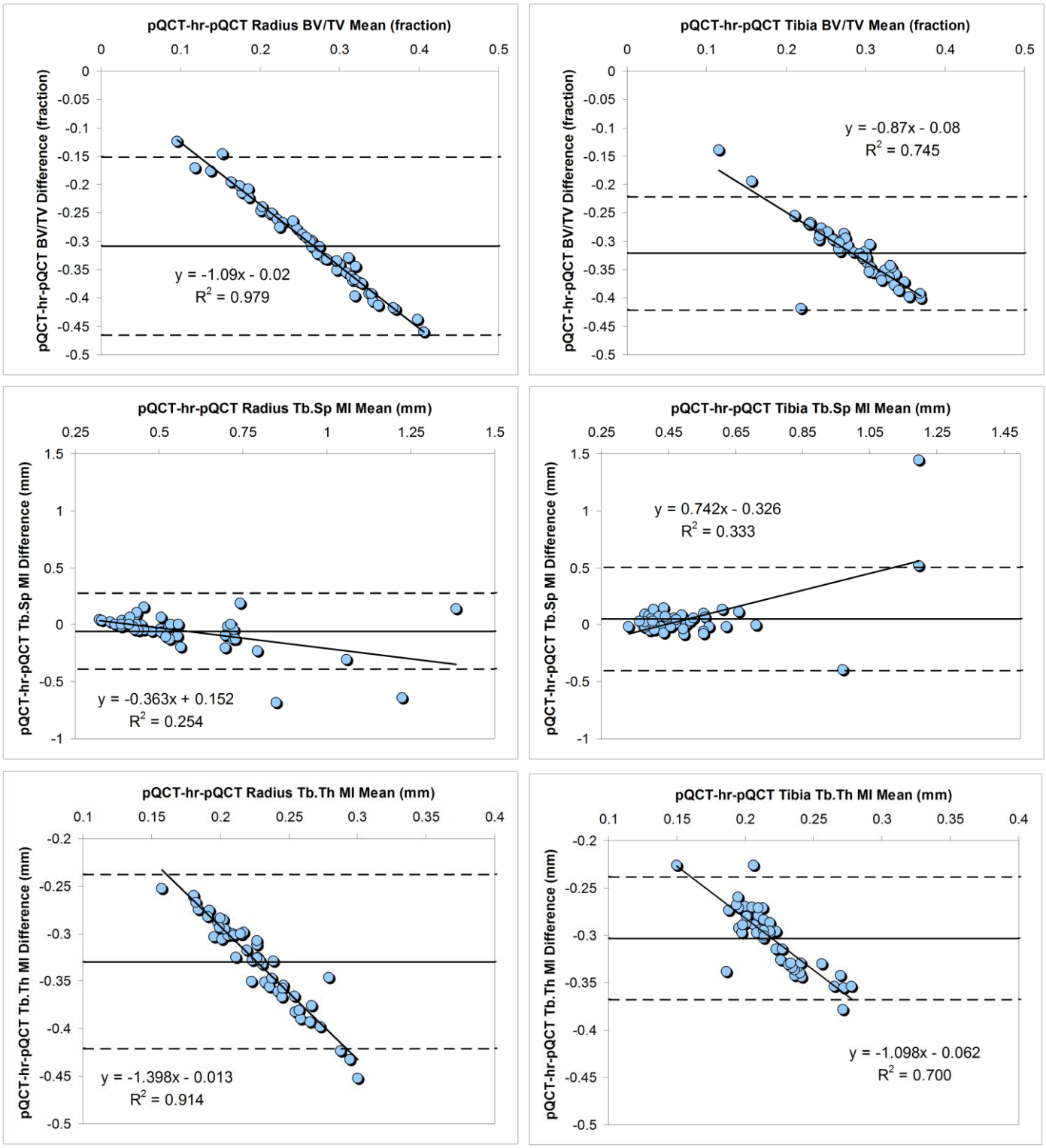

Figure 17. Bland-Altman plots for pQCT radius and tibia volumetric bone measure agreement with hr-pQCT. Bland-Altman plots for pQCT radius (left column) and tibia (right column) image-derived volumetric bone outcomes as compared to hr-pQCT at the corresponding anatomical location. Dashed lines indicate upper and lower limits. Linear regression was performed on all means versus inter-modality differences. MI = model-independent measures. Linear equations and regression coefficients are displayed in graphs where relevant.

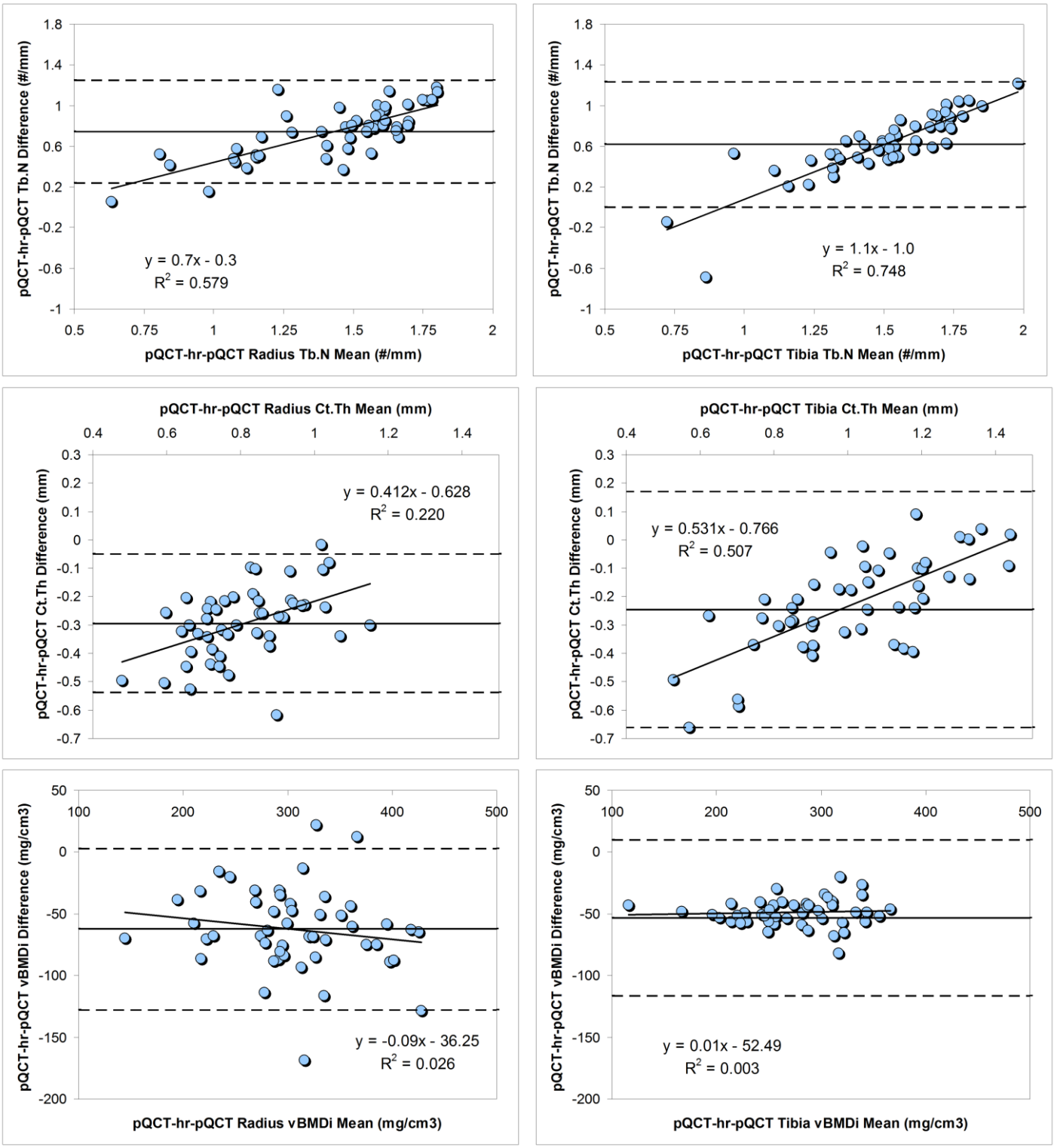

Figure 18. Bland-Altman plots for pQCT radius and tibia bone measure agreement with hr-pQCT. Continued. Bland-Altman plots for pQCT radius (left column) and tibia (right column) image-derived bone structural variables as compared to hr-pQCT at the corresponding anatomical location. Dashed lines indicate upper and lower limits. Linear regression was performed on all means versus inter-modality differences. MI = model-independent measures. Linear equations and regression coefficients are displayed in graphs where relevant.

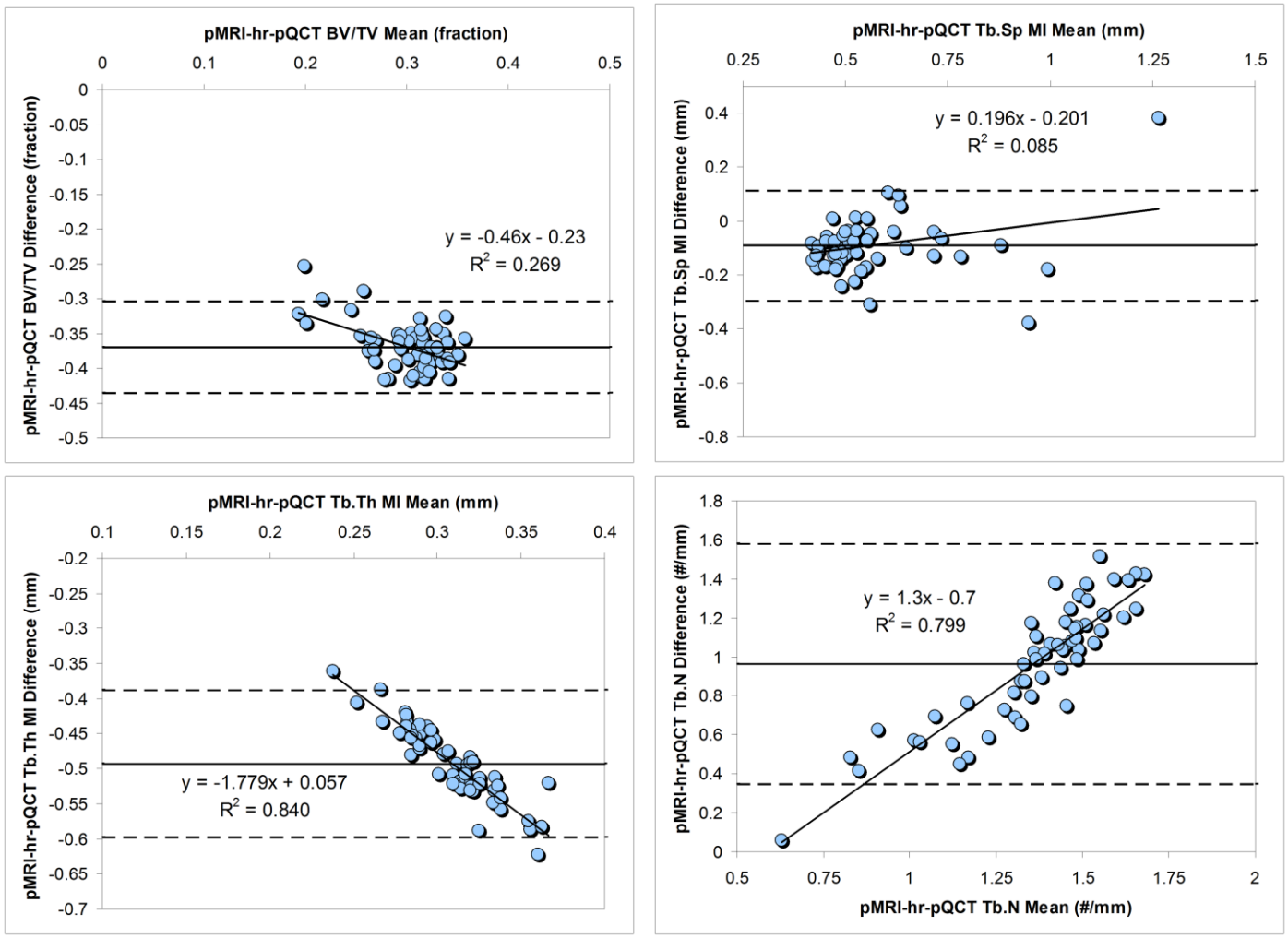

Figure 19. Bland-Altman plots for pMRI radius bone structure agreement with hr-pQCT.
Bland-Altman plots for pMRI bone structural variables as compared to hr-pQCT were plotted with dashed lines indicating upper and lower limits. Linear regression was performed on all means versus inter-modality differences. MI = model-independent measures. Linear equations and regression coefficients are displayed in graphs where relevant.

Table XXVI. Bland-Altman limits of agreement for pQCT radius and tibia volumetric bone measures compared to hr-pQCT

Agreement in the computed volumetric bone variables between hr-pQCT and each of pQCT radius and tibia measurements was assessed using upper (LOAU) and lower (LOAL) limits of agreement. Mean difference (Diff) and standard deviations (SD) were used to compute 95% confidence intervals representing LOAL and LOAU values.

	pQCT radius statistics				pQCT tibia statistics			
Bone structure variable	**Mean Diff**	**SD Diff**	**LOAU**	**LOAL**	**Mean Diff**	**SD Diff**	**LOAU**	**LOAL**
BV/TV (fraction)	-0.309	0.080	-0.152	-0.465	-0.321	0.051	-0.222	-0.421
Tb.Sp (mm)	-0.067	0.164	0.255	-0.388	0.051	0.231	0.503	-0.401
Tb.Sp MI (mm)	-0.056	0.170	0.277	-0.389	0.051	0.231	0.503	-0.401
Tb.Th (mm)	-0.330	0.047	-0.238	-0.421	-0.303	0.033	-0.239	-0.368
Tb.Th MI (mm)	-0.330	0.047	-0.238	-0.421	-0.303	0.033	-0.239	-0.368
Tb.N (#/mm)	0.7	0.3	1.3	0.2	0.6	0.3	1.2	0.0
Ct.Th (mm)	-0.294	0.124	-0.050	-0.537	-0.245	0.212	0.171	-0.661
$vBMD_i$ (mg/cm^3)	-62.49	33.44	3.05	-128.04	-53.40	32.24	9.79	-116.58
$vBMD_c$ (mg/cm^3)	-176.91	46.50	-85.78	-268.04	-170.27	104.53	34.62	-375.15
$vBMD_{tr}$ (mg/cm^3)	-26.86	16.03	4.55	-58.28	-35.39	24.09	11.83	-82.60

Table XXVII. Bland-Altman limits of agreement for pMRI bone structure compared to hr-pQCT

Agreement in bone structural variables between hr-pQCT and pMRI was assessed using upper (LOAU) and lower (LOAL) limits of agreement. Mean difference (Diff) and standard deviations (SD) were used to compute 95% confidence intervals representing LOAL and LOAU values.

Bone structure variable	**Mean Diff**	**SD Diff**	**LOAU**	**LOAL**
BV/TV (fraction)	-0.370	0.034	-0.304	-0.436
Tb.Sp (mm)	-0.110	0.124	0.133	-0.353
Tb.Sp MI (mm)	-0.091	0.105	0.114	-0.297
Tb.Th (mm)	-0.497	0.054	-0.391	-0.604
Tb.Th MI (mm)	-0.493	0.054	-0.387	-0.598
Tb.N (#/mm)	1.0	0.3	1.6	0.3

5.3 Reliability: RMSCV, RMSSD, Bland-Altman (Specific aim #2)

5.3.1 Short-term test-retest precision

Of all volumetric bone measures, BV/TV was the most reproducible across all modalities followed by Tb.N, Tb.Th and then Tb.Sp (Table XXVIII-Table XXXI). Hole geometry (H_A, H_M) and Cx at the radius demonstrated the poorest reproducibility for both pQCT and pMRI. Cortical and trabecular vBMD appeared to be more reproducible than integral vBMD for pQCT at the radius. At the tibia, reproducibility of integral and trabecular vBMD were superior to cortical vBMD. Precision of model-dependent and model-independent measures of Tb.Sp and Tb.Th were nearly identical in all analyses.

Test-retest reproducibility for all volumetric bone measures appeared similar between pMRI and pQCT scans at the radius. Tibial bone variables for pQCT were, in general, more reproducible compared to radial bone variables from either pQCT or pMRI. In particular, even hole geometry and connectivity were within 10% error. In fact, H_M at the more distal slice of the radius and tibia showed precision error below 5%. Co-registration and selection of anatomically analogous pMRI slices across participants resulted in only a slight improvement in reproducibility for all but Tb.Th. Test-retest limits of agreement for BV/TV, Tb.Sp and Tb.N were similar between pMRI and pQCT. Meanwhile, hole geometry and connectivity between repeated measures agreed to a lower extent on pQCT compared to pMRI. For pQCT, volumetric bone measures from the distal slice were more reproducible than the more proximal slice.

Table XXVIII. pMRI short-term test-retest statistics for all participants' full image sets
Distal radius scans obtained twice at the same study visit were analyzed without co-registration. Root mean square coefficients of variation (RMSCV) and standard deviations (RMSSD) were reported long with Bland-Altman limits of agreement (LOA).

MRI Bone Variable	N	RMSCV	RMSSD	Mean Diff	SD Diff	Lower LOA	Upper LOA
BV/TV (fraction)	42	0.043	0.019	0.002	0.027	-0.050	0.054
Tb.Sp (mm)	42	0.079	0.066	0.014	0.094	-0.169	0.198
Tb.Sp MI (mm)	43	0.067	0.047	0.011	0.066	-0.119	0.142
Tb.Th (mm)	42	0.059	0.033	0.014	0.045	-0.075	0.103
Tb.Th MI (mm)	43	0.062	0.034	0.016	0.047	-0.076	0.107
Tb.N (#/mm)	42	0.049	0.0	0.0	0.1	-0.1	0.1
H_M (mm^2)	42	0.166	6.99	-0.65	9.98	-20.21	18.91
H_A (mm^2)	42	0.212	1.32	0.10	1.89	-3.61	3.81
Cx (index)	42	0.923	1.17	-0.02	1.68	-3.32	3.27
Tot.Ar (mm^2)	42	0.102	16.48	-1.61	23.53	-47.73	44.51
Tb.Ar (mm^2)	42	0.128	9.78	-0.77	13.97	-28.16	26.61

Table XXIX. pMRI short-term test-retest statistics for all participants' co-registered images
Distal radius scans obtained twice at the same study visit were analyzed after co-registration. Only slices that shared the same anatomical region of interest were included. Root mean square coefficients of variation (RMSCV) and standard deviations (RMSSD) were reported long with Bland-Altman limits of agreement (LOA).

MRI Bone Variable	N	RMSCV	RMSSD	Mean Diff	SD Diff	Lower LOA	Upper LOA
BV/TV (fraction)	43	0.037	0.017	0.008	0.023	-0.037	0.053
Tb.Sp (mm)	43	0.059	0.043	0.002	0.062	-0.119	0.123
Tb.Sp MI (mm)	43	0.058	0.042	0.001	0.060	-0.116	0.119
Tb.Th (mm)	43	0.070	0.043	0.018	0.059	-0.097	0.134
Tb.Th MI (mm)	43	0.070	0.043	0.018	0.059	-0.097	0.133
Tb.N (#/mm)	43	0.055	0.0	0.0	0.1	-0.1	0.1
H_M (mm^2)	43	0.234	9.91	1.66	14.08	-25.94	29.26
H_A (mm^2)	43	0.192	1.00	0.09	1.43	-2.71	2.88
Cx (index)	43	0.488	1.42	-0.21	2.03	-4.18	3.76
Tot.Ar (mm^2)	43	0.102	16.45	3.97	23.19	-41.47	49.42
Tb.Ar (mm^2)	43	0.125	9.69	3.30	13.45	-23.07	29.66

Table XXX. pQCT radius short-term test-retest statistics for all participants
Distal radius scans (proximal slice, top and distal slice, bottom) obtained twice at the same study visit were analyzed for root mean square coefficients of variation (RMSCV), standard deviations (RMSSD), and Bland-Altman limits of agreement (LOA).

Bone Variable Proximal Slice	N	RMSCV	RMSSD	Mean Diff	SD Diff	Lower LOA	Upper LOA
BV/TV (fraction)	53	0.041	0.010	0.002	0.020	-0.030	0.040
Tb.Sp (mm)	53	0.061	0.070	0.009	0.100	-0.200	0.210
Tb.Sp MI (mm)	53	0.061	0.070	0.009	0.100	-0.200	0.210
Tb.Th (mm)	53	0.039	0.010	0.001	0.020	-0.040	0.040
Tb.Th MI (mm)	53	0.039	0.010	0.001	0.020	-0.040	0.040
Tb.N (#/mm)	53	0.050	0.04	0.00	0.05	-0.11	0.11
Ct.Th (mm)	53	0.044	0.040	-0.004	0.060	-0.120	0.110
$vBMD_i$ (mg/cm^3)	54	0.046	0.060	-0.002	0.080	-0.160	0.160
$vBMD_c$ (mg/cm^3)	54	0.113	28.47	-9.41	39.51	-86.85	68.02
$vBMD_{tr}$ (mg/cm^3)	54	0.023	22.40	0.30	31.97	-62.36	62.96
H_M (mm^2)	53	0.072	9.40	-0.21	13.42	-26.51	26.10
H_A (mm^2)	53	0.175	11.98	-3.68	16.70	-36.42	29.05
Cx (index)	53	0.221	2.39	0.36	3.39	-6.28	7.01
Tb.Ar (mm^2)	54	0.093	3.28	-0.77	4.61	-9.80	8.27
Tot.Ar (mm^2)	54	0.206	30.01	-1.46	42.82	-85.39	82.46
Bone Variable Distal Slice	**N**	**RMSCV**	**RMSSD**	**Mean Diff**	**SD Diff**	**Lower LOA**	**Upper LOA**
BV/TV (fraction)	54	0.035	0.010	0.000	0.020	-0.040	0.040
Tb.Sp (mm)	54	0.041	0.030	0.000	0.040	-0.080	0.070
Tb.Sp MI (mm)	54	0.041	0.030	0.000	0.040	-0.080	0.070
Tb.Th (mm)	54	0.040	0.010	0.000	0.020	-0.040	0.030
Tb.Th MI (mm)	54	0.040	0.010	0.000	0.020	-0.040	0.030
Tb.N (#/mm)	54	0.029	0.0	0.0	0.0	-0.1	0.1
Ct.Th (mm)	54	0.050	0.040	-0.010	0.060	-0.140	0.110
$vBMD_i$ (mg/cm^3)	54	0.050	0.06	-0.01	0.08	-0.17	0.14
$vBMD_c$ (mg/cm^3)	54	0.070	18.57	-8.04	25.24	-57.50	41.42
$vBMD_{tr}$ (mg/cm^3)	54	0.030	26.12	-4.99	36.95	-77.40	67.43
H_M (mm^2)	54	0.031	5.27	-0.64	7.49	-15.32	14.04
H_A (mm^2)	54	0.205	18.08	4.87	25.34	-44.78	54.53
Cx (index)	54	0.139	0.56	-0.02	0.80	-1.60	1.55
Tb.Ar (mm^2)	54	0.348	4.86	-1.02	6.85	-14.46	12.41
Tot.Ar (mm^2)	54	0.145	36.06	9.88	50.50	-89.11	108.86

Table XXXI. pQCT tibia short-term test-retest statistics for all participants
Distal tibia scans (proximal slice, top and distal slice, bottom) obtained twice at the same study visit were analyzed for root mean square coefficients of variation (RMSCV), standard deviations (RMSSD), and Bland-Altman limits of agreement (LOA).

Bone Variable Proximal Slice	N	RMSCV	RMSSD	Mean Diff	SD Diff	Lower LOA	Upper LOA
BV/TV (fraction)	54	0.026	0.010	0.000	0.010	-0.030	0.030
Tb.Sp (mm)	54	0.033	0.020	0.000	0.030	-0.060	0.050
Tb.Sp MI (mm)	54	0.033	0.020	0.000	0.030	-0.060	0.050
Tb.Th (mm)	54	0.025	0.010	0.000	0.010	-0.030	0.030
Tb.Th MI (mm)	54	0.025	0.010	0.000	0.010	-0.030	0.030
Tb.N (#/mm)	54	0.021	0.0	0.00	0.0	-0.1	0.1
Ct.Th (mm)	54	0.050	0.070	0.010	0.090	-0.180	0.190
$vBMD_i$ (mg/cm^3)	54	0.054	0.08	0.010	0.12	-0.22	0.23
$vBMD_c$ (mg/cm^3)	54	0.088	28.72	-1.52	40.98	-81.83	78.79
$vBMD_{tr}$ (mg/cm^3)	54	0.032	30.21	-2.55	43.04	-86.91	81.81
H_M (mm^2)	54	0.082	13.30	-0.13	18.99	-37.35	37.10
H_A (mm^2)	54	0.058	13.01	-0.43	18.57	-36.83	35.97
Cx (index)	54	0.097	0.43	-0.01	0.62	-1.21	1.20
Tb.Ar (mm^2)	54	0.141	10.43	-0.03	14.89	-29.22	29.15
Tot.Ar (mm^2)	54	0.109	51.82	2.84	73.92	-142.05	147.73
Bone Variable Distal Slice	**N**	**RMSCV**	**RMSSD**	**Mean Diff**	**SD Diff**	**Lower LOA**	**Upper LOA**
BV/TV (fraction)	54	0.016	0.010	-0.001	0.010	-0.020	0.020
Tb.Sp (mm)	54	0.025	0.010	0.003	0.020	-0.030	0.040
Tb.Sp MI (mm)	54	0.025	0.010	0.003	0.020	-0.030	0.040
Tb.Th (mm)	54	0.017	0.010	0.000	0.010	-0.020	0.020
Tb.Th MI (mm)	54	0.017	0.010	0.000	0.010	-0.020	0.020
Tb.N (#/mm)	54	0.016	0.0	0.0	0.0	-0.1	0.1
Ct.Th (mm)	54	0.050	0.060	0.001	0.080	-0.160	0.160
$vBMD_i$ (mg/cm^3)	54	0.052	0.07	0.00	0.10	-0.19	0.19
$vBMD_c$ (mg/cm^3)	54	0.026	7.98	-0.79	11.36	-23.07	21.48
$vBMD_{tr}$ (mg/cm^3)	54	0.011	10.32	0.65	14.71	-28.19	29.49
H_M (mm^2)	54	0.019	3.42	-0.35	4.87	-9.90	9.20
H_A (mm^2)	54	0.088	17.34	-0.48	24.75	-48.99	48.02
Cx (index)	54	0.080	0.22	-0.07	0.31	-0.68	0.55
Tb.Ar (mm^2)	54	0.098	5.67	-0.12	8.10	-16.00	15.75
Tot.Ar (mm^2)	54	0.048	30.06	-0.81	42.91	-84.91	83.28

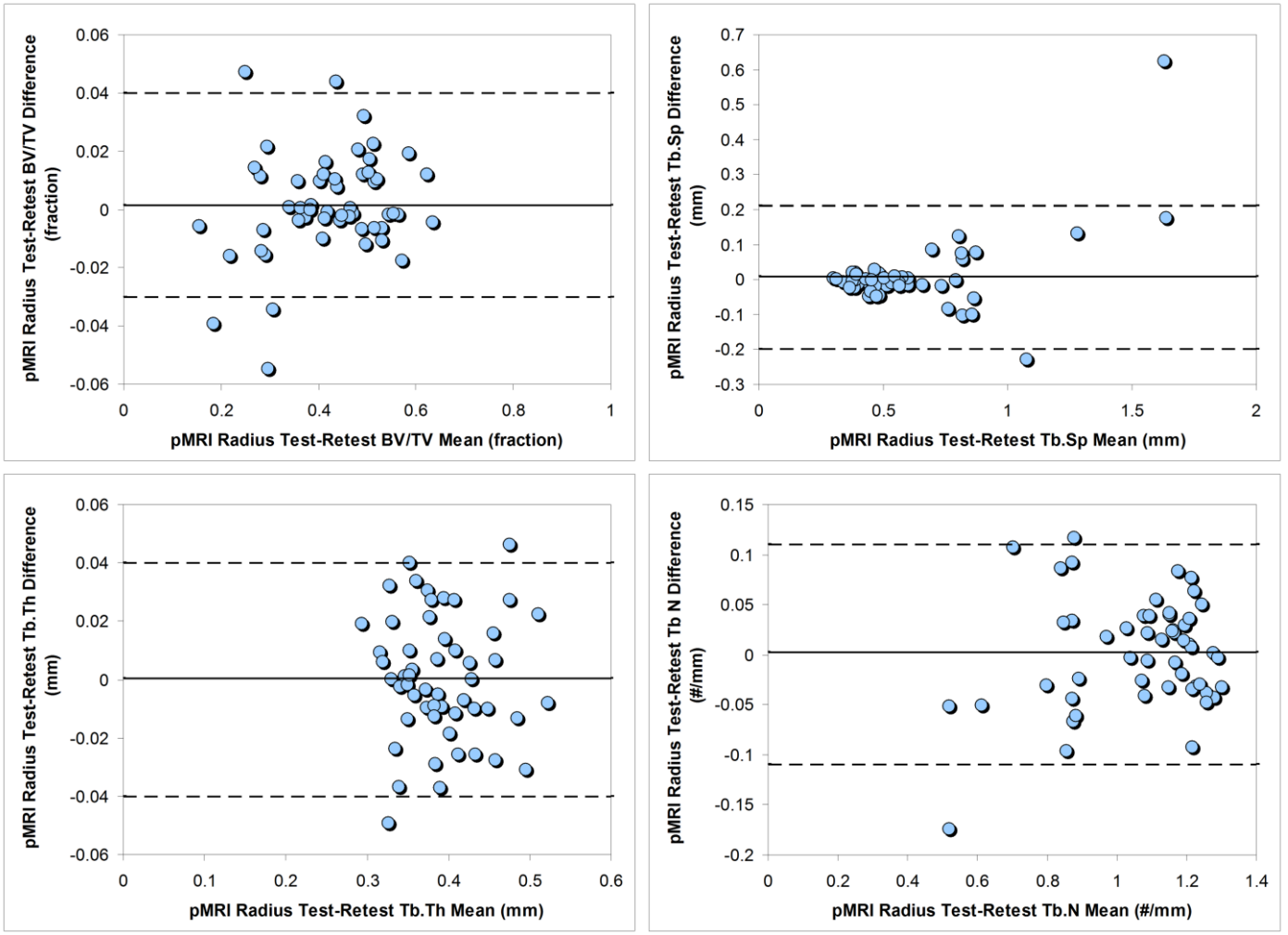

Figure 20. Bland-Altman plots of agreement between bone measures from repeated pMRI scans of the radius
Bland-Altman plots depict comparisons of pMRI radius bone structural variables between repeated scans. Dashed lines indicate upper and lower limits of agreement.

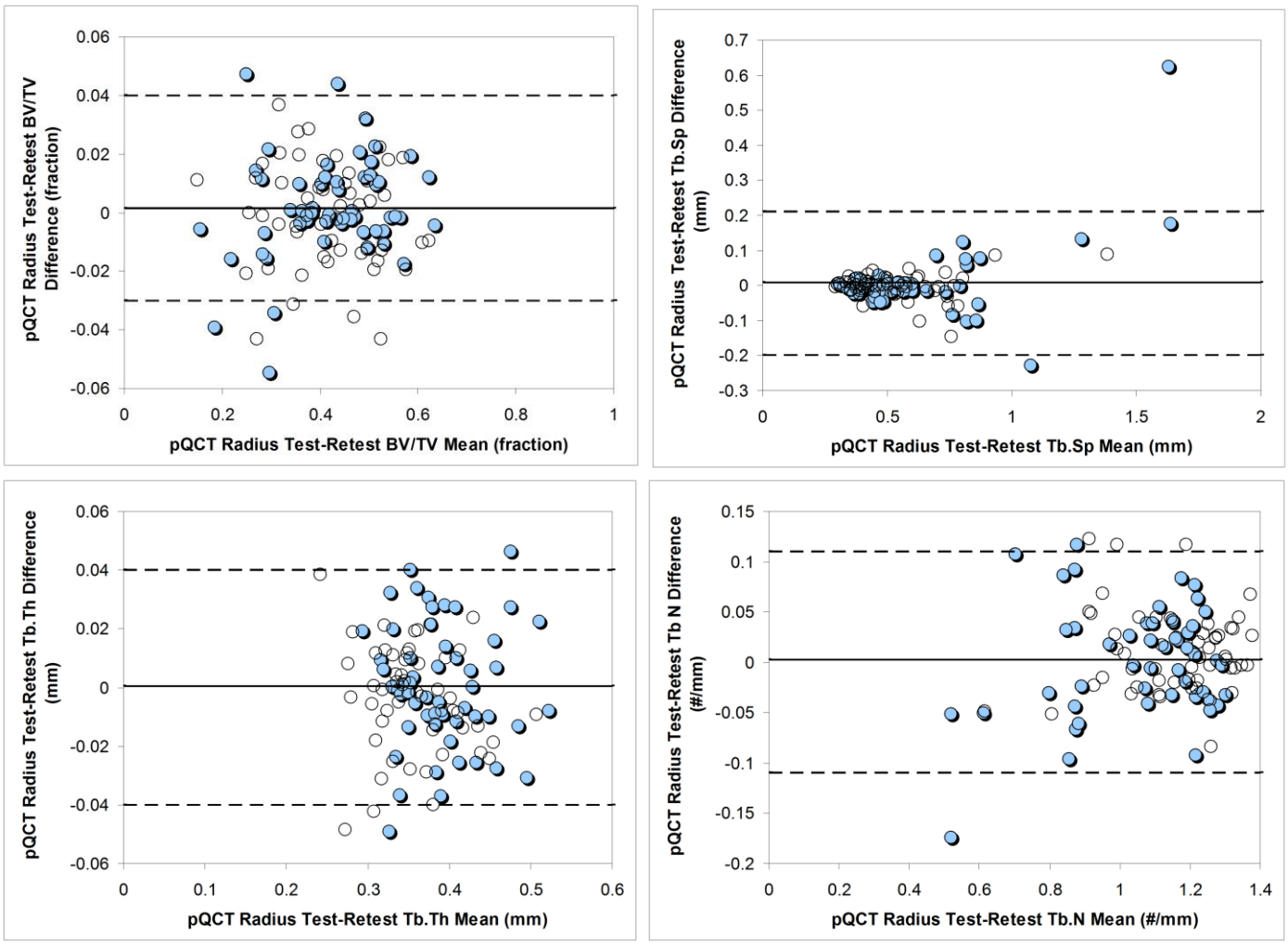

Figure 21. Bland-Altman plots of agreement between bone measures from repeated pQCT radius scans
Bland-Altman plots depicting comparisons of volumetric bone variables between repetitions of more proximal (solid circles) and more distal (open circles) pQCT radius scans. Dashed lines indicate upper and lower limits of agreement for only the proximal slice for simplicity.

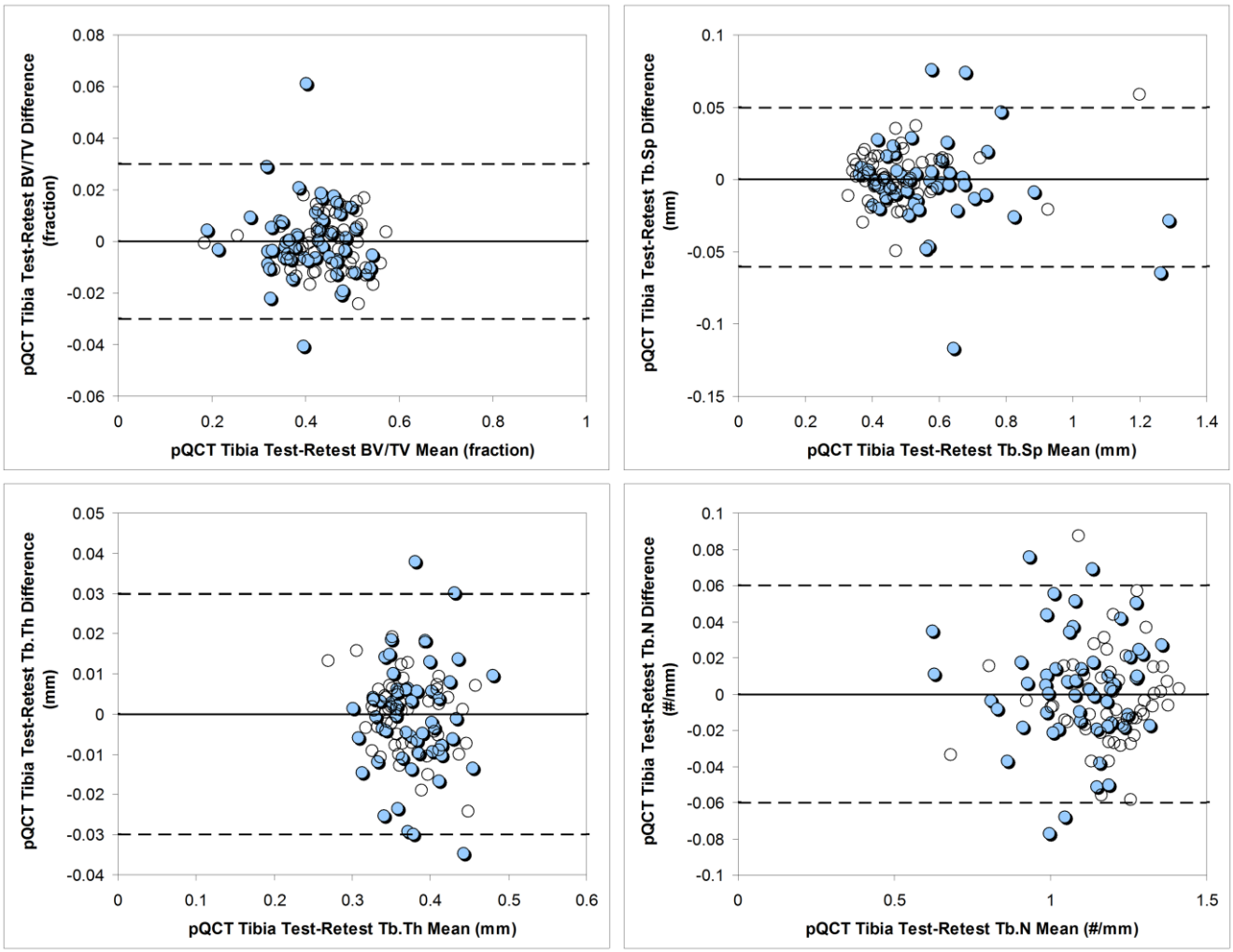

Figure 22. Bland-Altman plots of agreement between bone measures from repeated pQCT tibia scans
Bland-Altman plots depicting the comparison of volumetric bone variables between repetitions of more proximal (solid circles) and more distal (open circles) pQCT tibia slices. Dashed lines indicate upper and lower limits of agreement for only the proximal slice for simplicity.

<u>POST-HOC: Effect of co-registration on pMRI bone structure test-retest precision error</u>

After co-registering repeated pMR images with one another, the precision error was slightly reduced for most variables except for Tb.Th, Tb.N and hole geometry measures. Correspondingly, the Bland-Altman limits of agreement were also tighter. However, it should be noted that the reproducibility of the total area measurement was unaffected by co-registering the images (Table XXIX).

5.3.2 One-year follow-up long-term precision

The mean follow-up times for pMRI, pQCT and hr-pQCT were: 1.20 ± 0.14 years, 1.12 ± 0.12 years and 1.20 ± 0.15 years, respectively. The relative change over one-year was smallest for BV/TV, Tb.N and Tb.Sp (Table XXXIII- Table XXXVII). Like short-term precision, hole geometry and connectivity exhibited the largest relative change over time. For pQCT, the distal slice of the radius showed smaller changes in bone connectivity, bone density and Tb.Sp than the proximal slice, but larger changes in the overall amount of bone. Similarly for the distal slice of the tibia, all volumetric bone measures provided smaller one-year changes compared to the proximal slice. Changes at the tibia were generally smaller than any changes at the radius. However, for hr-pQCT, the opposite was true for Tb.Sp, Tb.Th and Tb.N. The integral, trabecular and cortical vBMD obtained from the more proximal pQCT slice of the radius showed a similar degree of change as one another. At the more distal slice, integral vBMD showed minimal change while one-year changes for both cortical and especially trabecular vBMD were considerably larger. At the tibia, trabecular vBMD showed larger one-year change compared to both cortical and integral vBMD at both slice locations. Differential vBMD changes were also observed for hr-pQCT images at the radius but only more mildly so at the tibia.

One-year longitudinal changes in volumetric bone measures derived from pMRI scans of the radius were similar to changes at the distal slice of the radius on pQCT images. Compared to pMRI, the proximal slice of pQCT yielded larger one-year change values. For most measures, hr-pQCT bone structure at the radius exhibited smaller one-year change values than those obtained on either pMRI or pQCT at the same site. In contrast,

Tb.N showed a larger one-year change when obtained using hr-pQCT compared to both pMRI and pQCT. One-year change in Tb.Sp was similar across all modalities.

POST-HOC: One-year change in those without fractures and not on antiresoprtives

By excluding individuals who have had a fragility fracture in the last 15 years or who were on antiresorptive therapy, the absolute change over one year was reduced for all volumetric bone measures except for H_M on pQCT and pMR images. The effect of excluding those with fractures or those on treatment was most dramatic for connectivity. For hr-pQCT, there was no change or even a slight increase in one-year change after excluding these individuals. Removing those without fractures and not taking antiresorptives did not affect the differential pattern of one-year changes in vBMD observed for pQCT or hr-pQCT at both anatomical locations.

POST-HOC: One-year change for pMRI-derived bone outcomes after co-registration

After co-registering baseline and one-year follow-up pMR images, there was only a reduced precision error for Tb.Sp, Tb.Th and Tb.N while other bone outcomes maintained a similar degree of one-year precision.

Table XXXII. pMRI one-year follow-up statistics for full image set in participants with and without fractures/on antiresorptive therapy

Distal radius scans obtained at baseline and one year later were analyzed with or without excluding participants who have had a fragility fracture or were on antiresorptive therapy. Root mean square coefficients of variation (RMSCV), standard deviations (RMSSD) and least significant change (LSC) were reported. Fx = fragility fractures.

	All Study Participants				No Fx & No Antiresorptive therapy			
Bone Variable	**N**	**RMSCV**	**RMSSD**	**LSC**	**N**	**RMSCV**	**RMSSD**	**LSC**
BV/TV (fraction)	48	0.051	0.023	0.063	17	0.037	0.018	0.049
Tb.Sp (mm)	48	0.172	0.088	0.245	17	0.067	0.042	0.116
Tb.Sp MI (mm)	48	0.169	0.081	0.224	17	0.062	0.038	0.104
Tb.Th (mm)	48	0.185	0.079	0.218	17	0.087	0.051	0.141
Tb.Th MI (mm)	48	0.185	0.078	0.215	17	0.087	0.050	0.138
Tb.N (#/mm)	48	0.170	0.5	1.4	17	0.066	0.1	0.2
H_M (mm^2)	48	0.163	6.07	16.82	17	0.181	6.85	18.98
H_A (mm^2)	48	0.215	0.97	2.69	17	0.199	0.59	1.62
Cx (index)	48	0.331	1.44	4.00	17	0.327	1.51	4.18
Tot.Ar (mm^2)	48	0.103	15.32	42.45	17	0.077	11.86	32.88
Tb.Ar (mm^2)	48	0.129	8.73	24.21	15	0.110	8.53	23.63

Table XXXIII. pMRI one-year follow-up statistics for co-registered images in participants with and without fractures/on antiresorptive therapy

Distal radius scans obtained at baseline and one year later were analyzed after co-registration and with or without excluding participants who have had a fragility fracture or were on antiresorptive therapy. Root mean square coefficients of variation (RMSCV), standard deviations (RMSSD) and least significant change (LSC) were reported. Fx = fragility fractures.

	All Study Participants				No Fx & No Antiresorptive therapy			
Bone Variable	**N**	**RMSCV**	**RMSSD**	**LSC**	**N**	**RMSCV**	**RMSSD**	**LSC**
BV/TV (fraction)	48	0.048	0.022	0.060	17	0.038	0.018	0.050
Tb.Sp (mm)	48	0.068	0.047	0.130	17	0.059	0.037	0.102
Tb.Sp MI (mm)	48	0.065	0.044	0.122	17	0.058	0.035	0.097
Tb.Th (mm)	48	0.090	0.050	0.140	17	0.071	0.039	0.109
Tb.Th MI (mm)	48	0.090	0.050	0.139	17	0.071	0.039	0.108
Tb.N (#/mm)	48	0.065	0.1	0.2	17	0.055	0.1	0.1
H_M (mm^2)	48	0.177	6.22	17.24	17	0.225	8.12	22.50
H_A (mm^2)	48	0.259	1.36	3.78	17	0.230	0.63	1.74
Cx (index)	48	0.354	1.69	4.69	17	0.273	1.49	4.13
Tot.Ar (mm^2)	48	0.114	18.04	49.99	17	0.104	15.67	43.45
Tb.Ar (mm^2)	48	0.136	10.06	27.88	17	0.120	9.40	26.06

Table XXXIV. pQCT radius one-year follow-up statistics for participants with and without fractures or on antiresorptive therapy

Distal radius pQCT scans at baseline and one year were analyzed with or without excluding participants who have had a fragility fracture or were on antiresorptive therapy. Root mean square coefficients of variation (RMSCV), standard deviations (RMSSD) and least significant change (LSC) were reported. Fx = fragility fractures.

Bone Variable	All Study Participants				No Fx & No Antiresorptive therapy			
Proximal Slice	**N**	**RMSCV**	**RMSSD**	**LSC**	**N**	**RMSCV**	**RMSSD**	**LSC**
BV/TV (fraction)	36	0.061	0.020	0.050	14	0.039	0.020	0.050
Tb.Sp (mm)	36	0.103	0.120	0.330	14	0.056	0.030	0.090
Tb.Sp MI (mm)	36	0.103	0.120	0.330	14	0.056	0.030	0.090
Tb.Th (mm)	36	0.072	0.030	0.080	14	0.046	0.020	0.050
Tb.Th MI (mm)	36	0.072	0.030	0.080	14	0.046	0.020	0.050
Tb.N (#/mm)	36	0.088	0.1	0.2	14	0.041	0.1	0.1
Ct.Th (mm)	36	0.101	0.110	0.300	14	0.076	0.080	0.210
$vBMD_i$ (mg/cm^3)	35	0.148	48.45	134.30	14	0.076	0.10	0.27
$vBMD_c$ (mg/cm^3)	35	0.191	164.18	455.08	14	0.078	27.45	76.10
$vBMD_{tr}$ (mg/cm^3)	35	0.138	19.99	55.42	14	0.178	153.50	425.49
H_M (mm^2)	36	0.134	12.29	34.08	14	0.029	4.83	13.38
H_A (mm^2)	36	0.192	2.26	6.27	14	0.105	8.77	24.32
Cx (index)	36	3.059	2.71	7.50	14	0.154	0.65	1.81
Ct.Ar (mm^2)	35	0.351	16.78	46.50	14	0.447	2.70	7.49
Tb.Ar (mm^2)	35	0.164	30.70	85.09	14	0.346	16.68	46.23
Tot.Ar (mm^2)	35	0.112	29.73	82.40	14	0.113	21.96	60.86
Distal Slice	**N**	**RMSCV**	**RMSSD**	**LSC**	**N**	**RMSCV**	**RMSSD**	**LSC**
BV/TV (fraction)	35	0.075	0.030	0.090	13	0.046	0.020	0.050
Tb.Sp (mm)	35	0.064	0.040	0.100	13	0.046	0.020	0.060
Tb.Sp MI (mm)	35	0.063	0.040	0.100	13	0.045	0.020	0.060
Tb.Th (mm)	35	0.092	0.040	0.110	13	0.050	0.020	0.050
Tb.Th MI (mm)	35	0.092	0.040	0.110	13	0.050	0.020	0.050
Tb.N (#/mm)	35	0.041	0.0	0.1	13	0.025	0.0	0.1
Ct.Th (mm)	35	0.103	0.090	0.260	13	0.108	0.110	0.290
$vBMD_i$ (mg/cm^3)	35	0.098	0.12	0.32	13	0.107	0.14	0.38
$vBMD_c$ (mg/cm^3)	35	0.156	39.30	108.94	14	0.078	20.52	56.87
$vBMD_{tr}$ (mg/cm^3)	35	0.390	259.64	719.69	14	0.400	257.78	714.53
H_M (mm^2)	35	0.118	19.33	53.58	14	0.033	5.95	16.49
H_A (mm^2)	35	0.272	27.54	76.35	13	0.230	21.01	58.23
Cx (index)	35	0.239	1.44	3.98	13	0.180	0.51	1.41
Ct.Ar (mm^2)	35	1.071	3.82	10.59	13	1.413	2.66	7.37
Tb.Ar (mm^2)	35	0.934	39.97	110.78	14	0.993	43.94	121.78
Tot.Ar (mm^2)	35	0.168	51.34	142.30	14	0.123	40.53	112.36

Table XXXV. pQCT tibia one-year follow-up statistics for participants with and without fractures/on antiresorptive therapy

Distal tibia scans at baseline and one year were analyzed with and without excluding participants who have had a fragility fracture or were on antiresorptive therapy. Root mean square coefficients of variation (RMSCV), standard deviations (RMSSD) and least significant change (LSC) were reported. Fx = fragility fractures.

Bone Variable	**All Study Participants**				**No Fx & No Antiresorptive therapy**			
Proximal Slice	**N**	**RMSCV**	**RMSSD**	**LSC**	**N**	**RMSCV**	**RMSSD**	**LSC**
BV/TV (fraction)	36	0.028	0.010	0.030	14	0.022	0.010	0.030
Tb.Sp (mm)	36	0.036	0.020	0.060	14	0.030	0.020	0.050
Tb.Sp MI (mm)	36	0.036	0.020	0.070	14	0.030	0.020	0.050
Tb.Th (mm)	36	0.030	0.010	0.030	14	0.023	0.010	0.030
Tb.Th MI (mm)	36	0.030	0.010	0.030	14	0.023	0.010	0.030
Tb.N (#/mm)	36	0.024	0.0	0.1	14	0.020	0.0	0.1
Ct.Th (mm)	36	0.049	0.070	0.190	14	0.045	0.060	0.170
$vBMD_i$ (mg/cm^3)	36	0.051	0.08	0.22	14	0.047	0.07	0.21
$vBMD_c$ (mg/cm^3)	36	0.119	36.11	100.10	14	0.056	19.92	55.22
$vBMD_{tr}$ (mg/cm^3)	36	0.100	85.74	237.65	14	0.077	67.00	185.70
H_M (mm^2)	36	0.095	14.34	39.76	14	0.040	6.42	17.79
H_A (mm^2)	36	0.054	11.54	31.97	14	0.074	16.24	45.01
Cx (index)	36	0.105	0.65	1.79	14	0.076	0.13	0.36
Ct.Ar (mm^2)	36	1.944	1.88	5.20	14	2.074	1.27	3.52
Tb.Ar (mm^2)	36	0.226	19.40	53.77	14	0.156	15.62	43.29
Tot.Ar (mm^2)	36	0.115	54.65	151.47	14	0.092	33.75	93.55
Distal Slice	**N**	**RMSCV**	**RMSSD**	**LSC**	**N**	**RMSCV**	**RMSSD**	**LSC**
BV/TV (fraction)	36	0.020	0.010	0.020	14	0.019	0.010	0.020
Tb.Sp (mm)	36	0.026	0.010	0.030	14	0.023	0.010	0.030
Tb.Sp MI (mm)	36	0.026	0.010	0.030	14	0.023	0.010	0.030
Tb.Th (mm)	36	0.020	0.010	0.020	14	0.021	0.010	0.020
Tb.Th MI (mm)	36	0.020	0.010	0.020	14	0.021	0.010	0.020
Tb.N (#/mm)	36	0.015	0.0	0.1	14	0.013	0.0	0.0
Ct.Th (mm)	36	0.047	0.050	0.150	14	0.052	0.060	0.170
$vBMD_i$ (mg/cm^3)	36	0.048	0.06	0.18	14	0.053	0.07	0.20
$vBMD_c$ (mg/cm^3)	36	0.023	7.39	20.48	14	0.025	8.09	22.42
$vBMD_{tr}$ (mg/cm^3)	36	0.167	130.31	361.21	14	0.141	112.23	311.07
H_M (mm^2)	36	0.021	3.79	10.50	14	0.016	2.88	7.99
H_A (mm^2)	36	0.072	15.36	42.59	14	0.077	17.94	49.72
Cx (index)	36	0.089	0.34	0.93	14	0.064	0.11	0.31
Ct.Ar (mm^2)	36	1.110	1.67	4.64	14	0.710	1.30	3.59
Tb.Ar (mm^2)	36	0.380	28.61	79.30	14	0.320	27.88	77.28
Tot.Ar (mm^2)	36	0.030	18.23	50.53	14	0.038	22.13	61.34

Table XXXVI. hr-pQCT radius one-year follow-up statistics for participants with and without fractures/on antiresorptive therapy

Distal radius scans at baseline and one year were analyzed with or without excluding participants who have had a fragility fracture or were on antiresorptive therapy. Root mean square coefficients of variation (RMSCV), standard deviations (RMSSD) and least significant change (LSC) were reported. Fx = fragility fractures.

	All Study Participants				No Fx & No Antiresorptive therapy			
Bone Variable	**N**	**RMSCV**	**RMSSD**	**LSC**	**N**	**RMSCV**	**RMSSD**	**LSC**
BV/TV (fraction)	40	0.026	0.002	0.007	13	0.017	0.002	0.006
Tb.Sp MI (mm)	40	0.062	0.038	0.106	13	0.068	0.032	0.088
Tb.Th MI (mm)	40	0.047	0.003	0.008	13	0.055	0.003	0.009
Tb.N (#/mm)	40	0.060	0.1	0.3	13	0.067	0.1	0.4
Ct.Th (mm)	40	0.056	0.037	0.102	13	0.055	0.038	0.104
$vBMD_i$ (mg/cm^3)	40	0.024	6.73	18.64	13	0.025	7.34	20.36
$vBMD_c$(mg/cm^3)	40	0.019	15.23	42.21	13	0.017	13.37	37.06
$vBMD_{tr}$ (mg/cm^3)	40	0.025	2.78	7.70	13	0.018	2.64	7.32
Ct.Ar (mm^2)	40	0.050	2.29	6.34	13	0.053	2.55	7.07
Tb.Ar (mm^2)	40	0.010	1.82	5.05	13	0.011	2.25	6.23

Table XXXVII. hr-pQCT tibia one-year follow-up statistics for participants with and without fractures/on antiresorptive therapy

Distal tibia scans at baseline and one year were analyzed with or without excluding participants who have had a fragility fracture or were on antiresorptive therapy. Root mean square coefficients of variation (RMSCV), standard deviations (RMSSD) and least significant change (LSC) were reported. Fx = fragility fractures.

	All Study Participants				No Fx & No Antiresorptive therapy			
Bone Variable	**N**	**RMSCV**	**RMSSD**	**LSC**	**N**	**RMSCV**	**RMSSD**	**LSC**
BV/TV (fraction)	40	0.020	0.002	0.005	13	0.010	0.001	0.003
Tb.Sp MI (mm)	40	0.077	0.040	0.112	13	0.081	0.041	0.113
Tb.Th MI (mm)	40	0.075	0.006	0.015	13	0.081	0.006	0.015
Tb.N (#/mm)	40	0.077	0.1	0.4	13	0.081	0.2	0.4
Ct.Th (mm)	40	0.032	0.024	0.068	13	0.025	0.024	0.067
$vBMD_i$ (mg/cm^3)	40	0.013	2.75	7.63	13	0.007	1.96	5.44
$vBMD_c$(mg/cm^3)	40	0.011	8.54	23.68	13	0.007	5.87	16.27
$vBMD_{tr}$ (mg/cm^3)	40	0.019	2.23	6.18	13	0.009	1.31	3.64
Ct.Ar (mm^2)	40	0.033	2.46	6.81	13	0.025	2.57	7.12
Tb.Ar (mm^2)	40	0.004	2.01	5.57	13	0.004	2.28	6.31

5.4 Detection limits & clinical sensitivity (Specific aim #3)

5.4.1 Detection limits: Standard error of the estimate

Standard errors of the estimate for apparent trabecular structure for pQCT radius images were smaller than for pMR images but the opposite was true for hole geometry and connectivity. Bone measures' SEE obtained from pQCT and pMR images were more comparable after excluding individuals with a history of fragility fractures and those currently on antiresorptive therapy. All but Tb.N's SEEs were smaller when obtained

Table XXXVIII. Comparison of radius bone variables' standard errors of the estimate for all modalities
Standard errors of the estimate (SEE) were determined from linear regression models for baseline and follow-up radius volumetric bone variables with (white header) and without (black header) including individuals who have had a fragility fracture in the last 15 years or who were on antiresorptive therapy.

Bone Variable	pMRI SEE (N=46)	pMRI SEE (N=15)	pQCT SEE (N=34)	pQCT SEE (N=12)	Hr-pQCT SEE (N=38)	Hr-pQCT SEE (N=11)
BV/TV (fraction)	0.026	0.018	0.028	0.023	0.003	0.003
Tb.Sp (mm)	0.060	0.040	0.166	0.038		
Tb.Sp MI (mm)	0.054	0.038	0.166	0.038	0.050	0.039
Tb.Th (mm)	0.050	0.046	0.038	0.026		
Tb.Th MI (mm)	0.050	0.046	0.038	0.026	0.004	0.004
Tb.N (#/mm)	0.1	0.1	0.1	0.1	0.1	0.2
Ct.Th (mm)			0.142	0.095	0.032	0.028
$vBMD_i$ (mg/cm^3)			60.99	37.88	5.27	5.53
$vBMD_c$ (mg/cm^3)			83.02	61.32	17.00	12.17
$vBMD_{tr}$ (mg/cm^3)			26.15	6.93	4.01	4.00
H_M (mm^2)	8.28	9.84	17.55	13.40		
H_A (mm^2)	1.85	0.53	2.34	0.58		
Cx (index)	1.85	1.52	3.71	3.58		
Ct.Ar (mm^2)			8.71	5.79		
Tb.Ar (mm^2)	12.69	13.20	41.59	31.79	1.98	2.01
Tot.Ar (mm^2)	22.87	22.84	40.59	33.99	1.79	2.08

using hr-pQCT as compared to both pMRI and pQCT by as much as double. However, excluding those with fractures or on antiresorptives resulted in trabecular vBMD values obtained by pQCT that was similar to hr-pQCT at the radius. At the tibia, similar differences in SEE magnitudes can be described between hr-pQCT versus pQCT images. However, Tb.Sp measured on pQCT at the tibia showed over three fold smaller SEEs compared to hr-pQCT. In contrast to the radius, exclusion of women with fractures or who were taking antiresorptive therapy did not made a considerable difference in the SEE values obtained at the tibia for either pQCT or hr-pQCT.

Table XXXIX. Comparison of tibia bone variables' standard errors of the estimate for all modalities

Standard errors of the estimate (SEE) were determined from linear regression models for baseline and follow-up tibia volumeric bone variables with (white header) and without (black header) including individuals who have had a fragility fracture in the last 15 years or who were on antiresorptive therapy.

Bone Variable	pQCT SEE (N=34)	pQCT SEE (N=12)	Hr-pQCT SEE (N=38)	Hr-pQCT SEE (N=11)
BV/TV (fraction)	0.011	0.011	0.003	0.002
Tb.Sp (mm)	0.015	0.013		
Tb.Sp MI (mm)	0.015	0.013	0.057	0.047
Tb.Th (mm)	0.011	0.012		
Tb.Th MI (mm)	0.011	0.012	0.007	0.007
Tb.N (#/mm)	0.02	0.02	0.19	0.19
Ct.Th (mm)	0.070	0.090	0.03	0.03
$vBMD_i$ (mg/cm^3)	10.37	10.72	3.67	2.63
$vBMD_c$ (mg/cm^3)	111.45	82.96	11.75	8.58
$vBMD_{tr}$ (mg/cm^3)	5.25	4.25	2.97	1.56
H_M (mm^2)	21.79	22.14		
H_A (mm^2)	0.32	0.11		
Cx (index)	2.26	1.78		
Ct.Ar (mm^2)	23.63	24.73	2.99	3.15
Tb.Ar (mm^2)	25.36	29.05	2.24	2.79
Tot.Ar (mm^2)	28.62	29.37		

Table XL. Comparison of radius bone variables' LSC for all modalities
Least significant change (LSC) values for baseline and follow-up radius bone variables with (white header) and without (black header) including individuals who have had a fragility fracture in the last 15 years or who were on antiresorptive therapy.

Bone Structural Variable	MRI LSC (N=48)	MRI LSC (N=17)	pQCT LSC (N=36)	pQCT LSC (N=14)	hr-pQCT LSC (N=40)	Hr-pQCT LSC (N=13)
BV/TV (fraction)	0.060	0.050	0.050	0.050	0.007	0.006
Tb.Sp (mm)	0.130	0.102	0.330	0.090		
Tb.Sp MI (mm)	0.122	0.097	0.330	0.090	0.106	0.088
Tb.Th (mm)	0.140	0.109	0.080	0.050		
Tb.Th MI (mm)	0.139	0.108	0.080	0.050	0.008	0.009
Tb.N (#/mm)	0.2	0.1	0.2	0.1	0.3	0.4
Ct.Th (mm)			0.300	0.210	0.102	0.104
vBMDi (mg/cm^3)			134.30	0.270	18.64	20.36
vBMDc (mg/cm^3)			455.08	76.10	42.21	37.06
vBMDtr (mg/cm^3)			55.42	425.49	7.70	7.32
H_M (mm^2)	17.24	22.50	34.08	13.38		
H_A (mm^2)	3.78	1.74	6.27	24.32		
Cx (index)	4.69	4.13	7.50	1.81		
Ct.Ar (mm^2)			46.50	7.49		
Tb.Ar (mm^2)			85.09	46.23	5.05	6.23
Tot.Ar (mm^2)	49.99	43.45	82.40	60.86	0.00	0.00

5.4.2 Clinical sensitivity: Least significant change

The same inter-modality differences were notable for LSC values as for SEE values. However, LSC for hole geometry and connectivity as measured from pQCT images became as small as or even smaller than those obtained from pMR images after excluding those with fractures or on antiresorptive therapy. The pattern of differential vBMD changes over one year for integral, cortical and trabecular computations mirrored the observations for SEE. Exclusion of women with fractures or on antiresorptives resulted in accentuation of the differential patterns in LSC values for vBMD for pQCT radius images.

This same pattern was observed from pQCT images of the tibia. Like SEEs, the LSC for model-independent Tb.Sp was comparable across modalities. In general, LSC values were at least twice the magnitude of SEE values (Table XXXVIII to Table XLI).

Table XLI. Comparison of tibia bone variables' LSC for all modalities
Least significant change (LSC) values for baseline and follow-up tibia bone variables with (white header) and without (black header) including individuals who have had a fragility fracture in the last 15 years or who were on antiresorptive therapy.

Bone Structural Variable	pQCT LSC (N=36)	pQCT LSC (N=14)	hr-pQCT LSC (N=40)	Hr-pQCT LSC (N=13)
BV/TV (fraction)	0.030	0.030	0.005	0.003
Tb.Sp (mm)	0.060	0.050		
Tb.Sp MI (mm)	0.070	0.050	0.112	0.113
Tb.Th (mm)	0.030	0.030		
Tb.Th MI (mm)	0.030	0.030	0.015	0.015
Tb.N (#/mm)	0.1	0.1	0.4	0.4
Ct.Th (mm)	0.190	0.170	0.068	0.067
vBMDi (mg/cm^3)	0.22	0.21	7.63	5.44
vBMDc (mg/cm^3)	100.10	55.22	23.68	16.27
vBMDtr (mg/cm^3)	237.65	185.70	6.18	3.64
H_M (mm^2)	39.76	17.79		
H_A (mm^2)	31.97	45.01		
Cx (index)	1.79	0.36		
Ct.Ar (mm^2)	5.20	3.52	6.81	7.12
Tb.Ar (mm^2)	53.77	43.29	5.57	6.31
Tot.Ar (mm^2)	151.47	93.55		

5.4.3 Clinical sensitivity: disease odds

Neither MRI nor pQCT yielded any bone outcomes that were significantly associated with individuals with a history of fragility fractures in the local cohort examined. For hr-pQCT, decrease in Ct.Th by an amount equivalent to the SD, LSC or SEE at the radius and tibia was associated with between 9 to 85% increase in the odds for a fragility fracture. Similarly, one unit SD, LSC or SEE decrease in cortical vBMD was associated with up to 86% increase in the odds for a fragility fracture. Although MRI did not generate any cortical measurements, pQCT-derived Ct.Th at the radius and tibia both showed ORs over 1.10 with confidence intervals erring towards a higher OR value but still crossed just below 1.00 and therefore did not reach significance. The similar case was true for pQCT-image-derived cortical vBMD at the tibia but not at the radius. Radius and tibia differences in fracture odds were apparent for many measures. For example, for Ct.Th obtained using hr-pQCT at the radius, a single unit decrease in the clinical LSC (0.104 mm) was associated with a 45% increase in the odds for a fragility fracture. For the tibia with a clinical LSC of 0.067 mm, a one unit decrease in Ct.Th would result in only 13% increase in the odds for a fragility fracture. Odds per difference in SD, LSC or SEE all demonstrated a similar finding but yielded different magnitudes of odds.

Table XLII. pMRI radius bone variables' association with fragility fractures
Magnitude of fracture odds associated with each standard deviation (SD), least significant change (LSC) or standard error of estimate (SEE) increase (+) or decrease (-) in radius bone variables obtained from pMR images was determined using a binary logistic regression model. Models were examined with and without adjusting for age. CI = 95% confidence interval (lower, upper).

	Unadjusted			Age-Adjusted		
Bone Variable	**OR(CI) per SD**	**OR(CI) per LSC**	**OR(CI) per SEE**	**OR(CI) per SD**	**OR(CI) per LSC**	**OR(CI) per SEE**
BV/TV (fraction)	1.04 (0.69,1.58)	1.04 (0.69,1.58)	1.02 (0.88,1.18)	0.94 (0.61,1.46)	0.94 (0.61,1.45)	0.98 (0.84,1.14)
Tb.Sp (mm)	1.17 (0.75,1.82)	1.08 (0.87,1.33)	1.03 (0.95,1.12)	1.07 (0.67,1.70)	1.03 (0.82,1.29)	1.01 (0.93,1.10)
Tb.Sp MI (mm)	1.16 (0.75,1.80)	1.09 (0.85,1.40)	1.04 (0.94,1.14)	1.06 (0.66,1.68)	1.03 (0.79,1.35)	1.01 (0.91,1.12)
Tb.Th (mm)	0.67 (0.43,1.05)	0.31 (0.08,1.16)	0.61 (0.35,1.07)	0.63 (0.39,1.03)	0.26 (0.06,1.08)	0.57 (0.31,1.03)
Tb.Th MI (mm)	0.70 (0.45,1.08)	0.34 (0.09,1.26)	0.64 (0.36,1.10)	0.66 (0.41,1.06)	0.29 (0.07,1.17)	0.59 (0.33,1.07)
Tb.N (#/mm)	1.25 (0.81,1.92)	1.32 (0.77,2.28)	1.13 (0.89,1.42)	1.18 (0.75,1.86)	1.23 (0.69,2.19)	1.09 (0.85,1.40)
H_M (mm^2)	1.10 (0.73,1.68)	1.16 (0.63,2.14)	1.07 (0.82,1.40)	1.03 (0.67,1.60)	1.05 (0.55,1.99)	1.02 (0.77,1.35)
H_A (mm^2)	0.99 (0.66,1.48)	0.99 (0.76,1.30)	1.00 (0.92,1.08)	0.94 (0.62,1.44)	0.96 (0.73,1.27)	0.99 (0.91,1.08)
Cx (index)	1.11 (0.74,1.68)	1.16 (0.66,2.02)	1.06 (0.86,1.30)	1.10 (0.72,1.69)	1.14 (0.64,2.03)	1.05 (0.85,1.30)

Table XLIII. pQCT radius bone variables' association with fragility fractures
Magnitude of odds for fragility fractures associated with each standard deviation (SD), least significant change (LSC) or standard error of estimate (SEE) increase (+) or decrease (-) in radius bone variables obtained from pQCT images was determined with a binary logistic regression model. Models were examined with and without adjusting for age. CI = 95% confidence interval (lower, upper).

	Unadjusted			Age-Adjusted		
Bone Variable	**OR(CI) per SD**	**OR(CI) per LSC**	**OR(CI) per SEE**	**OR(CI) per SD**	**OR(CI) per LSC**	**OR(CI) per SEE**
BV/TV (fraction)	0.91 (0.53,1.56)	0.96 (0.75,1.22)	0.98 (0.88,1.10)	0.84 (0.48,1.48)	0.92 (0.72,1.19)	0.96 (0.86,1.08)
Tb.Sp (mm)	1.08 (0.63,1.86)	1.03 (0.85,1.24)	1.01 (0.94,1.09)	0.96 (0.54,1.72)	0.99 (0.81,1.20)	1.00 (0.92,1.08)
Tb.Sp MI (mm)	1.08 (0.63,1.86)	1.03 (0.85,1.24)	1.01 (0.94,1.09)	0.96 (0.54,1.72)	0.99 (0.81,1.20)	1.00 (0.92,1.08)
Tb.Th (mm)	0.64 (0.36,1.15)	0.67 (0.39,1.13)	0.81 (0.62,1.07)	0.66 (0.36,1.18)	0.68 (0.40,1.16)	0.82 (0.62,1.08)
Tb.Th MI (mm)	0.64 (0.36,1.15)	0.67 (0.39,1.13)	0.81 (0.62,1.07)	0.66 (0.36,1.18)	0.68 (0.40,1.16)	0.82 (0.62,1.08)
Tb.N (#/mm)	1.18 (0.68,2.03)	1.11 (0.79,1.55)	1.05 (0.89,1.25)	1.04 (0.58,1.86)	1.03 (0.71,1.47)	1.01 (0.84,1.21)
Ct.Th (mm)	1.18 (0.69,2.02)	1.33 (0.53,3.35)	1.14 (0.75,1.73)	1.05 (0.60,1.86)	1.09 (0.41,2.92)	1.04 (0.67,1.62)
$vBMD_i$ (mg/cm^3)	1.12 (0.66,1.92)	1.00 (1.00,1.00)	1.07 (0.79,1.44)	1.02 (0.58,1.79)	1.00 (1.00,1.00)	1.01 (0.74,1.38)
$vBMD_c$ (mg/cm^3)	1.02 (0.60,1.74)	1.02 (0.58,1.79)	1.02 (0.65,1.60)	1.00 (0.58,1.73)	1.00 (0.56,1.78)	1.00 (0.63,1.59)
$vBMD_{tr}$ (mg/cm^3)	1.10 (0.64,1.88)	1.16 (0.48,2.81)	1.02 (0.91,1.14)	1.02 (0.58,1.80)	1.03 (0.41,2.61)	1.00 (0.89,1.13)
H_M (mm^2)	0.85 (0.50,1.45)	0.96 (0.82,1.11)	0.96 (0.82,1.11)	0.78 (0.45,1.38)	0.93 (0.80,1.09)	0.93 (0.80,1.10)
H_A (mm^2)	1.06 (0.61,1.86)	1.28 (0.14,11.49)	1.01 (0.95,1.06)	0.97 (0.54,1.74)	0.89 (0.09,8.98)	1.00 (0.94,1.05)
Cx (index)	0.71 (0.41,1.23)	0.95 (0.88,1.03)	0.90 (0.77,1.06)	0.70 (0.39,1.23)	0.95 (0.87,1.03)	0.90 (0.76,1.06)

Table XLIV. pQCT tibia bone variables' association with fragility fractures
Magnitude of odds for fragility fractures associated with each standard deviation (SD), least significant change (LSC) or standard error of estimate (SEE) increase (+) or decrease (-) in tibia bone variables obtained on pQCT was determined with a binary logistic regression model. Models were examined with and without adjusting for age. CI = 95% confidence interval (lower, upper).

	Unadjusted			Age-Adjusted		
Bone Variable	**OR(CI) per SD**	**OR(CI) per LSC**	**OR(CI) per SEE**	**OR(CI) per SD**	**OR(CI) per LSC**	**OR(CI) per SEE**
BV/TV (fraction)	0.94 (0.55,1.60)	0.97 (0.78,1.22)	0.99 (0.91,1.07)	0.88 (0.50,1.54)	0.95 (0.75,1.20)	0.98 (0.90,1.07)
Tb.Sp (mm)	1.10 (0.63,1.90)	1.03 (0.85,1.26)	1.01 (0.96,1.06)	0.98 (0.55,1.77)	1.00 (0.81,1.23)	1.00 (0.94,1.06)
Tb.Sp MI (mm)	1.10 (0.63,1.90)	1.03 (0.85,1.26)	1.01 (0.96,1.06)	0.98 (0.55,177)	0.99 (0.80,1.23)	1.00 (0.94,1.06)
Tb.Th (mm)	0.79 (0.46,1.36)	0.84 (0.56,1.26)	0.93 (0.79,1.10)	0.78 (0.44,1.37)	0.83 (0.55,1.26)	0.93 (0.78,1.10)
Tb.Th MI (mm)	0.79 (0.46,1.36)	0.84 (0.56,1.26)	0.93 (0.79,1.10)	0.78 (0.44,1.37)	0.83 (0.55,1.26)	0.93 (0.78,1.10)
Tb.N (#/mm)	1.20 (0.69,2.09)	1.08 (0.85,1.39)	1.03 (0.95,1.12)	1.11 (0.61,2.02)	1.05 (0.80,1.37)	1.02 (0.93,1.11)
Ct.Th (mm)	1.24 (0.72,2.13)	1.23 (0.73,2.10)	1.12 (0.84,1.48)	1.15 (0.65,2.04)	1.15 (0.66,2.01)	1.08 (0.80,1.45)
$vBMD_i$ (mg/cm^3)	1.13 (0.66,1.93)	1.00 (1.00,1.00)	1.02 (0.92,1.14)	1.02 (0.57,1.80)	1.00 (1.00,1.00)	1.00 (0.89,1.13)
$vBMD_c$ (mg/cm^3)	1.37 (0.75,2.52)	1.35 (0.76,2.41)	1.58 (0.66,3.75)	1.26 (0.71,2.24)	1.24 (0.72,2.16)	1.39 (0.61,3.17)
$vBMD_{tr}$ (mg/cm^3)	1.03 (0.60,1.76)	1.26 (0.02,80.5)	1.00 (0.91,1.11)	0.97 (0.55,1.72)	0.81 (0.01,68.5)	1.00 (0.90,1.10)
H_M (mm^2)	1.00 (0.59,1.71)	1.00 (0.93,1.08)	1.00 (0.91,1.10)	0.97 (0.55,1.71)	1.00 (0.92,1.08)	1.00 (0.90,1.10)
H_A (mm^2)	1.07 (0.61,1.87)	3.24 (0.00,99.9)	1.00 (0.98,1.03)	0.95 (0.53,1.70)	0.44 (0.00,99.9)	1.00 (0.97,1.02)
Cx (index)	0.85 (0.50,1.45)	0.99 (0.97,1.02)	0.97 (0.87,1.08)	0.83 (0.47,1.44)	0.99 (0.97,1.01)	0.96 (0.86,1.07)

Table XLV. hr-pQCT bone variables' association with fragility fractures
Magnitude of odds for fragility fractures associated with each standard deviation (SD), least significant change (LSC) or standard error of estimate (SEE) increase (+) or decrease (-) in bone variables obtained from pQCT images was determined with a binary logistic regression model. Models were examined with and without adjusting for age. CI = 95% confidence interval (lower, upper). Bold indicates significant statistic at $p < 0.05$.

	Unadjusted			**Age-Adjusted**		
Radius Variable	**OR(CI) per SD**	**OR(CI) per LSC**	**OR(CI) per SEE**	**OR(CI) per SD**	**OR(CI) per LSC**	**OR(CI) per SEE**
BV/TV (fraction)	0.90 (0.55,1.46)	0.98 (0.90,1.08)	0.99 (0.95,1.04)	0.85 (0.52,1.41)	0.97 (0.88,1.07)	0.98 (0.94,1.03)
Tb.Sp MI (mm)	0.88 (0.54,1.42)	1.07 (0.84,1.37)	1.03 (0.92,1.15)	0.78 (0.46,1.31)	1.13 (0.87,1.48)	1.06 (0.94, 1.19)
Tb.Th MI (mm)	0.97 (0.59,1.57)	0.97 (0.64,1.47)	0.99 (0.82,1.19)	0.99 (0.60,1.65)	0.99 (0.64,1.53)	1.00 (0.82,1.21)
Tb.N (#/mm)	0.87 (0.54,1.42)	0.88 (0.55,1.40)	0.94 (0.76,1.17)	0.78 (0.47,1.31)	0.79 (0.48,1.29)	0.90 (0.71,1.13)
Ct.Th (mm)	**1.85 (1.08,3.17)**	**1.45 (1.05,2.00)**	**1.10 (1.01,1.20)**	**1.74 (1.00,3.04)**	**1.40 (1.00,1.95)**	**1.09 (1.00,1.20)**
$vBMD_i$ (mg/cm^3)	1.42 (0.86,2.36)	1.13 (0.95,1.35)	1.03 (0.98,1.08)	1.33 (0.79,2.25)	1.10 (0.92,1.33)	1.03 (0.98,1.08)
$vBMD_c$ (mg/cm^3)	**1.86 (1.06,3.26)**	**1.42 (1.03,1.96)**	**1.12 (1.01,1.25)**	1.74 (0.97,3.12)	1.37 (0.98,1.91)	1.11 (0.99,1.24)
$vBMD_{tr}$ (mg/cm^3)	0.90 (0.56,1.47)	0.98 (0.89,1.08)	0.99 (0.94,1.04)	0.86 (0.52,1.42)	0.97 (0.88,1.07)	0.98 (0.93,1.04)
Tibia Variable	**OR(CI) per SD**	**OR(CI) per LSC**	**OR(CI) per SEE**	**OR(CI) per SD**	**OR(CI) per LSC**	**OR(CI) per SEE**
BV/TV (fraction)	0.90 (0.55,1.46)	0.99 (0.94,1.04)	0.99 (0.96,1.03)	0.84 (0.51,1.39)	0.98 (0.94,1.03)	0.99 (0.96,1.02)
Tb.Sp MI (mm)	0.97 (0.60,1.57)	1.02 (0.80,1.29)	1.01 (0.91,1.11)	0.89 (0.54,1.46)	1.06 (0.83,1.35)	1.02 (0.93,1.13)
Tb.Th MI (mm)	1.22 (0.74,2.01)	1.23 (0.73,2.08)	1.10 (0.86,1.41)	1.26 (0.75,2.13)	1.28 (0.74,2.21)	1.12 (0.87,1.45)
Tb.N (#/mm)	0.87 (0.54,1.42)	0.86 (0.51,1.46)	0.93 (0.73,1.19)	0.78 (0.47,1.30)	0.76 (0.44,1.33)	0.88 (0.68,1.14)
Ct.Th (mm)	1.72 (0.99,2.97)	**1.13 (1.00,1.27)**	**1.06 (1.00,1.11)**	1.60 (0.90,2.84)	1.11 (0.98,1.26)	1.05 (0.99,1.11)
$vBMD_i$ (mg/cm^3)	1.31 (0.78,2.20)	1.03 (0.98,1.08)	1.01 (0.99,1.04)	1.20 (0.69,2.06)	1.02 (0.97,1.07)	1.01 (0.98,1.03)
$vBMD_c$ (mg/cm^3)	**3.28 (1.16,9.34)**	**1.18 (1.02,1.37)**	**1.09 (1.01,1.18)**	3.05 (0.99,9.39)	**1.17 (1.00,1.37)**	**1.09 (1.00,1.18)**
$vBMD_{tr}$ (mg/cm^3)	0.90 (0.55,1.46)	0.99 (0.94,1.04)	1.00 (0.98,1.02)	0.84 (0.51,1.39)	0.98 (0.93,1.03)	0.99 (0.97,1.01)

NATIONAL STUDY RESULTS:

5.5 Descriptive statistics and diagnostics (Specific aim #4)

5.5.1 Study participant characteristics

At the time of analyses, only age, BMI and fractures history information was available in addition to the volumetric bone outcomes for hr-pQCT and pQCT. For pQCT, apparent microstructural analyses have yet to be performed so the following represents data for

Table XLVI. National cohort: hr-pQCT bone variables' normality and data distribution. Kolmogorov-Smirnov test of normality determined whether variable was suitable to be used in parametric or non-parametric statistical models.

Radius Variable	Skewness	Kurtosis	Norm	P-value	Parametric
BV/TV	0.059	-0.163	0.995	0.528	Yes
Tb.Sp	3.017	12.476	0.720	<0.001	No
Tb.Th	1.764	7.197	0.892	<0.001	No
Tb.N	-0.681	0.710	0.970	<0.001	No
Ct.Th	0.105	0.030	0.996	0.587	Yes
$vBMD_i$	0.348	0.292	0.991	0.078	Yes
$vBMD_c$	-0.758	0.621	0.965	<0.001	No
$vBMD_{tr}$	0.059	-0.166	0.995	0.528	Yes
Ct.Ar	-0.029	-0.154	0.996	0.633	Yes
Tb.Ar	0.495	0.290	0.984	0.002	No
Tibia Variable	**Skewness**	**Kurtosis**	**Norm**	**P-value**	**Parametric**
BV/TV	0.124	-0.142	0.995	0.522	Yes
Tb.Sp	3.375	22.654	0.777	<0.001	No
Tb.Th	0.494	0.210	0.982	0.001	No
Tb.N	-0.001	0.803	0.991	0.077	Yes
Ct.Th	0.063	-0.125	0.996	0.573	Yes
$vBMD_i$	0.227	0.305	0.991	0.065	Yes
$vBMD_c$	-0.815	1.706	0.959	<0.001	No
$vBMD_{tr}$	0.122	-0.141	0.995	0.541	Yes
Ct.Ar	-0.069	-0.028	0.996	0.726	Yes
Tb.Ar	0.285	-0.243	0.991	0.052	Yes

only volumetric density measurements from pQCT images derived from the manufacturer software and the full set of bone outcomes for hr-pQCT. For the 307 study participants examined in the national cohort study, the mean age was 67.9 ± 13.1 years and the mean BMI was 27.9 ± 5.5 kg/m^2. Of these individuals, 131 (42.7%) have had a history of one or more fragility fractures in the last 15 years.

5.5.2 Measures of normality, distribution and central tendency

Table XLVII. National cohort: Summary statistics for bone outcomes from hr-pQCT images
Measures of central tendency (mean for parametric (P) and median for non-parametric (NP) variables) and error (standard deviations (SD) for parametric and interquartile range (Q1-Q3) for non-parametric variables). MI = variables not computed based on Parfitt's model of parallel plates.

Variable	hr-pQCT-Mean ± SD	hr-pQCT Median (Q1-Q3)	hr-pQCT-Mean ± SD	hr-pQCT Median (Q1-Q3)
BV/TV ^{P}	0.117 (0.032)	0.12 (0.094, 0.138)	0.132 (0.029)	0.131 (0.111, 0.153)
Tb.Sp MI (mm) ^{NP}	0.524 (0.180)	0.477 (0.426, 0.565)	0.517 (0.138)	0.493 (0.430, 0.571)
Tb.Th MI (mm) ^{NP}	0.065 (0.012)	0.064 (0.058, 0.071)	0.076 (0.014)	0.076 (0.065, 0.084)
Tb.N (#/mm^2) ^{NP}	1.80 (0.37)	1.84 (1.59, 2.05)	1.76 (0.33)	1.75 (1.53, 1.97)
Ct.Th (mm) ^{P}	0.641 (0.207)	0.640 (0.490, 0.770)	0.915 (0.272)	0.900 (0.730, 1.100)
vBMD$_i$ (mg/cm^3) ^{P}	279.45 (68.10)	278.50 (230.60, 318.70)	259.16 (49.80)	260.70 (226.00, 288.10)
vBMD$_c$ (mg/cm^3) ^{NP}	798.58 (87.69)	808.4 (749.90, 863.50)	778.23 (78.97)	783.60 (737.20, 828.30)
vBMD$_{tr}$ (mg/cm^3) ^{P}	140.86 (38.86)	143.8 (113.20, 166.00)	158.93 (35.14)	157.70 (133.70, 183.70)
Ct.Ar (mm^2) ^{P}	43.98 (13.05)	43.40 (35.30, 52.90)	93.61 (25.43)	93.40 (78.50, 109.50)
Tb.Ar (mm^2) ^{NP}	211.67 (47.35)	207.40 (174.90, 243.30)	585.26 (112.12)	578.20 (504.10, 662.30)

Of all the bone outcomes derived from the national hr-pQCT dataset, trabecular outcomes appeared to be primarily non-normally distributed while cortical measures were normally distributed, with the exception of cortical vBMD. In particular, Tb.Sp and Tb.Th were largely right skewed with a majority of study participants exhibiting smaller spaces between trabeculae (leptokurtotic) but thinner trabecular bone. Few individuals showed

Table XLVIII. National cohort: pQCT radius bone variables normality and data distribution.
Kolmogorov-Smirnov test of normality determined whether variable is suitable to be used in parametric or non-parametric statistical models.

Radius Proximal	Skewness	Kurtosis	Norm	P-value	Parametric
vBMDi	0.827	1.154	0.961	<0.001	No
vBMDc	1.172	1.829	0.926	<0.001	No
vBMDtr	0.302	0.109	0.992	0.219	Yes
Tot.Ar	-0.624	2.243	0.971	<0.001	No
Ct.Ar	1.028	0.777	0.918	<0.001	No
Tb.Ar	-0.624	2.243	0.971	<0.001	No
Radius Distal	**Skewness**	**Kurtosis**	**Norm**	**P-value**	**Parametric**
vBMDi	0.018	-0.127	0.997	0.946	Yes
vBMDc	-0.402	0.006	0.984	0.021	No
vBMDtr	0.839	1.771	0.960	<0.001	No
Tot.Ar	0.315	-0.264	0.985	0.028	No
Ct.Ar	0.839	1.772	0.960	<0.001	No
Tb.Ar	0.088	-0.448	0.990	0.160	Yes

Table XLIX. National cohort: pQCT tibia bone variables normality and data distribution.
Kolmogorov-Smirnov test of normality determined whether variable is suitable to be used in parametric or non-parametric statistical models.

Tibia Proximal	Skewness	Kurtosis	Norm	P-value	Parametric
vBMDi	0.337	0.215	0.990	0.047	No
vBMDc	0.058	-0.365	0.996	0.632	Yes
vBMDtr	0.070	-0.276	0.995	0.547	Yes
Tot.Ar	-0.189	2.091	0.976	<0.001	No
Ct.Ar	0.889	1.429	0.956	<0.001	No
Tb.Ar	-0.189	2.091	0.976	<0.001	No
Tibia Distal	**Skewness**	**Kurtosis**	**Norm**	**P-value**	**Parametric**
vBMDi	0.388	0.219	0.989	0.036	No
vBMDc	0.530	0.498	0.979	<0.001	No
vBMDtr	0.269	0.249	0.993	0.205	Yes
Tot.Ar	-1.468	8.996	0.913	<0.001	No
Ct.Ar	1.505	3.230	0.885	<0.001	No
Tb.Ar	-1.468	8.995	0.913	<0.001	No

Table L. National cohort: Summary statistics for bone outcomes derived on pQCT
Measures of central tendency (mean for parametric (P) and median for non-parametric (NP) variables) and error (standard deviations (SD) for parametric and interquartile range (Q1-Q3) for non-parametric variables).

	Proximal Slice		Distal Slice	
Radius Variable	**pQCT Mean ± SD**	**pQCT Median (Q1-Q3)**	**pQCT Mean ± SD**	**pQCT Median (Q1-Q3)**
vBMDi (mg/cm^3) NP	269.26 (64.91)	265.20 (220.3, 308.9)	348.38 (80.85)	351.25 (279.65, 407.05)
vBMDc (mg/cm^3) NP	872.85 (72.39)	858.30 (828.2, 903.1)	970.45 (70.00)	969.70 (928.05, 1023.3)
vBMDtr (mg/cm^3) P	163.14 (40.44)	161.00 (133.8, 188.7)	156.5 (47.29)	154.75 (121.6, 191)
Tot.Ar (mm^2) NP	350.46 (76.71)	354.68 (305.72, 397.48)	259.26 (51.56)	252.72 (224.08, 289.08)
Ct.Ar (mm^2) NP	19.09 (14.34)	15.84 (7.44, 26.68)	38.35 (14.47)	38.40 (28.18, 48.54)
Tb.Ar (mm^2) NP	157.69 (34.52)	159.60 (137.56, 178.84)	116.65 (23.2)	113.70 (100.82, 130.08)
Tibia Variable	**pQCT Mean ± SD**	**pQCT Median (Q1-Q3)**	**pQCT Mean ± SD**	**pQCT Median (Q1-Q3)**
vBMDi (mg/cm^3) NP	276.81 (46.77)	274.20 (245.80, 302.60)	257.32 (42.49)	252.00 (228.20, 281.90)
vBMDc (mg/cm^3) NP	869.88 (44.79)	869.40 (836.90, 900.90)	825.17 (36.91)	822.90 (797.30, 846.50)
vBMDtr (mg/cm^3) P	207.18 (39.88)	206.60 (180.20, 233.70)	222.79 (40.66)	222.60 (194.10, 246.70)
Tot.Ar (mm^2) NP	961.25 (135.76)	947.88 (867.56, 1056.56)	1145.86 (162.6)	1154.12 (1059.80, 1248.88)
Ct.Ar (mm^2) NP	37.99 (20.45)	34.72 (23.56, 50.76)	20.15 (15.06)	16.16 (9.24, 27.84)
Tb.Ar (mm^2) NP	432.54 (61.09)	426.52 (390.40, 475.44)	515.62 (73.17)	519.32 (476.88, 561.96)

more elaborate separation spaces and some had thicker trabeculae. While the thickness and area of cortical bone remained relatively balanced across individuals, most women's vBMD was actually larger with few exhibiting considerably low cortical vBMD. In

contrast to the normally distributed areal measures for the hr-pQCT outcomes, pQCT areal measures deviated from a Gaussian distribution. Total and trabecular areas were equally left skewed while most individuals appeared to have a smaller cortical area in general. In addition, cortical and integral vBMD were both mostly right skewed while trabecular vBMD remained normally distributed.

All hr-pQCT bone outcome values were comparable between the national and the local datasets, with any discrepancies being well within 10% of a standard deviation. However, for pQCT, integral ($p<0.001$) and cortical ($p<0.001$) vBMD in the national cohort was significantly smaller than in the local cohort. The national pQCT dataset vBMD values were around the same order of magnitude as corresponding measures in the national hr-pQCT dataset at both radius and tibia. Areal measurements on pQCT were routinely smaller than hr-pQCT values at both anatomical sites. The distal slice of the radius exhibited bone outcome values that were more similar to corresponding hr-pQCT values compared to the proximal slice of pQCT. For the tibia, the same was true for the distal slice.

5.5.3 Region of interest comparison – national versus local study

From the tibial limb lengths obtained during pQCT scans, it was determined that the 4% region of interest site as prescribed in the national protocol (mean(SD) = 14.89 (1.02) mm proximal to the tibial endplate) was significantly smaller than the prescribed fixed distance utilized in the local study pQCT (24.5 and 29.5 mm, $p<0.001$) and hr-pQCT scan

(22.5 mm, p<0.001) protocols. Although the distance value of the 4% radius site used in the national study was significantly different from the prescribed 9.5 mm fixed distance (p=0.02), the absolute difference was small (9.78 (0.66) – 9.50 mm = 0.28 mm).

5.6 Inter-site cross-calibration

5.6.1 Technician-specific test-retest precision

All technicians' pQCT and hr-pQCT test-retest precision values for vBMD values were below 5% with cortical vBMD showing the highest degree of precision followed by trabecular and integral vBMD. Hr-pQCT measurements performed by technicians were more reproducible than pQCT measurements. Any inconsistencies in image acquisition methodology and in image analysis protocols were resolved during this small sample test-retest study procedure, thus ensuring that study protocol was nationally streamlined.

Table LI. Technician study centre-specific test-retest precision of pQCT and hr-pQCT bone outcome computation.
All technicians for pQCT and hr-pQCT scanned at least 7 study participants twice with complete removal in between scans. Test-retest precision was evaluated using RMSCV%.

pQCT site	vBMDi	vBMDtr	vBMDc
Vancouver	3.46	1.21	2.55
Saskatoon	3.59	2.55	1.73
Hamilton	2.49	2.44	0.59
Toronto	2.75	3.81	1.46
Kingston	0.51	0.75	0.89

hr-pQCT site	vBMDi	vBMDtr	vBMDc
Vancouver	3.46	1.21	2.55
Calgary	0.62	0.66	0.34
Saskatoon	1.40	2.10	1.50
Toronto	0.52	0.70	0.46

5.6.2 Phantom cross-calibration

Cross-calibration of pQCT and hr-pQCT scanners across the six sites using the EFP yielded calibration slopes close to unity for all bone variables. All intercepts were either within or in the same order of magnitude as short-term precision values (RMSSD) for the corresponding bone variable (Table LIII). However, what appeared to be most consistent was a systematically lower bone outcome obtained at all the other sites compared to the pQCT in Hamilton. Compared to other sites, calibration of $vBMD_{tr}$ for the pQCT in Vancouver yielded a slope over 10% larger than unity. At this study centre, where both XCT2000 and XCT3000 models of the pQCT were available, there did not appear to be any considerable between-model differences in calibration (Table LII).

Table LII. National cohort: pQCT cross-calibration equations for European forearm phantom (EFP).
Linear regression models were fitted to determine the slope and intercept describing the relationship of EFP image-derived bone variables between the referent Hamilton pQCT scanner (model: XCT2000) and each of the scanners below. 95% confidence intervals (CI) (lower, upper) for slope and intercepts were also reported.

	Vancouver XCT2000		Vancouver XCT3000	
Bone variable	**Slope (95%CI)**	**Intercept (95%CI)**	**Slope (95%CI)**	**Intercept (95%CI)**
Tot.Ar (mm^2)	1.02 (1.01,1.02)	5.90 (4.08,7.73)	1.02 (1.01,1.02)	5.31 (3.93,6.69)
$vBMD_i$ (mg/cm^3)	0.97 (0.94,1)	23.16 (10.88,35.45)	0.99 (0.97,1)	13.85 (6.2,21.49)
Ct.Ar (mm^2)	0.98 (0.89,1.06)	0.23 (-4.33,4.78)	1.00 (0.93,1.08)	1.04 (-2.76,4.83)
$vBMD_c$ (mg/cm^3)	0.98 (0.89,1.07)	17.77 (-58.59,94.12)	0.92 (0.84,1)	69.7 (1.58,137.83)
Tb.Ar (mm^2)	1.02 (1.01,1.02)	2.57 (1.72,3.43)	1.02 (1.01,1.02)	2.35 (1.75,2.94)
$vBMD_{tr}$ (mg/cm^3)	1.17 (1.1,1.24)	-27.17 (-44.85,-9.49)	1.19 (1.09,1.28)	-31.15 (-53.34,-8.96)

Table LIII. National cohort: pQCT cross-calibration equations for European forearm phantom (EFP). Continued.
Linear regression models were fitted to determine the slope and intercept describing the relationship of EFP image-derived bone variables between the referent Hamilton pQCT scanner (model: XCT2000) and each of the scanners in the cities below. 95% confidence intervals (CI) (lower, upper) for slope and intercepts were also reported.

	Saskatoon		Toronto		Kingston	
Bone Variable	**Slope (95%CI)**	**Intercept (95%CI)**	**Slope (95%CI)**	**Intercept (95%CI)**	**Slope (95%CI)**	**Intercept (95%CI)**
Tot.Ar (mm^2)	1.00 (1.00,1.00)	-0.18 (-1.36,1.00)	1.00 (1.00,1.00)	-0.75 (-1.76,0.25)	1.00 (1.00,1.00)	-0.57 (-1.45,0.32)
$vBMD_i$ (mg/cm^3)	1.00 (0.99,1.01)	-2.75 (-6.8,1.29)	1.01 (1.00,1.01)	-8.21 (-10.65,-5.76)	0.98 (0.97,0.99)	-3.92 (-7.39,-0.44)
Ct.Ar (mm^2)	0.99 (0.92,1.06)	-0.20 (-3.62,3.22)	0.97 (0.87,1.07)	0.65 (-4.57,5.86)	0.93 (0.84,1.02)	0.62 (-4.32,5.56)
$vBMD_C$ (mg/cm^3)	0.96 (0.83,1.09)	27.41 (-80.22,135.04)	0.91 (0.78,1.05)	67.96 (-43.67,179.59)	0.92 (0.81,1.02)	50.9 (-38.96,140.75)
Tb.Ar (mm^2)	1.00 (1.00,1.00)	-0.09 (-0.6,0.42)	1.00 (1.00,1.00)	-0.40 (-0.85,0.05)	1.00 (1.00,1.00)	-0.23 (-0.65,0.2)
$vBMD_{tr}$ (mg/cm^3)	0.99 (0.97,1.01)	0.79 (-3.98,5.57)	0.99 (0.97,1.01)	-2.54 (-8.93,3.86)	0.97 (0.96,0.98)	-0.91 (-3.84,2.01)

Table LIV. National cohort: hr-pQCT cross-calibration equations for European forearm phantom (EFP).
Linear regression models were fitted to determine the slope and intercept describing the relationship of EFP image-derived bone variables between the referent Toronto hr-pQCT scanner and each of the scanners in the cities below. 95% confidence intervals (CI) (lower, upper) for slope and intercepts were also reported.

	Vancouver		Calgary		Saskatoon	
Bone variable	**Slope (95%CI)**	**Intercept (95%CI)**	**Slope (95%CI)**	**Intercept (95%CI)**	**Slope (95%CI)**	**Intercept (95%CI)**
$vBMD_i$ (mg/cm^3)	1.04 (1.03,1.05)	-4.82 (-8,-1.63)	0.97 (0.96,0.99)	2.94 (-2.26,8.13)	0.96 (0.95,0.98)	-0.94 (-5.93,4.04)
Ct.Ar (mm^2)	1.06 (1.03,1.1)	-0.73 (-2.72,1.25)	1.00 (0.99,1.01)	-1.05 (-1.78,-0.32)	1.01 (1.00,1.01)	-0.35 (-0.89,0.19)
$vBMD_C$ (mg/cm^3)	1.28 (1.09,1.46)	-176.91 (-305.36,-48.47)	0.96 (0.83,1.09)	13.77 (-84.08,111.62)	1.04 (0.88,1.21)	-66.26 (-188.19,55.66)
Tb.Ar (mm^2)	0.99 (0.99,0.99)	-0.44 (-0.55,-0.32)	0.99 (0.99,0.99)	0.49 (0.12,0.86)	1.00 (1.00,1.00)	0.27 (-0.02,0.55)
$vBMD_{tr}$ (mg/cm^3)	1.09 (0.99,1.19)	-16.14 (-29.86,-2.43)	1.00 (0.99,1.02)	0.75 (-1.01,2.52)	0.98 (0.95,1.00)	-0.15 (-3.31,3.01)

5.6.3 Human cross-calibration

Integral, trabecular vBMD and cortical area demonstrated the best human calibrations with slopes closest to unity for both hr-pQCT and pQCT across all sites as compared to the referent machine. Cortical vBMD and trabecular area showed linear slopes deviating further away from 1.0 for pQCT calibration, with correspondingly wide confidence intervals at all study centres. Trabecular area calibration was poorer for hr-pQCT as compared to other bone variables. One notable discrepant observation was in integral and cortical vBMD for pQCT in Toronto, which yielded calibration slopes of 1.14 and 1.33, respectively. In addition, trabecular area had a much lower calibration slope for Toronto's pQCT than any other site with a value of 0.35. For hr-pQCT calibration slopes across sites, Calgary showed a larger slope of 1.15 for cortical area and Vancouver a larger slope of 1.11 for trabecular area compared to other sites. Aside from these minor deviations, calibration slopes for other bone variables were mostly similar across study centres.

Table LV. National cohort: *in vivo* pQCT cross-calibration equations.
Linear regression models were fitted to determine the slope and intercept describing the relationship of bone variables between *in vivo* images obtained from the referent Hamilton pQCT scanner (model: XCT2000) versus each of the scanners below. 95% confidence intervals (CI) (lower, upper) for slope and intercepts were also reported.

	Vancouver XCT2000		Vancouver XCT3000	
Bone variable	**Slope (95%CI)**	**Intercept (95%CI)**	**Slope (95%CI)**	**Intercept (95%CI)**
Tot.Ar (mm^2)	1.01 (0.98,1.04)	-18.91 (-145.06,107.24)	1.01 (0.97,1.04)	-31.1 (-176.23,114.02)
$vBMD_i$ (mg/cm^3)	0.96 (0.82,1.11)	34.68 (-31.93,101.29)	1.01 (0.92,1.11)	10.85 (-33.99,55.68)
Ct.Ar (mm^2)	0.95 (0.9,0.99)	14.99 (4.87,25.11)	0.93 (0.89,0.96)	17.47 (7.96,26.97)
$vBMD_C$ (mg/cm^3)	0.79 (0.56,1.02)	233.44 (-7.1,473.99)	0.9 (0.79,1.02)	120.2 (-2.52,242.92)
Tb.Ar (mm^2)	0.88 (0.64,1.12)	30.09 (-29.47,89.65)	0.88 (0.69,1.08)	28.04 (-21.11,77.19)
$vBMD_{tr}$ (mg/cm^3)	1.03 (0.98,1.09)	-3.90 (-13.84,6.04)	0.97 (0.86,1.08)	1.85 (-19.08,22.79)

	Saskatoon		Toronto		Kingston	
Bone variable	**Slope (95%CI)**	**Intercept (95%CI)**	**Slope (95%CI)**	**Intercept (95%CI)**	**Slope (95%CI)**	**Intercept (95%CI)**
Tot.Ar (mm^2)	1.02 (0.99,1.05)	-28.99 (-155.55,97.57)	1.08 (1.04,1.13)	-69.60 (-245.63,106.44)	1.09 (1.06,1.12)	-104.79 (-232.3,22.71)
$vBMD_i$ (mg/cm^3)	0.93 (0.84,1.02)	24.4 (-19.02,67.83)	1.14 (1,1.29)	-36.00 (-100.48,28.48)	1.02 (0.9,1.13)	7.43 (-45.26,60.12)
Ct.Ar (mm^2)	0.98 (0.94,1.01)	3.57 (-5.24,12.37)	1.00 (0.95,1.05)	-4.30 (-16.97,8.38)	0.98 (0.94,1.02)	8.09 (-2.16,18.34)
$vBMD_C$ (mg/cm^3)	0.85 (0.64,1.06)	161.2 (-61.72,384.11)	1.33 (0.9,1.75)	-344.23 (-797.54,109.08)	0.71 (0.54,0.88)	312.20 (131.86,492.53)
Tb.Ar (mm^2)	0.80 (0.48,1.12)	53.06 (-25.49,131.62)	0.35 (-0.01,0.71)	129.52 (10.61,248.43)	0.87 (0.52,1.22)	15.74 (-76.78,108.26)
$vBMD_{tr}$ (mg/cm^3)	0.98 (0.95,1)	-2.85 (-8.48,2.78)	1.02 (0.99,1.05)	-4.73 (-11.46,1.99)	0.96 (0.91,1.01)	-1.57 (-10.76,7.62)

Table LVI. National cohort: *in vivo* hr-pQCT cross-calibration equations.
Linear regression models were fitted to determine the slope and intercept describing the relationship of bone variables between *in vivo* images obtained from the referent Toronto hr-pQCT scanner versus each of the scanners in the cities below. 95% confidence intervals (CI) (lower, upper) for slope and intercepts were also reported.

	Vancouver		Calgary		Saskatoon	
Bone variable	**Slope (95%CI)**	**Intercept (95%CI)**	**Slope (95%CI)**	**Intercept (95%CI)**	**Slope (95%CI)**	**Intercept (95%CI)**
$vBMD_i$ (mg/cm^3)	0.99 (0.89,1.1)	-3.93 (-61.94,54.09)	0.97 (0.95,0.99)	19.06 (6.85,31.28)	1.03 (0.98,1.08)	-23.26 (-50.02,3.5)
Ct.Ar (mm^2)	0.89 (0.42,1.35)	23.85 (-74.49,122.19)	1.15 (-0.89,3.2)	-27.33 (-450.84,396.18)	0.96 (0.56,1.37)	3.58 (-84.35,91.51)
$vBMD_C$ (mg/cm^3)	1.04 (1.03,1.05)	-0.05 (-1.17,1.07)	1.05 (0.98,1.13)	-6.82 (-17.16,3.53)	0.99 (0.92,1.06)	-0.03 (-9.19,9.13)
Tb.Ar (mm^2)	1.11 (0.95,1.26)	-35.06 (-93.43,23.31)	0.71 (0.4,1.03)	108.11 (-14.15,230.37)	0.84 (-0.32,1.99)	54.51 (-402.19,511.2)
$vBMD_{tr}$ (mg/cm^3)	0.98 (0.92,1.05)	2.88 (-23.64,29.4)	0.95 (0.92,0.97)	22.82 (12.37,33.27)	1.03 (0.95,1.12)	-20.12 (-55.14,14.9)

5.7 External validation: clinical sensitivity in national cohort

Binary logistic regression models showed increased odds for fragility fractures associated with lower vBMD, Ct.Th, and smaller BV/TV at both the radius and tibia as obtained from hr-pQCT images in the national cohort (Table LVIII). As compared to the local study results for clinical sensitivity, the national cohort yielded a greater number of significant statistics. Smaller integral vBMD demonstrated the highest odds for a fragility fracture, followed by Ct.Th and BV/TV. Odds were increased after adjusting for age, and were higher when observed at the ultadistal tibia compared to the radius in general. Specifically at the radius, lower Tb.N was associated with higher odds for fractures, but not at the tibia. At the tibia, thinner trabeculae were associated with fractures, but not at the radius. Trabecular vBMD at the tibia appeared to associate with fractures to a higher degree than at the radius for hr-pQCT. For pQCT, the same was true, but in addition,

cortical vBMD demonstrated stronger associations with fractures at the radius compared to at the tibia, where there was no association with fractures (Table LVII). Lower integral vBMD obtained using pQCT was consistently associated with fractures at both the utlradistal radius and tibia. The magnitude of odds for fragility fractures per unit SD, SEE or LSC was larger overall for pQCT versus hr-pQCT. While most confidence intervals were relatively narrow, the OR confidence interval for trabecular vBMD at the tibia as obtained using pQCT was wider than other bone variables measured from pQCT images when examined per unit of LSC.

Table LVII. pQCT bone variables' association with fragility fractures
Magnitude of odds for fragility fractures associated with each standard deviation (SD), least significant change (LSC) or standard error of estimate (SEE) increase (+) or decrease (-) in radius bone variables obtained from pQCT images was determined with a binary logistic regression model. Models were examined with and without adjusting for age. CI = 95% confidence interval (lower, upper). Bold indicates significant at $p < 0.05$

	Unadjusted			**Age-Adjusted**		
Radius Bone Variable	**OR(CI) per SD**	**OR(CI) per LSC**	**OR(CI) per SEE**	**OR(CI) per SD**	**OR(CI) per LSC**	**OR(CI) per SEE**
$vBMD_i$ (mg/cm^3)	**1.43 (1.09,1.86)**	1.00 (1.00,1.00)	**1.23 (1.05,1.44)**	**1.57 (1.18,2.09)**	1.00 (1.00,1.00)	**1.30 (1.10,1.54)**
$vBMD_c$ (mg/cm^3)	**1.30 (1.00,1.69)**	**1.31 (1.00,1.73)**	**1.24 (1.00,1.56)**	**1.37 (1.04,1.80)**	**1.39 (1.04,1.85)**	**1.30 (1.04,1.64)**
$vBMD_{tr}$ (mg/cm^3)	1.08 (0.84,1.39)	1.11 (0.78,1.57)	1.01 (0.97,1.06)	1.10 (0.85,1.44)	1.15 (0.80,1.64)	1.02 (0.97,1.06)
Tibia Bone Variable	**OR(CI) per SD**	**OR(CI) per LSC**	**OR(CI) per SEE**	**OR(CI) per SD**	**OR(CI) per LSC**	**OR(CI) per SEE**
$vBMD_i$ (mg/cm^3)	1.26 (0.99,1.61)	1.00 (1.00,1.00)	**1.06 (1.00,1.13)**	**1.43 (1.09,1.87)**	1.00 (1.00,1.00)	**1.09 (1.02,1.17)**
$vBMD_c$ (mg/cm^3)	0.93 (0.73,1.18)	0.89 (0.63,1.28)	0.84 (0.50,1.44)	0.97 (0.75,1.26)	0.96 (0.65,1.42)	0.94 (0.53,1.69)
$vBMD_{tr}$ (mg/cm^3)	**1.34 (1.05,1.71)**	**3.81 (1.24,11.69)**	**1.03 (1.00,1.06)**	**1.48 (1.13,1.94)**	**6.04 (1.77,20.62)**	**1.04 (1.01,1.07)**

Table LVIII. National cohort: hr-pQCT bone variables' association with fragility fractures
Magnitude of odds for fragility fractures associated with each standard deviation (SD), least significant change (LSC) or standard error of estimate (SEE) increase (+) or decrease (-) in bone variables obtained from pQCT images was determined with a binary logistic regression model. Models were examined with and without adjusting for age. CI = 95% confidence interval (lower, upper). Bold indicates significant at $p < 0.05$.

	Unadjusted			**Age-Adjusted**		
Radius Variable	**OR(CI) per SD**	**OR(CI) per LSC**	**OR(CI) per SEE**	**OR(CI) per SD**	**OR(CI) per LSC**	**OR(CI) per SEE**
BV/TV (fraction)	1.21 (0.96,1.52)	1.04 (0.99,1.08)	**1.02 (1.00,1.04)**	**1.33 (1.04,1.71)**	**1.06 (1.01,1.11)**	**1.03 (1.00,1.05)**
Tb.Sp MI (mm)	1.22 (0.96,1.54)	0.91 (0.81,1.02)	0.96 (0.91,1.01)	1.30 (0.99,1.71)	0.88 (0.77,1.00)	0.94 (0.89,1.00)
Tb.Th MI (mm)	1.00 (0.80,1.25)	1.00 (0.85,1.18)	1.00 (0.93,1.08)	1.07 (0.84,1.36)	1.05 (0.88,1.25)	1.02 (0.95,1.10)
Tb.N (#/mm)	1.21 (0.96,1.52)	1.20 (0.96,1.50)	1.09 (0.98,1.20)	**1.31 (1.01,1.69)**	**1.29 (1.01,1.65)**	**1.13 (1.00,1.26)**
Ct.Th (mm)	1.24 (0.99,1.57)	1.12 (0.99,1.25)	**1.03 (1.00,1.06)**	**1.41 (1.09,1.82)**	**1.19 (1.04,1.35)**	**1.05 (1.01,1.08)**
$vBMD_i$ (mg/cm^3)	**1.28 (1.02,1.62)**	**1.08 (1.00,1.16)**	**1.02 (1.00,1.04)**	**1.47 (1.13,1.90)**	**1.12 (1.04,1.22)**	**1.03 (1.01,1.05)**
$vBMD_c$ (mg/cm^3)	1.20 (0.95,1.50)	1.08 (0.98,1.18)	1.02 (0.99,1.06)	**1.31 (1.02,1.68)**	**1.12 (1.01,1.24)**	**1.04 (1.00,1.07)**
$vBMD_{tr}$ (mg/cm^3)	1.21 (0.96,1.52)	1.04 (0.99,1.08)	**1.02 (1.00,1.04)**	**1.33 (1.04,1.71)**	**1.06 (1.01,1.11)**	**1.03 (1.00,1.06)**
Tibia Variable	**OR(CI) per SD**	**OR(CI) per LSC**	**OR(CI) per SEE**	**OR(CI) per SD**	**OR(CI) per LSC**	**OR(CI) per SEE**
BV/TV (fraction)	**1.30 (1.03,1.63)**	**1.03 (1.00,1.05)**	**1.02 (1.00,1.03)**	**1.39 (1.09,1.78)**	**1.03 (1.01,1.06)**	**1.02 (1.01,1.04)**
Tb.Sp MI (mm)	1.08 (0.86,1.35)	0.94 (0.78,1.13)	0.98 (0.90,1.05)	1.11 (0.86,1.43)	0.92 (0.75,1.12)	0.97 (0.89,1.05)
Tb.Th MI (mm)	**1.25 (1.00,1.58)**	**1.27 (1.00,1.62)**	**1.12 (1.00,1.25)**	**1.30 (1.02,1.66)**	**1.33 (1.02,1.72)**	**1.14 (1.01,1.29)**
Tb.N (#/mm)	1.08 (0.87,1.36)	1.11 (0.84,1.47)	1.05 (0.92,1.19)	1.14 (0.89,1.48)	1.18 (0.86,1.62)	1.08 (0.93,1.25)
Ct.Th (mm)	**1.38 (1.09,1.74)**	**1.08 (1.02,1.15)**	**1.04 (1.01,1.06)**	**1.49 (1.15,1.93)**	**1.10 (1.04,1.18)**	**1.04 (1.02,1.08)**
$vBMD_i$ (mg/cm^3)	**1.50 (1.18,1.91)**	**1.04 (1.02,1.07)**	**1.02 (1.01,1.04)**	**1.69 (1.30,2.21)**	**1.06 (1.03,1.09)**	**1.03 (1.01,1.04)**
$vBMD_c$ (mg/cm^3)	1.22 (0.97,1.53)	1.04 (0.99,1.09)	**1.02 (1.00,1.05)**	**1.28 (1.00,1.63)**	**1.05 (1.00,1.10)**	**1.03 (1.00,1.05)**
$vBMD_{tr}$ (mg/cm^3)	**1.30 (1.03,1.63)**	**1.03 (1.00,1.05)**	**1.01 (1.00,1.02)**	**1.39 (1.08,1.78)**	**1.03 (1.01,1.06)**	**1.02 (1.00,1.03)**

5.8 National reference data

The number of women across the age categories by half decades was normally distributed for pQCT and hr-pQCT with the fewest individuals in the 85+ age category. For pMRI, a larger number of older women were imaged. Volumetric bone outcomes for pQCT (Table LIX & Table LX), hr-pQCT (Table LXI & Table LXII) and 1.0T pMRI (Table LXIII) categorized by age groups are displayed below. While there was an overall pattern of deteriorating bone towards older age groups, the 85+ age category deviated from this trend for all measures within pQCT variables. In addition, the 55-60 years old age group exhibited lower bone outcome values for hr-pQCT at the radius and in the non-fractured group at the tibia, compared to the 60-65 age group. A small number of individuals were identified in both these age categories. For pMRI, smaller numbers of individuals were categorized into each age group compared to pQCT and hr-pQCT, plus age-related trends were not apparent. For the more distal slice of the radius in pQCT, only one data point was available, as was the case for the distal radius in the non-fractured group for hr-pQCT. In general, the differences between fractured and non-fractured groups appeared to become larger towards the older age groups for all modalities. This difference was noticed earlier for Ct.Th, cortical and trabecular vBMD compared to other bone outcomes on hr-pQCT. The pooled data showed a similar pattern of age-related vBMD and bone structure loss as both fractured and non-fractured groups. The means for each age category for hr-pQCT situated between the values for the more proximal and more distal slices of pQCT. For the radius, hr-pQCT values were actually closer to values at the more proximal slice but for the tibia, both slices faired closely to the corresponding hr-pQCT

Age Category	NO FRACTURE				ONE OR MORE FRACTURE			
More proximal slice	**N**	**vBMDi (mg/cm^3)**	**vBMDtr (mg/cm^3)**	**vBMDc (mg/cm^3)**	**N**	**vBMDi (mg/cm^3)**	**vBMDtr (mg/cm^3)**	**vBMDc (mg/cm^3)**
60-65 years	25	291.36 ± 58.75	174.04 ± 29.63	882.86 ± 50.67	23	275.41 ± 69.68	161.22 ± 33.08	895.70 ± 94.60
65-70 years	37	281.27 ± 62.19	155.98 ± 41.26	896.09 ± 87.41	32	253.37 ± 56.83	169.73 ± 46.66	850.63 ± 56.65
70-75 years	28	263.94 ± 57.29	168.69 ± 35.57	851.61 ± 60.45	22	265.22 ± 55.86	169.03 ± 31.88	858.04 ± 59.51
75-80 years	19	295.73 ± 96.57	166.62 ± 51.44	893.23 ± 89.93	18	241.84 ± 48.44	151.94 ± 32.15	845.82 ± 50.79
80-85 years	19	266.87 ± 66.73	159.46 ± 58.76	882.10 ± 69.24	14	231.42 ± 56.05	143.60 ± 39.68	854.47 ± 60.36
85+ years	3	277.77 ± 79.56	172.27 ± 46.92	878.97 ± 81.98	5	298.78 ± 78.12	161.74 ± 16.20	904.28 ± 94.83
More distal slice	**N**	**vBMDi (mg/cm^3)**	**vBMDtr (mg/cm^3)**	**vBMDc (mg/cm^3)**	**N**	**vBMDi (mg/cm^3)**	**vBMDtr (mg/cm^3)**	**vBMDc (mg/cm^3)**
60-65 years	21	397.81 ± 90.98	164.79 ± 40.77	1016.39 ± 62.37	19	352.62 ± 65.64	155.94 ± 42.53	993.91 ± 68.44
65-70 years	27	356.03 ± 69.56	160.32 ± 52.40	982.71 ± 57.20	31	321.16 ± 81.62	159.85 ± 41.43	941.77 ± 76.09
70-75 years	24	346.16 ± 66.26	165.34 ± 42.81	964.43 ± 59.74	22	352.84 ± 86.13	156.33 ± 40.47	964.84 ± 75.82
75-80 years	15	368.73 ± 107.68	148.95 ± 59.77	984.61 ± 71.75	18	329.32 ± 61.21	147.04 ± 38.20	949.72 ± 60.23
80-85 years	15	343.75 ± 74.34	162.01 ± 64.84	952.37 ± 64.40	12	302.91 ± 84.25	124.83 ± 54.97	946.72 ± 73.77
85+ years	1	450.00	238.10	1058.10	3	356.63 ± 101.84	129.67 ± 37.71	985.60 ± 105.56

Age Category	POOLED			
More proximal slice	**N**	**vBMDi (mg/cm^3)**	**vBMDtr (mg/cm^3)**	**vBMDc (mg/cm^3)**
60-65 years	48	283.72 ± 64.03	167.90 ± 31.66	889.01 ± 74.44
65-70 years	69	268.33 ± 60.96	162.36 ± 44.06	875.01 ± 77.65
70-75 years	50	264.50 ± 56.09	168.84 ± 33.66	854.44 ± 59.51
75-80 years	37	269.51 ± 80.73	159.48 ± 43.20	870.17 ± 76.41
80-85 years	33	251.83 ± 64.01	152.73 ± 51.43	870.38 ± 66.10
85+ years	8	290.90 ± 73.58	165.69 ± 28.44	894.79 ± 85.03
More distal slice	**N**	**vBMDi (mg/cm^3)**	**vBMDtr (mg/cm^3)**	**vBMDc (mg/cm^3)**
60-65 years	40	376.34 ± 82.20	160.59 ± 41.32	1005.71 ± 65.47
65-70 years	58	337.39 ± 77.59	160.07 ± 46.43	960.83 ± 70.46
70-75 years	46	349.35 ± 75.61	161.03 ± 41.49	964.62 ± 67.13
75-80 years	33	347.23 ± 86.38	147.91 ± 48.37	965.58 ± 67.01
80-85 years	27	325.60 ± 80.04	145.49 ± 62.42	949.86 ± 67.41
85+ years	4	379.98 ± 95.36	156.78 ± 62.35	1003.73 ± 93.50

Table LIX. National pQCT reference data for distal radius by half decades

Means and standard deviations (SD) for each volumetric bone outcome was computed separately for each age category. Analyses were separated according to those without fractures (top left), with fractures (top right) and pooled (bottom).

Age Category	NO FRACTURE				ONE OR MORE FRACTURE			
More proximal slice	**N**	**vBMDi (mg/cm^3)**	**vBMDtr (mg/cm^3)**	**vBMDc (mg/cm^3)**	**N**	**vBMDi (mg/cm^3)**	**vBMDtr (mg/cm^3)**	**vBMDc (mg/cm^3)**
60-65 years	24	294.96 ± 42.23	218.15 ± 36.05	887.43 ± 44.85	26	292.33 ± 45.02	213.92 ± 42.62	904.38 ± 39.9
65-70 years	48	290.01 ± 43.76	210.97 ± 38.41	882.18 ± 35.86	36	275.45 ± 49.88	203.78 ± 40.19	866.82 ± 40.3
70-75 years	34	278.75 ± 34.95	213.03 ± 32.24	855.32 ± 36.79	32	276.52 ± 43.87	206.65 ± 36.06	876.28 ± 39.11
75-80 years	20	266.54 ± 52.48	201.48 ± 43.67	867.98 ± 44.12	18	260.74 ± 41.84	205.91 ± 39.27	844.31 ± 37.22
80-85 years	16	256.47 ± 40.33	201.81 ± 47.45	840.41 ± 44.47	13	236.92 ± 54.66	176.15 ± 45.74	842.97 ± 57.18
85+ years	2	326.9 ± 80.19	265.4 ± 30.97	870.05 ± 143.19	4	216.4 ± 19.16	164.6 ± 13.16	822.93 ± 25.69
More distal slice	**N**	**vBMDi (mg/cm^3)**	**vBMDtr (mg/cm^3)**	**vBMDc (mg/cm^3)**	**N**	**vBMDi (mg/cm^3)**	**vBMDtr (mg/cm^3)**	**vBMDc (mg/cm^3)**
60-65 years	25	273.36 ± 42.91	237.04 ± 43	837.4 ± 32.6	26	267.7 ± 36.99	222.96 ± 39.45	853.75 ± 41.36
65-70 years	46	266.95 ± 38.68	225.97 ± 38.85	833.23 ± 31.21	39	255.02 ± 41.9	216.59 ± 37.62	826.42 ± 37.18
70-75 years	33	256.67 ± 33.65	226.01 ± 32.5	815.26 ± 28.62	33	256.91 ± 38.94	222.1 ± 36.46	829.17 ± 34.62
75-80 years	20	259.21 ± 57.45	228.1 ± 55.95	815.25 ± 36.81	18	243.68 ± 36.69	220.19 ± 34.49	805.75 ± 25.83
80-85 years	17	240.17 ± 42.05	220.91 ± 49.08	800.66 ± 32.03	13	224.33 ± 49.1	194.75 ± 43.43	806.62 ± 41.38
85+ years	2	308.35 ± 62.58	279.2 ± 25.6	862.75 ± 68.66	3	203.13 ± 16.52	181.1 ± 8.85	777.27 ± 13.06

Age Category	POOLED			
More proximal slice	**N**	**vBMDi (mg/cm^3)**	**vBMDtr (mg/cm^3)**	**vBMDc (mg/cm^3)**
60-65 years	50	293.6 ± 43.28	215.95 ± 39.26	896.24 ± 42.77
65-70 years	84	283.77 ± 46.75	207.89 ± 39.11	875.6 ± 38.36
70-75 years	66	277.67 ± 39.23	209.93 ± 34.03	865.48 ± 39.09
75-80 years	38	263.79 ± 47.19	203.58 ± 41.15	856.76 ± 42.18
80-85 years	29	247.71 ± 47.43	190.31 ± 47.66	841.56 ± 49.62
85+ years	6	253.23 ± 69.01	198.2 ± 54.82	838.63 ± 71.34
More distal slice	**N**	**vBMDi (mg/cm^3)**	**vBMDtr (mg/cm^3)**	**vBMDc (mg/cm^3)**
60-65 years	51	270.47 ± 39.7	229.86 ± 41.43	845.73 ± 37.86
65-70 years	85	261.48 ± 40.39	221.67 ± 38.35	830.1 ± 34.04
70-75 years	66	256.79 ± 36.11	224.05 ± 34.33	822.22 ± 32.29
75-80 years	38	251.85 ± 48.73	224.35 ± 46.58	810.75 ± 32.02
80-85 years	30	233.31 ± 45.13	209.57 ± 47.78	803.24 ± 35.83
85+ years	5	245.22 ± 66.61	220.34 ± 55.59	811.46 ± 58.79

Table LX. National pQCT reference data for distal tibia by half decades

Means and standard deviations (SD) for each volumetric bone outcome was computed separately for each age category. Analyses were separated according to those without fractures (top left), with fractures (top right) and pooled (bottom).

Table LXI. National hr-pQCT reference data for distal radius by half decades

Means and standard deviations (SD) for each volumetric bone outcome was computed separately for each age category. Reference datasets were generated for individuals without fractures (Fx-, top), individuals with fractures (Fx+, middle) and combined (bottom).

Radius – Fx-

Age Category	N	BV/TV (frac)	Tb.Sp (mm)	Tb.Th (mm)	Tb.N (#/mm)	Ct.Th (mm)	vBMDi (mg/cm^3)	vBMDtr (mg/cm^3)	vBMDc (mg/cm^3)
55-60 years	8	0.126 ± 0.014	0.466 ± 0.056	0.067 ± 0.009	1.90 ± 0.21	0.855 ± 0.127	342.84 ± 43.78	151.70 ± 17.28	908.01 ± 38.33
60-65 years	37	0.127 ± 0.032	0.467 ± 0.093	0.065 ± 0.010	1.93 ± 0.29	0.739 ± 0.193	313.22 ± 69.97	152.09 ± 38.38	838.31 ± 71.05
65-70 years	47	0.119 ± 0.034	0.507 ± 0.103	0.066 ± 0.013	1.80 ± 0.32	0.682 ± 0.174	290.47 ± 64.01	142.91 ± 40.53	810.77 ± 72.2
70-75 years	26	0.118 ± 0.022	0.491 ± 0.075	0.064 ± 0.009	1.83 ± 0.23	0.641 ± 0.179	275.42 ± 51.42	141.73 ± 26.13	784.12 ± 82.28
75-80 years	27	0.115 ± 0.043	0.577 ± 0.261	0.066 ± 0.016	1.74 ± 0.51	0.577 ± 0.215	263.28 ± 70.08	137.40 ± 51.38	762.18 ± 103.18
80-85 years	14	0.117 ± 0.045	0.545 ± 0.239	0.063 ± 0.01	1.81 ± 0.49	0.499 ± 0.184	246.61 ± 63.98	140.44 ± 54.20	748.89 ± 69.64
85+ years	1	0.070	0.653	0.049	1.42	0.600	214.80	83.60	863.50

Radius – Fx+

Age Category	N	BV/TV (frac)	Tb.Sp (mm)	Tb.Th (mm)	Tb.N (#/mm)	Ct.Th (mm)	vBMDi (mg/cm^3)	vBMDtr (mg/cm^3)	vBMDc (mg/cm^3)
55-60 years	6	0.127 ± 0.038	0.469 ± 0.064	0.067 ± 0.018	1.89 ± 0.21	0.843 ± 0.286	336.62 ± 119.23	152.52 ± 45.76	866.53 ± 76.68
60-65 years	27	0.118 ± 0.028	0.538 ± 0.212	0.068 ± 0.018	1.79 ± 0.42	0.719 ± 0.180	292.73 ± 58.34	141.17 ± 33.45	829.39 ± 75.39
65-70 years	31	0.115 ± 0.029	0.528 ± 0.140	0.065 ± 0.010	1.76 ± 0.36	0.588 ± 0.167	264.02 ± 56.11	138.61 ± 35.02	774.77 ± 82.43
70-75 years	37	0.111 ± 0.032	0.572 ± 0.274	0.065 ± 0.012	1.73 ± 0.42	0.616 ± 0.196	268.32 ± 66.91	133.50 ± 38.90	789.43 ± 76.62
75-80 years	28	0.105 ± 0.036	0.597 ± 0.319	0.062 ± 0.011	1.67 ± 0.40	0.564 ± 0.213	253.43 ± 73.64	126.42 ± 42.79	773.67 ± 87.46
80-85 years	12	0.110± 0.032	0.579 ± 0.250	0.066 ± 0.012	1.68 ± 0.39	0.514 ± 0.251	244.58 ± 62.12	131.73 ± 38.48	730.66 ± 127.56
85+ years	5	0.100 ± 0.030	0.574 ± 0.216	0.059 ± 0.007	1.69 ± 0.41	0.476 ± 0.233	223.84 ± 69.37	120.50 ± 36.13	749.94 ± 128.30

Radius - Pooled

Age Category	N	BV/TV (frac)	Tb.Sp (mm)	Tb.Th (mm)	Tb.N (#/mm)	Ct.Th (mm)	vBMDi (mg/cm^3)	vBMDtr (mg/cm^3)	vBMDc (mg/cm^3)
55-60 years	14	0.127 ± 0.026	0.467 ± 0.057	0.067 ± 0.013	1.89 ± 0.21	0.850 ± 0.201	340.17 ± 80.68	152.05 ± 31.09	890.24 ± 59.22
60-65 years	64	0.123 ± 0.030	0.497 ± 0.157	0.066 ± 0.014	1.87 ± 0.35	0.730 ± 0.186	304.57 ± 65.63	147.49 ± 36.51	834.55 ± 72.46
65-70 years	78	0.118 ± 0.032	0.515 ± 0.119	0.066 ± 0.012	1.78 ± 0.33	0.645 ± 0.176	279.96 ± 62.00	141.20 ± 38.26	796.46 ± 77.95
70-75 years	63	0.114 ± 0.029	0.539 ± 0.218	0.065 ± 0.011	1.77 ± 0.36	0.626 ± 0.188	271.25 ± 60.65	136.90 ± 34.22	787.24 ± 78.40
75-80 years	55	0.110 ± 0.039	0.587 ± 0.290	0.064 ± 0.014	1.70 ± 0.45	0.571 ± 0.212	258.26 ± 71.42	131.81 ± 47.09	768.03 ± 94.79
80-85 years	26	0.114 ± 0.039	0.561 ± 0.240	0.064 ± 0.011	1.75 ± 0.44	0.506 ± 0.213	245.68 ± 61.86	136.42 ± 46.89	740.47 ± 98.83
85+ years	6	0.095 ± 0.029	0.587 ± 0.196	0.057 ± 0.007	1.65 ± 0.38	0.497 ± 0.214	222.33 ± 62.15	114.35 ± 35.65	768.87 ± 123.77

Table LXII. National hr-pQCT reference data for distal tibia by half decades

Means and standard deviations (SD) for each volumetric bone outcome was computed separately for each age category. Reference datasets were generated for individuals without fractures (Fx-, top), individuals with fractures (Fx+, middle) and combined (bottom).

Tibia – Fx-

Age Category	N	BV/TV (frac)	Tb.Sp (mm)	Tb.Th (mm)	Tb.N (#/mm)	Ct.Th (mm)	vBMDi (mg/cm^3)	vBMDtr (mg/cm^3)	vBMDc (mg/cm^3)
55-60 years	8	0.133 ± 0.020	0.515 ± 0.076	0.078 ± 0.004	1.71 ± 0.21	1.226 ± 0.290	308.64 ± 36.07	159.34 ± 24.74	876.03 ± 59.79
60-65 years	37	0.135 ± 0.034	0.496 ± 0.108	0.075 ± 0.013	1.81 ± 0.33	1.113 ± 0.242	289.10 ± 48.39	162.38 ± 40.33	825.51 ± 72.18
65-70 years	48	0.139 ± 0.031	0.506 ± 0.106	0.080 ± 0.016	1.76 ± 0.30	0.983 ± 0.198	273.65 ± 47.14	166.87 ± 37.26	789.79 ± 57.61
70-75 years	27	0.134 ± 0.025	0.505 ± 0.085	0.077 ± 0.012	1.76 ± 0.27	0.857 ± 0.244	251.34 ± 41.69	161.15 ± 30.15	756.35 ± 93.01
75-80 years	28	0.137 ± 0.032	0.519 ± 0.137	0.079 ± 0.013	1.76 ± 0.43	0.832 ± 0.307	253.78 ± 57.01	164.09 ± 38.00	746.26 ± 89.04
80-85 years	15	0.132 ± 0.038	0.579 ± 0.326	0.080 ± 0.021	1.70 ± 0.42	0.734 ± 0.165	236.59 ± 41.86	158.30 ± 45.75	741.36 ± 54.40
85+ years	1	0.137	0.410	0.065	2.10	0.510	214.60	164.80	676.90

Tibia – Fx+

Age Category	N	BV/TV (frac)	Tb.Sp (mm)	Tb.Th (mm)	Tb.N (#/mm)	Ct.Th (mm)	vBMDi (mg/cm^3)	vBMDtr (mg/cm^3)	vBMDc (mg/cm^3)
55-60 years	5	0.146 ± 0.019	0.456 ± 0.057	0.079 ± 0.019	1.90 ± 0.26	1.236 ± 0.334	307.64 ± 61.65	175.34 ± 22.85	828.06 ± 40.45
60-65 years	28	0.131 ± 0.028	0.489 ± 0.089	0.072 ± 0.015	1.83 ± 0.30	0.933 ± 0.156	257.86 ± 39.18	156.88 ± 33.97	805.64 ± 44.61
65-70 years	33	0.124 ± 0.028	0.548 ± 0.144	0.075 ± 0.013	1.67 ± 0.32	0.872 ± 0.247	242.02 ± 43.38	148.83 ± 33.38	766.49 ± 87.10
70-75 years	37	0.129 ± 0.026	0.541 ± 0.172	0.077 ± 0.013	1.71 ± 0.35	0.898 ± 0.212	252.78 ± 44.95	155.22 ± 30.91	774.10 ± 58.20
75-80 years	29	0.127 ± 0.026	0.519 ± 0.089	0.074 ± 0.013	1.73 ± 0.28	0.804 ± 0.262	243.31 ± 47.27	152.14 ± 31.49	754.70 ± 62.12
80-85 years	12	0.131 ± 0.040	0.536 ± 0.144	0.076 ± 0.012	1.72 ± 0.41	0.783 ± 0.346	240.83 ± 49.70	157.31 ± 48.02	727.24 ± 116.76
85+ years	6	0.119 ± 0.027	0.542 ± 0.102	0.071 ± 0.013	1.67 ± 0.31	0.525 ± 0.215	197.60 ± 49.67	142.50 ± 31.87	677.65 ± 78.06

Tibia - Pooled

Age Category	N	BV/TV (frac)	Tb.Sp (mm)	Tb.Th (mm)	Tb.N (#/mm)	Ct.Th (mm)	vBMDi (mg/cm^3)	vBMDtr (mg/cm^3)	vBMDc (mg/cm^3)
55-60 years	13	0.138 ± 0.020	0.493 ± 0.073	0.078 ± 0.011	1.78 ± 0.24	1.230 ± 0.293	308.25 ± 45.01	165.49 ± 24.43	857.58 ± 56.75
60-65 years	65	0.133 ± 0.031	0.493 ± 0.099	0.074 ± 0.014	1.82 ± 0.32	1.035 ± 0.226	275.64 ± 46.98	160.01 ± 37.54	816.95 ± 62.20
65-70 years	81	0.133 ± 0.030	0.523 ± 0.124	0.078 ± 0.015	1.73 ± 0.31	0.938 ± 0.224	260.76 ± 47.99	159.52 ± 36.61	780.30 ± 71.53
70-75 years	64	0.131 ± 0.025	0.526 ± 0.142	0.077 ± 0.013	1.73 ± 0.31	0.881 ± 0.225	252.17 ± 43.27	157.73 ± 30.49	766.61 ± 74.72
75-80 years	57	0.132 ± 0.029	0.519 ± 0.114	0.076 ± 0.013	1.75 ± 0.36	0.818 ± 0.283	248.45 ± 52.08	158.01 ± 35.05	750.55 ± 75.96
80-85 years	27	0.132 ± 0.038	0.560 ± 0.258	0.078 ± 0.018	1.71 ± 0.41	0.756 ± 0.256	238.47 ± 44.65	157.86 ± 45.86	735.09 ± 86.09
85+ years	7	0.121 ± 0.025	0.523 ± 0.106	0.070 ± 0.012	1.73 ± 0.33	0.523 ± 0.196	200.03 ± 45.80	145.69 ± 30.29	677.54 ± 71.26

Table LXIII. National 1.0T pMRI reference data (Hamilton cohort) for distal radius by half decades

Means and standard deviations (SD) for each volumetric bone outcome was computed separately for each age category. Reference datasets were generated for individuals without fractures (top), individuals with fractures (middle) and combined (bottom).

No Fracture										
Age Category	**N**	**BV/TV** (fraction)	**Tb.Sp** (mm)	**Tb.Sp MI** (mm)	**Tb.Th** (mm)	**Tb.Th MI** (mm)	**Tb.N** (#/mm)	**Cx** (index)	**H_A** (mm^2)	**H_M** (mm^2)
55-60 years	3	0.447 ± 0.024	0.611 ± 0.118	0.605 ± 0.115	0.483 ± 0.046	0.479 ± 0.043	0.9 ± 0.1	5.47 ± 3.85	3.72 ± 1.98	31.91 ± 7.11
60-65 years	4	0.494 ± 0.014	0.535 ± 0.050	0.531 ± 0.049	0.517 ± 0.045	0.515 ± 0.045	1.0 ± 0.1	7.08 ± 4.40	2.30 ± 0.49	43.22 ± 13.77
65-70 years	9	0.461 ± 0.049	0.665 ± 0.156	0.646 ± 0.130	0.542 ± 0.028	0.538 ± 0.030	0.8 ± 0.1	5.81 ± 2.88	3.91 ± 2.13	41.38 ± 14.40
70-75 years	7	0.465 ± 0.053	0.635 ± 0.152	0.614 ± 0.125	0.526 ± 0.042	0.520 ± 0.038	0.9 ± 0.1	5.41 ± 3.49	3.89 ± 3.77	52.65 ± 26.18
75-80 years	9	0.487 ± 0.034	0.581 ± 0.156	0.554 ± 0.094	0.519 ± 0.028	0.519 ± 0.026	0.9 ± 0.1	8.42 ± 2.42	2.83 ± 2.16	32.48 ± 10.19
80-85 years	8	0.456 ± 0.075	0.687 ± 0.294	0.673 ± 0.274	0.531 ± 0.020	0.528 ± 0.020	0.9 ± 0.1	6.58 ± 3.31	3.89 ± 3.21	39.05 ± 11.39
Fractured										
Age Category	**N**	**BV/TV** (fraction)	**Tb.Sp** (mm)	**Tb.Sp MI** (mm)	**Tb.Th** (mm)	**Tb.Th MI** (mm)	**Tb.N** (#/mm)	**Cx** (index)	**H_A** (mm^2)	**H_M** (mm^2)
60-65 years	9	0.482 ± 0.022	0.590 ± 0.071	0.581 ± 0.068	0.538 ± 0.025	0.535 ± 0.024	0.9 ± 0.1	7.36 ± 2.54	2.90 ± 1.14	39.20 ± 12.86
65-70 years	11	0.482 ± 0.056	0.638 ± 0.268	0.604 ± 0.184	0.544 ± 0.035	0.537 ± 0.034	0.9 ± 0.1	6.68 ± 2.49	3.61 ± 4.04	35.52 ± 11.87
70-75 years	7	0.480 ± 0.020	0.603 ± 0.070	0.591 ± 0.063	0.546 ± 0.031	0.542 ± 0.029	0.9 ± 0.1	6.28 ± 2.68	2.90 ± 0.80	41.95 ± 10.17
75-80 years	8	0.479 ± 0.025	0.603 ± 0.072	0.595 ± 0.070	0.546 ± 0.052	0.542 ± 0.048	0.9 ± 0.1	6.09 ± 3.52	2.98 ± 1.07	40.67 ± 10.81
80-85 years	12	0.465 ± 0.053	0.657 ± 0.190	0.639 ± 0.170	0.542 ± 0.048	0.538 ± 0.045	0.9 ± 0.1	6.31 ± 2.90	3.27 ± 1.69	39.90 ± 9.06
85+ years	13	0.432 ± 0.074	0.796 ± 0.390	0.743 ± 0.288	0.528 ± 0.045	0.522 ± 0.048	0.8 ± 0.2	5.24 ± 3.77	4.44 ± 4.19	53.53 ± 21.83
Pooled										
Age Category	**N**	**BV/TV** (fraction)	**Tb.Sp** (mm)	**Tb.Sp MI** (mm)	**Tb.Th** (mm)	**Tb.Th MI** (mm)	**Tb.N** (#/mm)	**Cx** (index)	**H_A** (mm^2)	**H_M** (mm^2)
55-60 years	3	0.447 ± 0.024	0.611 ± 0.118	0.605 ± 0.115	0.483 ± 0.046	0.479 ± 0.043	0.9 ± 0.1	5.47 ± 3.85	3.72 ± 1.98	31.91 ± 7.11
60-65 years	13	0.486 ± 0.02	0.573 ± 0.069	0.565 ± 0.065	0.532 ± 0.032	0.529 ± 0.031	0.9 ± 0.1	7.27 ± 3.03	2.72 ± 1.01	40.44 ± 12.7
65-70 years	20	0.473 ± 0.053	0.65 ± 0.219	0.623 ± 0.16	0.543 ± 0.031	0.538 ± 0.031	0.9 ± 0.1	6.29 ± 2.64	3.74 ± 3.24	38.16 ± 13.06
70-75 years	14	0.472 ± 0.039	0.619 ± 0.115	0.602 ± 0.096	0.536 ± 0.037	0.531 ± 0.034	0.9 ± 0.1	5.84 ± 3.02	3.4 ± 2.67	47.3 ± 19.87
75-80 years	17	0.483 ± 0.03	0.591 ± 0.121	0.573 ± 0.084	0.532 ± 0.042	0.53 ± 0.038	0.9 ± 0.1	7.33 ± 3.13	2.9 ± 1.68	36.33 ± 11
80-85 years	20	0.462 ± 0.06	0.668 ± 0.226	0.652 ± 0.207	0.538 ± 0.04	0.534 ± 0.037	0.9 ± 0.1	6.41 ± 2.97	3.5 ± 2.29	39.59 ± 9.68
85+ years	13	0.432 ± 0.074	0.796 ± 0.39	0.743 ± 0.288	0.528 ± 0.045	0.522 ± 0.048	0.8 ± 0.2	5.24 ± 3.77	4.44 ± 4.19	53.53 ± 21.83

volume. Trabecular number showed low variability across age groups for pMRI and hr-pQCT. However, hr-pQCT was able to measure larger inter-individual variability in Tb.N. All Tb.N values were rounded to one decimal place, resulting in near identical results for all age groups for pMRI. Graphical data from Bland-Altman analyses for pMRI-hr-pQCT validation (Table XXVII) revealed the true variability for values that were not rounded.

Overall bone volume was higher, and trabeculae thicker at the tibia compared to the radius but density was similar between the two sites as demonstrated by hr-pQCT. Differences between fracture and non-fractured groups were most evidently shown for Tb.Sp, Ct.Th and cortical vBMD (Table LXIV). Statistical analyses were not performed here as significance of between-group differences were already highlighted by OR and confidence intervals in section 5.7. Although density differences between fractured and non-fractured groups were not large for trabecular vBMD as obtained by hr-pQCT at the radius (0.78 mg/cm^3), pQCT was able to demonstrate as large as 27.64 mg/cm^3 difference at the more distal slice of the radius. A similar magnitude of difference was observed at the more distal slice of the tibia as well (Table LXV). Differences between fractured and non-fractured groups were most evident at the more distal slice for both the ultradistal radius and tibia for pQCT, as compared to the more proximal slice. The largest differences were observed with integral vBMD between fractured and non-fractured individuals. Aside from BV/TV and hole geometry measures, pMRI revealed sizeable differences between fractured and non-fractured groups – although, Tb.Th appeared larger in the fractured group versus the non-fractured. Like hr-pQCT, differences in Tb.N between groups were minimal for pMRI (Table LXVI).

Table LXIV**. National cohort: descriptive summary of hr-pQCT data by fracture groups**
Means ± standard deviation for each volumetric bone outcome were summarized across all study participants collapsing age-categories for the ultradistal radius and tibia in the national cohort study according to whether (+) or not (-) they had history of fragility fractures (Fx).

Anatomy	N	BV/TV (fraction)	Tb.Sp (mm)	Tb.Th (mm)	Tb.N (#/mm)
Radius - Fx-	160	0.113 ± 0.020	0.529 ± 0.068	0.063 ± 0.006	1.78 ± 0.17
Radius – Fx+	146	0.112 ± 0.009	0.551 ± 0.043	0.065 ± 0.003	1.74 ± 0.08
Radius – Pooled	306	0.114 ± 0.012	0.536 ± 0.046	0.064 ± 0.003	1.77 ± 0.09
Tibia – Fx-	164	0.134 ± 0.003	0.504 ± 0.050	0.076 ± 0.005	1.80 ± 0.14
Tibia – Fx+	150	0.128 ± 0.011	0.519 ± 0.034	0.075 ± 0.003	1.75 ± 0.09
Tibia – Pooled	314	0.131 ± 0.005	0.520 ± 0.023	0.076 ± 0.003	1.75 ± 0.04
Anatomy	**N**	**Ct.Th (mm)**	**vBMDi (mg/cm^3)**	**vBMDtr (mg/cm^3)**	**vBMDc (mg/cm^3)**
Radius - Fx-	160	0.656 ± 0.116	278.09 ± 42.43	135.70 ± 23.64	816.54 ± 57.24
Radius – Fx+	146	0.617 ± 0.126	269.08 ± 36.60	134.92 ± 10.45	787.77 ± 46.54
Radius – Pooled	306	0.632 ± 0.126	274.60 ± 38.89	137.17 ± 12.21	797.98 ± 50.03
Tibia – Fx-	164	0.894 ± 0.240	261.10 ± 31.92	162.42 ± 3.06	773.17 ± 64.40
Tibia – Fx+	150	0.864 ± 0.212	248.86 ± 32.46	155.46 ± 10.20	761.98 ± 49.68
Tibia – Pooled	314	0.883 ± 0.222	254.82 ± 33.27	157.76 ± 5.97	769.23 ± 57.93

Table LXV. National cohort: descriptive summary of pQCT data by fracture groups
Means ± standard deviation for each volumetric bone densitometric outcome were summarized across all study participants collapsing age-categories for the ultradistal radius and tibia in the national cohort study according to non-fractured, fractured and combined groups.

	NO FRACTURES			
Anatomy	**N**	**vBMDi**	**vBMDtr**	**vBMDc**
Radius Proximal Slice	131	279.49 ± 12.74	166.18 ± 7.14	880.81 ± 15.81
Radius Distal Slice	103	377.08 ± 40.81	173.25 ± 32.32	993.09 ± 38.53
Tibia Proximal Slice	144	285.61 ± 24.79	218.47 ± 23.89	867.23 ± 17.33
Tibia Distal Slice	143	267.45 ± 22.96	236.21 ± 21.71	827.43 ± 21.88
	ONE OR MORE FRACTURES			
Anatomy	**N**	**vBMDi**	**vBMDtr**	**vBMDc**
Radius Proximal Slice	114	261.01 ± 24.30	159.54 ± 10.13	868.16 ± 25.14
Radius Distal Slice	105	335.91 ± 21.66	145.61 ± 14.92	963.76 ± 21.72
Tibia Proximal Slice	129	259.73 ± 28.25	195.17 ± 19.84	859.62 ± 28.95
Tibia Distal Slice	132	241.80 ± 23.99	209.62 ± 17.48	816.50 ± 26.07
	POOLED			
Anatomy	**N**	**vBMDi**	**vBMDtr**	**vBMDc**
Radius Proximal Slice	245	271.47 ± 13.97	162.83 ± 6.06	875.63 ± 14.51
Radius Distal Slice	208	352.65 ± 21.51	155.31 ± 6.88	975.05 ± 23.65
Tibia Proximal Slice	273	269.96 ± 18.01	204.31 ± 9.10	862.38 ± 21.73
Tibia Distal Slice	275	253.19 ± 12.97	221.64 ± 6.75	820.58 ± 15.53

Table LXVI. National cohort: descriptive summary of 1.0T pMRI data by fracture groups
Means ± standard deviation for each distal radius volumetric bone outcome were summarized across all study participants in the Hamilton cohort collapsing age-categories and separated according to non-fractured (Fx-), fractured (Fx) and pooled groups.

Group	**N**	**BV/TV** (fraction)	**Tb.Sp** (mm)	**Tb.Sp MI** (mm)	**Tb.Th** (mm)	**Tb.Th MI** (mm)
Fx-	40	0.470 ± 0.049	0.627 ± 0.177	0.609 ± 0.153	0.526 ± 0.033	0.523 ± 0.032
Fx+	60	0.468 ± 0.052	0.658 ± 0.235	0.633 ± 0.179	0.540 ± 0.040	0.535 ± 0.039
Pooled	100	0.469 ± 0.050	0.646 ± 0.214	0.624 ± 0.169	0.534 ± 0.038	0.530 ± 0.037
Group	**N**	**Tb.N** (#/mm)	**Cx** (index)	**H_A** (mm^2)	**H_M** (mm^2)	
Fx-	40	0.9 ± 0.1	6.61 ± 3.18	3.47 ± 2.54	40.61 ± 16.28	
Fx+	60	0.9 ± 0.1	6.29 ± 2.99	3.43 ± 2.72	42.1 ± 14.69	
Pooled	100	0.9 ± 0.1	6.41 ± 3.05	3.45 ± 2.64	41.52 ± 15.27	

6 Discussion

6.1 Summary of Results

In the local cohort of women with mean age 74 years and BMI 27.65 kg/m^2, study procedure uptake was at least 50% for follow-up, repeat and multi-modality activities. MR images encountered more motion artifact followed by pQCT and hr-pQCT images, which demonstrated the highest image quality. Model-independent Tb.Sp as measured from pMR images, Ct.Th and vBMD from pQCT images all showed strong correlations with corresponding values derived from hr-pQCT images and yielded slopes near unity. However, ICCs suggested that Tb.Sp from pMR images did not agree with those from hr-pQCT images as well as other bone variables did. Closer examination of agreement from Bland-Altman analyses suggested a relationship between mean value and degree of agreement for multiple pQCT-derived volumetric bone outcomes. The angular difference in anatomical orientation between MRI and hr-pQCT images made little impact on these linear relationships. Co-registration and selection of only anatomically comparable slices between participants resulted in an improvement in BV/TV correlation but worsened Tb.Sp correlation between pMRI and hr-pQCT. Short-term reproducibility of bone outcomes was highest for BV/TV and other macrostructural densitometric variables and lowest for trabecular outcomes related to hole geometry and connectivity. The precision errors yielded from these analyses were lower at the tibia for pQCT images as compared to the radius, and lower for pQCT images at the radius as compared to pMR images. Co-registration of repeated pMR images contributed to mild improvement in precision error. One-year changes were larger for the radius than for the tibia, and smallest for hr-pQCT

followed by pMRI and then pQCT for the majority of variables except for Tb.N, showing the opposite trend. One-year changes in Tb.Sp were similar across the three modalities. Exclusion of individuals who were on antiresorptive therapy or who have had a fragility fracture in the last 15 years resulted in further decrease in one-year change. Least significant change and SEE yielded considerably different odds for fractures for most bone variables. In the local cohort, only Ct.Th and cortical vBMD revealed any association with fragility fractures using hr-pQCT images. Although certain trabecular measures dervied from pMR and pQCT images erred towards an increased odds for fragility fractures, confidence intervals overlapped 1.0. In the national dataset, the associations for Ct.Th and vBMD with fractures were externally validated for hr-pQCT and became significant for pQCT. In addition, other bone variables revealed increased odds for fractures as well, albeit to a smaller magnitude. This investigation also generated a number of useful outputs for reference including a national reference dataset for each modality by age, one-year LSC, SEE, cross-calibration equations, multi-centre phantom and human calibration equations.

6.2 Study design strengths and limitations

6.2.1 Recruitment and selection

Selection biases were present in the local Hamilton cohort of women due to various logistical and volunteerism-related conditions. Although these limitations could have reduced the degree to which this cohort represented Canadian women over 50 years of age, most conditions were not anticipated to affect at least short-term precision error and in some cases, the long-term changes over time.

Local Hamilton Cohort

Selection biases: Transportation: Because of the amount of travel (70 km) required for completing hr-pQCT procedures, only participants sufficiently capable of traveling longer distances agreed to completing these study procedures. To reduce the bias towards a cohort with greater access to transportation options, taxis and a van fleet were offered to participants who did not have immediate access to a vehicle or a peer willing to accompany the participant to their study appointment. One could argue that more mobile study participants may inherently have superior locomotor skills and be able to remain still during a scan. More importantly, their bone health may be better maintained relative to individuals who are less mobile and thus unable or unwilling to participate in the study. Syddall showed that women with no car access had a higher risk for fractures and lower bone strength as measured by pQCT in the Hertfordshire Cohort Study (181). Hence, it is plausible that women with poorer bone strength may be missed as a result of the poorer participation rate from those who were unable or unwilling to travel long distances.

Sex: Although this cohort focused only on women, it was not anticipated that volumetric bone outcome validity and short-term precision would be significantly affected by sex differences. Long-term precision, LSCs, SEEs and ORs for fractures, on the other hand, can be influenced by sex-differences in the rate and timing of bone loss with chronological age (15,182). While evidence supporting this idea was focused on changes at the hip and lumbar spine, the results may be translatable to the ultradistal radius and tibia sites, which similarly involve a combination of cortical and trabecular bone support.

Sode et al. showed that the region exhibiting major differences between the sexes is located at the inner anterior aspect of the ultradistal radius and tibia, as quantified from hr-pQCT (183). Using pQCT, MacIntyre also showed that loss of trabecular bone connectivity and increases in mean hole area was significantly more rapid in women than in men (119).

Employment/retirement age and mobility: Due to the fact that some younger women were still employed and had difficulty creating availability to complete study procedures; and a greater proportion of older women lacked mobility and were similarly unable to attend; there was an inherent bias towards women closer to retirement age. It was unknown whether age contributed towards test-retest precision biologically. It was not anticipated that outcome validation would be affected by age alone, except to the extent that tendency to move in the scanner would be correlated with age. Kalisch et al revealed that increasing age was related to greater errors in joint position sense acuity of the dominant and non-dominant hand (184) suggesting that repositioning to the right joint angulation in the scanner may be more of a problem for older adults. This point highlights the importance of consistent technician-guided positioning. However, age-related differences in fracture odds could contribute towards a different clinical sensitivity between women.

Weight-restrictions: Weight limitations to scanner positioning chairs prevented heavier women from participating in the study. One study participant was excluded from pMRI and hr-pQCT scans due to this restriction. One previous investigation did suggest that

increased body size was associated with an increased test-retest precision error on pQCT (185) – a proposition that could extend to precision error for pMRI and hr-pQCT examinations requiring a similar degree of limb immobilization or involving a similar degree of motion sensitivity. Although an element of balance may be involved in maintaining immobility during scans, BMI was not found to be a determining factor in functional balance or mobility test reliability according to another study (186).

National Study

Selection biases: Volunteer/retention-driven bias: The accumulation of 16 years of volunteerism progressively filtered those who were not interested or were unable to continue with the study for a number of reasons. Reviewing historical reasons for loss-to-follow-up, the most common causes were 1) refusal (46%) which includes lack of time and health complications, 2) death (38%), 3) no contact or unable to reach (16%) (CaMos query). From the initial recruitment of CaMos participants, 42% agreed to participate (187), and to date, study retention has been 44% for the six sites at which pQCT and hr-pQCT scans were performed (CaMos BQS internal reference). Many participants who remained in the CaMos cohort from which the national dataset was sampled, displayed active health-seeking behaviour and in particular had more direct concerns regarding their risk for osteoporosis (187). Consequently, the national sample may overestimate bone structure and density in Canadian women. A review of occupational history among existing participants reveals a large proportion of individuals who were or currently are in

a professional specialty occupation including nurses and teachers (37.4%) or who were or are currently in the field of administrative support (21.4%).

Cultural/Geographical bias: The local health policies surrounding access to bone imaging technologies contributed towards regional biases in participation. In Ontario, British Columbia and Alberta where access to bone density testing using DXA scanners is widespread, the attraction of a study offering free access to bone imaging may not be uniquely appealing. However, in Saskatchewan, where scanner access is low and level 4 estimated maximum wait time has been 75 days (188), the advertisement of free immediate access to bone imaging technologies was more attractive. Another more immediate regional bias is the prominence of inclement weather (snow storms, floods) reducing study participation in mid-central Canada (primarily Saskatchewan and Alberta).

Ethical practices: Although study procedures have been largely streamlined, ethical practices were both nationally approved and locally fine-tuned. The interpretation of the Tri-Council Policy Statement (TCPS2, 2012) differed by jurisdiction. The most influential difference was whether or not study participants were allowed to receive any compensation beyond that which covered their cost for transportation and parking. The availability of extra compensation could have contributed towards increased participation and may therefore have influenced further regional differences in recruitment rates, centred on a socio-economical imbalance.

Radiation beliefs: Cohort differences in perceptions of radiation safety may exist within the intended sample. Those participants having been exposed to World War II to various degrees may have developed a fear for even minute amounts of radiation. The media also played a significant role in increasing caution to radiation sources in light of recent events (Fukushima Daiichi Nuclear Disaster, Japan, 2011). Proximity to sources of radiation may have been an added concern for some participants (Vancouver coastline radiation from Japanese tsunami; Ontario nuclear power plant). Because multiple technologies involving radiation (hr-pQCT, pQCT) were the subject of proposed study activities, participants may have exercised heightened caution when interpreting implications of radiation on their health. To provide a fair balance of radiation caution to participants, a comparison of radiation exposure from both natural and medical sources was provided to help participants make a better informed decision on participation. However, despite such efforts, some women declined study participation due to exposure to unnecessary harm.

Additional biases related to age, sex, and weight-restrictions described in the local Hamilton cohort section also apply to the national cohort.

6.2.2 Bone outcome availability

Due to technological differences and the lack of cross-platform applicable algorithms, the number of bone outcomes derived on each modality were different. pQCT was able to benefit from the technology of ionizing radiation in yielding densitometric measures yet at the same time, the OsteoQ foresting algorithm can be applied to pQCT image slices. Consequently, pQCT image analyses generated both densitometric outcomes as well as

hole geometry and trabecular connectivity measurements. While specialized for bone microstructural and density computations, manufacturer software for hr-pQCT was not equipped to compute direct hole geometry and connectivity measurements. Images derived from hr-pQCT scans in DICOM format can be read using the OsteoQ algorithm, but the 110 image slices obtained by hr-pQCT would need to be analyzed individually.

Although MR images were analyzed by OsteoQ to generate bone structure and hole geometry measurements, MR technology is currently not equipped to generate direct measurements of vBMD. Instead, efforts to estimate vBMD have been attempted. One study performed on ex-vivo metacarpal condyle bones of thoroughbreds showed that MR signal intensity as quantified from a T_1-weighted sequence was negatively correlated with vBMD as obtained by QCT ($R^2 = 0.77$) (189). In a similar study performed in 28 healthy men's femoral heads in vivo, vBMD obtained by QCT was correlated with T_2 relaxation time as determined using MRI (190). It is possible that these correlations reflect a biological relationship between bone marrow fat and bone density within the same region of interest, rather than a true linear correlation between density of compact bone and MR signal as reflecting bone material properties. Studies performed on compact bone examining the relationship between T_2 relaxation time and vBMD would need to be performed.

A larger repertoire of bone measurements can be generated from both OsteoQ and Scanco manufacturer algorithms than reported here. Those reported in this study were a limited

selection that has previously been shown to associate with clinical outcomes (139,180,191). Mechanical properties of bone were not discussed here, but could also contribute towards an improved understanding of fracture risk. Although mechanical strength can be more accurately determined using finite element analysis, this procedure requires information about the material properties of bone, which cannot be derived using MRI. Simpler structurally-related mechanical measures such as buckling ratio and cross-section moments of inertia could be derived from MRI, pQCT and hr-pQCT images by measuring the geometric properties of bone.

6.2.3 Timing of repeated study procedures

Because of the large number of study procedures demanded of study participants, coordination of all events within a short time-frame was a challenge. Consequently, pMRI, pQCT and hr-pQCT procedures were performed within 6 months of one another and one-year follow-up periods were given a margin of error of 3 months. The actual mean between-modality time discrepancy was 15 ± 28 days, with a maximum of 6 months and a minimum of 0 days. Follow-up times were closer to 13-15 months rather than one-year. It was not anticipated that between-modality comparisons would be affected by a maximum of 6 month time-delay as long as participants were not afflicted with any acute primary or secondary bone loss due to altered metabolism or iatrogenic causes (192). Of the participants examined in the local study, none were on long-term glucocorticoid therapy, had undergone any organ transplantation, had primary or secondary hyper- or hypoparathyroidism, or had recently been immobilized due to injury.

6.2.4 Statistical models and methods

Linear regression models reported all calibration slopes and intercepts for both parametric and non-parametric bone variables. Although it was shown that the non-parametric generalized additive model revealed confidence intervals around the slope and intercept that were wider than for a linear regression model, this difference in data variability was minimal. Despite the lack of differences between these models, it was clear that for certain non-parametric variables, such as Tb.Sp, that much of the data were skewed towards one end of the scale (See Figure 16) with only few data points forming the opposite end of values, and shaping the overall trend line. When the same variable was observed using an ICC, the results were dramatically different since ICCs are sensitive to larger mean differences between measurements despite a strong correlation. In addition, ICCs are largely influenced by small inter-individual variability, which was the case for a majority of individuals' Tb.Sp values. Although Chronbach's alpha is often chosen to quantify internal consistency even when the precision of each instrument (ie. the three modalities in question) is different, it remains sensitive to skewed data distributions (193). Instead, in this study, a third procedure, the Bland-Altman analysis was performed to address the limitations of these first two methods. Bland-Altman plots enable the visualization of the magnitude of agreement for all cases across a range of mean values regardless of the data distribution (194). For example, from the Bland-Altman plots, it is clear that despite having a strong correlation between modalities, Tb.Sp as measured by different scanners remains divergent when values are large (See Figure 17 and Figure 19).

For test-retest reliability, RMSCV was used as a global measure for inter-variable comparisons. While it represents the reliability of measurements upon repetition, it hinges on a critical assumption that variations of the repeated measurements are random and are normally distributed (177). Although several variables were found not to follow a Gaussian distribution, their RMSCV values were not particularly high as compared to variables fitting a Gaussian distribution. Though, extreme between-repetition differences did in fact contribute partially to a larger RMSCV value. In such cases where the pattern of agreement was not immediately apparent when observing RMSCV values, Bland-Altman analyses were useful to clarify at which values there may be a lack of reproducibility.

Detection limits were represented by SEE and LSC as examined in the context of clinical outcomes. Overall, SEEs yielded smaller absolute values as compared to the LSC. The SEE represented a characteristic of the scanner in question, addressing the question of how small a change the technique can actually detect (178). Standard errors of the estimate putatively remove the contribution of biological changes that can occur within a year by using the least squares regression method for adjusting for correlated differences (178). However, it assumes that changes are linear, which may not be necessarily the case with bone loss in post-menopausal women over the span of multiple years. Considering a relatively short period of one year, this assumption may, however, be valid.

LSCs were designed as a threshold beyond which clinical significance can be appreciated. However, its construction is based on a 95% confidence, an element of precision in the instrument and an adjustment factor related to the number of measurements made at baseline and follow-up as would be indicated in a clinical setting (179). This latter factor was based on the observation that confidence interval lengths decrease inversely proportional to the square root of the number of replications. Because there is no direct clinical implication associated with an LSC, it becomes difficult to assess to what extent an individual with such a quantified change over time will be at risk for an outcome.

To address this last problem, binary logistic regression models were fitted to data to quantify the odds for fragility fractures associated with each unit difference in bone variables, expressed in terms of SD, LSC and SEE. This method attributed clinical sensitivity to units of detection limit and to inter-individual variability. The limitation of a binary logistic regression model is that the direction of causality would be difficult to define, as data are analyzed in a cross-sectional point in time, or like in the present study with fractures, was evaluated retrospectively. Ideally a Cox proportional hazards model would report true fracture risk expressed as a HR, but this would require at minimum three years of follow-up and sufficient prospectively determined fractures over this period to provide adequate statistical power. In the case of an outcome such as a fragility fracture, the rate of which is relatively infrequent, an OR can approximate a HR (risk) (195). Hence, the odds for fractures outlined here can be a reasonable estimate of risk per unit difference in bone outcomes.

6.3 Region of interest location

6.3.1 Identifying ROI across modalities

Rationale for ROI selection

The poorer flexibility of the software interface provided by the hr-pQCT manufacturer limited the ease of customizing a more comparable ROI across modalities. Using a different ROI than one recommended by the manufacturer resulted in exclusion of the acquired images from the analysis database and the generation of different, incomplete outputs by default. More custom manipulation of the software is required to reconstitute the required variables in analyses generated from the usual ROI. In addition, it was desirable to adhere to a protocol that was utilized in most studies employing hr-pQCT in the past (from 2005-2013) (98,138,162,163,180,183,196-198). In order to maximize comparability, pQCT and pMRI protocols were tailored to match the hr-pQCT protocol. Although no scientific rationale from the manufacturer was provided for the selection of a fixed 9.5 mm distance for locating the volume of interest at the radius, Mueller showed that bone strength (encompassing mechanical properties of bone) determined from this location correlated the best with whole-bone strength ($r^2 = 0.98$) quantified over a span of 50 mm from the radial endplate. More proximal ($r^2 = 0.83$) and more distal ($r^2 = 0.93$) locations were less representative of whole-bone strength. In fact, only minor increases in the ability to predict bone failure (3-5% more) (199) can be obtained by examining the whole bone versus just the 9.02 mm span of bone located at 9.5 mm proximal to the radial endplate. While there have been no similar reports on the tibia 22.5 mm site, it is possible that Mueller's explanation that the greater amount of trabecular bone at the site

contributes to bone failure estimation can be further extended to what occurs at the tibia. However, one must be cautious as to the difference in biomechanics between the radius and tibia, since the tibia is weight-bearing and load distribution can be further affected by knee and hip joint alignment.

The differently sized ROIs across the modalities would also contribute to discrepancies in bone outcomes obtained. However, the focus of the present study was to evaluate the overall scan protocols and technologies (including number of slices, thickness of slices, total ROI, scan orientation, positioning) of each modality by examining the bone outputs, rather than simply looking at site-specific (matched) differences in bone driven purely by the science behind the technologies. As such, the validation procedures and comparison of reliability analyses have taken into account the fact that the ROI for pMRI was 10 mm, for hr-pQCT was approximately 9.02 mm but for pQCT was only 2.5 ± 0.3 mm. While it may have been desirable to increase coverage of bone using pQCT to 10.0 mm (4 slices), the time required to complete the procedure (about 20 minutes) would preclude the ability to acquire acceptable quality images suitable for analyses, largely due to motion. Instead, this study permitted one to determine how well less detailed and lower resolution bone images derived from single or thicker slices could represent bone from a more detailed and higher resolution image.

Landmark identification

Conceptually, scans obtained using pQCT and pMRI were performed such that slices were localized to within the 9.02 mm spanned distance measured on hr-pQCT. However, in each case, distance relative to an anatomical landmark guided the placement of the ROI at the ultradistal location. Angulation of the wrist or ankle could have led to a different view observed on scouts, particularly with pQCT and hr-pQCT where single projection scans were obtained. Because these scout views were two-dimensional, projection of a front of the bone that casts radio-opacity over an anatomical feature such as the radial endplate tuberosity would obscure its visibility. Although for pMRI, a series of slices of the anatomy were acquired, creating a better view of the anatomy, neither pMRI nor pQCT were consistently able to display the radial endplate tuberosity found on hr-pQCT. A relative position landmark measuring midway between the beginning and end of the radial tilt was used, which may have differed from the true radial endplate tuberosity by several millimetres. Boyd noted that with a 0.5 mm shift in ROI, there could be as much as a 2% and 6% difference in integral vBMD for the radius and tibia, respectively (167). Hence, it is probable that the discrepancy in radial endplate tuberosity localization could contribute towards error in validation models where bone variable values were compared between hr-pQCT and each of pQCT and pMRI. This issue was further addressed by co-registration procedures, the results of which were described in Section 5.2.1.

Relative (national) versus absolute (local) distance from reference line

In the national study, where the 4% site of the ultradistal radius and tibia was examined, there was found to be a significant difference as compared to the fixed distance used in the local study. While the almost 10 mm difference at the tibia in the national protocol would create a substantial discrepancy (>6%) with the more proximal location utilized in the local study, the 0.28 mm distance discrepancy at the radius would only incur a small penalty in position / ROI-placement error (<2%) as per Boyd's recommendations (167). Using a relative ROI like the 4% site has the advantage of correctly representing a region bearing an analogous proportion of trabecular versus cortical bone. In individuals with longer limb lengths, trabecular bone may have been higher in volume, thicker and its separation smaller. Conversely, in individuals with shorter limb lengths, cortical bone may have been thicker, trabecular bone lower in volume, thinner and more separated apart – relative to bone from individuals with the mean limb length. In children, the use of the percentage site is critical due to the dramatic differences in limb length with growth (126). In the current study, radius length ranged from 190 mm to 270 mm and tibia length ranged from 323 mm to 435 mm. With this wide range of lengths, it is plausible that the fixed distance ROI may have resulted in inaccurate representation of the same ultradistal site across individuals.

6.3.2 Limb angulation and scan orientation

The geometry of bone within the selected ROI was also affected by the angle at which the study participant positioned their hand into the scanner. As previously mentioned, the

ability to maintain a fixed angle could be affected by joint position sense acuity. While effort was made to straighten the participant's arm in the scanner's gantry, minor angulation in the anterioposterior and mediolateral directions could contribute to retesting error and to distorted overall geometry, especially thickness measures. This issue was more of a challenge for the two QCT modalities than for pMRI since QCT scans are only limited to axial orientation imaging. With pMRI, scan orientation can be recalibrated to an oblique direction on coronal and sagittal scout views. Angulation of hr-pQCT scans was quantified relative to pMRI scans assuming that all pMRI scans were correctly aligned with axial slices perpendicular to the shaft of the radius. The mean angular deviation was $4.46^{o} \pm 2.28^{o}$ with a range of 0.4^{o} to as much as 10.5^{o} malalignment. Certainly, a 10^{o} angle deviated from the zero axial axis could result in differences in bone structure, though perhaps not as dramatically for vBMD. The less than 5% variance in pMRI-hr-pQCT deviation for Tb.Th and less than 1% in difference for other bone structural measures explained by angular deviation suggested that the angulation of QCT scans due to limb positioning did not make a significant contribution to the validation procedures examined between pMRI and hr-pQCT. Although a similar investigation has not been performed by other investigators at the ultradistal radius and tibia on any of the modalities examined here, the precision of mandibular measurement from full body QCT scans was previously investigated at different gantry alignment angles demonstrating as much as 2-51% precision error due to angulation of 5^{o} up to 30^{o} (200).

6.4 Accuracy of volumetric bone characteristics

6.4.1 Trabecular separation and large holes

While an equally right skewed distribution for both Tb.Sp and H_M was observed, there were differences in what was represented by these two measurements. Trabecular separation was calculated as the fraction of marrow volume averaged over the total number of trabeculae. Thus, any particularly larger spaces between trabeculae would not be easily represented. Although the Tb.Sp SD measurement quantifies the degree of heterogeneity of Tb.Sp within an image, this outcome was not available on either pQCT or pMRI. For H_M, circles were circumscribed within inter-trabecular spaces to obtain a more accurate representation of spatial distribution. Several individuals were noted to have a single particularly large space within the medullary region, forming a cavity within the bone (Figure 23). Although it may be possible that a more proximal ROI was selected, reminiscent of the gradual transition from densely packed to sparse and no trabeculae at the diaphysis, many of these cases were actually observed towards the ultradistal segment of both radius and tibia. Through consultation with rheumatologists and radiologists, this characteristic may coincide with the development of a cyst. Unfortunately, the 3D gradient echo sequence utilized to quantify bone structure was not appropriate for visualizing cystic lesions or areas with fluid build-up. A fat-suppressed spin echo sequence would have been necessary to help confirm this proposition (201). Whether or not the loss of trabeculae in this region would contribute towards fracture risk remains unknown. However, this feature was not thought to contribute to any error in test-retest reproducibility or validity between modalities. Theoretically, the ability to identify such large holes would be limited by use of single-slice imaging, but in fact, 5 individuals with large holes were consistently identified in hr-pQCT, pMRI and pQCT image sets of the

radius. Meanwhile at the tibia, only 3 individuals with large holes were identified using pQCT but 8 were found on hr-pQCT. Bone cysts at the distal tibia were previously reported only in several case studies of children who experienced recent fracture, trauma or implants (202-205). From young adults with humeral and femoral bone cysts detected by MRI, Pireau demonstrated bone cyst index as related to minimum cortical thickness and cystic diameter, was associated with an increased odds for fractures (206). Buie et al more recently examined the effect of focal bone defects including bone

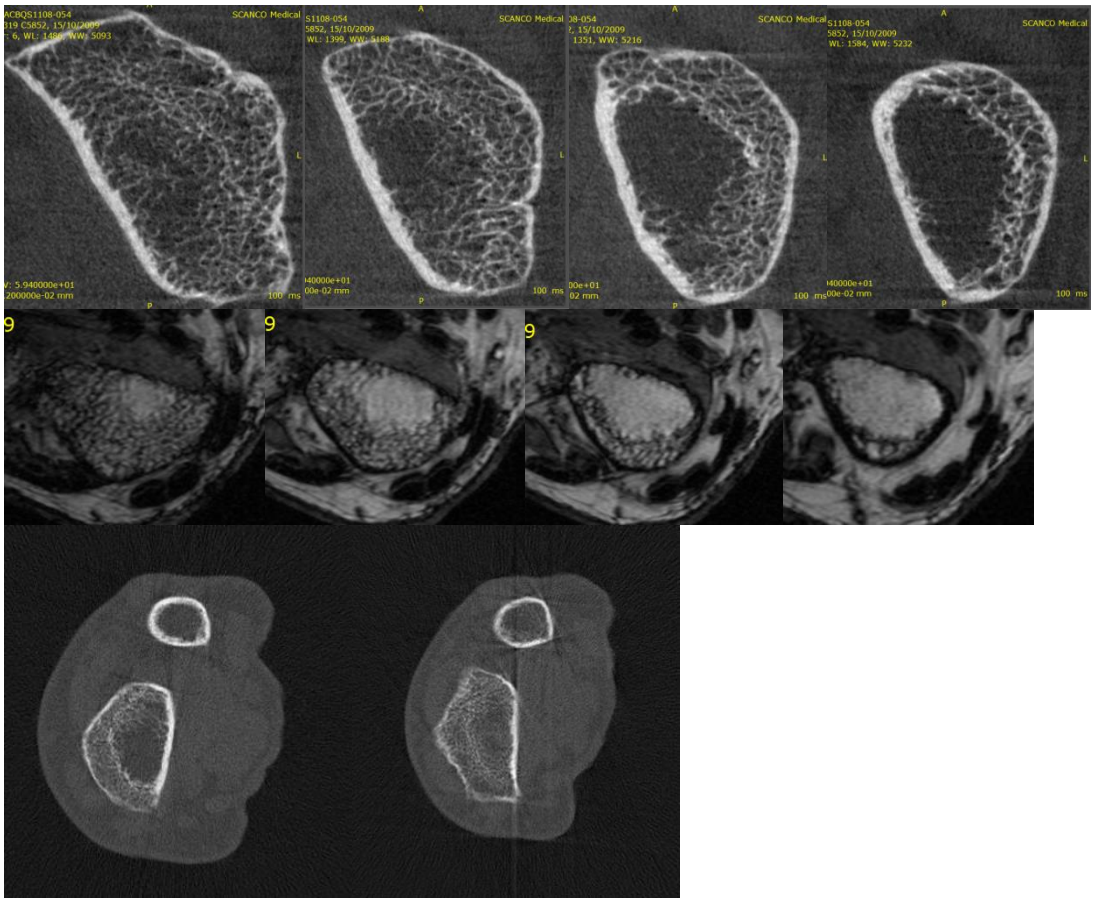

Figure 23. Comparison of large hole phenotype across modalities.
Elaborate inter-trabecular holes were identified at the ultradistal radius using hr-pQCT (top), pMRI (middle), and pQCT (bottom row). Borders of these elaborate holes were marked by increased linear attenuation on CT scans and lower signal on MRI scans.

cysts on the quantification of trabecular microstructure using µCT in burr-hole model rats for fracture healing and osteolytic bone metastasis model rats (207). They found that such focal lesions in the burr-hole model significantly increased mean Tb.Sp, Tb.Sp SD and maximum separation by 27.6%, 113% and 72.8%, respectively, relative to controls. Supporting the proposition discussed here, these results motivate special attention towards understanding large hole pathology and ramifications on fracture risk.

6.4.2 In-plane resolution and partial volume artifact

Effect of resolution on thickness quantification

All hr-pQCT scans were acquired with isotropic voxels of 82 µm, serving as the reference standard for comparisons in volumetric bone outcomes examined in this study. While µCT technology at resolutions down to 4 µm isotropic would be the ideal standard, the ionizing radiation (0.98 mSv/second from a direct beam) involved would be detrimental for human exposure (annual dose limit for public as per Health Canada: 1 mSv (208)) – not to mention the gantry size available at these resolutions are too small to accommodate a human wrist. At the 82 µm resolution, Tb.Th can only be approximated at best. For a mean Tb.Th of 205.4 ± 29.9 µm, as determined from previous iliac crest biopsies (209), a maximum of two voxels can span across without interruption. An additional maximum of two voxels can also span the borders of the trabecular bone. Depending on the anatomy, Tb.Th can range from 50 to 300 µm (95). At the higher end of this scale, 3 voxels can span across with a maximum of two voxels crossing the borders of the trabecular bone. Hence, any trabecular bone less than 246 µm (3 pixels at 82 µm each) in thickness may

be inaccurately measured using hr-pQCT. This limitation in resolution becomes more serious for pMRI (in-plane pixel resolution: 195 μm) and pQCT (in-plane pixel resolution: 200 μm), which could only have one pixel spanning the trabecular bone at best. Augat et al demonstrated this problem with the limited accuracy of Ct.Th and vBMD measurements on pQCT, with the primary culprit being partial voluming at the end voxels overlapping the bone boundaries, especially with thinner cortices (152). Hangartner also showed that peak cortical vBMD was reached only when the width of the structure can be represented by more than 6 pixels across. To address this problem, Hangartner suggested to use a segmentation threshold equal to the average between bone and soft tissues, at a value that most closely approximates a viable bone density, to obtain mineral content information; and a second but lower threshold to separately quantify area so as not to encounter areal overestimation (210). This method would limit the inaccuracies of quantifying cortical vBMD as it relates to thickness. Although these two investigations were focused on cortical bone, the conclusions could be extended to trabecular bone.

Contribution of segmentation method to thickness accuracy

Interpolation of trabecular bone boundaries on grey scale images was achieved with a dual-threshold-based algorithm for hr-pQCT, where edges of the trabecular bone represented by a partially bone-filled voxel may bare a density value equivalent to a fraction of compact bone. In this scenario, the threshold utilized and the fraction of bone overlapping the voxel will together determine whether that voxel would be considered bone or marrow (a binary result). For pQCT, bone was segmented from outer soft tissues

by applying a threshold equal to 2 times the SD above the mean soft tissue signal; and marrow was separated from bone using a threshold value determined using the Otsu method (211), after applying a series of image filters. For pQCT analyses, partial voluming effects at the edges of trabecular bone may still present as a problem but because image filters and a voxel-intensity histogram equalization procedure were applied to enhance bone signal dynamic range, the edges between bone and marrow would be smoothed. It remains unknown whether these enhancement procedures contribute to any improvements or degradations in accuracy. However, Li et al showed that histogram equalization of voxel intensity in MR images reduced the false positives for focal gray matter lesions identified in the brain using voxel-based morphometry (212).

Unlike pQCT and hr-pQCT analyses which rely on bone density thresholds for segmentation, pMRI bone segmentation was guided by image greyscale value, image gradient and pixel relative position to high contrast boundaries. The image foresting transform algorithm segmented bone from marrow and from soft tissue using these features, a method which may be less sensitive to partial voluming effects at the edge of bone (117). It is unknown whether the image foresting algorithm is superior to thresholding techniques in yielding more accurate measures of bone thickness. Aside from the data presented here, Falcao's image foresting transform algorithm was applied to segment parasites from microscopy fields of view, yielding 98.22% correct segmentations with over 90% sensitivity and 98% specificity for correct identification of species using different classifiers (213). To overcome the lack of density information from MRI,

Engelke previously described intra-image calibrated thresholding to binarize bone from soft tissue. The method was based on an average of air, tendon and cortical bone signals (ATC) standardized by that of subcutaneous fat (FAT), and adjusted empirically by a factor d, using the equation:

$$\text{Threshold (TH)} = \text{ATC} + d * (1 - \text{ATC/FAT}) \qquad (214)$$

Equation 20. Threshold selection based on air, tendon, cortical bone and fat signals.

However, the choice of d was arbitrary and the group adjusted d so that BV/TV was 20%. This method also lacked a statistical rationale, particularly regarding the probability that a signal of a certain magnitude would be considered bone.

In-plane and out-of-plane partial volume artifact

The partial voluming effects at the pixels surrounding the edges of bone presented problems with thickness measurements as discussed above. The overall sum of this effect then translated to total bone volume and density measurements that relied on this same element. In addition to the in-plane limitations of resolution, the thickness of slices was also subject to partial voluming. With a larger slice thickness, a greater amount of bone information was averaged within a single voxel. For CT modalities, this averaging effect was due to the back projection and integration of CT values across the volume of of voxel. For pMRI, this effect was due to the summation of signals of varying energies emitted from protons resonating greater or lesser from the focused RF. The greyscale value reflecting this average can be misinterpreted as low density bone depending on what

threshold was selected and what percentage of the voxel actually contains bone. In the case of MRI analyses, the averaged greyscale value can lead to mistaken Euclidean distances from seeded points in bone. With a thickness of 82 µm, hr-pQCT would suffer less from this limitation, followed by pMRI with a slice thickness of 1.0 mm and finally pQCT with thickness as large as 2.5 mm. Unfortunately, the limits of the collimator prevents pQCT slices from being any smaller. However, for pMRI, slice thickness can be altered at the expense of longer scan times, lower SNR and potential cross-talk between slices given a constant volume of interest. Engelke showed that in 1.5T MR images of the calcaneus at 1.0 mm slice thickness and 195 µm in-plane resolution, partial volume artifacts prevented accurate determination of bone structure compared to histomorphometry even after multiple 1 µm microtome-sectioned slices were averaged, repixelated to 208 µm in-plane and Gaussian blurred to simulate MR image slices (214).

The OsteoQ algorithm segmented cortical bone from soft tissue using a within-image calibration equal to 2.0 SD above the mean background signal. However, this did not account for the halo region described by Rittweger, representing partial voluming of the periosteal surface of cortical shell. While the Stratec manufacturer did not have an implemented algorithm to address this halo effect, Rittweger corrected for pQCT-derived cortical bone partial voluming artifact errors by up to 80% by using an equation developed with an aluminum and silicon phantom on the XCT2000 model (215). Here, they modeled the bone, background and halo regions around bone based on densities, areas, and circumference around each bone phantom, including the voxel edge length.

They applied the assumption that pixels in the halo region closer in proximity to the bone or background would bear a density closer to them, respectively. By applying corrections for errors in estimating mass and the threshold detection algorithm, an equation for better estimating material density was generated (See equation A13 of manuscript and appendix for full derivations (215)). Because the geometry of trabecular bone is more intricate, and marrow density is non-uniform, the definitions of circumference and modeling of how density is distributed within the halo region around the trabecular bone would require a different series of equations. No studies have been performed to date correcting for trabecular partial volume artifact.

6.4.3 Motion and other image artifacts

Motion artifact

Motion was a greater problem for pMRI followed by pQCT and most minimally hr-pQCT. The duration for which participants had to remain still was likely the reason for more motion in one modality compared to another – with pMRI scan time being 17-20 minutes versus 10-15 minutes for pQCT and 8 minutes for hr-pQCT, considering positioning and number of slices obtained. In participants with tremors, one scan was performed to gauge the participant's ability to remain still but was not repeated for any further analyses when image quality was poor on first try. For example, one participant with Parkinson's disease displayed a tremor on a follow-up visit. Consequently, the retest scan was cancelled.

While images with more severe motion were excluded from analyses, images with minor motion artifact were retained in analyses and could contribute to loss of accuracy and

reproducibility of bone outcomes. In CT images, motion streaks can mimic higher linear attenuation in areas that are otherwise non-radio-opaque. In MR images, areas of higher signal intensity, mostly marrow in this case, would overlap regions of bone that do not have any signal. As a result, CT images bearing motion exhibit an overestimation of BV/TV and conversely, MR images bearing motion artifact yield an underestimation of BV/TV. Indeed, Pauchard demonstrated that Tb.N was increased with participant motion, but both vBMD and Ct.Th decreased from hr-pQCT images (163). In addition, precision was reduced in images with a motion grade above 3, thus justifying their use of this selection threshold in quality control procedures (162), one which was also applied in the current study. The effect of grade 3 and above motion on precision was more dramatic for structural measures and more robust for vBMD. Although this study was applied to hr-pQCT images, the same observation could extend to pQCT. The algorithm described quantifying translational and longitudinal motion could prove useful for objective quality control during scans (162).

With MR images, a similar algorithm for quantifying motion in the translational and longitudinal directions has been described by Bhagat (164) using the normalized gradient squared (NGS) metric. It was determined that increased magnitude of displacement resulted in 9 to 45% differences in structural measures of bone from the same image. In addition, differences previously found to occur between two groups of participants (younger and older) was obscured by mimicking motion to their images through k-space (164). A technique called autofocusing, that involved manipulations to k-space for both

translational and rotational motions (216) improved NGS to a level just under 1%, which was superior compared to other similar but translation-only navigator techniques applied to k-space. Because the 1.0T pMRI unit utilized in the study did not come equipped with programming capability, it was not possible to apply image post-processing techniques to image k-space for motion correction. Future generations of the pMRI unit will have this research feature available (GE Healthcare internal communication).

Chemical shift artifact and magnetic susceptibility

The abnormally thin cortical shell in the anterior aspect of the radius could be explained by two image artifacts. Specific to MR images, the electronic shielding of protons of one nuclei is affected by neighbouring molecules' electron cloud configurations. When the influence is large enough, the precessional frequency of the proton can be changed significantly, as a consequence of a change in the local magnetic field (217), as suggested by:

$$\omega_{eff} = \gamma \cdot B_{eff}$$

Equation 21. Effective precessional frequency of a molecule (218).

where ω_{eff} is the effective precessional frequency, which is influenced by γ, the gyromagnetic ratio specific to the molecule of interest and B_{eff}, the effective magnetic field strength (a function of the external B_0 and local magnetic fields). Within bone marrow, the largest difference in precessional frequency is water and fat (219). For example, for the 1.0T field strength used in this study with a main magnetic field resonant

frequency (ω_0) of 42.58 MHz, given that the resonant frequency shift (Δf_{cs}) between fat and water is 3.5 ppm (220), the relative chemical shift frequency difference δ can be calculated:

$$\delta = \Delta f_{cs} * \omega_0 / 10^6$$

Equation 22. Relative chemical shift frequency difference (219).

$$= 3.5 \text{ ppm} * 42.58 \text{ MHz} (\times 10^6 \text{ Hz/ Mhz}) / 10^6$$

$$= 149.03 \text{ Hz} \quad \text{or} \quad \text{period} = 6.7 \text{ ms}$$

which means that for every period of 6.7 ms, fat and water signals will be exactly in phase; for TE's coinciding with periods in between cycles of this 6.7 ms, a combination of fat and water signals will be additive; and finally for TE's falling at the middle of the 6.7 ms period (ie. 3.35 ms), fat and water signals will be completely out of phase. This phenomenon manifests in an apparent spatial misregistration of MR image data, which would explain the loss of cortical bone at the anterior segment of the radius as shown in Figure 24, where bone was otherwise overlapped by signal shifted due to fat-water chemical shift. Since gradient echo sequences do not have a 180^o refocusing of spins like spin-echo sequences do, chemical shift artifacts are more apparent. Ways of reducing this artifact include changing the direction of frequency and phase-encoding directions – but this simply changes the direction of the spatial misregistration; using a wider receiver bandwidth, allowing a larger data collection interval per pixel with the cost of reduced SNR (217); and applying a fat suppression technique such as inversion-recovery to minimize the signal contribution of fat. Although magnetic field strength cannot be changed in the present setup, stronger magnetic fields actually precipitate the problem of

chemical shift artifacts. Thus, despite the small voxel size and higher SNR capable on magnets up to 7.0T field strength, these modalities may face an even more serious problem with chemical shift in SPGR imaging.

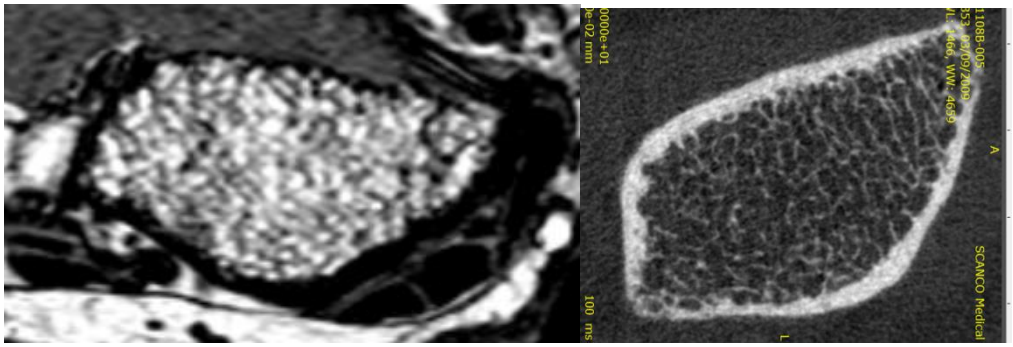

Figure 24. Comparison of MR image to CT image of the same bone.
Chemical shift artifact is apparent at the anterior aspect of the radius cortical bone as signal from the bone marrow shifted over due to precessional frequency differences between fat and water. One can also note thicker trabeculae in MR images compared to CT due to lower resolution but possibly with a contribution from magnetic susceptibiltiy differences resulting in signal loss or geometric distortion at bone-bone marrow boundaries.

A second possible contributor to the image artifact observed at the bone-bone marrow interface is occurrence of magnetic susceptibility differences between tissues. When molecules in proximity to one another exhibit very different capacities to be internally magnetized by an external field, local distortions in the magnetic field are possible. The resultant static magnetic field inhomogeneities can result in dephasing of spins and frequency shifts, manifesting in overall signal loss, geometric distortion or spatial misregistration of the image (221,222). Not only could this affect the cortical bone boundaries observed in Figure 24, the thickness of trabeculae can also be overestimated with susceptibility-driven signal loss of the bone marrow, rather than the normal lack of signal where bone is present. One study demonstrated with a magnetometer that the

frequency shift due to magnetic susceptibility differences between bone and soft tissue is as much as 9 ppm (222), amounting to phase shift with a period of 2.6 ms:

$\delta = \Delta f_{cs} * \omega_0 / 10^6$

$= 9.0 \text{ ppm} * 42.58 \text{ MHz} (\times 10^6 \text{ Hz/ Mhz}) / 10^6$

$= 383.22 \text{ Hz}$ or period = 2.6 ms

Although the authors believed the shift of as much as 1 mm was negligible with the resolution typically examined on MRI, the size of this shift would be as much as five times the pixel size in the present study. With 1.5T MR imaging of the femur, as much as a 2.5 mm shift due to magnetic susceptibility differences was described at the bone-tissue interface (223).

Aside from these two major sources of geometric anomalies described above, a number of other factors can also contribute towards misregistration of MR images including scaling error and lack of linearity in gradient fields, gradient shimming and magnetic field eddy currents (222). Gradient scale and linearity is calibrated on the machine and with regular maintenance, drift in these parameters should not be a major problem. However, proper gradient shimming may be a minor contributor especially with small RF leaks in the Faraday cage or at times improper coil fixation.

Beam hardening and ringing artifact

Although not immediately apparent on CT images, beam hardening could contribute towards a decreased Ct.Th and additional streaking artifacts reminiscent of motion. While

lower energy photons are attenuated by material in the path of the X-ray beam, their filtration generates a higher energy beam that passes through the remainder of the object. Material that can once attenuate lower energy photons can no longer attenuate this higher energy beam. The linear attenuation profile for the assumed beam spectrum is therefore underestimated in areas with more material through which photons must pass (224). When the signals around a circular object like the radius is integrated across all detectors, the result is an image bearing density around the cortical shell that is lower than it actually is. When routine thresholding is applied to these images, what may once be considered cortical bone may cross into trabecular bone territory, manifesting in smaller Ct.Th. For beams passing through soft tissue, the apparent low attenuation profile creates streaks along the path of the X-ray originating from a region of high density and thickness. On the CT images, this appears as darker bands compared to the surrounding tissue (224). In the present study, it was difficult to distinguish streaks originating from beam hardening when they coincided with streaks that were due to motion. However, individually, motion streaks were typically flanked by both higher and lower intensity streaks whereas beam hardening streaks only exhibit a lower intensity streak flanking the cortical bone. Filters on pQCT were available to compensate for some of the beam hardening effects by first attenuating the lower energy photons with a metal filament. The pQCT system was also pre-calibrated (built in to system) to cortical bone of the radius and tibia while adjusting for potential beam hardening artifacts within a physiological range of bone densities. While this range of bone densities have not been reported by the manufacturer, it is possible that individuals whose bone densities may fall beyond this

calibrated range could have insufficiently corrected beam hardening artifacts, leading to loss of cortical vBMD and Ct.Th accuracy.

Ringing artifacts noted from hr-pQCT scans were due to faulty CCDs at a specific location along the gantry of the scanner (224). This was consistent with the fact that the ringing artifact appeared at the same location within all image fields of view. As the periodicity of the waves of the ring was high, the hills and troughs of the waves did not directly mask trabecular or cortical bone features. Aside from minor discrepancies in density, it is not believed that the ringing artifact would contribute significantly to any deviations in structural measures of bone for hr-pQCT. There is the possibility that connectivity measures can be compromised when the skeletonization procedure identifies additional bone free ends as a consequence to the ring-induced interruptions in bone. However, the ringing artifacts were not present in pQCT images and connectivity assessment was not performed on hr-pQCT images here.

6.4.4 Comparison of radius bone outcomes across modalities

Because tibial scans were not performed on pMRI due to challenges with foot plantar flexion, only radial bone outcomes were compared across the three modalities. Like Kazakia who performed 3T MRI scans at 156 μm in-plane resolution at the radius with 0.5 mm slice thickness (131), the present study also demonstrated significant differences between pMRI and hr-pQCT, with a similar pattern of differences observed between hr-pQCT and pQCT. Notably, BV/TV and Tb.Th from MRI both exhibited between 3 to 4

fold larger values compared to hr-pQCT for both the present study and from Kazakia's analysis. At the higher resolution used by Kazakia, the 3T MRI-hr-pQCT difference for Tb.N was actually within the precision error for MRI-derived Tb.N. Meanwhile, the 40-60% smaller Tb.N observed here using 1T pMRI compared to hr-pQCT was actually much larger than the RMSSD for Tb.N on 1T pMRI. The fact that similar conclusions could be reached with even slightly better resolution demonstrates that the magnitude of this discrepancy cannot be explained by just resolution alone. Although there has not been a study correlating pQCT with hr-pQCT bone outcomes, it is anticipated that if resolution was truly the major determinant of the discrepancies observed here, that similar patterns of inter-modality bone outcome differences could be observed.

6.4.5 pQCT and pMRI validity - calibration equations

pMRI and pQCT correlations and linear equations for Tb.Sp

Although Tb.Sp showed slopes closest to unity for pMRI, its correlation coefficient with hr-pQCT was 0.65. The modest correlation coefficient could be reflective of more motion observed in MR image sets versus hr-pQCT. Lack of spatial resolution also factors into the unexplained variance. That model-independent Tb.Sp on pMRI correlated with the same on hr-pQCT better than model-dependent Tb.Sp, suggested that there are inherent differences between the two methods of computing Tb.Sp that may result in discrepancies when comparing this outcome across modalities. Calder also demonstrated significant differences between the (parallel plate) model-dependent and (mean intercept length) model-independent method of Tb.Sp computation for pQCT (200 x 200 µm x 2.5 mm), the agreement of which was dependent on the mean value of Tb.Sp (225). The similar but

smaller slope between model-dependent Tb.Sp obtained by pQCT versus hr-pQCT compared to between pMRI and hr-pQCT perhaps reflected the difference in image volumes between pQCT and each of pMRI and hr-pQCT.

Among pQCT images, the radius showed a stronger correlation against hr-pQCT for Tb.Sp than at the tibia, but the calibration slope was closer to unity at the tibia than at the radius. This observation can be explained by the greater heterogeneity of bone at the radius versus at the tibia sites. At the radius, within a volume spanning a 9.02 mm distance for hr-pQCT scans, there was a greater within-sample difference in the amount of trabecular versus cortical bone from distal to proximal ends. This feature was also shown by Calder (225). However, for the same fixed volume at the tibia, the distribution was not as dramatically different. Hence, a single slice pQCT scan centred about the tibia may actually be more representative of the full 9.02 mm span volume from hr-pQCT images as compared to one slice of the radius to a corresponding 9.02 mm span radius volume. The smaller inter-modality correlation coefficients observed at the tibia versus the radius can be explained by greater inter-individual variability in Tb.Sp at the ultradistal tibia. In comparison, a single slice of the radius, particularly at the more proximal slice, would show a larger void space where trabeculae are similarly sparse across different individuals. In contrast to pMRI, validity of pQCT-derived model-independent Tb.Sp was no different than model-dependent Tb.Sp for comparison against hr-pQCT. It was possible that BV/TV (larger in multi-slice pMRI versus single slice

pQCT) factored into the equation for model-independent Tb.Sp played a major role in dictating the discrepancy between pQCT and pMRI.

Examining the same 9.5 mm site of the ultradistal radius in 52 women with a mean age of 55 years, Kazakia et al observed the highest correlation between hr-pQCT and 3T MRI (156 x 156 μm x 2 mm) for Tb.Sp with an R^2 of 0.54 for the radius and 0.60 for the tibia (131). These values were slightly lower but similar in order of magnitude to what was observed in the present study ($R^2 = 0.65$). Although they showed a similarly high variability with larger Tb.Sp values, the slope described in the present study (m = 0.97) was closer to unity than what was observed by Kazakia (m = 1.69, axes reversed to match the present study). In a similar analysis in women (mean age 56 years, N=31) scanned using the same 3T MRI protocol, Folkesson from the same research group showed Tb.Sp correlations at the radius with hr-pQCT, which was similar to the one reported here (R^2 = 0.67, NS) when a dual-threshold method was applied to MR images (116). However, when she employed Fuzzy logic cluster segmentation, a method that binarized images based on image pixel intensity and anisotropy, the correlation became larger for Tb.Sp ($R^2 = 0.88$, $p<0.001$) (226). Krug et al used a similar imaging protocol on 3T MRI (156 x 156 x 500 μm) and saw a correlation against hr-pQCT for Tb.Sp of 0.83 based on the parallel-plate model at the distal radius, but as high as 0.92 for a model-independent analysis (132). The directionality of the increase was same as what was observed here but the present study revealed a slightly larger model-independent slope.

pMRI and pQCT correlations and linear equations for BV/TV

Both pQCT and hr-pQCT algorithms segmented bone from soft tissue by using density-based thresholds, albeit, the threshold values utilized for the former was based on surrounding soft tissue, and for the latter was fixed. In both cases, what was considered bone was very similar. In contrast to these density-based techniques, the algorithm used for pMR images segmented bone based on grey-scale contrast, cost-minimizing functions and Euclidean distances. Bone volume fraction was calculated as the trabecular vBMD divided by a mean 1200 mg HA/cm^3 for hr-pQCT and as the area of total bone divided by total mask area for pQCT. Considering this difference, BV/TV for pQCT remained highly correlated with hr-pQCT even though the amount of bone present in the single slice may be under-representing the full volume as obtained by hr-pQCT. This under-representation was reflected in the slope being less than unity. Similar to Tb.Sp, BV/TV obtained by pQCT at the radius was better correlated with hr-pQCT than at the tibia, but the slope was larger at the tibia. This observation can similarly be explained by the difference in cortical versus trabecular bone distributions at the radius versus tibia. For pMRI, although the calibration slope for BV/TV was larger than pQCT, the correlation coefficient was smaller due largely to the differences in algorithms and technology (magnetic resonance versus X-ray linear attenuation) used. pMRI algorithms for bone segmentation relied on a measurable contrast between bone and soft tissue edges. The CNR would have been greatly affected by any motion and partial volume artifacts.

Kazakia et al observed a smaller correlation between 3T MRI and hr-pQCT-derived BV/TV ($r^2 = 0.25$) than reported here ($r^2 = 0.53$) at the ultradistal radius, but their slope (m = 1.43) was larger by almost three-fold (131) than reported here (m = 0.48), but equally divergent from unity. However, they registered the analyzed high-resolution MR image set with a lower resolution volume that actually captured the full distal endplate anatomy. Rather than relying on a scout view for localization of the 9.5 mm site, the full three-dimensional low-resolution image set would have been more accurate. On the other hand, they observed a slope of 0.80 at the distal tibia, suggesting that MRI overestimated BV/TV relative to hr-pQCT, like in the present study. Similar to Kazakia's study, but employing the fuzzy logic segmentation method, Folkesson revealed an R^2 of 0.75 for BV/TV, compared to an R^2 of 0.39 when dual threshold segmentation was used. In both cases, the slope (m = 1.82 for dual threshold, and m= 2.27 for fuzzy logic) was at least as large as what was reported by Kazakia (226), and over three-fold larger than in the current study. Krug et al showed that a spin echo sequence generated smaller BV/TV values (by over 9%) compared to gradient echo sequences, the latter of which was employed in the current study. At the distal radius, the R^2 of 0.67 between 3T MRI and hr-pQCT was larger than what was observed here (132).

pMRI and pQCT correlations and linear equations for Tb.Th

Spatial resolution could be a contributing factor to the small slope observed for Tb.Th for both pQCT and pMRI in relation to hr-pQCT. Each of pMRI and pQCT have pixel sizes of approximately 200 μm. With only one or two pixels spanning most trabeculae, the

interpolation of any Tb.Th value would be limited to a small range of values. In fact, when the data were examined closely for pMRI, the SD represented less than 10% of the mean Tb.Th value. In comparison, other volumetric bone measures showed inter-individual SD that were between 30-80% of the measure's mean. For this reason, pMRI correlations were not significant and slopes were near zero, compounded by the fact that other factors related to discrepancy between technologies may be contributing to the unexplained variance. As described above, this discrepancy could be due to differences in bone segmentation technique – for CT based on linear attenuation and for MRI based on image foresting.

The difference between fuzzy logic (MRI-hr-pQCT Tb.Th $r^2 = 0.15$, $p<0.05$) and dual threshold segmentation (MRI-hr-pQCT Tb.Th $r^2 = 0.32$, NS) techniques described by Folkesson accounted for a difference in Tb.Th correlation with hr-pQCT of 17% (226). In either case, the correlations were small but larger than what was observed with the image foresting technique in this study. Hence, it is possible that the large unexplained variance is due to poor spatial resolution compared to hr-pQCT but also to the segmentation method used to define bone boundaries. Notably, Folkesson's fuzzy C-means clustering technique enabled bone enhancement by overcoming partial volume artifact and suppressing noise from the background, and relying mostly on probabilities of voxels bearing membership to one class of tissue versus another (116). The higher apparent SNR generated from this enhancement likely resulted in superior bone boundary definitions and thus Tb.Th quantification. Like BV/TV, correlations for MR image-derived Tb.Th

against hr-pQCT as described by Kazakia were small (r^2 = 0.13 for radius and 0.33 for tibia), but the slopes were much closer to unity (m = 1.29 for radius and m = 0.71 for tibia) than was reported here (m = 0.02) (131). Like Folkesson's study, Kazakia also employed a bone enhancement fuzzy C-means clustering technique for segmentation. In contrast, the dual-threshold method used in Krug's study resulted in the best correlation of 0.52 for model-independent computations and 0.63 for model-dependent computations for Tb.Th as compared against hr-pQCT (132). The difference between model-dependent and independent methods of calculating Tb.Th in Krug's study contrasts with the lack of difference observed in the present investigation. This discrepancy could be due to the low contrast yielded from MR images obtained from the present study and the fact that bone enhancement techniques were not applied here.

pMRI and pQCT correlations and linear equations for Tb.N

Like BV/TV, correlation coefficients for Tb.N were modest for both pMRI- and pQCT-hr-pQCT comparisons. However, it was the only bone measure that was routinely underestimated compared to hr-pQCT. Since Tb.N was computed as a function of BV/TV and Tb.Th, it was logical that a similar observation as BV/TV was demonstrated, tempered by the fact that the more inaccurate Tb.Th measurement rendered the correlation coefficient lower. By over-representing Tb.Th or underestimating the total perimeter of bone (P_B), due to larger pixel sizes, Tb.N (=BV/TV / ↑**Tb.Th** or =↓$\mathbf{P_B}$ / A_T) could be underestimated.

Kazakia et al showed a higher correlation (R^2 = 0.52) between MRI and hr-pQCT-derived Tb.N compared to the present study (R^2 = 0.38) but a larger slope of 3.1 versus 2.1 in this investigation (131). The slope derived from the fuzzy logic method (m = 2.5) was actually more similar to what was observed in this study as compared to the dual-threshold segmentation method (m = 3.1). In either case, correlations (R^2 = 0.73 for dual-threshold and R^2 = 0.83 for fuzzy logic segmentation) were over twice as large as in the present study (226). Unlike the calibration equation described here, both Kazakia and Folkesson demonstrated hr-pQCT-derived Tb.N values that were routinely larger than MRI-derived values by over 1 trabecula per mm as suggested by the x-intercept. Using the dual-threshold segmentation method, both model-dependent (R^2 = 0.95) and model-independent (R^2 = 0.93) methods yielded Tb.N correlations that were closest to unity.

pQCT correlations and linear equations for Ct.Th

For pMRI, Ct.Th was not computed due to the challenges of cortical bone loss resulting from chemical shift and magnetic susceptibility artifacts. For pQCT, like Tb.Th, Ct.Th measurement was compromised by poor in-plane resolution. Although beam hardening could also have contributed to lack of accuracy in Ct.Th, partial voluming artifact due to poor in-plane resolution was the key player. However, because Ct.Th is on average larger than any trabecula, the effects of partial voluming on the overall correlation coefficient for Ct.Th was less dramatic than for Tb.Th. Modest correlations were noted at all anatomical sites except for the more distal slice of the ultradistal radius, as this location contained smaller Ct.Th and was thus more sensitive to the effects of poorer resolution.

Both integral and trabecular vBMD showed strong correlations for pQCT against hr-pQCT with slopes close to unity. However, cortical vBMD suffered from smaller correlation coefficients and cortical vBMD was on average underestimated at a number of anatomical sites by pQCT. The poorer correlation observed for cortical vBMD could be explained by the same reasoning as for Ct.Th as related to poor spatial resolution. By averaging a given bone mass over an overestimated cortical area extrapolated by partial volumed voxels, the resultant cortical vBMD would be underestimated. As trabecular and integral vBMD did not rely as greatly on accurate segmentation of bone as for Ct.Th, the correlation with hr-pQCT remained high and slopes remained near unity.

Kazakia also reported the inability to compute cortical measures from radius MRI scans. However, they noted that the primary reason was due to the natural thinning towards the distal end at the wider diaphysis and not due to chemical shift artifact. In their study, only the proximal half of the corresponding hr-pQCT radius volume on MRI could be analyzed but data were not presented (131). While significant chemical shift artifact was noted in the MR images described in the present study, MR images observed from Kazakia or Folkesson's studies did not display a dramatic or visibly apparent chemical shift (131,132,226). The MR sequence utilized in the two studies was similarly a 3D gradient echo, but a larger bandwidth of 122 Hz/pixel was employed, almost 10 times larger than that used in the current study. This high bandwidth would explain the lack of chemical shift artifact observed, coupled with a larger SNR and CNR. Supporting this

hypothesis, the study by Krug used a bandwidth similar to the present study and yielded images that showed some chemical shift as depicted from their manuscript (Figure 25).

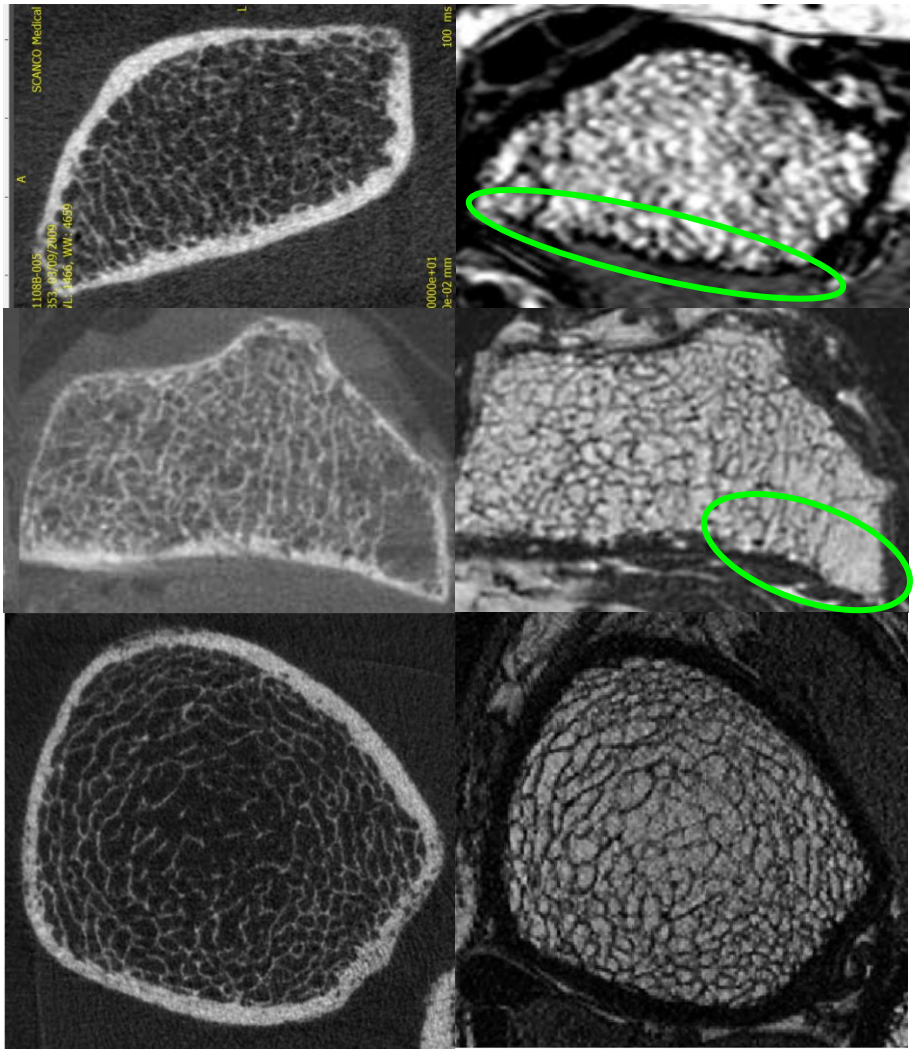

Figure 25. Chemical shift artifact of MR images obtained at different bandwidths.
Left column are hr-pQCT images and right column corresponding registered slice on MRI. Images obtained from the present study (top row) at 15 Hz, from Krug's study (middle row) at 15.63Hz and from Kazakia's study (bottom row) at 122 Hz were compared. Chemical shift artifact was most apparent (indicated by circled areas) in the present study followed by Krug's and Kazakia with no evidence of visible chemical shift.

Unlike the radius, tibia cortical bone was more prominent. From results obtained at the distal tibia in Kazakia's study, correlation between 3T MRI and hr-pQCT for Ct.Th was 0.59 with a slope of 1.67 (131). Louis showed that cortical area as measured by T1-weighted MRI and pQCT explained up to 88% and 87% of variance from a reference standard using planimetry of sectioned cadaveric specimens (227), respectively.

Overall validation challenges

Aside from Tb.Th, all bone structural measures obtained by pQCT and pMRI could be considered valid outcomes as referenced to hr-pQCT. In addition to the factors affecting accuracy described above, out-of-plane inconsistencies could also have contributed to poorer accuracy for all bone measures. Partial voluming artifact due to the larger slice thickness of pQCT (2.5 ± 0.3 mm) followed by pMRI (1.0 mm) was a major culprit for the quantification of trabecular geometry and to a lesser degree, cortical vBMD. Within a thicker slice, any structural elements of bone within the volume would have been integrated together during image reconstruction. Trabecular bone from more distant z-coordinates within the slice can appear as lower intensity linear attenuation values. Depending on the threshold selected for segmentation, these partial volume bone voxels may or may not be considered bone in the final analyses.

Although larger slice thicknesses on pMRI provide higher SNR, the less precise RF focusing within the slice means that the finer details of individual sections of bone within the volume may not be well represented in the final image slice acquired. In addition, the

sequence utilized for MR imaging of the radius involved 0 mm gap between slices, which could have contributed to decreased image contrast arisen from inter-slice cross-talk. Cross-talk occurs because the slice selection gradient and excitation profiles may not be uniform. Consequently, a single excitation pulse may be applied to adjacent slices at the same location, causing saturation of the signal and yielding little image detail in certain regions within slices (228). Of all MRI scans obtained, 4% exhibited mild to advanced forms of cross-talk. Two examples of cross-talk are illustrated in Figure 26.

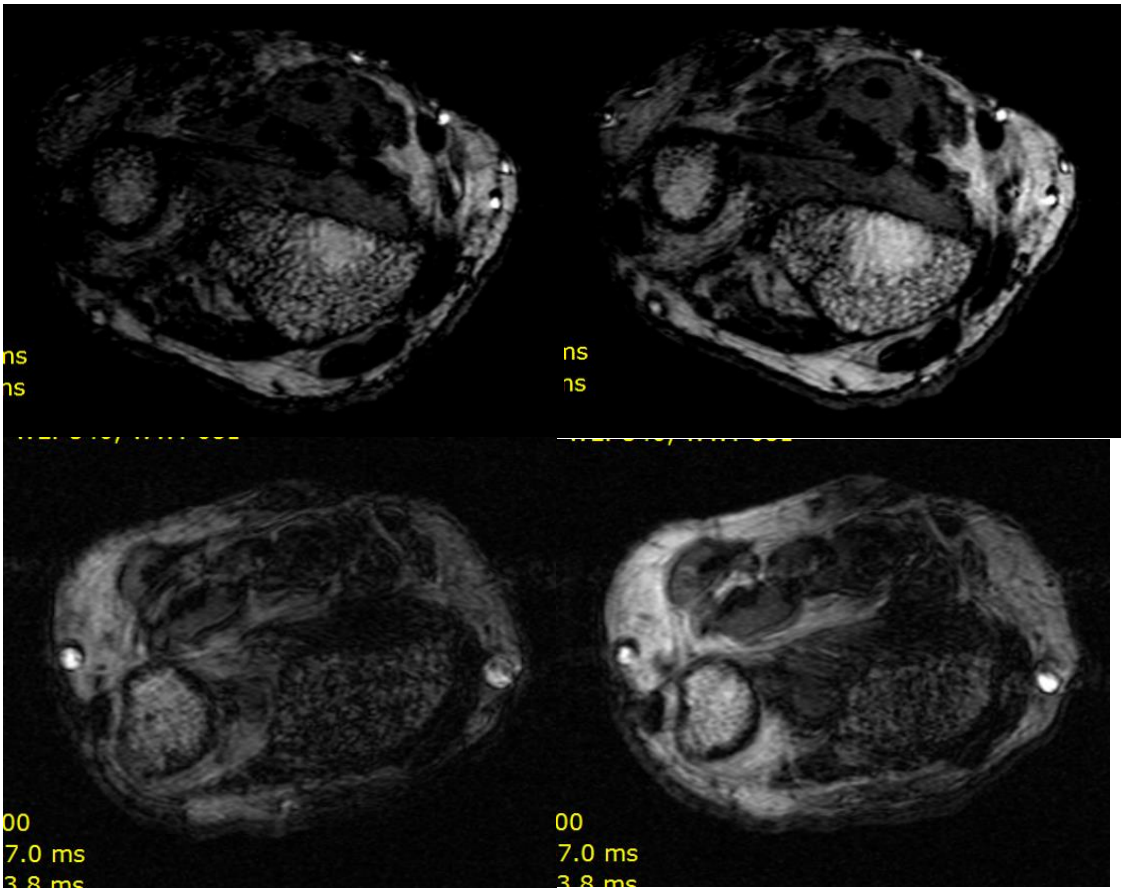

Figure 26. Inter-slice cross-talk resulting in localized image saturation.
Non-uniform slice selection gradient and excitation profiles resulting in excitation of adjacent slices at the same anatomical location, yielding localized image saturation. Each row represents one image set, and each image within the row illustrating various degrees of cross-talk.

pMRI Validation after co-registration

The improvement in linear slope between pMRI and hr-pQCT-derived BV/TV after co-registration suggests that positional error did in fact contribute to differential bone volume computation. However, the fact that isolating only slices that were relatively congruent did not improve correlations for Tb.N and Tb.Th between these modalities suggested that the advantage of slice matching was offset by perhaps the drawback of averaging fewer slices. With a larger volume of interest examined, the inter-modality errors would have been buffered by a larger proportion of matching features. In fact, inter-modality correlations were actually decreased for Tb.Sp after co-registration and isolating only anatomically analogous slices. Future validation efforts should begin with a larger volume of interest such that any co-registration efforts that filter out mismatched slices would not inadvertently trim the total volume to a smaller averaged volume that would render inter-modality errors more impactful on the overall inter-modality correlation. With a standard acquisition protocol yielding 9.02 mm for hr-pQCT, only 8 pMRI slices were found to be matched with hr-pQCT and located at the same region of interest across all individuals.

Co-registration was guided by visual inspection of overlaid colour schemes applied to each image set. Because of the difference in image contrast and angled axial image planes of MRI versus CT scans, it was challenging to consistently utilize any fixed anatomical landmarks or bone-soft tissue interfaces as guiding points for the co-registration process on every image set without multi-planar reformatting. For this same reason, 3D rigid registration techniques were not employed as was performed by Folkesson (226). Instead, unique anatomical features guided co-registration on an image-by-image basis while only

translational and rotational transformations were applied. Because multi-planar reformatting of the images was not desired – due to the degradation in resolution achieved by oblique rotation – it was not possible to perfectly co-register a number of images. The malalignment angles were quantified in a separate analysis. One previous study by Sun et al suggested that scans remaining within ±20 mm^2 (tibia) or ±10 mm^2 (radius) of the first image set's cross-sectional area for the ROI should be considered sufficiently matched (170). Although using area as a guide for co-registration may improve this step further, area determined from hr-pQCT and pMRI differed in their definition. In hr-pQCT images, trabecular area was determined after peeling away the cortical and the trabecularized cortical transition zone. From the pMRI OsteoQ algorithm, trabecular area was defined by user-guided segmentation of the medullary region which included this transition zone. With the definitions of area mismatched, using area as a guide was not feasible.

Blumenfeld first described a B-spline or grey-scale nearest neighbour interpolation method for automatic registration of MR image sets from baseline to follow-up (229). Compared to this automatic registration method, manual registration qualitatively guided by 2D colour subtraction and 3D surface renderings, as was also performed in the present study, showed an average sum of squares that was 19.37 ± 0.07 % higher in Blumenfeld's study. However, the authors demonstrated that the actual trabecular bone structural measures calculated from both registration methods did not differ significantly and test-retest precision error remained well within 5% (137). In these studies, Blumenfeld utilized a higher in-plane resolution and thinner slice (156 x 156 x 500 μm) than the present study. Hence, their conclusions may not fully apply to the images obtained here,

as partial volume effects here were twice as evident and trabecular features may not be as enhanced. Indeed, Carpenter within Majumdar's group investigated reproducibility of bone structure quantification of the proximal femur after co-registration at a 1 mm slice thickness using MRI. Compared to the lower precision error of 2.0-4.5% reported by Blumenfeld, Carpenter from the same group saw as high as 6.5-13.5% test-retest error when slice thickness was twice as large, even after co-registration (137,230).

Effect of angular deviation on inter-modality correlation

Because CT image acquisition was limited to the axial orientation relative to the scanner's axis, it was not possible to realign images relative to the long axis of the radius without reformatting and compromising further on resolution. For pMRI, oblique image acquisition was possible and correct anatomical alignment was not a major concern. The pMRI-hr-pQCT image malalignment angles did not significantly explain the magnitude of deviation identified between pMRI and hr-pQCT likely because the majority of the unexplained variance is due to larger key players such as inherent differences between CT and MR technologies and image artifacts. The effect size of 3-5% inter-modality standard deviation explained by malalignment angle represented less than 5% of the total correlation between modalities. Furthermore, greater degrees of malalignment may not necessarily mean a worse inter-modality deviation. Instead, slight degrees of malalignment may already result in quantifiable differences between modalities and, within a window of values, any further deviation may not result in any poorer mismatch between the modalities' bone outcomes. However, even when severity of malalignment

was binarized to above and below the third quartile of 5.91^{o}, there was not found to be any difference in inter-modality SDs. Although SDs used to describe the inter-modality deviation may underrepresent the degree of variability across individuals, coefficients of variation were also used in analyses, yielding similar results. There have been no studies examining the effect of image malalignment angle as a continuous outcome on quantified bone outcome. One report by Blumenfeld did report a mean post-registration angular deviation of 0.2 ± 0.1^{o} (137).

6.4.6 pQCT and pMRI ICC's and Bland-Altman analyses

Agreement of trabecular vBMD from pQCT of the radius against that of hr-pQCT was reflected by an ICC below 0.900 in contrast to a value of 0.936 at the tibia, which can be justified by the greater error of measurements at the radius due to motion. In addition, the reference landmark used for the tibia (the plateau portion of the end plate) was more consistent than using the reference site for the radius (half way between the proximal and distal ends of the radial tilt). Despite the modest correlation coefficients for Tb.Sp observed between hr-pQCT and each of pMRI and pQCT's images, the ICCs obtained were actually lower than any other bone outcome. pMRI still yielded an ICC of over 0.80 for Tb.Sp but for pQCT, it was well below 0.40. A poorer pQCT-hr-pQCT correlation coefficient (<0.30) for Tb.Sp measured at the distal tibia could explain these low ICC values, but at the distal radius, correlation coefficients for pQCT-derived Tb.Sp (> 0.50) were similar in magnitude to Tb.N and Tb.Th. Bland and Altman (1990) suggested that the ICCs alone were not sufficient to assess inter-method agreement. Because ICC's are

an average of correlations across all possible pairings between the compared groups, it ignores the order or assignment of one method or another to the independent (X) or dependent (Y) variable (194). This statistic assumes the two methods compared represent a random sample of all methods available. However, in the present study, there were essential differences between the technologies compared that warrant careful treatment of the order of assignment to X and Y variables. In addition, Bland and Altman demonstrated that Lee's application of ICCs to inter-method agreement fails when inter-individual variability is low (231) – that despite values being similar between methods, the low variability across individuals renders the overall ICC values small. Thus, it is possible that by virtue of having a cohort with low Tb.Sp heterogeneity, the ICC values yielded were small. Other studies showed an equally low or even lower Tb.Sp heterogeneity within the cohorts examined (98,139,142,232).

Indeed, Bland-Altman plots revealed the low degree of heterogeneity for Tb.Sp for pQCT at smaller values (Figure 16), despite several outliers at the higher end of the scale. Examining the 95% confidence interval range, it was apparent that pQCT-hr-pQCT limits of agreement represented over 50% of the median value for Tb.Sp, suggesting that Tb.Sp quantification for pQCT may be limited in validity. In comparison, pMRI limits of agreement were within 25% of the median Tb.Sp value. Bland-Altman plots were also informative on the conditions under which inter-modality differences were greatest. For BV/TV, and Tb.Th a decreasing mean value was associated with poorer inter-modality agreement for both pMRI and pQCT, which can be explained by the greater sensitivity of smaller trabecular features to repositioning. When larger amounts of bone are present in

an expanse network of trabeculae, small repositioning errors would still yield very similar bone structural values. Consequently larger BV/TV and Tb.Th values would be more resilient to inter-modality differences. While Tb.N exhibited the opposite trend, larger deviations with higher Tb.N values could be explained by the ease of quantification of the perimeter of bone for individuals with fewer trabeculae. Since Tb.N is defined by perimeter of bone averaged over the total area of the mask, the easier the different algorithms can trace the trabecular bone perimeter, the more likely the final result would be common between modalities. In a study examining radius specimen bone structure on 1.5T MRI using the fuzzy logic segmentation method, Carballido-Gamio showed a limits of agreement for Tb.N of 0.015 to 0.025, representing as much as 55% of the mean measurement (233). However, in this ex vivo study, there were no evident patterns towards poorer agreement with higher Tb.N values.

The limits of agreement for pQCT-derived integral vBMD of the radius being larger than at the tibia, could be explained by the vast difference in trabecular bone distribution with shifts towards the proximal or distal directions at the distal radius. Boyd demonstrated that a ± 0.5 mm difference in distance can be attributed to as much as 6% error in integral vBMD for the radius and 2% error for the tibia (167). Differences in Ct.Th are typically sizeable along the axial length of the ultradistal radius. However, a smaller pQCT-hr-pQCT limit of agreement was shown for radial Ct.Th as compared to the tibia, which could be because there is a lack of variation in Ct.Th at the most distal end of the radius where Ct.Th is already minimal. Zebaze showed that even with different segmentation methods, cortical area measurement can be underestimated by as much as 7.15 mm^2 from

hr-pQCT radius scans (234). Underestimation of medullary area by segmenting out cortical bone from attenuation profiles appeared to be more dramatic for larger areas, which could partly explain deviations in Ct.Th measurement.

6.5 Precision of measurements

6.5.1 Short-term precision

The superior reproducibility of BV/TV for all modalities compared to other bone outcome measures can be reconciled by the fact that this measurement was computed as a ratio of total bone area to total mask area, thus reducing the variance contribution of each of these individual variables. Moreover, the fraction of bone may not differ as dramatically with repositioning as more minute features of bone such as its connectivity or trabecular geometries. Although other trabecular outcomes were derived from BV/TV, they were also dictated by finer trabecular details such as Tb.N and is therefore subjected to greater influence from motion and repositioning differences than BV/TV alone. Consequently, other outcomes would plausibly yield a higher precision error. While a similar pattern was observed for hr-pQCT-derived BV/TV by Kazakia (131) and Boutroy (98) at the radius and tibia, 3T MRI yielded a precision error of 6.7% for BV/TV at the radius, which was higher than all other bone outcomes in their study (131). Nevitt et al revealed a BV/TV short-term precision error of 5.2% when examining the 7 mm site proximal to the radial endplate, which was reduced to 3.7% when values were averaged over a 7.5 mm distance and further reduced to 2.2% after excluding a single participant with a low SNR image. These values were more comparable to those shown in the present study (235).

The fact that short-term precision errors for all measures were similar between pMRI and pQCT suggests that the similar in-plane resolution between the two modalities was a large factor in dictating the degree of precision achievable. Supporting this proposition, short-term precision for hr-pQCT, with an in-plane resolution of 82 µm, was previously found to be considerably lower than for either pQCT or pMRI in the present study (See Table LXVII). Resolution may be more important for microstructural measures but even with an in-plane resolution of 500 µm using pQCT, Sievanen et al still yielded an RMSCV of 2.2% for trabecular vBMD (134). While distal tibia measures were not obtained using pMRI, tibial quantities of bone structure were more reproducible than at the radius for pQCT because of the greater ability to keep the lower limb stationary. One previous study quantifying involuntary movements using surface electromyography (EMG) demonstrated that EMG differences due to parallel and rotational shifts were smaller at the tibialis anterior versus both wrist extensor and flexors (236). Meanwhile, Kazakia did not note differences in reproducibility between these sites (131).

Despite the poor reproducibility of trabecular connectivity and hole size measures at the radius reported in this study overall, the less than 5% precision error observed for H_M at the distal slice of both radius and tibia using pQCT showed promise for its potential use as an outcome, especially after further improvements to trabecular segmentation. Consistent with the present study, Gordon showed a 5.5% precision error for H_A. In fact, even Cx exhibited a short-term precision error of 5.1% (154). The authors noted that with 20% differences in the area of the region of interest, both Cx and H_A measures were affected by only within 1% difference. MacIntyre reported an RMSSD of 1.87 for Cx and

8.14 mm^2 for H_M, values which were slightly smaller than those reported here, even when the repeated measurement was performed approximately one week from the first (147). There were little to no differences in reproducibility for model-dependent versus the model-independent counterpart for Tb.Sp and Tb.Th. For either case, the difference lies in the way Tb.N was computed. For model-independent measures, Tb.N was the inverse of mean Euclidean distances between the ridges of trabecular bone computed in three dimensions. For model-dependent measures, Tb.N was computed as a ratio of bone perimeter to total mask area within a single slice. The two methods yielded values that were highly correlated. However, model-dependent and independent measures differ when there is a larger discrepancy in the actual thickness of bone segmented from each method, leading to a larger perimeter of bone, a situation that would occur when comparing between modalities imaging bone at different spatial resolutions. Newitt compared 2D Parfitt-model computed bone structural measures (5.2% precision error for all images, and 2.2% excluding low SNR image) with 3D model-independent (5.5% for all images, and 2.4% excluding low SNR image) computations, demonstrating that BV/TV was actually comparable between the two methods (235).

Among pQCT scans, the distal slice proved to be more reproducible than the proximal slice. Although it was tempting to attribute this pattern to the order in which scans were obtained (assuming more involuntary motion over time), at the radius, the proximal slice was actually acquired before the distal – for the tibia, the order was the opposite. A viable

Table LXVII. hr-pQCT short-term test-retest statistics from previous study on same machine.
Mean age was 44.2 (range: 20-69) years with 25 women and 6 men. Participants were scanned twice at the same study visit on the same hr-pQCT scanner utilized in the present study. Scan protocol, image analyses and technician were identical to those used here. Reproduced with permission from Cheung et al (237).

Parameter	Radius		Tibia	
	RMSCV	RMSSD	RMSCV	RMSSD
BV/TV (fraction)	0.007	0.001	0.004	<0.000
Tb.Sp (mm)	0.048	0.023	0.041	0.022
Tb.Th (mm)	0.046	0.003	0.037	0.003
Tb.N (mm^{-1})	0.048	0.09	0.041	0.07
Ct.Th (mm)	0.013	0.010	0.005	0.006
vBMDi (mg/cm^3)	0.005	1.77	0.002	0.76
vBMDc (mg/cm^3)	0.005	3.93	0.002	1.73
vBMDtr (mg/cm^3)	0.007	1.01	0.004	0.69

explanation for the superior reproducibility at the distal site may be the ease with which trabecular bone can be delineated from the marrow. At the more distal site, trabeculae are denser and thicker, allowing for a clearer decision on what would be considered bone and what would be marrow space compared to the more proximal site where trabeculae are thin and sparse. Capozza et al also showed that the more distal tibia had higher total bone mineral content than a location just proximal to it (238). The lower attenuation values at the more proximal site could contribute to poorer ability to segment the bone. Gordon also demonstrated that the more distal radius exhibited higher connectivity and smaller trabecular mean hole size than a more proximal slice (154).

Co-registration of pMRI slices from test-retest scans actually improved precision error slightly for most variables, except for Tb.Th and Tb.N, in contrast to the degradation in inter-modality correlation observed for the validation study. Since bone perimeter was a

common denominator in the computation of Tb.Th and Tb.N, it was reasonable that both measures suffered from poorer precision after co-registration. The increased error in computing bone perimeter after co-registration may be derived from the reduction in the number of slices averaged for analyses. Bone perimeter may be more sensitive than other bone measures to overall differences in area and volume since it is computed directly from the geometry of bone without any further averaging or division operations like with other bone measures. Newitt showed that image registration without inter-slice interpolation resulted in improvements in longitudinal change for Tb.Th but made no effect for either BV/TV or Tb.Sp (235). Although signal inhomogeneity was not a concern for the RF coils utilized in the present study, low pass filter correction for quadrature and birdcage coils used by Newitt further rendered any previously found significant longitudinal changes to be minimal (235). Such conclusions could be extended to short-term precision, assuming that co-registration and adjustment for signal homogeneity could reduce overall measurement error.

Short-term reproducibility of hr-pQCT bone outcomes

Study participants were not scanned twice at baseline to quantify short-term precision error for hr-pQCT as this had already been done on the same hr-pQCT scanner by the same technician utilized for baseline hr-pQCT scans. These data were reported previously by Cheung et al and are shown in Table LXVII. In addition to having the smallest precision error out of the three modalities, hr-pQCT-derived bone outcomes' RMSCV at the tibia was smaller than at the radius. In particular, cortical and integral vBMD showed

as low as 0.2% precision error. However, the mean age of the cohort where these data were examined was younger than the present study (mean age 44.2 years). Comparing data from Cheung's study where Ct.Th displayed a precision error of 1.3% at the radius and 0.5% at the tibia, Burghardt saw a similar 3.9% error at the radius and 1.5% error at the tibia in older women (mean age: 61 ± 10 years). Meanwhile, in their younger cohort of men and women with a mean age of 26 ± 3 years, radius precision error for Ct.Th was lower (1.3%) but tibia precision was not different from the older cohort (3.9%) (161). Similar to the above findings for pQCT, both Burghardt and Cheung cautioned about the higher precision error found for bone structural measures versus densitometry.

6.5.2 Short-term Bland-Altman agreement

The poorer test-retest agreement observed from Bland-Altman plots for connectivity and hole geometry measures for pQCT compared to pMRI could be reasoned by the smaller overall volume of interest for pQCT slices over which the measures were obtained. While no major trends in repeat scan deviations was observed for most structural measures, the greater short-term test-retest deviation observed with larger Tb.Sp was most notable for both pMRI and pQCT. It is possible that at the lower end of the scale, the interpolation of Tb.Sp achieved when resolution was poor resulted in values that were very similar. With larger values of Tb.Sp, measurement became more accurate and was met with greater measurement variability. In addition, the actual size of spaces between trabeculae may not differ that much with slight rotation of the anatomy when the geometry is small. However, when the size of the inter-trabecular space is larger, small rotations can lead to more

dramatic changes in apparent geometry due to parallax, especially when considering slice thickness and partial volume artifact. Over the imaged length of the radius, Kazakia showed that BV/TV and Tb.N variability within an hr-pQCT image volume represented as much as 58% of its mean value, which could translate to significant variation in Tb.Sp at the proximal radius. In contrast to these data, Mueller showed that test-retest RMSCV of Tb.Sp as obtained by hr-pQCT was smaller towards the proximal region of the radius but BV/TV test-retest RMSCV actually increased proximally (239). It is possible that poorer test-retest agreement for Tb.Sp at the ultradistal radius in vivo could be the result of poorer fixation at the more distal region of the wrist.

6.6 Detection limit and clinical sensitivity

6.6.1 One-year change

One-year change computations were made within three months of one year from baseline measurements for all three modalities. The minor discrepancy in timing across modalities (1-3 months) was not expected to translate significantly to any additional changes in bone measures. As a point of reference, one year change in bone density for women in the CaMos study investigating antiresorptive therapy was less than 1.5% (182). It was logical that the larger one-year changes observed coincided with bone measures that exhibited poorer short-term precision error, in particular, hole geometry and connectivity. Following the same pattern as short-term reproducibility, radius and tibia measures at the more distal slice showed smaller one-year changes than the proximal slice for pQCT. Changes in the more proximal slice of the ultradistal radius obtained from pQCT being larger than the more distal slice, could also be explained by the higher degree of bone

turnover exhibited by regions with more trabecular bone compared to cortical bone. Similarly, due to the smaller precision error shown for hr-pQCT, its corresponding one-year changes were considerably smaller than that of bone outcomes obtained on either pMRI or pQCT. The fact that one-year change in Tb.N measured from hr-pQCT images was larger than both pQCT and pMRI, could be justified by the fact that Tb.N computed using the OsteoQ software for pQCT and pMRI relied on the calculation of bone perimeter. With a lower image resolution, bone perimeter differences may not be immediately apparent, thus translating to very similar Tb.N values both within and between individuals. Although other variables also rely on bone perimeter or area, their computation is buffered by other measures that reduce the overall reliance on this parameter. That distal radius changes were more pronounced than tibial bone changes could be explained by the lack of weight-bearing on the radius site. Without constant load applied to the radius, bone loss may not be counteracted by load-induced bone formation as dictated by Wolff's law (65). Another more obvious explanation is the poorer precision of measurements made at the radius compared to the tibia by virtue of the higher probability of motion at the radius.

The reduction in one-year change in most bone outcomes after exclusion of individuals with a history of fragility fractures may also be justified by differences in bone turnover. High bone turnover is one of the etiologies of osteoporotic fractures (240). Thus by excluding individuals with a previous fragility fracture, people with lower bone turnover will remain, explaining the lower one-year change over time. In addition, exclusion of those who are currently on antiresorptive therapy could modify the cohort bone turnover

status – though in which direction depends on the degree to which antiresorptives lowered the participants' bone turnover. Some may exhibit a baseline high bone turnover that only became partly blunted by antiresorptives while others on more potent therapy could exhibit a lower bone turnover than average. Moreover, there may be participants who were not treated with antiresorptives but actually have high bone turnover and poor bone structural integrity. When bone turnover is low, there is more time for mineral to accumulate resulting in a higher vBMD. However, the rate of replacing old bone with new matrices is slowed, which could actually result in the lack of bone formation (241,242). Indeed, it has been shown that antiresorptives, known to inhibit the activity of osteoclasts, in turn blunt osteoblastic activity since these latter players rely on active osteoclasts to function (243). In a study of women (age: 56 ± 4 years) on alendronate therapy, Folkesson showed that MRI-derived Tb.Th actually showed a significant decrease of 0.49% in the treatment group versus a non-significant 0.24% decrease in the control group at the radius after one year, while no significant changes were observed in the other bone outcomes until 24 months of therapy (226). Compared to the present study, these change values, although significant in Folkesson's study, were well within the 7.1% one-year RMSCV precision error for Tb.Th for 1.0T pMRI for individuals not on antiresoprtive therapy. In another study examining zoledronic acid therapy versus placebo in 152 women using paired bone biopsies, the antiresorptive treatment resulted in higher Tb.N, Cx and lower Tb.Sp than the placebo group that was significant after three years of treatment. However, this study did not measure actual change over time with paired biopsies. Other differences in duration (3 vs. 1 years) and formulation (intravenous vs.

oral) of treatment between this study by Recker and the previous study examining alendronate by Folkesson also explain differences in the changes in bone structure observed (244). In a randomized controlled trial of L-arginine versus placebo, Baecker et al showed that the placebo group of postmenopausal women (mean age 54.5 ± 4.1 years) decreased in pQCT image-derived trabecular vBMD at the radius by 3.2 mg/cm^3 (2.0%, NS) and at the tibia by 0.2 mg/cm^3 (0.1%, NS). Similarly, cortical vBMD non-significantly decreased by 0.8% at the radius and 0.7% at the tibia in the placebo group (245). The corresponding one-year changes in trabecular (radius RMSCV: 17.8%; tibia RMSCV: 7.7%) and cortical (radius RMSCV: 7.8%; tibia RMSCV: 5.6%) vBMD in the present study were also much larger than those reported in this clinical trial. Given that the same region of interest was examined with a lower resolution by Baecker et al than the current study, it is possible they did not have adequate power to observe such changes over one year. In another RCT of 33 individuals on alendronate versus placebo, Burghardt similarly showed that trabecular vBMD was the only bone outcome that demonstrated significant decrease by over 2.25% at the radius and 1.75% at the tibia within one year using hr-pQCT (166). Although not significant, overall cortical bone thickness and area appeared to decrease as well. In contrast to the previous study employing pQCT, these percentage decreases were actually larger than the corresponding one-year RMSCV values (trabecular vBMD for radius: 1.8% and tibia: 0.9%) reported in the present study.

There have not been studies performed previously examining longitudinal changes in Cx and hole geometry measures from any of the three modalities investigated. The more

dramatic reduction in one-year change for Cx after excluding individuals with fractures or on antiresorptive therapy compared to other outcomes could be explained by the lower precision error or greater ability to remain still among the remaining individuals. No literature has reported any association between fractures and ability to remain still, but two studies did demonstrate that falsely diagnosed fractures could arise from motion artifact (246,247).

6.6.2 Detection limit and long-term precision: SEE

The patterns observed for SEE and LSC were consistent with the one-year changes described for all bone outcomes at the various locations. The SEE values being smaller than LSC values indicate that changes over time would exceed SEE sooner than LSC, should the former be used as any reference of change. The SEE was previously described as a more appropriate measure for long-term precision compared to the SD because it accounts for the expected correlation between time points and putative biological changes over time, thus reflecting the intrinsic long-term precision of the machine (178). However, the SEE applied to bone outcomes utilized in this study made the assumption that changes in bone were linear. For the short-term, this approximation could be more accurate than longer term bone dynamics (248). Using the SEE measure and confidence intervals of bone changes over time, Verheij was able to recommend intervals between bone density follow-up scans (248). However, for individual patients, the precision of bone density measurements can be poorer with a greater amount of soft-tissue around the region of interest and a lower BMD value at baseline (249). There has been a lack of studies

reporting longitudinal changes in volumetric bone outcomes using SEE. Few have examined SEE in the context of DXA measurements over time (250,251).

6.6.3 Clinically meaningful detection limit: LSC

It was logical that LSC values, just like SEE, were comparable for many bone outcomes between pQCT and pMRI since the two have very similar in-plane resolutions. However, unlike SEE, LSC for connectivity, hole geometry and Tb.Th measures were discrepant between the modalities, which could be explained by the fact that baseline-follow-up correlations adjusted by SEE technique enabled proper adjustment for biological change whereas LSC values did not adjust for this. Hence, LSC values, in contrast to SEE, may represent more than just the intrinsic detection ability of modalities. Biological change has been incorporated into the LSC statistic, which suggests that the amount of change required to be considered clinically significant can be altered by reducing the uncertainty in the measurement through acquiring multiple baseline and follow-up scans (248). While uncertainty may pose a problem to the accurate estimation of relevant clinical change in bone, the prescription of multiple scans means greater exposure to radiation, particularly for DXA, yielding 10 µSv per scan including total hip and lumbar spine. For any of the modalities examined: pQCT (1 µSv/site), hr-pQCT (3 µSv per site) or pMRI (none), radiation would not be a major concern and reducing LSC could indeed be feasible by performing multiple baseline and follow-up scans at the same region of interest. However, for pMRI, time would be a major challenge as the entire procedure can take up to 15 minutes with repositioning. Additional scans would especially be subject to further

increases in motion artifact. Although the LSC values were twice as large as the SEE observed, there is potential to narrow the LSC values to smaller estimates that preclude more uncertainty surrounding the baseline and follow-up measurements. However, there remains the problem that any changes estimated over one year, even though they could be more accurately quantified, may not necessarily translate to any clinical significance if no attributable clinical endpoint can be associated with the volumetric bone outcome.

Same-day or one-week LSC values were previously reported for hr-pQCT by Cheung (237) and Burghardt (161), the values of which were twice as large in Burghardt's cohort of older women as in the younger adults in Cheung's study, but the bone outcome values were around the same order of magnitude. Repeat scans within two months were performed to quantify LSC in one study by Rinaldi et al (252), yielding values for cortical vBMD that were three times as large as same-day hr-pQCT LSC reported by Cheung (237), almost twice as large as one-week (maximum) hr-pQCT LSC reported by Burghardt (161), and half the size of one-year pQCT LSC reported in the present study at the radius. This same pattern of increased LSC with increasing time to scan repeat was also displayed with Ct.Th and integral vBMD. Microstructural outcomes were not reported in this study of two-month LSC for pQCT. However, no previous study has reported one-year LSC values for any of hr-pQCT, MRI or pQCT. Within pQCT imaging, LSC values for integral, cortical and trabecular vBMD were dramatically different between analyses with and without excluding individuals with fractures or were on antiresorptive therapy. The fact that the cohort size decreased from 36 to 14 participants

by applying these exclusion criteria could account for the higher sensitivity of the LSC measure to outlying participants exhibiting wider changes over time. However, the fact that this large discrepancy resided only with vBMD measures suggests that perhaps the discrepancy is not structurally-dependent. One possibility may be the artificially increased density conferred by motion surrounding the cortical bone.

6.6.4 Clinical sensitivity: odds for fractures

That neither pMRI nor pQCT yielded any bone outcomes that showed associations with fractures could be due to the lack of statistical power given the larger short-term precision error of measurements compared to hr-pQCT. Even with hr-pQCT, only Ct.Th and vBMD showed increases in odds for fragility fractures of 10-86%. Although not significant, pQCT Ct.Th and vBMD demonstrated a trend towards an increased odds for fractures per LSC or SEE-unit decrease in Ct.Th, suggesting that cortical measures do in fact bear an important effect size for fractures association. Because of the varying magnitudes of SD, SEE and LSC units, the ORs yielded were different. In particular, the detection limit representative, SEE, showed the lowest OR. Although LSC comprises an element of RMSSD precision error, expression of odds per SD of the measurement across individuals generated a higher OR than LSC, which accounts only for within-individual variation. The interpretation of the OR from each case can correspondingly be put into context: 1) Increased fracture odds per lowest unit change detectable by the instrument (SEE), 2) Increased fracture odds per lowest unit of intra-individual clinically meaningful change (LSC); and 3) Increased fracture odds per standardized unit of inter-individual

clinical change (SD). Although the first contextual example references a property of the machine (detection limit) and can be comparable across individuals, it lacks a clinical rationale and thus translation of this knowledge into practice may not immediately make sense to physicians and patients. Contextual example two provides a clearer reference to the patient but intra-individual change may be sensitive to cohort effects. The third contextual example considers inter-individual differences but not intra-individual change. However, when the population examined becomes highly diverse, the meaning of the unit of SD may be more difficult to interpret, similar to contextual example two with LSC. Since LSC and SDs are simply population statistics with fixed values, the odds for fractures for both scenarios could be compared in making the final interpretation of fracture odds.

The OR computed from binary logistic regression analysis is based on cross-sectional data and therefore is subject to questions about whether causation can be implied or about the direction of causality. However, when the rate of events such as fragility fractures is low, the OR closely approximates the HR, a statistic that estimates the risk of a future fractures based on longitudinal data (195). Indeed, it is possible that individuals who have previously sustained a fragility fracture, depending on the anatomical location, may suffer from reduced mobility, further leading to disuse osteoporosis. This condition may most likely be relevant for individuals who have recently had a fracture rather than those who experienced one a greater number of years ago. The present study did not adjust for time since last fracture, which could have improved the gradient of risk estimated. Also,

fractures were not subcategorized into type, location, clinical or sub-clinical. Another helpful procedure would be to distinguish fracture location according to whether cortical bone is dominant or whether trabecular bone is more prominent. Bone turnover at trabecular interfaces are higher compared to cortical bone (253). Hence, one would expect that trabecular bone measurements would better associate with fractures at sites whether there is a predominance of trabeculae versus cortical bone, for example the vertebrae. Since bone outcomes were examined only at the radius and tibia, there is also suspicion as to how and to what degree bone at such distal locations relate biologically to more clinically-relevant sites such as the hip and spine, which were associated with the majority of fracture-related mortalities previously reported (9). Liu et al showed that there was a correlation between tibial integral vBMD obtained by hr-pQCT and stiffness of the proximal femur (r=0.75). Similarly, vertebral stiffness was correlated with trabecular vBMD of the distal radius (r = 0.58) (232). In another study, Melton showed that lumbar spine integral vBMD and vertebral Ct.Th correlated with Tb.Sp at the 9.5 mm distal radius as measured by hr-pQCT (r=-0.58 and r=-0.48, respectively) (140). These studies may be limited by the fact that different modalities and in-plane resolutions were used to examine the central versus peripheral site, though one study by Horikoshi used pQCT (XCT3000 with a larger gantry than XCT2000) to quantify bone outcomes at both femoral neck and distal radius. In this study, integral, trabecular and cortical vBMD displayed correlations between the femoral neck and distal radius (r=0.639, r=0.517 and r=0.351, respectively) (254). Explaining up to 50% of the variance in the more clinically

relevant hip and spine sites, it is plausible that peripheral bone outcomes could serve as potential predictors of vertebral and hip fractures.

Despite the smaller sample size used to examine odds for fractures in the local study sample, there were no major model fit issues. Confidence intervals were relatively tight, suggesting that the bone measurements examined were not overly skewed and that statistical power was not a major influence on the precision of the parameter estimate. Whereas the effect size for ORs associated with SD differences in Ct.Th and vBMD were larger than either SEE or LSC, the corresponding confidence interval just overlapped 1.0 after adjusting for age. It is anticipated that with a larger sample size, the age-adjusted ORs would remain significant. Statistical power was preserved by limiting the number of covariates in the model to age. Although it would be desirable to include aBMD as an additional covariate to examine the added contribution of bone outcomes to fracture odds assessment, concurrent aBMD data were not available. The most recent DXA scans were performed at least five years ago and the time difference would have led to significant offsets in the odds for fractures obtained. Regardless, having unadjusted and minimally-adjusted models would serve as a useful reference for future comparison of ORs, especially in situations where other covariates such as aBMD may not be available.

Literature on odds for fractures related to bone outcomes from each modality will be discussed at the end of the national study section on the corresponding odds for fractures.

6.7 National study component

6.7.1 Descriptive statistics – national versus local studies

The national cohort of women examined at the six study centres were on average younger than the local cohort of Hamiltonians, with a smaller proportion of women bearing a history of fragility fractures. Between the two cohorts, BMI was similar. Unfortunately at this point in time, the 1.0 pMRI modality was not available at the other study centres. Consequently, the national dataset focused on pQCT and hr-pQCT, one or both of which were available at all centres. Aside from Tb.Th and cortical vBMD, all other bone measures' data distributions were comparable between the national and local cohorts. The smaller sample of the local cohort could have contributed towards a greater imbalance in bone outcome value distributions.

The pQCT investigation comparing fixed (local) and relative (national) region of interest localization protocols showed significant but minor distance or ROI-related differences at the radius but larger differences at the tibia. Assuming a linear relationship between positioning error and bone outcome precision error, the 0.28 mm mean positional difference at the radius could translate to just over 3% error attributable to variable ROI selection (167). At the tibia, the over 10 mm difference in ROI position would yield over 30% error for comparing to a different ROI. Hence, one would not expect major differences in bone outcome observations at the radius but for results generated at the 4% versus the distal 22.5 mm tibia, bone outcome analyses could vary significantly. Since the local protocol employed the same fixed distance ROI for all modalities, this discrepancy

would not present as a problem. However, for comparison of local versus national studies, caution should be exercised in any tibial bone interpretations. Despite these study design-related differences in imaging protocols, technican site-specific test-retest values for vBMD were all below 5% and imaging procedures were streamlined to ensure consistency across study centres (Table LI).

6.7.2 Inter-modality and inter-site calibrations

The near unity phantom cross-site calibration slopes along with tight confidence intervals around the parameter estimate provided confidence that both pQCT and hr-pQCT measurements made across Canada could be reliably compared. That the intercepts of the linear equations fell within the RMSSD value for each corresponding measure suggests that the systematic error between sites would not severely impact pooled data analyses. The close to 20% underestimation of trabecular vBMD at the Vancouver site pQCT scanners cannot be explained by the different model of pQCT used since both models (XCT2000 and XCT3000) exhibited a similar pattern with comparison against the pQCT scanner in Hamilton (XCT2000). One possible explanation may be the fact that the Vancouver XCT2000 scanner was purchased earlier (2001) compared to the other scanners (mostly 2007) across Canada. Minor differences in CdTe detector and X-ray crystal installation and fabrication could lead to different distributions of image noise and spatial frequency (255). In addition, the calibration phantom used to standardize the machine upon installation could also affect the final computed bone outcome value. The fact that only trabecular vBMD from the Vancouver site was affected and not cortical

vBMD or any of the other bone outcomes suggests perhaps that the lower end of the linear attenuation scale was subject to the deviations observed in comparison to other sites. Incidentally, cortical vBMD and to a lesser degree trabecular vBMD obtained by hr-pQCT at the same Vancouver site also displayed just below 30% and 10% underestimation compared to the Toronto site scanner, respectively. As one individual performed all scans using the same phantom, operator-dependent errors may not likely have been the source of this larger deviation here. Conversely, the slopes were close to unity for trabecular vBMD on pQCT and hr-pQCT for the human cross-calibrations. Cortical vBMD varied more widely across sites with slopes ranging between 0.71 and 1.33 for the human calibration. Given the variable performance of these measures between sites, future multi-centre studies may benefit from adjusting for vBMD measurement by applying these linear calibration equations. Whether to use the phantom or human calibration equations to adjust for future human scans becomes another question to address. Since microstructural information was not available on the morphometric European Forearm Phantom, any trabecular variables would need to be adjusted using the equations describing bone structure from human calibration. The human calibration equations quantifying inter-site relations in volumetric bone outcomes comprise also the degree of participant positioning and movement-related error, which are not relevant for purely calibration purposes. Blake did suggest from one study that phantom calibration may not always yield reliable results compared to in vivo test-retesting (256). In this analysis, cross-calibration of newer to older DXA scanners showed 0.2% error with a Hologic phantom but up to 2% error with in vivo measurement, which

was replicated by another phantom not from the same manufacturer. Genant's previous study also supported errors closer to 2% for linear-equation-calibrated values using both a cohort of participants and using a European spine phantom (257). No trabecular structure phantom was available at the time that the present study was performed. The construction of a trabecular bone phantom compatible with MRI and QCT is met with the challenge that the soft tissue surrounding bone must have the correct radio-opacity as soft tissue, yet bear the correct T_2 relaxation properties as muscle. In addition, real bone may erode over time with the shear stress generated from liquids flowing over its surface.

While no MRI and QCT-compatible bone structure phantom has been constructed to date, Burghardt first described the construction of a QCT-compatible extremity bone structure phantom by embedding a cadaveric bone specimen in a polymethylmethacrylate and polyethylene resin with the same radio-opacity as soft tissue (138). Because no liquid phase was required, as this phantom was not designed for MR imaging, long-term stability of the phantom was not a major problem. This phantom was imaged across nine study centres to determine within-centre short-term reproducibility, yielding between 0.3-0.6% RMSCV for bone densitometric outcomes and just over 1% for Ct.Th. No calibration equations were obtained from this study, but between-centre test-retest reproducibility showed RMSCV values just within 5% for density and microstructural outcomes (Ct.Th, Tb.N, Tb.Sp, Tb.Th) (138). Similar to the trabecular vBMD value reported for a single study centre in the present study, Burghardt also demonstrated that individual study centres deviated to different extents from others depending on the class

of bone variable examined. For example, one study centre routinely demonstrated the largest integral, trabecular and cortical vBMD compared to the other study centres while another centre was an outlier for cortical measures. The authors did note that error intrinsic to the scanner itself is common, and can be partly explained by the apparent spatial resolution and SNR of resultant images. However, this same centre did not exhibit the lowest SNR or lowest spatial resolution compared to others (138). An additional contributor to the variability among sites for QCT-derived bone outcomes may be the X-ray current or X-ray spectrum. Since pQCT functions under the same principles guiding X-ray scintillation and photomultipliers as hr-pQCT, these same observations can be extended to deviations observed for pQCT. One multi-centre study examined phantom-guided calibration across four pQCT machines and found deviations not more than 2.9 g/cm^3 for integral density with a mean test-retest precision of 0.21% and a mean inter-site precision of 0.18% (258).

6.7.3 External validation: clinical sensitivity

The similar increases in odds for fragility fractures observed for vBMD for hr-pQCT and pQCT in the national cohort study externally validated the results obtained from the local study – the participants of which did not form part of the national cohort. The fact that tibial vBMD demonstrated larger ORs compared to the radius for both pQCT and hr-pQCT could be reasoned by the potential connection between weight-bearing at the tibia and the similarly weight-bearing status of the sites where fractures have occurred. According to the breakdown of fractures in the CaMos dataset, the majority comprised of

other fractures that were not any of: hip, spine, pelvis, rib or wrist, followed by forearm, vertebral, rib, hip and lastly pelvic fractures. When summated together, fracture sites that were weight-bearing comprised 40.2%, forming the majority of all fractures, versus 24.9% for forearm and wrists, with a remaining 34.9% that may comprise a combination of both weight-bearing and non-weight-bearing fracture sites (CaMos internal reference).

The larger effect sizes observed for pQCT versus hr-pQCT was not expected since hr-pQCT demonstrated a superior degree of precision and ORs would not have been influenced by measurement error as much as for pQCT. It is possible that the 4% tibia examined by pQCT, which deviated as much as 10 mm more distal than the fixed 22.5 mm site observed by hr-pQCT, provided more trabecular information that better correlated with fractures than the more proximal hr-pQCT site that comprised of less trabecular bone. However, this argument can be buffered by the observation that pQCT image-derived trabecular vBMD in particular, demonstrated a wider confidence interval when expressed per unit LSC, suggesting that precision error is in fact influencing the large variability in the OR parameter estimate. Unlike the local cohort study, adjustment for age actually increased the association with fractures while preserving the tightness of confidence intervals, suggesting that the bone outcome associations observed were not confounded by differences in volumetric bone properties due to age.

At the time of analyses, pQCT apparent microstructural information was not computed. Only vBMD and Ct.Th data were generated from the original Stratec manufacturer's

software. For hr-pQCT, Ct.Th and BV/TV revealed the next strongest associations with fragility fractures after vBMD. At both tibia and radius, it appeared that these cortical or macrostructural measures were more relevant than the trabecular measures in dictating the odds for fractures. One would expect that trabecular bone measures would better associate with fractures at sites with a predominance of trabeculae. However, the analyses in this study were not decomposed according to fracture types to address this proposition. One study by Szulc et al actually demonstrated that all volumetric bone outcomes showed stronger associations with low trauma fragility fractures compared to just peripheral fragility fractures alone, albeit, only by under 10% further increase in odds (259).

A number of studies have examined the association between volumetric bone outcomes and fractures using hr-pQCT at the radius (121,140,160,180,196,197,259-261) and tibia (160,180,197,259,261). However, only few have investigated the same using either pQCT (122,141,262,263) or MRI (139,264-266). A summary of these studies comparing ORs and 95% CI for various conditions is displayed in Table LXVIII for the distal radius and in Table LXIX for the distal tibia. One analysis by Cortet et al demonstrated significant associations between MRI-derived bone outcomes and fractures, but acknowledged the fact that fewer outcomes were significant compared to hr-pQCT performed on the same study participants (266). In general, one SD difference in volumetric bone outcomes derived from hr-pQCT, pQCT or MRI were able to yield significantly increased odds for fractures between 1.32 to 16.67 at the ultradistal radius site, with an average OR across

Table LXVIII. Comparison of odds ratios for fractures associated with distal radius bone outcomes.

Odds ratios (OR) and 95% confidence intervals for fractures associated with various bone outcomes obtained at the distal tibia are compared from multiple sources. The ultradistal tibia was defined as the 22.5 mm site proximal to the tibial endplate for hr-pQCT and as the 4% site for pQCT. Various conditions for each study are displayed. **Bold** = significant at the 95% confidence level.

Lead Author	Year	Modality	Resolution (μm)	Mean age	Fx Type	N (F/M)	Covariates	BV/TV (OR)
1. Melton	2007	hr-pQCT	89 x 89 x 89	68.1 ± 11.4	Forearm Fx	36F	age	N/A
2. Melton	2007	hr-pQCT	82 x 82 x 82	78.6 ± 9.0	Vert Fx r	80F	age	1.1 (0.6–2.0)
3. Boutroy	2008	hr-pQCT	82 x 82 x 82	73.4 ± 6.0	Low trauma FFx r	66F	N/A	N/A
4. Sornay-Rendu	2009	hr-pQCT	82 x 82 x 82	72.2 ± 8.2	Vert Fx r	462F	age, spine aBMD	N/A
5. Sornay-Rendu	2009	hr-pQCT	82 x 82 x 82	72.2 ± 8.2	Vert Fx r	462F	age, hip aBMD	N/A
6. Cejka	2011	hr-pQCT	82 x 82 x 82	59 ± 15	Low trauma FFx r	34F40M	age	**2.17 (1.12-4.17)**
7. Szluc	2011	hr-pQCT	82 x 82 x 82	71 ± 8	Low trauma FFx r	920M	age, weight	N/A
8. Szluc	2011	hr-pQCT	82 x 82 x 82	71 ± 8	Peripheral FFx	920M	age, weight	N/A
9. Vilayphiou	2011	hr-pQCT	82 x 82 x 82	71 ± 10	Low trauma FFx r	327M	age, height, weight	N/A
10. Majumdar	1999	MRI 1.5T	156 x 156 x 500	72.2 ± 9.2	Hip Fx	39F	N/A	1.84 (0.87-3.99)
11. Cortet	2000	MRI 1.5T	195 x 195 x 2000	69 ± 7	Vert Fx r	20F	N/A	NS
12. Laib	2002	MRI 1.5T	156 x 156 x 500	62.2 ± 6.4	Vert Fx r	148F	age	**1.60 (1.02-2.50)**
13. Gorai	2001	pQCT	500 x 500 x 2500	66.4 ± 10.3	Vert Fx r	621F	age	N/A
14. MacIntyre	2003	pQCT	330 x 330 x 2500	57.7 ± 15.3	Wrist Fx	42F	radial aBMD	N/A
15. Jamal	2006	pQCT	250 x 250 x 2500	65.8 ± 9.0	Low trauma FFX r	36M16F	age, weight, sex	N/A

Lead Author	Year	Tb.Sp (OR)	Tb.Th (OR)	Tb.N (OR)	Ct.Th (OR)	vBMDi (OR)	vBMDtr (OR)	vBMDc (OR)
1. Melton	2007	0.6 (0.2-1.3)	1.7 (0.8-3.6)	**2.3 (1.02-5.1)**	**4.0 (1.4-11.0)**	**4.2 (1.4-12.0)**	**2.7 (1.1-6.4)**	**2.7 (1.1-6.4)**
2. Melton	2007	0.7 (0.4–1.4)	1.1 (0.6–1.9)	1.1 (0.6–2.0)	**c 2.1 (1.1–4.1)**	**c 2.2 (1.1–4.3)**	N/A	N/A
3. Boutroy	2008	N/A	N/A	**3.60 (1.73-7.47)**	**5.14 (2.16-12.26)**	**5.38 (2.17-13.30)**	**2.54 (1.35-4.80)**	N/A
4. Sornay-Rendu	2009	N/A	N/A	N/A	**2.04 (1.02-4.00)**	N/A	N/A	N/A
5. Sornay-Rendu	2009	N/A	N/A	N/A	**2.08 (1.13-3.83)**	N/A	N/A	N/A
6. Cejka	2011	N/A	1.33 (0.76-2.33)	**2.86 (1.37-5.56)**	**1.85 (1.01-3.33)**	1.82 (0.99-3.33)	**2.17 (1.12-4.17)**	1.27 (0.74-2.13)
7. Szluc	2011	**1.38 (1.19-1.61)**	**1.39 (1.15-1.68)**	**1.45 (1.21-1.72)**	**1.54 (1.26-1.89)**	**1.61 (1.32-1.97)**	**1.57 (1.30-1.90)**	**1.36 (1.13-1.64)**
8. Szluc	2011	**1.33 (1.13-1.58)**	**1.32 (1.04-1.67)**	**1.47 (1.19-1.82)**	1.26 (0.98-1.61)	**1.43 (1.12-1.83)**	**1.55 (1.23-1.96)**	1.12 (0.89-1.42)
9. Vilayphiou	2011	1.15 (0.80-1.64)	1.10 (0.78-1.56)	1.14 (0.83-1.57)	1.18 (0.78-1.79)	1.36 (0.84-2.20)	1.31 (0.85-2.02)	1.01 (0.70-1.44)
10. Majumdar	1999	1.33 (0.72-2.46)	1.07 (0.60-1.93)	**2.14 (1.00-4.61)**	N/A	N/A	N/A	N/A
11. Cortet	2000	**3.25 (1.39-6.90)**	N/A	N/A	N/A	N/A	N/A	N/A
12. Laib	2002	**1.91 (1.25-2.89)**	1.27 (0.84-1.92)	**2.03 (1.31-3.15)**	N/A	N/A	N/A	N/A
13. Gorai	2001	N/A	N/A	N/A	N/A	**2.10 (1.63-2.70)**	**2.17 (1.69-2.77)**	**1.56 (1.21-2.00)**
14. MacIntyre	2003	N/A	N/A	N/A	N/A	1.28 (0.32-5.09)	0.51 (0.13-1.93)	1.87 (0.52-6.76)
15. Jamal	2006	N/A	N/A	N/A	**3.26 (1.36-7.87)**	N/A	1.18 (0.60-2.33)	**16.67 (2.94-83.33)**

Table LXIX. Comparison of odds ratios for fractures associated with distal tibia bone outcomes.

Odds ratios (OR) and 95% confidence intervals for fractures associated with various bone outcomes obtained at the distal tibia are compared from multiple sources. The ultradistal tibia was defined as the 22.5 mm site proximal to the tibial endplate for hr-pQCT and as the 4% site for pQCT. Various conditions for each study are displayed. **Bold** = significant at the 95% confidence level.

Lead Author	Year	Modality	Resolution (μm)	Mean age (yrs)	Fx Type	N (F/M)	Covariates	BV/TV (OR)
1. Cejka	2011	hr-pQCT	82 x 82 x 82	59 (+-) 15	Low trauma FFx r	34F40M	age	**3.45 (1.52-8.33)**
2. Szluc	2011	hr-pQCT	82 x 82 x 82	71 (+-) 8	Low trauma FFx r	920M	age, weight	N/A
3. Szluc	2011	hr-pQCT	82 x 82 x 82	71 (+-) 8	Peripheral FFx	920M	age, weight	N/A
4. Vilayphiou	2011	hr-pQCT	82 x 82 x 82	71 (+-) 10	Low trauma FFx r	327M	age, height, weight	N/A
5. Sheu	2011	pQCT	500 x 500 x 2500	78.0 (+-) 5.3	Low trauma Nonspine Fx	1143M	age, BMI, FN aBMD	N/A

Lead Author	Year	Tb.Sp (OR)	Tb.Th (OR)	Tb.N (OR)	Ct.Th (OR)	vBMDi (OR)	vBMDtr (OR)	vBMDc (OR)
1. Cejka	2011	N/A	1.04 (0.63-1.61)	**2.86 (1.39-5.88)**	**2.56 (1.30-5.00)**	**2.86 (1.29-5.80)**	**3.70 (1.59-8.33)**	**1.89 (1.02-3.57)**
2. Szluc	2011	**1.44 (1.24-1.68)**	1.18 (0.99-1.41)	**1.53 (1.27-1.83)**	**1.59 (1.31-1.91)**	**1.59 (1.32-1.92)**	**1.54 (1.28-1.85)**	**1.44 (1.22-1.71)**
3. Szluc	2011	**1.32 (1.11-1.56)**	1.10 (0.89-1.37)	**1.49 (1.19-1.87)**	**1.42 (1.13-1.78)**	**1.43 (1.14-1.79)**	**1.45 (1.15-1.79)**	**1.28 (1.05-1.55)**
4. Vilayphiou	2011	1.01 (0.74-1.39)	1.20 (0.93-1.55)	1.02 (0.77-1.35)	**1.40 (1.03-1.89)**	1.32 (0.96-1.81)	1.20 (0.87-1.65)	1.24 (0.93-1.66)
5. Sheu	2011	N/A	N/A	N/A	N/A	**1.7 (1.1-2.6)**	1.2 (0.8-1.8)	N/A

studies for all bone outcomes of 2.24. Odds ratios at the ultradistal tibia ranged from 1.28 to 3.70 with a mean of 1.65 across studies. The larger OR reported by Jamal of 16.67 was identified for cortical vBMD from pQCT images in a sample of 52 dialysis study participants, both men and women. The larger confidence interval observed (2.94-83.33) could be an indication of imprecision from *inter alia*, a small sample size poorly representative of the population, or could be an error due to an overabundance of cell frequencies of 0. This latter scenario could occur when subgroups represented by combinations of independent variables yield no dichotomy in the dependent outcome of fractures (ie. all individuals have no fractures) (267). Excluding this larger OR, ORs derived from volumetric bone outcomes from the tibia were on average larger than those obtained at the ultradistal radius. Caution must be taken in considering this general observation due to variable imaging conditions applied for each study (most importantly: type of modality, exact ROI localization and resolution). In comparison to the present study, all ORs were still larger than the highest OR derived from age-adjusted models using MRI (1.23 (0.69-2.19)) in the local cohort. However, most hr-pQCT and pQCT-derived outcomes in the national cohort of the present study expressed per SD difference exhibited ORs (hr-pQCT range of 1.28-1.69; and pQCT range of 1.37-1.57) that were comparable to those reported by other studies. In a study examining a similarly sized cohort of women with mean age 72.2 years, Sornay-Rendu measured a larger OR for Ct.Th at the distal radius compared to the present study using hr-pQCT. This larger effect size could be explained by the fact that this group limited fractures to radiologically confirmed vertebral fractures. With the exception of Tb.N, all other bone outcomes that

Szulc and Sheu examined demonstrated ORs similar to those reported by hr-pQCT and pQCT at both radius and tibia, even though their cohorts consisted of all men (122,259). At this time, only one study by MacIntyre evaluated ORs for hole size measurements but because they based their logistic regression models on specific cutoff values rather than on units of SD, it was difficult to compare the values yielded to the present study (141).

6.7.4 National reference data

The establishment of a reference dataset is useful for comparison to individual patients in the clinic or for evaluating cohort effects, diseases and interventions by use of controls or reference populations. However, the task of establishing a reference range is challenged with selecting the population for comparison. In the case of aBMD, DXA scanner manufacturers and the NHANES survey have used sex-matched young adult means for comparison (268). It is recognized that there is a natural course of bone structure and volumetric density decline with aging (15,269,270) that would inadvertently exceed values below the young adult reference. Consequently, using a young adult mean would label a larger number of individuals as having low aBMD. If treatment decisions were calibrated based on determining the optimal bone outcome level for treatment, setting an arbitrary threshold may not be a major problem. However, if no guidance is provided on the potential fracture risks and threshold for treatment, there may be danger in over-diagnosing patients using a young adult mean. An older adult reference dataset was established in the present study. One would expect a smaller number of individuals identified as having bone outcome values beyond a given threshold when this older

cohort is used as compared to a younger adult population. The decision on where to set the threshold will depend on the ultimate decision to be made, contextualized by other secondary risk factors for osteoporosis.

Another challenge of creating a reference dataset is defining what is healthy or normal. With different study protocols, clinical populations or geographical regions (10), the reference state may vary and a standard reference dataset bearing a single set of cohort characteristics may not be ideal. Some investigators who generated reference ranges for bone data excluded individuals who were likely to have an altered bone metabolism – including a previous history of fractures, hyperparathyroidism, hypoparathyroidism, diabetes mellitus, renal disease or hormone replacement therapy (135,263). Other investigators reasoned that the goal was to describe overall variability in the cohort and to describe the norm representative of the population examined, and therefore did not exclude individuals on these characteristics (271,272). A report of the two types of cohorts could provide flexibility for future studies desiring different parameters of comparison. Nonetheless, previous manufacturers have compared individuals' bone density to historical reference data in populations, relied on reference datasets from other manufacturers, or from an established research study centre (268,273). In such these two latter cases, validation is required, and comparisons must be performed under the assumption that the equipment examined is similarly calibrated and would produce similarly reliable results.

Certainly, variations in an imaging modality's scan protocol could confer drastic differences to the study results obtained. This is particularly true when differences in resolution are a component of these variations. As demonstrated in the validation and reproducibility portions of this investigation, minute features such as trabecular structural details could be largely affected. The decision to choose a fixed or relative region of interest for the distal radius and particularly the tibia was an important one, especially for reporting national reference data to which future studies could compare. For most individuals in this study, the 4% ultradistal radius and tibia localized to a distance that was less than 9.5 mm and 22.5 mm proximal to the end plate, respectively, thus accounting for the observed differences between national and local cohort vBMD values for pQCT. This condition also explained the difference in cross-sectional area values between pQCT and hr-pQCT images in the national cohort. The proximal image slice obtained by pQCT, being closer to the actual region of interest for hr-pQCT scans, was consequently comparable in vBMD values. It is notable that even though cortical and trabecular vBMD values were between 20-70 mg/cm^3 larger on pQCT compared to hr-pQCT, the overall integral vBMD on pQCT was up to 10 mg/cm^3 smaller than hr-pQCT. This corollary follows from the fact that the total area with which integral vBMD was computed was actually larger than cortical and trabecular areas combined for pQCT.

The national reference datasets generated for pQCT, hr-pQCT and 1.0T pMRI in section 5.8 were expressed as means ± standard deviations for sake of comparison with other studies reporting the same previously. Few studies (135,263,271,274) have actually

reported a reference dataset with a breakdown of volumetric bone measures in older adults by age group. Meanwhile, several other investigators reported age-specific pQCT-derived bone outcomes in children and in adolescents (275-277).

Comparison of national pQCT age-specific reference values to literature

Compared to Gorai's study of pQCT (500 x 500 μm x 2.5 mm) at the distal radius separated also by half decades in age (263), the more proximal pQCT slice investigated in the present study showed smaller integral vBMD but larger trabecular vBMD for all half decades between 60 to 90 years. Conversely, the distal slice here was closer in values to Gorai's study but still yielded up to 30 mg/cm^3 larger values for both integral and trabecular vBMD than their study. In addition, Gorai's cohort showed vBMD differences for total and trabecular regions by as much as 70 mg/cm^3 and 30 mg/cm^3, respectively from the 60-64 age group to the 85-89 age group. The present study only exhibited differences of up to 30 mg/cm^3 for integral and 15-20 mg/cm^3 for trabecular vBMD at both slices. Cortical vBMD was more similar between the two cohorts, but again the difference from 60 to 90 years of age in the present study was only half as large as the difference (60 mg/cm^3) shown in Gorai's study. One major difference between the studies is that Gorai's cohort consisted of all Japanese women whereas the current study comprised largely of Caucasian Canadian women. However, Gorai et al did note that the rate of integral vBMD loss (-1.28%) was within the range of a Caucasian population, though their trabecular vBMD loss (-1.37%) was higher than in Caucasians. No structural information was available from this study.

Guglielmi reported pQCT-derived (500 x 500 µm x 2.5 mm) radius vBMD measures as well but only by full decades in healthy Italian women not receiving hormonal replacement (135). Comparing their data to the proximal slice of the distal radius in the present study, the 60-69 decade reported by Guglielmi was larger for both integral and trabecular vBMD, similar to the findings from Gorai's study. Trabecular vBMD in Guglielmi's study was still larger than the more distal slice of the radius in the present study but their integral vBMD was 30 mg/cm^3 smaller. Similar but more accentuated results were observed when examining their 70-81 year age group as compared to the 70-75 and 75-80 age group in the present study. Again, these contrasting results at the two slices obtained by pQCT demonstrated the importance of selecting a similar region of interest for comparison. No cortical bone reference data were available and no structural information were computed from Guglielmi's study.

Schneider also reported German reference ranges graphically for men and women using pQCT (resolution unreported) but the data were not tabulated by age categories (274). Judging by visual inspection, the mean trabecular vBMD for women between the 60-70 age group was not more than 150 mg/cm^3 and similar to that reported for the distal slice in the present study. The slight decline from the 60-70 towards the 70-80 age group was more consistent with the amount of difference in the present study compared to that observed in both Gorai and Guglielmi's studies. In contrast, integral vBMD was smaller than the distal slice observed here but larger than the proximal slice in the current study, with values for integral vBMD decreasing from the 60-70 to the 70-80 age group to a

greater extent than trabecular vBMD, but not to as large a difference than observed in the present study at both proximal and distal slices. No structural information was obtained in this study.

Comparison of national hr-pQCT age-specific reference values to literature

Macdonald (271), Khosla (14) and Dalzell (272) each reported age-related differences in volumetric bone outcomes using hr-pQCT in population-based cohorts but none tabulated reference values for separate age groups. Graphical representations of age versus bone outcomes were interpreted for comparison to the present study. It was apparent in women that after age 60, there was a gradual decline in BV/TV, Tb.N and Tb.Th that accelerated towards 80 years and beyond at the distal radius (271). In comparison to the national CaMos BQS cohort (part of the cohort consisted of Calgarian women, data for whom were collected after January 1, 2012 and thus not part of Macdonald's study), Macdonald's local cohort of Calgarian women showed hr-pQCT-derived BV/TV values and a rate of decline from age 60 to 85 years that were similar to those radius values reported in the present study within women who have not fractured a bone. Although a decrease was observed in the fractured group here as well, the magnitude was not as dramatic as in the non-fractured group. The same pattern of age-related decline was true for Tb.N between Macdonald's and the pooled analysis of present study, though here, the amount of decline was slightly larger from age 60 to 85. Both Macdonald's and the present study's Tb.Th values showed only minimal decline from the 60s to just before the mid 70s. Like BV/TV, Tb.Th and Tb.N median values in the present study were similar to

MacDonald's. Although Macdonald's regression model for Tb.Sp on age was not significant (no graphical representation), her data showed a trend towards an apparent increase in Tb.Sp with age that was larger than in men. Compared to the median hr-pQCT-derived Tb.Sp in the present study, the median Tb.Sp of 0.471 mm and 0.503 mm for the radius and tibia of Macdonald's cohort was only within a 0.010 mm difference. At the tibia, both in Macdonald's study and in the present analysis, rates of decline in bone structure were modest compared to the radius. It is likely that these similarities in both bone structural values and age-related declines between Macdonald's and the present study were derived from the fact that the cohort of Canadian women examined in both cases exhibited similar demographics. No age-specific densitometric data were displayed in Macdonald's study.

In the American cohort derived from the Rochester Epidemiology Project (MN, USA), Khosla computed BV/TV from hr-pQCT-derived images at the radius that was similar in both the mean value and the average decline between age 60 to above age 85 as in the present study (14). In contrast to both Macdonald's and the present Canadian study, Tb.N in the Americans was larger by more than half a trabecula per mm but Tb.Th smaller by 0.015 mm. The amount of decline in BV/TV and Tb.N with aging in Americans appeared only slightly faster than both the present study and Macdonald's study of Canadian women. However, the present Canadian study displayed an almost two-fold larger Tb.Sp compared to the Americans in the Rochester study and revealed over twice as rapid an age-related increase in Tb.Sp. Thus it appears that American women have more, but

thinner, trabeculae that are not separated as far apart as Canadians, but Canadian women are better at maintaining bone volume by preserving trabecular thickness even though the amount of separation between them increases more rapidly than Americans. Age-specific densitometric data from hr-pQCT were not displayed in Khosla's manuscript.

In a cohort of Norfolk, English study participants, Dalzell used hr-pQCT and computed normative reference values for volumetric bone outcomes with and without excluding individuals with self-reported fractures, osteoporosis or other conditions that would affect bone metabolism. They did not find a significant difference in the fit of their regression models for radius and tibia bone outcomes on age after exclusion of the 28 participants who met these criteria (272). From the available graphical data, it appeared that English women shared a common starting point as Canadians with integral vBMD averaging around 300 mg/cm^3 for both radius and tibia but showed a sharper decline towards age 80 and beyond compared to the present Canadian cohort. The same was true for trabecular and cortical vBMD, ignoring the 50-55 age decade, which showed an abnormally lower vBMD in Canadians. Although Canadians' Tb.Sp displayed a median around the same values as English participants, the amount of increase from 60 to beyond 80 years of age was not as great in Canadians who had a fracture but was similar to the English cohort in Canadians who have not had a fracture. Similar to both the present Canadian study and Khosla's Rochester cohort, BV/TV in the English cohort shared a similar starting point and rate of decline starting from age 60 to 80 for the radius but a faster decline at the tibia. In contrast, Tb.N in Dalzell's study was similar to the present study but there was not a

noticeable decline with age observed at either site. The largest difference between the cohorts was found in Ct.Th, where values at the radius in the English study started at about the same level but declined by over 50% compared to the only 30% decline in the present study. Incidentally, cortical density and thickness measures also demonstrated the largest sex-differences in the English cohort. Taken together, Canadians and the English shared similar bone structural integrity beginning at age 60 but the English showed sharper declines in Ct.Th primarily with more rapid loss of vBMD and overall bone volume. Like the Americans, the English are better at preserving a smaller Tb.Sp and larger number of trabeculae compared to Canadians.

Comparison of summarized national hr-pQCT reference values to literature

Because of the lack of age-category-specific bone outcomes available for fracture versus non-fractured groups in the literature, overall summary statistics for volumetric bone outcomes from other fracture association studies was compiled into Table LXX (radius) and Table LXXI (tibia). Only one former cohort study out of those examining bone outcomes and fractures (Table LXX & Table LXXI) had reported at least Tb.Sp's median and interquartile range for images obtained by hr-pQCT (259). Compared to the overall median reported in the present study using hr-pQCT images, the median Tb.Sp in Szulc's control group was 20 µm smaller but demonstrated a tighter interquartile range. The larger separation and wider distribution of data reported here was likely because the median comprised of a slightly older cohort and the sex examined was women versus men in Szulc's study. Sex differences in bone density and structure, particularly after 65

years of age, are most apparent (120). In men, Eckstein showed that trabeculae are more plate-like, thicker and have smaller separation spaces at the distal radius and femoral neck compared to women (278). This observation explains the minor discrepancy observed between the present study and the control data from Szulc's study. Bone volume fraction obtained from hr-pQCT images here matched most closely to Melton's mean fraction of 0.121 compared to other studies employing hr-pQCT. Cortical vBMD, Ct.Th, Tb.Th and integral vBMD were more in line with values reported by previous hr-pQCT studies but Tb.N and trabecular vBMD obtained from hr-pQCT here were on average larger than those observed from hr-pQCT studies previously described (Table LXX). While all scan protocols were mostly similar across all hr-pQCT studies including the current investigation, the sample size reported here was larger than many others except one study performed in men by Szulc and one done in women by Sornay-Rendu. In addition to differences in statistical power, population characteristics of Canadians versus many of the American studies and few European studies could also explain these differences.

Comparison of summarized national pQCT reference values to literature

Despite observing a higher overall trabecular vBMD value in the current study obtained from pQCT images, integral vBMD was similar to other studies reported using pQCT. The heterogeneity of cortical vBMD was high among the four studies reporting pQCT measures, but the values identified here were closest to Gorai's study of Japanese women. Although not explicitly described in the manuscripts of each of these studies in Table LXX, the difference across these studies may lie in the differential use of segmentation

thresholds for separating cortical from trabecular bone as suggested by Kontulainen (169). At this point in time, aside from the present study, only the MrOS study employed the OsteoQ software for computing apparent bone structure from pQCT images. However, these measurements have yet to be reported by MrOS investigators. Consequently, no comparable studies were available for volumetric bone structure measurements.

Comparison of summarized national MRI reference values to literature

To date, there have been no studies reporting age-specific population-based MR image-derived volumetric bone structural outcomes. In the single larger cohort study by Laib et al (156 x 156 x 500 µm) performed in postmenopausal American women from San Francisco, CA and Seattle, WA (139), the correlations between each of the bone structural outcomes and age (ranged from 46-96) were virtually zero ($r^2 < 0.01$, $p > 0.05$). Because of the lower resolution and larger slice thickness employed in the present study, BV/TV (by 0.125), Tb.Th (by over 200 µm), Tb.Sp (by over 100 µm) and Tb.N (by over 0.5 #/mm) were larger than values reported by Laib et al. While the present study showed a similar 30 µm difference for Tb.Sp between fractured and non-fractured groups (Table LXVI) as did Laib, BV/TV and Tb.N did not reveal a difference between groups here in contrast to Laib's study. However, like the present study, Tb.Th reported in Laib's fractured group was actually slightly larger than the non-fractured group but this comparison was not significant. Women in Laib's study were on average younger than in the present study. Majumdar used a similar MR imaging protocol (156 x 156 x 500 µm) as Laib to examine a smaller group of women who were closer in age (72.2 ± 9.2) to

those examined here (265) and found similar Tb.Th and Tb.N values as reported in the current study. Although, their reported SD for Tb.Th was over 20 fold larger than reported here, which could explain why they did not observe any differences between groups with and without fractures. In Majumdar's study, BV/TV was closely matched with values obtained by Laib, both of which were over half the value reported here. Like Tb.Th, Tb.Sp's SD was almost twice as large as what was observed here and their mean value was about 300 µm larger. Supporting the notion that resolution played a major role in the observed deviations among studies, Cortet used a similar resolution as the present study (195 x 195 µm x 2 mm) and yielded both BV/TV and Tb.Sp values that were similar in mean values and inter-individual variability as shown here.

The range of differences observed across various cohort studies in separate geographies for pQCT, hr-pQCT and MRI reveal the importance of establishing country-specific reference data. It is not new that fracture risk varies by region and the diagnosis of osteoporosis can differ significantly around the world (31). At this time, MRI did not have any substantial reference data available from previous studies. The establishment of a population-based cohort would require a larger sample size or a larger number of scanners for wider cohort access. Currently, with four pMRI units within Canada (only two available for access) and more expensive access to full body MRI units, there are serious feasibility challenges that must be overcome in order to meet this goal. The mean or median bone outcome values along with corresponding measures of between-individual distributions in this study could be used as a point of reference for future

studies. While individual patient data could be compared to this reference dataset, its clinical meaning would remain questionable until a longitudinal study examining prospective risk of fractures could be conducted, accounting for the standard of care: assessment of risk factors for osteoporosis in combination with aBMD of the total hip and lumbar spine (35).

Table LXX. Comparison of mean volumetric ultradistal radius bone outcomes across different studies

Summary statistics were compared across multiple studies employing one or more of the three modalities: hr-pQCT, pQCT and MRI. Different imaging conditions are listed for comparison. All studies examining the ultradistal (UD) radius reporting one or more of the indicated bone outcomes were compared here. Values are expressed as mean ± SD.

Author	Year	Modality	Resolution (um)	Anatomy	ROI	Mean age (years)	N (F/M)	BV/TV (%)
1. Boutroy	2008	hr-pQCT	82 x 82 x 82	UD Radius	9.5 mm	73.4 ± 6.0	66F	
2. Cejka	2011	hr-pQCT	82 x 82 x 82	UD Radius	9.5 mm	59 ± 15	34F/40M	9.75 ± 1.1
3. Melton	2007	hr-pQCT	89 x 89 x 89	UD Radius	7 mm	68.1 ± 11.4	36F	
4. Melton	2007	hr-pQCT	82 x 82 x 82	UD Radius	9.5 mm	78.6 ± 9.0	80F	12.1 ± 4.2
5. Sornay-Rendu	2009	hr-pQCT	82 x 82 x 82	UD Radius	9.5 mm	72.2 ± 8.2	462F	9.8 ± 4
6. Szulc	2011	hr-pQCT	82 x 82 x 82	UD Radius	9.5 mm	71 ± 8	920M	
7. Vico	2008	hr-pQCT	82 x 82 x 82	UD Radius	9.5 mm	71.5 ± 10.5	166F	9.4 ± 4
8. Vilayphiou	2011	hr-pQCT	82 x 82 x 82	UD Radius	9.5 mm	71 ± 10	327M	
9. Cortet	2000	MRI 1.5T	195 x 195 x 2000	UD Radius	Coronal	69 ± 7	20F	40.1 ± 4.62
10. Laib	2002	MRI 1.5T	156 x 156 x 500	UD Radius	14 mm	62.2 ± 6.4	148F	34 ± 6.4
11. Majumdar	1999	MRI 1.5T	156 x 156 x 500	UD Radius	joint line	72.2 ± 9.2	39F	27 ± 10
12. Gorai	2001	pQCT	500 x 500 x 2500	UD Radius	4%	66.4 ± 10.3	621F	
13. Jamal	2006	pQCT	250 x 250 x 2500	UD Radius	4%	65.8 ± 9.0	16F/36M	
14. MacIntyre	2003	pQCT	330 x 330 x 2500	UD Radius	4%	57.7 ± 15.3	42F	
15. Schneider	2001	pQCT	500 x 500 x 2500	UD Radius	4%	45-85	107F	

Author	Tb.Sp (µm)	Tb.Th (µm)	Tb.N (#/mm)	Ct.Th (µm)	vBMDi (mg/cm^3)	vBMDtr (mg/cm^3)	vBMDc (mg/cm^3)
1. Boutroy	0.716 ± 377	0.068 ± 0.012	1.4 ± 0.32	0.545 ± 0.204	239 ± 70	115 ± 39	786 ± 84
2. Cejka		0.061 ± 0.004	1.53 ± 0.115	0.600 ± 0.067	255 ± 21	115 ± 12	793 ± 24
3. Melton	0.695 ± 0.280	0.075 ± 0.010	1.45 ± 0.4				
4. Melton	0.625 ± 0.330	0.080 ± 0.010	1.55 ± 0.4				
5. Sornay-Rendu	0.748.5 ± 0.530	0.070 ± 0.010	1.39 ± 0.5	0.582 ± 0.180	251 ± 67	117 ± 43	808 ± 84
6. Szulc	0.476 ± 0.080	0.076 ± 0.012	1.82 ± 0.26	0.665 ± 0.220	282 ± 63	167 ± 39	792 ± 79
7. Vico	0.828 ± 0.590		1.33 ± 0.49	0.744 ± 0.259		114 ± 47	873 ± 118
8. Vilayphiou	0.488 ± 0.116		1.81 ± 0.26	0.654 ± 0.228	280 ± 61	166 ± 37	
9. Cortet	0.585 ± 0.140						
10. Laib	0.518 ± 0.100	0.300 ± 0.026	1.48 ± 0.15				
11. Majumdar	0.955 ± 0.470	0.510 ± 0.990	0.88 ± 0.19				
12. Gorai					284 ± 80	109 ± 50	841 ± 66
13. Jamal				1.845 ± 0.590		160 ± 65	1127 ± 64
14. MacIntyre					297 ± 67	133 ± 41	568 ± 109
15. Schneider					282 ± 85	119 ± 43	429 ± 92

Table LXXI. Comparison of mean volumetric ultradistal tibia bone outcomes across different studies

Summary statistics were compared across multiple studies employing one or more of the three modalities: hr-pQCT, pQCT and MRI. Different imaging conditions are listed for comparison. All studies examining the ultradistal (UD) tibia reporting one or more of the indicated bone outcomes were compared here. Values are expressed as mean ± SD.

Author	Year	Modality	Resolution (μm)	Anatomy	ROI	Mean age (years)	N (F/M)	BV/TV (%)
1. Cejka	2011	hr-pQCT	82 x 82 x 82	UD Tibia	22.5 mm	59 ± 15	34F/40M	10.25 ± 0.9
2. Sornay-Rendu	2009	hr-pQCT	82 x 82 x 82	UD Tibia	22.5 mm	72.2 ± 8.2	462F	11.05 ± 4
3. Szluc	2011	hr-pQCT	82 x 82 x 82	UD Tibia	22.5 mm	71 ± 8	920M	
4. Vico	2008	hr-pQCT	82 x 82 x 82	UD Tibia	22.5 mm	71.5 ± 10.5	166F	11.3 ± 3.9
5. Vilayphiou	2011	hr-pQCT	82 x 82 x 82	UD Tibia	22.5 mm	71 ± 10	327M	

Author	Tb.Sp (μm)	Tb.Th (μm)	Tb.N (#/mm)	Ct.Th (μm)	vBMDi (mg/cm^3)	vBMDtr (mg/cm^3)	vBMDc (mg/cm^3)
1. Cejka		0.072 ± 0.005	1.46 ± 0.104	0.786 ± 0.081	216 ± 15	121 ± 10	776 ± 20
2. Sornay-Rendu	0.736 ± 0.600	0.080 ± 0.020	1.38 ± 0.48	0.824 ± 0.260	228 ± 53	132 ± 48	782 ± 104
3. Szluc	0.508 ± 0.104	0.082 ± 0.013	1.69 ± 0.31	1.140 ± 0.310	279 ± 58	166 ± 37	824 ± 85
4. Vico	0.650 ± 0.429		1.51 ± 0.47	0.718 ± 0.283		136 ± 46	748 ± 107
5. Vilayphiou	0.538 ± 0.157		1.68 ± 0.31	1.136 ± 0.315	278 ± 58	164 ± 36	

Table LXXII. Meta-descriptive summary of volumetric bone outcomes across studies
Summary statistics for volumetric bone outcomes (radius: top, tibia: bottom) from multiple studies (all studies from **Table LXX** and **Table LXXI**) employing one or more of the three modalities: hr-pQCT, pQCT and MRI, were summarized to provide a meta-mean and SD according to the control (fx-), fractured (fx+) groups and the entire cohort of each study. Meta-ANOVA analysis compared means between fractured and control groups. **[a] indicates** significant difference before Bonferroni correction, and **[b] indicates** significant difference after Bonferroni correction.

Radius	BV/TV (%)	Tb.Sp (µm)	Tb.Th (µm)	Tb.N (#/mm)	Ct.Th (µm)	vBMDi (mg/cm^3)	vBMDtr (mg/cm^3)	vBMDc (mg/cm^3)
Fx-	20.5 ± 12.9	0.587 ± 0.122	0.150 ± 0.161	1.58 ± 0.25	0.908 ± 0.496	287 ± 19	146 ± 18	841 ± 158
Fx+	17.6 ± 12.5	**0.740 ± 0.196**[a]	0.142 ± 0.152	**1.35 ± 0.27**[a]	0.697 ± 0.364	**239 ± 41**[b]	**117 ± 30**[a]	795 ± 131
Total	19.1 ± 12.7	0.663 ± 0.155	0.146 ± 0.156	1.46 ± 0.25	0.802 ± 0.429	263 ± 27	131 ± 23	818 ± 144

Tibia	BV/TV (%)	Tb.Sp (µm)	Tb.Th (µm)	Tb.N (#/mm)	Ct.Th (µm)	vBMDi (mg/cm^3)	vBMDtr (mg/cm^3)	vBMDc (mg/cm^3)
Fx-	12.6 ± 0.1	0.545 ± 0.051	0.084 ± 0.001	1.65 ± 0.10	1.040 ± 0.197	280 ± 21	162 ± 13	810 ± 28
Fx+	**9.8 ± 0.5**[b]	0.672 ± 0.161	0.079 ± 0.004	**1.48 ± 0.19**[a]	0.869 ± 0.237	244 ± 37	**137 ± 24**[a]	**760 ± 49**[a]
Total	11.2 ± 0.2	0.608 ± 0.105	0.081 ± 0.001	1.57 ± 0.15	0.954 ± 0.217	262 ± 29	150 ± 18	785 ± 38

7 Conclusions and recommendations

7.1 Summary of findings

The present study compared three technologies capable of quantifying bone structural and densitometric properties at the ultradistal radius and tibia. Short- and long-term reproducibility was the highest for hr-pQCT followed by pQCT and pMRI. Because of the similarity in in-plane resolution, pMRI and pQCT demonstrated comparable precision error for most measurements. Trabecular separation and BV/TV were the most valid measures obtained by pMRI and pQCT but Bland-Altman plots showed that larger Tb.Sp values were less reliable. Connectivity and hole geometry measures proved poorer reliability because of their sensitivity to positioning. Correspondingly, they exhibited the largest one-year changes. Short and long-term errors appeared to be affected largely by motion artifact, which in turn could be resulted from longer scan times. Although measurements from pMR images were shown to be valid, it is apparent that at least for cortical bone, chemical shift artifact presents a major challenge for structural quantification on 1.0T pMRI. Sensitivity analyses showed little effect of image co-registration and angular misalignment on validity and reliability of measurements. Instead, a larger volume of interest examined appeared to reduce random error and maintain a higher reproducibility. Exclusion of individuals with a previous history of fractures or currently on antiresorptive therapy reduced the amount of change measured over time. Standard errors of the estimate reflected only the machine-associated detection limit while LSC values were larger and incorporated the notion of biological change over one year. Although the local cohort showed significant associations with fragility fractures for

Ct.Th and vBMD for just hr-pQCT, there was a trend towards significance for pQCT, which was externally validated by the national cohort where this trend was significant. Trabecular measurements showed smaller effect sizes, but they also demonstrated significant associations with fractures in a larger sample. Bone measures' association with fractures were stronger at the tibia than at the radius in general due to potential effects of weight-bearing on affecting bone turnover rates. This study generated a sizeable national dataset of bone structural and densitometric measures for pQCT and hr-pQCT but only a smaller reference dataset for 1.0T pMRI. National and local cohorts showed very similar ranges in bone measures but due to the difference in ROI selected, pQCT values were more discrepant at the more proximal slice compared to the more distal slice.

7.2 Recommendations and caution

7.2.1 pMRI recommendations

Due to the longer scan times required, influence of chemical shift artifact and magnetic susceptibility differences, it is not recommended that 1.0T pMRI be used as a routine tool for monitoring bone structure, particularly with the number of slices prescribed here. To increase feasibility and reliability of measurement, slice number could be reduced. Indeed, pQCT was shown to successfully associate single-slice bone outcome values to fractures and the same could hold true with pMRI when selecting a similar region of interest. While pMRI may be appropriate for quantifying bone structure in research studies, caution must be exercised when deciding on the duration of follow-up due to the larger LSC achievable compared to hr-pQCT. In addition, the lack of densitometric information

obtained by pMRI attributes to it another disadvantage. pMRI was investigated in the present study, bearing a smaller gantry thus enabling superior RF focusing and correspondingly higher SNR than a full body system. However, it is anticipated that similar conclusions can be extended to full body MRI scanners with minor error contributions from correct ROI positioning . Higher magnetic strength machines could also demonstrated even more severe chemical shift problems and will encounter a greater contribution of error due to magnetic susceptibility differences if other contributing variables such as bandwidth were not adjusted. MRI's contraindication against those with metal implants and pace makers prevents its utility for a small population. However, MRI benefits from the absence of ionizing radiation and would be appropriate for those who have concerns over radiation dose, in particular pregnant women and children.

7.2.2 pQCT recommendations

The pQCT modality proved to provide acceptable reliability for most bone measures and demonstrated validity against hr-pQCT while yielding information with exposure to a low amount of ionizing radiation (1 μSv) per slice. Although only two slices were obtained within 5-10 minutes, even single slice data were associated with fractures in the national dataset. With motion artifact, streaking could present a problem for accurate measurement of cortical bone density and thickness. It would be advisable to apply the OsteoQ algorithm to pQCT images rather than utilizing simple threshold-based techniques to perform segmentation of bone from soft tissue as per the manufacturer's software. Computation of trabecular measurements within a region representing 45% of the total

bone mask was feasible for avoiding the transition zone between cortical bone to trabecular bone, the inclusion of which could markedly increase the estimation of trabecular thickness. Rather than acquiring single slices, scanning multiple slices in tandem could help overcome potential problems with slice-matching for quantifying change over follow-up periods. However, in a cohort where significant motion could be a concern, a single slice would be recommended as the probability of encountering significant motion artifact causing failed quality assurance would be lower. Despite the longer scan time required compared to previous studies, the 10 mm/s scan speed demonstrated utility for quantifying apparent measures of bone structure at 200 μm in-plane resolution that correlated with fractures and would be recommended for future investigations. Previous studies employing 15 mm/s scan protocols would suffer from a difference of 7.27 standardized SNR units and 5.60 standardized CNR units, representing 24.6% and 25.8% lower SNR and CNR than the 10 mm/s protocol, respectively. This sizeable difference in SNR and CNR could affect clearer delineation of bone from soft tissue, thus affecting the computation of bone structural outcomes, particularly those involving thickness and connectivity measurement.

7.2.3 hr-pQCT recommendations

With the high degree of short and long-term precision, hr-pQCT is an optimal candidate for quantifying bone structural and densitometric outcomes. The scan time was shorter than either pQCT or pMRI and the number of failed QA procedures or high motion scans were lower. By virtue of the higher in-plane and out-of-plane resolution (or slice

thickness) of 82 μm, combined with the large number of image slices acquired, hr-pQCT was powered to yield bone outcomes that demonstrated small detection limits and significant associations with fractures. In addition, the ability to reproducibly match the same region of interest over follow-up periods is less problematic compared to pQCT since a sizeable volume can be matched. Of the three modalities, hr-pQCT confers the highest mount of radiation (3 μSv) per scan but this amount of radiation remains well within the amount of average daily radiation conferred by the sun (8 μSv) and three times less than a hip and spine bone density scan (10 μSv). For studies requiring shorter follow-up periods and those desiring the ability to detect smaller amounts of change, hr-pQCT would be an ideal candidate for quantifying bone outcomes. However, because the ROI prescribed by the manufacturer software was fixed at 9.5 mm proximal to the radial end plate and 22.5 mm proximal to the tibial end plate, the actual region examined may differ substantially between individuals who vary in radius and tibia lengths. Custom algorithms for computing bone outcomes using hr-pQCT images would benefit from the ability to select a percentage site relative to a reference landmark. In addition, selection of a reference landmark for the radius such as the base of the radial tilt would better enable future comparisons between hr-pQCT and pQCT data. In theory, the OsteoQ algorithm can be applied to hr-pQCT images but it has not been cross-adapted to interpret full three-dimensional datasets and would require slice-by-slice analysis of the full 110-slice volume. However, with the higher resolution scans available, semi- or full-automation of image segmentation procedures could not only improve analysis efficiency but could further reduce the precision error between analysis-reanalyses.

7.3 Future avenues of research

7.3.1 Mechanical properties of bone

Structural properties of bone were examined in this study for all modalities in addition to volumetric density for pQCT and hr-pQCT. With the combination of these features of bone, mechanical properties can be estimated by determining the distribution of bone voxels around the central axis using cross-sectional moments of inertia or similar measures such as stress-strain index that also relies on simple geometric distribution. With volumetric data generated from there-dimensional reconstructed bone images, hr-pQCT has been capable of yielding such data using micro finite element analysis within reasonable reliability (279,280). The densitometric information available from hr-pQCT also aids in the estimation of material properties, a requirement for assessing bone mechanical properties. However, μFEA has been performed on high-resolution MR images as well, by applying assumptions of material properties of bone, albeit, the reproducibility was poorer than hr-pQCT (235). One study showed that relaxation time of proton spins could be used to estimate mechanical properties of bone, but the study also revealed that pQCT was superior at predicting bone mechanical properties (281). pQCT has been able to estimate mechanical properties of bone by assuming a single cross-section can be extended to a cylindrical bone. Measures of polar stress-strain index, buckling ratio and cross-sectional moments of inertia can be derived by simply calculating the distribution of bone voxels from the central axis. In the CaMos BQS national study, mechanical properties of bone will be examined further and compared to combined elements of structure and density in predicting prospective fractures.

7.3.2 Comparison to the standard of care

The present study was focused on comparing the ability of pMRI, pQCT and hr-pQCT to compute bone outcomes and did not specifically examine the value added clinically over the current standard of care: bone density testing and assessment of primary and secondary risk factors for osteoporosis. There remains the possibility that measurements obtained at the ultradistal radius and tibia lack associations with more clinically relevant sites such as the spine and hip. In addition, there has been a lack of study comparing the relative differences in odds or hazard ratios for fractures identified for bone outcomes obtained at the peripheral sites versus outcomes determined from images of the hip and spine. Logistic regression models that include bone density and other risk factors for osteoporosis as covariates would better inform on how the observed associations reported here can remain robust and independent of these predictors. Despite the limitation of this study in not having these variables, the simple univariable binary logistic regression models and multivariable models including age could be used to compare with other study models where other risk factor information is not available.

7.3.3 Longitudinal study on fracture risk

In light of the limitations of the cross-sectional analyses described here, a longitudinal study will be equipped to better address the direction of causality between bone outcomes and incident fragility fractures. However, a larger sample size will be required to adequately power a Cox proportional hazard model used to address this question. The

national component of the present study will continue for the next five years to conduct the proposed longitudinal analysis. At the same time, bone density information will be included in Cox proportional hazard models to evaluate the independence of bone outcomes for predicting fragility fractures. Within a longitudinal analysis, a follow-up visit can be implemented to examine how changes in bone outcomes could relate to alterations in fracture risk and to prospective fractures. The ability to quantify change with and without treatment will provide confidence of true clinical sensitivity. Furthermore, quantifying such changes in different cohorts could prove the utility of this measure across a wider population and perhaps in individuals with different disease states.

The true evaluation of the success of pMRI, pQCT and hr-pQCT-derived bone outcomes for association with fractures would be a meta-Cox-proportional hazard analysis from a compilation of multiple studies. Currently, there are at least two collective efforts to combine hr-pQCT data across multiple population-based cohort studies to specifically address this goal (led by Bouxsein and Kiel). However, there have not been efforts to date to compile data for pQCT or pMRI bone outcomes. The major impediment to this milestone is the present lack of consistency in the way pQCT scans have been acquired, preventing the ability to combine the measures. Specifically, the 10 mm/s scan protocol yielding an in-plane resolution of 200 μm capable of computing apparent bone microstructure has only been implemented at one study centre and more recently has been disseminated for use in the national CaMos BQS study. For pMRI, the greatest hurdle is

the small number of pMRI modalities available or the lack of communication between investigators owning an extremity MRI unit.

7.3.4 Trade-off comparisons and technology assessments

The fact that a single slice of pQCT was able to demonstrate correlation with fragility fractures suggested that a volume as large as the 110 slices from hr-pQCT may not be necessary to yield a similarly large effect size. To determine the effect of volume of interest on fracture associations, cumulative slice number versus fracture association curves can be plotted to observe a maximum fracture association. The minimum slice number yielding the optimum fracture association could inform on the time-benefit or risk(radiation)-benefit relationship for acquiring more slices versus the information yielded. In addition to knowing the value of different volumes of interest, single-scan pQCT actually costs less on average than a hr-pQCT scan, with lower annual maintenance costs and a total smaller acquisition cost. If the development of bone outcomes reaches the point of clinical application, one would be concerned about the cost-benefit relationship. Clinical value can be expressed by percentage increase in fracture risk detectable but for comparison to policy standards, utility measures such as quality adjusted life years (QALY) would be standard. At this stage, there is not sufficient data to judge the number of quality adjusted life years saved from obtaining knowledge about an individual's risk for fracture based on pQCT or hr-pQCT bone outcome versus bone density alone.

7.3.5 Additional MRI techniques for quantifying bone

Magnetic susceptibility was discussed here as a drawback to being able to accurately quantify apparent bone microstructure. However, by measuring magnetic susceptibility differences using the T_2^* relaxation time, previous studies showed correlations with vBMD. This was a milestone in MR imaging of bone since bone density or the mineral content of bone cannot be measured directly using MRI technology (190,281). The physics behind this idea is based on the degree of magnetic susceptibility discontinuities as a function of trabecular thickness. With more bone separating bone marrow with higher magnetic susceptibility, T_2^* relaxation time is lowered, effectively affording an inverse relation with trabecular vBMD. This technique would be useful for sites bearing a higher proportion of trabecular bone such as the ultradistal radius, tibia sites as well as the lumbar spine. Femoral neck measurements may not benefit from this method due to the lack of trabecular bone but one study did demonstrate significant inverse correlations between T_2^* and proximal femur vBMD (190).

8 References

1. Brown JP, Josse RG 2002 2002 clinical practice guidelines for the diagnosis and management of osteoporosis in Canada. Cmaj **167**(10 Suppl)**:**S1-34.
2. Lu Y, Genant HK, Shepherd J, Zhao S, Mathur A, Fuerst TP, Cummings SR 2001 Classification of osteoporosis based on bone mineral densities. J Bone Miner Res **16**(5)**:**901-910.
3. Wiktorowicz ME, Goeree R, Papaioannou A, Adachi JD, Papadimitropoulos E 2001 Economic implications of hip fracture: health service use, institutional care and cost in Canada. Osteoporos Int **12**(4)**:**271-278.
4. Tarride JE, Hopkins RB, Leslie WD, Morin S, Adachi JD, Papaioannou A, Bessette L, Brown JP, Goeree R 2012 The burden of illness of osteoporosis in Canada. Osteoporos Int **23**(11)**:**2591-2600.
5. Goeree R, O'Brien B, Pettitt D, Cuddy L, Ferraz M, Adachi JD 1996 An assessment of the burden of illness due to osteoporosis in Canada. J Soc Obstet Gynaecol Can **18**(Suppl July)**:**15-24.
6. Canadian Institute for Health Information 2009 Health Indicators 2009, Ottawa, ONT, Canada.
7. Hiligsmann M, Ethgen O, Richy F, Reginster JY 2008 Utility values associated with osteoporotic fracture: a systematic review of the literature. Calcif Tissue Int **82**(4)**:**288-292.
8. Lips P, van Schoor NM 2005 Quality of life in patients with osteoporosis. Osteoporos Int **16**(5)**:**447-455.
9. Ioannidis G, Papaioannou A, Hopman WM, Akhtar-Danesh N, Anastassiades T, Pickard L, Kennedy CC, Prior J, Olszynski WP, Davison KS, Goltzman D, Thabane L, Gafni A, Papadimitropoulos E, Brown JP, Josse R, Hanley DA, Adachi JD 2009 Relation between fractures and mortality: results from the Canadian Multicentre Osteoporosis Study. CMAJ **181**(5)**:**1-7.
10. Langsetmo L, Hanley DA, Kreiger N, Jamal SA, Prior J, Adachi JD, Davison KS, Kovacs C, Anastassiades T, Tenenhouse A, Goltzman D 2008 Geographic variation of bone mineral density and selected risk factors for prediction of incident fracture among Canadians 50 and older. Bone **43**(4)**:**672-678.
11. Cooper C, Atkinson EJ, O'Fallon WM, Melton LJ, 3rd 1992 Incidence of clinically diagnosed vertebral fractures: a population-based study in Rochester, Minnesota, 1985-1989. J Bone Miner Res **7**(2)**:**221-227.
12. Lonnroos E, Kautiainen H, Karppi P, Huusko T, Hartikainen S, Kiviranta I, Sulkava R 2006 Increased incidence of hip fractures. A population based-study in Finland. Bone **39**(3)**:**623-627.
13. van Staa TP, Dennison EM, Leufkens HG, Cooper C 2001 Epidemiology of fractures in England and Wales. Bone **29**(6)**:**517-522.
14. Khosla S, Riggs BL, Atkinson EJ, Oberg AL, McDaniel LJ, Holets M, Peterson JM, Melton LJ, 3rd 2006 Effects of sex and age on bone microstructure at the

ultradistal radius: a population-based noninvasive in vivo assessment. J Bone Miner Res **21**(1)**:**124-131.

15. Lang TF, Sigurdsson S, Karlsdottir G, Oskarsdottir D, Sigmarsdottir A, Chengshi J, Kornak J, Harris TB, Sigurdsson G, Jonsson BY, Siggeirsdottir K, Eiriksdottir G, Gudnason V, Keyak JH 2012 Age-related loss of proximal femoral strength in elderly men and women: the Age Gene/Environment Susceptibility Study--Reykjavik. Bone **50**(3)**:**743-748.
16. Kanis JA, Johnell O, Oden A, Dawson A, De Laet C, Jonsson B 2001 Ten year probabilities of osteoporotic fractures according to BMD and diagnostic thresholds. Osteoporos Int **12**(12)**:**989-995.
17. Crabtree NJ, Kroger H, Martin A, Pols HA, Lorenc R, Nijs J, Stepan JJ, Falch JA, Miazgowski T, Grazio S, Raptou P, Adams J, Collings A, Khaw KT, Rushton N, Lunt M, Dixon AK, Reeve J 2002 Improving risk assessment: hip geometry, bone mineral distribution and bone strength in hip fracture cases and controls. The EPOS study. European Prospective Osteoporosis Study. Osteoporos Int **13**(1)**:**48-54.
18. Schuit SC, van der Klift M, Weel AE, de Laet CE, Burger H, Seeman E, Hofman A, Uitterlinden AG, van Leeuwen JP, Pols HA 2004 Fracture incidence and association with bone mineral density in elderly men and women: the Rotterdam Study. Bone **34**(1)**:**195-202.
19. Sornay-Rendu E, Munoz F, Garnero P, Duboeuf F, Delmas PD 2005 Identification of osteopenic women at high risk of fracture: the OFELY study. J Bone Miner Res **20**(10)**:**1813-1819.
20. Nguyen ND, Eisman JA, Center JR, Nguyen TV 2007 Risk factors for fracture in nonosteoporotic men and women. J Clin Endocrinol Metab **92**(3)**:**955-962.
21. Fink HA, Harrison SL, Taylor BC, Cummings SR, Schousboe JT, Kuskowski MA, Stone KL, Ensrud KE 2008 Differences in site-specific fracture risk among older women with discordant results for osteoporosis at hip and spine: study of osteoporotic fractures. J Clin Densitom **11**(2)**:**250-259.
22. Popp AW, Senn C, Franta O, Krieg MA, Perrelet R, Lippuner K 2009 Tibial or hip BMD predict clinical fracture risk equally well: results from a prospective study in 700 elderly Swiss women. Osteoporos Int **20**(8)**:**1393-1399.
23. Riggs BL, Melton LJ, 3rd, Robb RA, Camp JJ, Atkinson EJ, Oberg AL, Rouleau PA, McCollough CH, Khosla S, Bouxsein ML 2006 Population-based analysis of the relationship of whole bone strength indices and fall-related loads to age- and sex-specific patterns of hip and wrist fractures. J Bone Miner Res **21**(2)**:**315-323.
24. van Helden S, van Geel AC, Geusens PP, Kessels A, Nieuwenhuijzen Kruseman AC, Brink PR 2008 Bone and fall-related fracture risks in women and men with a recent clinical fracture. The Journal of bone and joint surgery **90**(2)**:**241-248.
25. Joakimsen RM, Fonnebo V, Magnus JH, Tollan A, Sogaard AJ 1998 The Tromso Study: body height, body mass index and fractures. Osteoporos Int **8**(5)**:**436-442.
26. Lunt M, Felsenberg D, Adams J, Benevolenskaya L, Cannata J, Dequeker J, Dodenhof C, Falch JA, Johnell O, Khaw KT, Masaryk P, Pols H, Poor G, Reid D, Scheidt-Nave C, Weber K, Silman AJ, Reeve J 1997 Population-based geographic

variations in DXA bone density in Europe: the EVOS Study. European Vertebral Osteoporosis. Osteoporos Int **7**(3)**:**175-189.
27. Beck TJ, Petit MA, Wu G, LeBoff MS, Cauley JA, Chen Z 2009 Does obesity really make the femur stronger? BMD, geometry, and fracture incidence in the women's health initiative-observational study. J Bone Miner Res **24**(8)**:**1369-1379.
28. Travison TG, Araujo AB, Esche GR, Beck TJ, McKinlay JB 2008 Lean mass and not fat mass is associated with male proximal femur strength. J Bone Miner Res **23**(2)**:**189-198.
29. Cummings SR, Nevitt MC, Browner WS, Stone K, Fox KM, Ensrud KE, Cauley J, Black D, Vogt TM 1995 Risk factors for hip fracture in white women. Study of Osteoporotic Fractures Research Group. N Engl J Med **332**(12)**:**767-773.
30. Kanis JA, Borgstrom F, De Laet C, Johansson H, Johnell O, Jonsson B, Oden A, Zethraeus N, Pfleger B, Khaltaev N 2005 Assessment of fracture risk. Osteoporos Int **16**(6)**:**581-589.
31. McCloskey EV, Johansson H, Oden A, Kanis JA 2009 From relative risk to absolute fracture risk calculation: the FRAX algorithm. Current osteoporosis reports **7**(3)**:**77-83.
32. Siminoski K, Leslie WD, Frame H, Hodsman A, Josse RG, Khan A, Lentle BC, Levesque J, Lyons DJ, Tarulli G, Brown JP 2007 Recommendations for bone mineral density reporting in Canada: a shift to absolute fracture risk assessment. J Clin Densitom **10**(2)**:**120-123.
33. Leslie WD, Berger C, Langsetmo L, Lix LM, Adachi JD, Hanley DA, Ioannidis G, Josse RG, Kovacs CS, Towheed T, Kaiser S, Olszynski WP, Prior JC, Jamal S, Kreiger N, Goltzman D 2011 Construction and validation of a simplified fracture risk assessment tool for Canadian women and men: results from the CaMos and Manitoba cohorts. Osteoporos Int **22**(6)**:**1873-1883.
34. Richards JB, Leslie WD, Joseph L, Siminoski K, Hanley DA, Adachi JD, Brown JP, Morin S, Papaioannou A, Josse RG, Prior JC, Davison KS, Tenenhouse A, Goltzman D 2007 Changes to osteoporosis prevalence according to method of risk assessment. J Bone Miner Res **22**(2)**:**228-234.
35. Papaioannou A, Morin S, Cheung AM, Atkinson S, Brown JP, Feldman S, Hanley DA, Hodsman A, Jamal SA, Kaiser SM, Kvern B, Siminoski K, Leslie WD 2010 2010 clinical practice guidelines for the diagnosis and management of osteoporosis in Canada: summary. CMAJ **182**(17)**:**1864-1873.
36. Leslie WD, Lix LM, Langsetmo L, Berger C, Goltzman D, Hanley DA, Adachi JD, Johansson H, Oden A, McCloskey E, Kanis JA 2011 Construction of a FRAX(R) model for the assessment of fracture probability in Canada and implications for treatment. Osteoporos Int **22**(3)**:**817-827.
37. Kanis JA, Oden A, Johnell O, Johansson H, De Laet C, Brown J, Burckhardt P, Cooper C, Christiansen C, Cummings S, Eisman JA, Fujiwara S, Gluer C, Goltzman D, Hans D, Krieg MA, La Croix A, McCloskey E, Mellstrom D, Melton LJ, 3rd, Pols H, Reeve J, Sanders K, Schott AM, Silman A, Torgerson D, van Staa T, Watts NB, Yoshimura N 2007 The use of clinical risk factors

enhances the performance of BMD in the prediction of hip and osteoporotic fractures in men and women. Osteoporos Int **18**(8)**:**1033-1046.

38. Robey PG, Boskey AL, Asbmr 2009 Chapter 6. The Composition of Bone Primer on the Metabolic Bone Diseases and Disorders of Mineral Metabolism. John Wiley & Sons, Inc., pp 32-38.
39. Zhu W, Robey PG, Boskey AL 2007 The regulatory role of matrix proteins in mineralization of bone. In: Marcus R, Feldman D, Nelson DA, Rosen CJ (eds.) Osteoporosis 3rd Edition, vol. 1. Academic Press, San Diego, CA, USA, pp 191-240.
40. Lees S 2003 Mineralization of type I collagen. Biophysical journal **85**(1)**:**204-207.
41. Stoffel W, Jenke B, Block B, Zumbansen M, Koebke J 2005 Neutral sphingomyelinase 2 (smpd3) in the control of postnatal growth and development. Proceedings of the National Academy of Sciences of the United States of America **102**(12)**:**4554-4559.
42. Aubin I, Adams CP, Opsahl S, Septier D, Bishop CE, Auge N, Salvayre R, Negre-Salvayre A, Goldberg M, Guenet JL, Poirier C 2005 A deletion in the gene encoding sphingomyelin phosphodiesterase 3 (Smpd3) results in osteogenesis and dentinogenesis imperfecta in the mouse. Nature genetics **37**(8)**:**803-805.
43. Bonewald LF, Asbmr 2009 Chapter 4. Osteocytes Primer on the Metabolic Bone Diseases and Disorders of Mineral Metabolism. John Wiley & Sons, Inc., pp 22-27.
44. Feng JQ, Clinkenbeard EL, Yuan B, White KE, Drezner MK 2013 Osteocyte regulation of phosphate homeostasis and bone mineralization underlies the pathophysiology of the heritable disorders of rickets and osteomalacia. Bone **54**(2)**:**213-221.
45. Rhee Y, Bivi N, Farrow E, Lezcano V, Plotkin LI, White KE, Bellido T 2011 Parathyroid hormone receptor signaling in osteocytes increases the expression of fibroblast growth factor-23 in vitro and in vivo. Bone **49**(4)**:**636-643.
46. Ross FP, Asbmr 2009 Chapter 3. Osteoclast Biology and Bone Resorption Primer on the Metabolic Bone Diseases and Disorders of Mineral Metabolism. John Wiley & Sons, Inc., pp 16-22.
47. Krause C, de Gorter DJJ, Karperien M, ten Dijke P, Asbmr 2009 Chapter 2. Signal Transduction Cascades Controlling Osteoblast Differentiation Primer on the Metabolic Bone Diseases and Disorders of Mineral Metabolism. John Wiley & Sons, Inc., pp 10-16.
48. Hens JR, Wilson KM, Dann P, Chen X, Horowitz MC, Wysolmerski JJ 2005 TOPGAL mice show that the canonical Wnt signaling pathway is active during bone development and growth and is activated by mechanical loading in vitro. J Bone Miner Res **20**(7)**:**1103-1113.
49. Khosla S 2001 Minireview: the OPG/RANKL/RANK system. Endocrinology **142**(12)**:**5050-5055.
50. Hirao M, Hashimoto J, Yamasaki N, Ando W, Tsuboi H, Myoui A, Yoshikawa H 2007 Oxygen tension is an important mediator of the transformation of osteoblasts to osteocytes. Journal of bone and mineral metabolism **25**(5)**:**266-276.

51. Zahm AM, Bucaro MA, Srinivas V, Shapiro IM, Adams CS 2008 Oxygen tension regulates preosteocyte maturation and mineralization. Bone **43**(1)**:**25-31.
52. Frost HM 1963 Measurement of human bone formation by means of tetracycline labelling. Canadian journal of biochemistry and physiology **41:**31-42.
53. Hattner R, Epker BN, Frost HM 1965 Suggested sequential mode of control of changes in cell behaviour in adult bone remodelling. Nature **206**(983)**:**489-490.
54. Eriksen EF, Hodgson SF, Eastell R, Cedel SL, O'Fallon WM, Riggs BL 1990 Cancellous bone remodeling in type I (postmenopausal) osteoporosis: quantitative assessment of rates of formation, resorption, and bone loss at tissue and cellular levels. J Bone Miner Res **5**(4)**:**311-319.
55. Karsdal MA, Martin TJ, Bollerslev J, Christiansen C, Henriksen K 2007 Are nonresorbing osteoclasts sources of bone anabolic activity? J Bone Miner Res **22**(4)**:**487-494.
56. Dai XM, Zong XH, Akhter MP, Stanley ER 2004 Osteoclast deficiency results in disorganized matrix, reduced mineralization, and abnormal osteoblast behavior in developing bone. J Bone Miner Res **19**(9)**:**1441-1451.
57. Zhao C, Irie N, Takada Y, Shimoda K, Miyamoto T, Nishiwaki T, Suda T, Matsuo K 2006 Bidirectional ephrinB2-EphB4 signaling controls bone homeostasis. Cell metabolism **4**(2)**:**111-121.
58. Ryu J, Kim HJ, Chang EJ, Huang H, Banno Y, Kim HH 2006 Sphingosine 1-phosphate as a regulator of osteoclast differentiation and osteoclast-osteoblast coupling. The EMBO journal **25**(24)**:**5840-5851.
59. Eriksen EF 2010 Cellular mechanisms of bone remodeling. Reviews in endocrine & metabolic disorders **11**(4)**:**219-227.
60. Kaigler D, Krebsbach PH, Polverini PJ, Mooney DJ 2003 Role of vascular endothelial growth factor in bone marrow stromal cell modulation of endothelial cells. Tissue engineering **9**(1)**:**95-103.
61. Downey PA, Siegel MI 2006 Bone biology and the clinical implications for osteoporosis. Physical therapy **86**(1)**:**77-91.
62. Buckwalter JA, Glimcher MJ, Cooper RR, Recker R 1996 Bone biology. I: Structure, blood supply, cells, matrix, and mineralization. Instructional course lectures **45:**371-386.
63. Barak MM, Lieberman DE, Hublin JJ 2011 A Wolff in sheep's clothing: trabecular bone adaptation in response to changes in joint loading orientation. Bone **49**(6)**:**1141-1151.
64. Dalle Carbonare L, Giannini S 2004 Bone microarchitecture as an important determinant of bone strength. Journal of endocrinological investigation **27**(1)**:**99-105.
65. Frost HM 2004 A 2003 update of bone physiology and Wolff's Law for clinicians. The Angle orthodontist **74**(1)**:**3-15.
66. Bikle DD, Sakata T, Halloran BP 2003 The impact of skeletal unloading on bone formation. Gravit Space Biol Bull **16**(2)**:**45-54.
67. Carmeliet G, Vico L, Bouillon R 2001 Space flight: a challenge for normal bone homeostasis. Critical reviews in eukaryotic gene expression **11**(1-3)**:**131-144.

68. Alexandre C, Vico L 2011 Pathophysiology of bone loss in disuse osteoporosis. Joint Bone Spine **78**(6)**:**572-576.
69. Rittweger J, Gerrits K, Altenburg T, Reeves N, Maganaris CN, de Haan A 2006 Bone adaptation to altered loading after spinal cord injury: a study of bone and muscle strength. Journal of musculoskeletal & neuronal interactions **6**(3)**:**269-276.
70. Park SH, Silva M 2004 Neuromuscular electrical stimulation enhances fracture healing: results of an animal model. J Orthop Res **22**(2)**:**382-387.
71. Zerath E, Canon F, Guezennec CY, Holy X, Renault S, Andre C 1995 Electrical stimulation of leg muscles increases tibial trabecular bone formation in unloaded rats. J Appl Physiol **79**(6)**:**1889-1894.
72. Vico L, Alexandre C 1992 Microgravity and bone adaptation at the tissue level. J Bone Miner Res **7 Suppl 2:**S445-447.
73. Duncan RL, Hruska KA 1994 Chronic, intermittent loading alters mechanosensitive channel characteristics in osteoblast-like cells. The American journal of physiology **267**(6 Pt 2)**:**F909-916.
74. Rubinacci A, Benelli FD, Borgo E, Villa I 2000 Bone as an ion exchange system: evidence for a pump-leak mechanism devoted to the maintenance of high bone K(+). American journal of physiology Endocrinology and metabolism **278**(1)**:**E15-24.
75. Isaacson BM, Bloebaum RD 2010 Bone bioelectricity: what have we learned in the past 160 years? Journal of biomedical materials research Part A **95**(4)**:**1270-1279.
76. Hughes JM, Petit MA 2010 Biological underpinnings of Frost's mechanostat thresholds: the important role of osteocytes. Journal of musculoskeletal & neuronal interactions **10**(2)**:**128-135.
77. Siris ES, Miller PD, Barrett-Connor E, Faulkner KG, Wehren LE, Abbott TA, Berger ML, Santora AC, Sherwood LM 2001 Identification and fracture outcomes of undiagnosed low bone mineral density in postmenopausal women: results from the National Osteoporosis Risk Assessment. Jama **286**(22)**:**2815-2822.
78. 1994 Assessment of fracture risk and its application to screening for postmenopausal osteoporosis. Report of a WHO Study Group. World Health Organization technical report series **843:**1-129.
79. Bolotin HH 2004 The significant effects of bone structure on inherent patient-specific DXA in vivo bone mineral density measurement inaccuracies. Medical physics **31**(4)**:**774-788.
80. Bolotin HH 2007 DXA in vivo BMD methodology: an erroneous and misleading research and clinical gauge of bone mineral status, bone fragility, and bone remodelling. Bone **41**(1)**:**138-154.
81. Iki M, Tamaki J, Kadowaki E, Sato Y, Dongmei N, Winzenrieth R, Kagamimori S, Kagawa Y, Yoneshima H 2013 Trabecular bone score (TBS) predicts vertebral fractures in Japanese women over 10 years independently of bone density and prevalent vertebral deformity: The Japanese population-based osteoporosis (JPOS) cohort study. J Bone Miner Res.

82. Krueger D, Fidler E, Libber J, Aubry-Rozier B, Hans D, Binkley N 2013 Spine Trabecular Bone Score Subsequent to Bone Mineral Density Improves Fracture Discrimination in Women. J Clin Densitom.
83. Jee WS 2005 The past, present, and future of bone morphometry: its contribution to an improved understanding of bone biology. Journal of bone and mineral metabolism **23 Suppl:**1-10.
84. Parfitt AM, Drezner MK, Glorieux FH, Kanis JA, Malluche H, Meunier PJ, Ott SM, Recker RR 1987 Bone histomorphometry: standardization of nomenclature, symbols, and units. Report of the ASBMR Histomorphometry Nomenclature Committee. J Bone Miner Res **2**(6)**:**595-610.
85. Weinstein RS, Majumdar S 1994 Fractal geometry and vertebral compression fractures. J Bone Miner Res **9**(11)**:**1797-1802.
86. van Gaalen SM, Kruyt MC, Geuze RE, de Bruijn JD, Alblas J, Dhert WJ 2010 Use of fluorochrome labels in in vivo bone tissue engineering research. Tissue engineering Part B, Reviews **16**(2)**:**209-217.
87. Recker RR, Kimmel DB, Dempster D, Weinstein RS, Wronski TJ, Burr DB 2011 Issues in modern bone histomorphometry. Bone **49**(5)**:**955-964.
88. Christiansen BA, Bouxsein ML, Asbmr 2009 Chapter 7. Assessment of Bone Mass and Microarchitecture in Rodents Primer on the Metabolic Bone Diseases and Disorders of Mineral Metabolism. John Wiley & Sons, Inc., pp 38-45.
89. Boyd SK, Moser S, Kuhn M, Klinck RJ, Krauze PL, Muller R, Gasser JA 2006 Evaluation of three-dimensional image registration methodologies for in vivo micro-computed tomography. Annals of biomedical engineering **34**(10)**:**1587-1599.
90. Aichinger H 2012 Production and Measurement of X-Rays. In: Dierker J, Joite-Barfuß S, Säbel M (eds.) Radiation Exposure and Image Quality in X-Ray Diagnostic Radiology Physical Principles and Clinical Applications, Second Edition. ed. Berlin, Heidelberg, Springer Berlin Heidelberg :, pp 13-14.
91. Jiang Y, Zhao JJ, Mitlak BH, Wang O, Genant HK, Eriksen EF 2003 Recombinant human parathyroid hormone (1-34) [teriparatide] improves both cortical and cancellous bone structure. J Bone Miner Res **18**(11)**:**1932-1941.
92. Dempster DW, Cosman F, Kurland ES, Zhou H, Nieves J, Woelfert L, Shane E, Plavetic K, Muller R, Bilezikian J, Lindsay R 2001 Effects of daily treatment with parathyroid hormone on bone microarchitecture and turnover in patients with osteoporosis: a paired biopsy study. J Bone Miner Res **16**(10)**:**1846-1853.
93. Bouxsein ML, Seeman E 2009 Quantifying the material and structural determinants of bone strength. Best practice & research Clinical rheumatology **23**(6)**:**741-753.
94. Ferretti JL 1999 Peripheral quantitative computed tomography (pQCT) for evaluating structural and mechanical properties of small bone. In: An YH, Draughn RA (eds.) Practical guide for mechanical testing of bone. CRC Press, Boca Raton, FL.

95. Morgan EF, Barnes GL, Einhorn TA 2010 The Bone Organ System: Form and Function. In: Marcus R, Feldman D, Nelson DA, Rosen CJ (eds.) Fundamentals of Osteoporosis. Elsevier Inc., San Diego, CA, pp 8.
96. Commission CNS 2012 Introduction to Radiation. Minister of Public Works and Government Services Canada, CNSC, Ottawa, Ontario.
97. AG SM 2005 XtremeCT User's Guide, Bruettisellen, Switzerland, pp 117.
98. Boutroy S, Bouxsein ML, Munoz F, Delmas PD 2005 In vivo assessment of trabecular bone microarchitecture by high-resolution peripheral quantitative computed tomography. J Clin Endocrinol Metab **90**(12)**:**6508-6515.
99. Weishaupt D 2006 How Does MRI Work? An Introduction to the Physics and Function of Magnetic Resonance Imaging. In: Köchli VD, Marincek B (eds.), Second Edition. ed. Berlin, Heidelberg, Springer-Verlag Berlin Heidelberg.
100. Gore J, Kennan R 1999 Physical principles and physiological basis of magnetic relaxation. In: Stark D, Bradley WJ (eds.) Magnetic resonance imaging, 3rd ed, vol. Book no.33. Mosby-Year, Mosby, St. Louis.
101. Duerk J 1997 Relaxation and contrast in MR imaging. In: Riederer S, Wood M (eds.) Categorical course in physics: the basic physics of MR imaging, vol. Book no.19. RSNA Publications, Oakbrook, IL, USA.
102. Wehrli FW 1997 Spatial encoding and k-space. In: Riederer S, Wood M (eds.) Categorical course in physics: The basic physics of MR imaging, vol. Book no.31. RSNA Publications, Oakbrook, IL, USA.
103. Wehrli FW, Song HK, Saha PK, Wright AC 2006 Quantitative MRI for the assessment of bone structure and function. NMR in biomedicine **19**(7)**:**731-764.
104. Wehrli FW 2007 Structural and functional assessment of trabecular and cortical bone by micro magnetic resonance imaging. JMagn ResonImaging **25**(2)**:**390-409.
105. Haacke EM, Frahm J 1991 A guide to understanding key aspects of fast gradient-echo imaging. Journal of magnetic resonance imaging : JMRI **1**(6)**:**621-624.
106. Elster AD 1993 Gradient-echo MR imaging: techniques and acronyms. Radiology **186**(1)**:**1-8.
107. Ernst R, Anderson W 1966 Application of Fourier transform to magnetic resonance spectroscopy. Rev Sci Instrum **37:**93-98.
108. Damilakis J, Maris T, Papadokostakis G, Sideri L, Gourtsoyiannis N 2004 Discriminatory ability of magnetic resonance T2* measurements in a sample of postmenopausal women with low-energy fractures: a comparison with phalangeal speed of sound and dual x-ray absorptiometry. Investigative radiology **39**(11)**:**706-712.
109. Link TM, Majumdar S, Augat P, Lin JC, Newitt D, Lane NE, Genant HK 1998 Proximal femur: assessment for osteoporosis with T2* decay characteristics at MR imaging. Radiology **209**(2)**:**531-536.
110. Yoshioka H, Schlechtweg P, Kose K 2009 Chapter 3 – Magnetic Resonance Imaging. In: Weissman B, Caroll C (eds.) Imaging of Arthritis and Metabolic Bone Disease. Elsevier, Philadelphia, PA.

111. Chung M, Dahabreh IJ, Hadar N, Ratichek SJ, Gaylor JM, Trikalinos TA, Lau J 2011 Emerging MRI Technologies for Imaging Musculoskeletal Disorders Under Loading Stress, Rockville (MD).
112. Pritchard JM, Giangregorio LM, Atkinson SA, Beattie KA, Inglis D, Ioannidis G, Punthakee Z, Adachi JD, Papaioannou A 2012 Association of larger holes in the trabecular bone at the distal radius in postmenopausal women with type 2 diabetes mellitus compared to controls. Arthritis care & research **64**(1)**:**83-91.
113. Pal N, Pal S 1993 A review on image segmentation techniques. Pattern Recog **26:**1277-1294.
114. Sharma N, Aggarwal LM 2010 Automated medical image segmentation techniques. Journal of medical physics / Association of Medical Physicists of India **35**(1)**:**3-14.
115. Pham DL, Xu C, Prince JL 2000 Current methods in medical image segmentation. Annual review of biomedical engineering **2:**315-337.
116. Folkesson J, Carballido-Gamio J, Eckstein F, Link TM, Majumdar S 2010 Local bone enhancement fuzzy clustering for segmentation of MR trabecular bone images. Medical physics **37**(1)**:**295-302.
117. Falcao AX, Stolfi J, de Alencar Lotufo R 2004 The image foresting transform: theory, algorithms, and applications. IEEE transactions on pattern analysis and machine intelligence **26**(1)**:**19-29.
118. Parfitt AM, Mathews CH, Villanueva AR, Kleerekoper M, Frame B, Rao DS 1983 Relationships between surface, volume, and thickness of iliac trabecular bone in aging and in osteoporosis. Implications for the microanatomic and cellular mechanisms of bone loss. The Journal of clinical investigation **72**(4)**:**1396-1409.
119. MacIntyre NJ, Adachi JD, Webber CE 1999 Gender differences in normal age-dependent patterns of radial bone structure and density: a cross-sectional study using peripheral quantitative computed tomography. J Clin Densitom **2**(2)**:**163-173.
120. Kaptoge S, Dalzell N, Loveridge N, Beck TJ, Khaw KT, Reeve J 2003 Effects of gender, anthropometric variables, and aging on the evolution of hip strength in men and women aged over 65. Bone **32**(5)**:**561-570.
121. Boutroy S, Van Rietbergen B, Sornay-Rendu E, Munoz F, Bouxsein ML, Delmas PD 2008 Finite element analysis based on in vivo HR-pQCT images of the distal radius is associated with wrist fracture in postmenopausal women. J Bone Miner Res **23**(3)**:**392-399.
122. Sheu Y, Zmuda JM, Boudreau RM, Petit MA, Ensrud KE, Bauer DC, Gordon CL, Orwoll ES, Cauley JA 2011 Bone strength measured by peripheral quantitative computed tomography and the risk of nonvertebral fractures: the osteoporotic fractures in men (MrOS) study. J Bone Miner Res **26**(1)**:**63-71.
123. Hulley SB, Martin JN, Cummings SR 2007 Planning the Measurements: Precision and Accuracy. In: Hulley SB, Cummings SR, Browner WS, Grady DG, Newman TB (eds.) Designing Clinical Research, vol. 3rd Edition. Lippincott Williams & Wilkins, Philadelphia, PA, pp 37-47.

124. Pardue HL 1997 The inseparable triad: analytical sensitivity, measurement uncertainty, and quantitative resolution. Clinical chemistry **43**(10)**:**1831-1837.
125. Engelke K, Adams JE, Armbrecht G, Augat P, Bogado CE, Bouxsein ML, Felsenberg D, Ito M, Prevrhal S, Hans DB, Lewiecki EM 2008 Clinical use of quantitative computed tomography and peripheral quantitative computed tomography in the management of osteoporosis in adults: the 2007 ISCD Official Positions. J Clin Densitom **11**(1)**:**123-162.
126. Zemel B, Bass S, Binkley T, Ducher G, Macdonald H, McKay H, Moyer-Mileur L, Shepherd J, Specker B, Ward K, Hans D 2008 Peripheral quantitative computed tomography in children and adolescents: the 2007 ISCD Pediatric Official Positions. J Clin Densitom **11**(1)**:**59-74.
127. MacNeil JA, Boyd SK 2007 Accuracy of high-resolution peripheral quantitative computed tomography for measurement of bone quality. Medical engineering & physics **29**(10)**:**1096-1105.
128. Ashe MC, Khan KM, Kontulainen SA, Guy P, Liu D, Beck TJ, McKay HA 2006 Accuracy of pQCT for evaluating the aged human radius: an ashing, histomorphometry and failure load investigation. Osteoporos Int **17**(8)**:**1241-1251.
129. Laib A, Ruegsegger P 1999 Calibration of trabecular bone structure measurements of in vivo three-dimensional peripheral quantitative computed tomography with 28-microm-resolution microcomputed tomography. Bone **24**(1)**:**35-39.
130. Liu XS, Zhang XH, Rajapakse CS, Wald MJ, Magland J, Sekhon KK, Adam MF, Sajda P, Wehrli FW, Guo XE 2010 Accuracy of high-resolution in vivo micro magnetic resonance imaging for measurements of microstructural and mechanical properties of human distal tibial bone. J Bone Miner Res **25**(9)**:**2039-2050.
131. Kazakia GJ, Hyun B, Burghardt AJ, Krug R, Newitt DC, de Papp AE, Link TM, Majumdar S 2008 In vivo determination of bone structure in postmenopausal women: a comparison of HR-pQCT and high-field MR imaging. JBone MinerRes **23**(4)**:**463-474.
132. Krug R, Carballido-Gamio J, Burghardt AJ, Kazakia G, Hyun BH, Jobke B, Banerjee S, Huber M, Link TM, Majumdar S 2008 Assessment of trabecular bone structure comparing magnetic resonance imaging at 3 Tesla with high-resolution peripheral quantitative computed tomography ex vivo and in vivo. OsteoporosInt **19**(5)**:**653-661.
133. Swinford RR, Warden SJ 2010 Factors affecting short-term precision of musculoskeletal measures using peripheral quantitative computed tomography (pQCT). Osteoporos Int **21**(11)**:**1863-1870.
134. Sievanen H, Koskue V, Rauhio A, Kannus P, Heinonen A, Vuori I 1998 Peripheral quantitative computed tomography in human long bones: evaluation of in vitro and in vivo precision. J Bone Miner Res **13**(5)**:**871-882.
135. Guglielmi G, De Serio A, Fusilli S, Scillitani A, Chiodini I, Torlontano M, Cammisa M 2000 Age-related changes assessed by peripheral QCT in healthy Italian women. European radiology **10**(4)**:**609-614.
136. Ouyang X, Selby K, Lang P, Engelke K, Klifa C, Fan B, Zucconi F, Hottya G, Chen M, Majumdar S, Genant HK 1997 High resolution magnetic resonance

imaging of the calcaneus: age-related changes in trabecular structure and comparison with dual X-ray absorptiometry measurements. Calcif Tissue Int **60**(2)**:**139-147.

137. Blumenfeld J, Carballido-Gamio J, Krug R, Blezek DJ, Hancu I, Majumdar S 2007 Automatic prospective registration of high-resolution trabecular bone images of the tibia. Annals of biomedical engineering **35**(11)**:**1924-1931.
138. Burghardt AJ, Pialat JB, Kazakia GJ, Boutroy S, Engelke K, Patsch JM, Valentinitsch A, Liu D, Szabo E, Bogado CE, Zanchetta MB, McKay HA, Shane E, Boyd SK, Bouxsein ML, Chapurlat R, Khosla S, Majumdar S 2012 Multi-center precision of cortical and trabecular bone quality measures assessed by HR-PQCT. J Bone Miner Res.
139. Laib A, Newitt DC, Lu Y, Majumdar S 2002 New model-independent measures of trabecular bone structure applied to in vivo high-resolution MR images. Osteoporos Int **13**(2)**:**130-136.
140. Melton LJ, 3rd, Riggs BL, Keaveny TM, Achenbach SJ, Hoffmann PF, Camp JJ, Rouleau PA, Bouxsein ML, Amin S, Atkinson EJ, Robb RA, Khosla S 2007 Structural determinants of vertebral fracture risk. J Bone Miner Res **22**(12)**:**1885-1892.
141. MacIntyre NJ, Adachi JD, Webber CE 2003 In vivo measurement of apparent trabecular bone structure of the radius in women with low bone density discriminates patients with recent wrist fracture from those without fracture. JClinDensitom **6**(1)**:**35-43.
142. Boutry N, Cortet B, Dubois P, Marchandise X, Cotten A 2003 Trabecular bone structure of the calcaneus: preliminary in vivo MR imaging assessment in men with osteoporosis. Radiology **227**(3)**:**708-717.
143. Baim S, Wilson CR, Lewiecki EM, Luckey MM, Downs RW, Jr., Lentle BC 2005 Precision assessment and radiation safety for dual-energy X-ray absorptiometry: position paper of the International Society for Clinical Densitometry. J Clin Densitom **8**(4)**:**371-378.
144. Riggs BL, Melton Iii LJ, 3rd, Robb RA, Camp JJ, Atkinson EJ, Peterson JM, Rouleau PA, McCollough CH, Bouxsein ML, Khosla S 2004 Population-based study of age and sex differences in bone volumetric density, size, geometry, and structure at different skeletal sites. J Bone Miner Res **19**(12)**:**1945-1954.
145. Kreiger N, Tenenhouse A, Joseph L, MacKenzie T, Poliquin S, Brown JP, Prior JC, Rittmaster RS 1999 Research notes: The Canadian Multicentre Osteoporosis Study (CaMos) - background, rationale, methods. Can J Aging **18**(3)**:**12.
146. Ashe MC, Liu-Ambrose T, Khan KM, White N, McKay HA 2005 Optimizing results from pQCT: reliability of operator-dependent pQCT variables in cadavers and humans with low bone mass. J Clin Densitom **8**(3)**:**335-340.
147. MacIntyre NJ, Adachi JD, Webber CE 1999 In vivo detection of structural differences between dominant and nondominant radii using peripheral quantitative computed tomography. J Clin Densitom **2**(4)**:**413-422.
148. MacIntyre NJ, Inglis D, Adachi JD, Webber CE 2005 Is there a relationship between apparent trabecular bone structure as measured by peripheral quantitative

computed tomography and disease severity in patients recently diagnosed with rheumatoid arthritis? Clin Exp Rheumatol **23**(Suppl 6)**:**745.

149. Boyd SK 2009 Micro-computed tomography. Reconstructions and Caveats. In: Sensen CW, Hallgrimsson B (eds.) Advanced Imaging in Biology and Medicine: Technology, Software Environments, Applications. Springer-Verlag, Heidelberg, Berlin.
150. Buie HR, Campbell GM, Klinck RJ, MacNeil JA, Boyd SK 2007 Automatic segmentation of cortical and trabecular compartments based on a dual threshold technique for in vivo micro-CT bone analysis. Bone **41**(4)**:**505-515.
151. Laib A, Hauselmann HJ, Ruegsegger P 1998 In vivo high resolution 3D-QCT of the human forearm. Technol Health Care **6**(5-6)**:**329-337.
152. Augat P, Gordon CL, Lang TF, Iida H, Genant HK 1998 Accuracy of cortical and trabecular bone measurements with peripheral quantitative computed tomography (pQCT). Phys Med Biol **43**(10)**:**2873-2883.
153. Stratec 2004 XCT Research Series Manual Software, vol. Version 5.50.
154. Gordon CL, Webber CE, Adachi JD, Christoforou N 1996 In vivo assessment of trabecular bone structure at the distal radius from high-resolution computed tomography images. Phys Med Biol **41**(3)**:**495-508.
155. Zhang T, Suen C 1984 A fast parallel algorithm for thinning digital patterns. Commun Assoc Comput Mach **27:**236-239.
156. Compston JE, Garrahan NJ, Croucher PI, Wright CD, Yamaguchi K 1993 Quantitative analysis of trabecular bone structure. Bone **14**(3)**:**187-192.
157. Smith JM, Jee WS 1983 Automated skeletal histomorphometry. In: Recker R (ed.) Bone Histomorphometry Techniques and Interpretations. CRC Press, Boca Raton, FL.
158. Whitehouse WJ 1974 The quantitative morphology of anisotropic trabecular bone. Journal of microscopy **101**(Pt 2)**:**153-168.
159. Falcao AX, Bergo FP 2004 Interactive volume segmentation with differential image foresting transforms. IEEE transactions on medical imaging **23**(9)**:**1100-1108.
160. Cejka D, Patsch JM, Weber M, Diarra D, Riegersperger M, Kikic Z, Krestan C, Schueller-Weidekamm C, Kainberger F, Haas M 2011 Bone microarchitecture in hemodialysis patients assessed by HR-pQCT. Clin J Am Soc Nephrol **6**(9)**:**2264-2271.
161. Burghardt AJ, Buie HR, Laib A, Majumdar S, Boyd SK 2010 Reproducibility of direct quantitative measures of cortical bone microarchitecture of the distal radius and tibia by HR-pQCT. Bone **47**(3)**:**519-528.
162. Pauchard Y, Liphardt AM, Macdonald HM, Hanley DA, Boyd SK 2012 Quality control for bone quality parameters affected by subject motion in high-resolution peripheral quantitative computed tomography. Bone **50**(6)**:**1304-1310.
163. Pauchard Y, Ayres FJ, Boyd SK 2011 Automated quantification of three-dimensional subject motion to monitor image quality in high-resolution peripheral quantitative computed tomography. Phys Med Biol **56**(20)**:**6523-6543.

164. Bhagat YA, Rajapakse CS, Magland JF, Wald MJ, Song HK, Leonard MB, Wehrli FW 2011 On the significance of motion degradation in high-resolution 3D muMRI of trabecular bone. Academic radiology **18**(10)**:**1205-1216.
165. MacNeil JA, Boyd SK 2008 Improved reproducibility of high-resolution peripheral quantitative computed tomography for measurement of bone quality. Medical engineering & physics **30**(6)**:**792-799.
166. Burghardt AJ, Kazakia GJ, Sode M, de Papp AE, Link TM, Majumdar S 2010 A longitudinal HR-pQCT study of alendronate treatment in postmenopausal women with low bone density: Relations among density, cortical and trabecular microarchitecture, biomechanics, and bone turnover. J Bone Miner Res **25**(12)**:**2558-2571.
167. Boyd SK 2008 Site-specific variation of bone micro-architecture in the distal radius and tibia. J Clin Densitom **11**(3)**:**424-430.
168. Rauch F, Tutlewski B, Schoenau E 2001 Peripheral quantitative computed tomography at the distal radius: cross-calibration between two scanners. Journal of musculoskeletal & neuronal interactions **2**(2)**:**153-155.
169. Kontulainen S, Liu D, Manske S, Jamieson M, Sievanen H, McKay H 2007 Analyzing cortical bone cross-sectional geometry by peripheral QCT: comparison with bone histomorphometry. J Clin Densitom **10**(1)**:**86-92.
170. Sun L, Beller G, Felsenberg D 2009 Quantification of bone mineral density precision according to repositioning errors in peripheral quantitative computed tomography (pQCT) at the radius and tibia. Journal of musculoskeletal & neuronal interactions **9**(1)**:**18-24.
171. Pearson J, Ruegsegger P, Dequeker J, Henley M, Bright J, Reeve J, Kalender W, Felsenberg D, Laval-Jeantet AM, Adams JE, et al. 1994 European semi-anthropomorphic phantom for the cross-calibration of peripheral bone densitometers: assessment of precision accuracy and stability. Bone and mineral **27**(2)**:**109-120.
172. Emaus N, Berntsen GK, Joakimsen R, Fonnebo V 2005 Bone mineral density measures in longitudinal studies: the choice of phantom is crucial for quality assessment. The Tromso study, a population-based study. Osteoporos Int **16**(12)**:**1597-1603.
173. Shepherd JA, Lu Y, Wilson K, Fuerst T, Genant H, Hangartner TN, Wilson C, Hans D, Leib ES 2006 Cross-calibration and minimum precision standards for dual-energy X-ray absorptiometry: the 2005 ISCD Official Positions. J Clin Densitom **9**(1)**:**31-36.
174. Makan S, Bayley HS, Webber CE 1997 Precision and accuracy of total body bone mass and body composition measurements in the rat using x-ray-based dual photon absorptiometry. Canadian journal of physiology and pharmacology **75**(10-11)**:**1257-1261.
175. Doros G, Lew R 2010 Design Based on Intra-Class Correlation Coefficients. Am J Biostat **1**(1)**:**1-8.
176. Krug R, Carballido-Gamio J, Burghardt AJ, Kazakia G, Hyun BH, Jobke B, Banerjee S, Huber M, Link TM, Majumdar S 2008 Assessment of trabecular bone

structure comparing magnetic resonance imaging at 3 Tesla with high-resolution peripheral quantitative computed tomography ex vivo and in vivo. Osteoporos Int **19**(5)**:**653-661.

177. Gluer CC, Blake G, Lu Y, Blunt BA, Jergas M, Genant HK 1995 Accurate assessment of precision errors: how to measure the reproducibility of bone densitometry techniques. Osteoporos Int **5**(4)**:**262-270.
178. Bonnick SL, Johnston CC, Jr., Kleerekoper M, Lindsay R, Miller P, Sherwood L, Siris E 2001 Importance of precision in bone density measurements. J Clin Densitom **4**(2)**:**105-110.
179. Bonnick SL, Lewis LA 2013 Bone Densitometry for Technologists. Springer.
180. Sornay-Rendu E, Cabrera-Bravo JL, Boutroy S, Munoz F, Delmas PD 2009 Severity of vertebral fractures is associated with alterations of cortical architecture in postmenopausal women. J Bone Miner Res **24**(4)**:**737-743.
181. Syddall HE, Evandrou M, Dennison EM, Cooper C, Sayer AA 2012 Social inequalities in osteoporosis and fracture among community-dwelling older men and women: findings from the Hertfordshire Cohort Study. Archives of osteoporosis **7**(1-2)**:**37-48.
182. Berger C, Langsetmo L, Joseph L, Hanley DA, Davison KS, Josse R, Kreiger N, Tenenhouse A, Goltzman D 2008 Change in bone mineral density as a function of age in women and men and association with the use of antiresorptive agents. Cmaj **178**(13)**:**1660-1668.
183. Sode M, Burghardt AJ, Kazakia GJ, Link TM, Majumdar S 2010 Regional variations of gender-specific and age-related differences in trabecular bone structure of the distal radius and tibia. Bone **46**(6)**:**1652-1660.
184. Kalisch T, Kattenstroth JC, Kowalewski R, Tegenthoff M, Dinse HR 2012 Age-related changes in the joint position sense of the human hand. Clinical interventions in aging **7:**499-507.
185. Swinford RR, Warden SJ Factors affecting short-term precision of musculoskeletal measures using peripheral quantitative computed tomography (pQCT). Osteoporos Int.
186. Busse ME, Tyson SF 2007 Functional balance and mobility tests in healthy participants: reliability, error and influencing factors. Physiother Res Int **12**(4)**:**242-250.
187. Kmetic A, Joseph L, Berger C, Tenenhouse A 2002 Multiple imputation to account for missing data in a survey: estimating the prevalence of osteoporosis. Epidemiology **13**(4)**:**437-444.
188. Saskatchewan Go 2013 Bone Mineral Densitometry (BMD) Wait Times Saskatchewan Diagnostic Imaging, vol. 2013.
189. Olive J, d'Anjou MA, Alexander K, Beauchamp G, Theoret CL 2010 Correlation of signal attenuation-based quantitative magnetic resonance imaging with quantitative computed tomographic measurements of subchondral bone mineral density in metacarpophalangeal joints of horses. American journal of veterinary research **71**(4)**:**412-420.

190. Arokoski MH, Arokoski JP, Vainio P, Niemitukia LH, Kroger H, Jurvelin JS 2002 Comparison of DXA and MRI methods for interpreting femoral neck bone mineral density. J Clin Densitom **5**(3)**:**289-296.
191. Graeff C, Marin F, Petto H, Kayser O, Reisinger A, Pena J, Zysset P, Gluer CC 2013 High resolution quantitative computed tomography-based assessment of trabecular microstructure and strength estimates by finite-element analysis of the spine, but not DXA, reflects vertebral fracture status in men with glucocorticoid-induced osteoporosis. Bone **52**(2)**:**568-577.
192. Epstein S, Inzerillo AM, Caminis J, Zaidi M 2003 Disorders associated with acute rapid and severe bone loss. J Bone Miner Res **18**(12)**:**2083-2094.
193. Stemler SS, Tsai J 2008 Best practices in interrater reliability. In: Osborne J (ed.) Best practices in quantitative methods. Sage Publications Inc., Thousand Oaks, CA, pp 38-39.
194. Bland JM, Altman DG 1990 A note on the use of the intraclass correlation coefficient in the evaluation of agreement between two methods of measurement. Computers in biology and medicine **20**(5)**:**337-340.
195. Symons MJ, Moore DT 2002 Hazard rate ratio and prospective epidemiological studies. Journal of clinical epidemiology **55**(9)**:**893-899.
196. Sornay-Rendu E, Boutroy S, Munoz F, Delmas PD 2007 Alterations of cortical and trabecular architecture are associated with fractures in postmenopausal women, partially independent of decreased BMD measured by DXA: the OFELY study. J Bone Miner Res **22**(3)**:**425-433.
197. Vico L, Zouch M, Amirouche A, Frere D, Laroche N, Koller B, Laib A, Thomas T, Alexandre C 2008 High-resolution pQCT analysis at the distal radius and tibia discriminates patients with recent wrist and femoral neck fractures. J Bone Miner Res **23**(11)**:**1741-1750.
198. Nishiyama KK, Macdonald HM, Buie HR, Hanley DA, Boyd SK Postmenopausal women with osteopenia have higher cortical porosity and thinner cortices at the distal radius and tibia than women with normal aBMD: an in vivo HR-pQCT study. J Bone Miner Res **25**(4)**:**882-890.
199. Mueller TL, Christen D, Sandercott S, Boyd SK, van Rietbergen B, Eckstein F, Lochmuller EM, Muller R, van Lenthe GH 2011 Computational finite element bone mechanics accurately predicts mechanical competence in the human radius of an elderly population. Bone **48**(6)**:**1232-1238.
200. Sforza NM, Franchini F, Lamma A, Botticelli S, Ghigi G 2007 Accuracy of computerized tomography for the evaluation of mandibular sites prior to implant placement. The International journal of periodontics & restorative dentistry **27**(6)**:**589-595.
201. Hayashi D, Guermazi A, Kwoh CK, Hannon MJ, Moore C, Jakicic JM, Green SM, Roemer FW 2011 Semiquantitative assessment of subchondral bone marrow edema-like lesions and subchondral cysts of the knee at 3T MRI: a comparison between intermediate-weighted fat-suppressed spin echo and Dual Echo Steady State sequences. BMC musculoskeletal disorders **12:**198.

202. Haft GE, Buckwalter JA 2003 Aneurysmal bone cyst following tibial fracture: a case report. The Iowa orthopaedic journal **23:**100-102.
203. Pecht S, Raschka C 2006 [A 15-year-old boy with spontaneous pain in the lower leg]. MMW Fortschritte der Medizin **148**(15)**:**46, 48.
204. Shiels WE, 2nd, Mayerson JL 2013 Percutaneous doxycycline treatment of aneurysmal bone cysts with low recurrence rate: a preliminary report. Clinical orthopaedics and related research **471**(8)**:**2675-2683.
205. Sturz H, Witt AN 1979 [Solitary bone cysts of the ulna (author's transl)]. Archives of orthopaedic and trauma surgery **94**(2)**:**105-108.
206. Pireau N, De Gheldere A, Mainard-Simard L, Lascombes P, Docquier PL 2011 Fracture risk in unicameral bone cyst. Is magnetic resonance imaging a better predictor than plain radiography? Acta orthopaedica Belgica **77**(2)**:**230-238.
207. Buie HR, Bosma NA, Downey CM, Jirik FR, Boyd SK 2013 Micro-CT evaluation of bone defects: Applications to osteolytic bone metastases, bone cysts, and fracture. Medical engineering & physics.
208. Canada H 2008 Radiation Doses Health Concerns, vol. 2013. Goverment of Canada.
209. Beaupied H, Chappard C, Basillais A, Lespessailles E, Benhamou CL 2006 Effect of specimen conditioning on the microarchitectural parameters of trabecular bone assessed by micro-computed tomography. Phys Med Biol **51**(18)**:**4621-4634.
210. Hangartner TN, Short DF 2007 Accurate quantification of width and density of bone structures by computed tomography. Medical physics **34**(10)**:**3777-3784.
211. Nobuyuki O 1979 A threshold selection method from gray-level histograms. IEEE Trans Sys Man Cyber **13**(1)**:**146-165.
212. Li X, Messe A, Marrelec G, Pelegrini-Issac M, Benali H 2010 An enhanced voxel-based morphometry method to investigate structural changes: application to Alzheimer's disease. Neuroradiology **52**(3)**:**203-213.
213. Suzuki CT, Gomes JF, Falcao AX, Papa JP, Hoshino-Shimizu S 2013 Automatic segmentation and classification of human intestinal parasites from microscopy images. IEEE transactions on bio-medical engineering **60**(3)**:**803-812.
214. Engelke K, Hahn M, Takada M, Vogel M, Ouyang X, Delling G, Genant HK 2001 Structural analysis of high resolution in vitro MR images compared to stained grindings. Calcif Tissue Int **68**(3)**:**163-171.
215. Rittweger J, Michaelis I, Giehl M, Wusecke P, Felsenberg D 2004 Adjusting for the partial volume effect in cortical bone analyses of pQCT images. Journal of musculoskeletal & neuronal interactions **4**(4)**:**436-441.
216. Lin W, Ladinsky GA, Wehrli FW, Song HK 2007 Image metric-based correction (autofocusing) of motion artifacts in high-resolution trabecular bone imaging. Journal of magnetic resonance imaging : JMRI **26**(1)**:**191-197.
217. Parizel PM, van Hasselt BA, van den Hauwe L, Van Goethem JW, De Schepper AM 1994 Understanding chemical shift induced boundary artefacts as a function of field strength: influence of imaging parameters (bandwidth, field-of-view, and matrix size). European journal of radiology **18**(3)**:**158-164.

218. Babcock EE, Brateman L, Weinreb JC, Horner SD, Nunnally RL 1985 Edge artifacts in MR images: chemical shift effect. Journal of computer assisted tomography **9**(2)**:**252-257.
219. Hood MN, Ho VB, Smirniotopoulos JG, Szumowski J 1999 Chemical shift: the artifact and clinical tool revisited. Radiographics : a review publication of the Radiological Society of North America, Inc **19**(2)**:**357-371.
220. Szumowski J, Simon JH 1994 Proton chemical shift imaging. In: Stark D, Bradley W (eds.) Magnetic resonance imaging. Mostby-Year Book, St. Louis, MO, pp 479-521.
221. Peh WC, Chan JH 2001 Artifacts in musculoskeletal magnetic resonance imaging: identification and correction. Skeletal radiology **30**(4)**:**179-191.
222. Sumanaweera TS, Glover GH, Binford TO, Adler JR 1993 MR susceptibility misregistration correction. IEEE transactions on medical imaging **12**(2)**:**251-259.
223. Burkhardt S, Schweikard A, Burgkart R 2003 Numerical determination of the susceptibility caused geometric distortions in magnetic resonance imaging. Medical image analysis **7**(3)**:**221-236.
224. Barrett JF, Keat N 2004 Artifacts in CT: recognition and avoidance. Radiographics : a review publication of the Radiological Society of North America, Inc **24**(6)**:**1679-1691.
225. Calder K, Inglis D, MacIntyre NJ 2010 Comparison of pQCT-based measures of radial bone geometry and apparent trabecular bone structure using manufacturer and in-house developed algorithms. J Clin Densitom.
226. Folkesson J, Goldenstein J, Carballido-Gamio J, Kazakia G, Burghardt AJ, Rodriguez A, Krug R, de Papp AE, Link TM, Majumdar S 2011 Longitudinal evaluation of the effects of alendronate on MRI bone microarchitecture in postmenopausal osteopenic women. Bone **48**(3)**:**611-621.
227. Louis O, Cattrysse E, Scafoglieri A, Luypaert R, Clarys JP, de Mey J 2010 Accuracy of peripheral quantitative computed tomography and magnetic resonance imaging in assessing cortical bone cross-sectional area: a cadaver study. Journal of computer assisted tomography **34**(3)**:**469-472.
228. Brown MA, Semelka RC 2010 Extrinsic parameters MRI: Basic Principles and Applications 4th Edition. John Wiley & Sons, Hoboken, NJ, pp 95.
229. Blumenfeld J, Studholme C, Carballido-Gamio J, Carpenter D, Link TM, Majumdar S 2008 Three-dimensional image registration of MR proximal femur images for the analysis of trabecular bone parameters. Medical physics **35**(10)**:**4630-4639.
230. Carpenter D, Krug R, Banerjee R, Majumdar S 2006 Analyzing Trabecular Bone Structure in the Proximal Femur with High-Resolution Parallel Magnetic Resonance Imaging International Bone Densitometry Workshop, Kyoto, Japan.
231. Lee J, Koh D, Ong CN 1989 Statistical evaluation of agreement between two methods for measuring a quantitative variable. Computers in biology and medicine **19**(1)**:**61-70.
232. Liu XS, Cohen A, Shane E, Yin PT, Stein EM, Rogers H, Kokolus SL, McMahon DJ, Lappe JM, Recker RR, Lang T, Guo XE 2010 Bone density, geometry,

microstructure, and stiffness: Relationships between peripheral and central skeletal sites assessed by DXA, HR-pQCT, and cQCT in premenopausal women. J Bone Miner Res **25**(10)**:**2229-2238.

233. Carballido-Gamio J, Phan C, Link TM, Majumdar S 2006 Characterization of trabecular bone structure from high-resolution magnetic resonance images using fuzzy logic. Magnetic resonance imaging **24**(8)**:**1023-1029.
234. Zebaze R, Ghasem-Zadeh A, Mbala A, Seeman E 2013 A new method of segmentation of compact-appearing, transitional and trabecular compartments and quantification of cortical porosity from high resolution peripheral quantitative computed tomographic images. Bone **54**(1)**:**8-20.
235. Newitt DC, van Rietbergen B, Majumdar S 2002 Processing and analysis of in vivo high-resolution MR images of trabecular bone for longitudinal studies: reproducibility of structural measures and micro-finite element analysis derived mechanical properties. Osteoporos Int **13**(4)**:**278-287.
236. Hashimoto T, Shindo M, Morita H, Yanagisawa N, Ikeda S 2005 On the errors in assessment of severity of involuntary movements using surface EMG. Journal of electromyography and kinesiology : official journal of the International Society of Electrophysiological Kinesiology **15**(3)**:**316-322.
237. Cheung AM, Chan C, Ahmed F, Hu H, Demaras A, Polidoulis I 2008 Intra-operator precision for in vivo high resolution pQCT scans. In: ISCD (ed.) International Society for Clinical Densitometry 14th Annual Meeting, San Francisco 12–15 March 2008.
238. Capozza RF, Feldman S, Mortarino P, Reina PS, Schiessl H, Rittweger J, Ferretti JL, Cointry GR 2010 Structural analysis of the human tibia by tomographic (pQCT) serial scans. Journal of anatomy **216**(4)**:**470-481.
239. Mueller TL, Stauber M, Kohler T, Eckstein F, Muller R, van Lenthe GH 2009 Non-invasive bone competence analysis by high-resolution pQCT: an in vitro reproducibility study on structural and mechanical properties at the human radius. Bone **44**(2)**:**364-371.
240. Brown JP, Albert C, Nassar BA, Adachi JD, Cole D, Davison KS, Dooley KC, Don-Wauchope A, Douville P, Hanley DA, Jamal SA, Josse R, Kaiser S, Krahn J, Krause R, Kremer R, Lepage R, Letendre E, Morin S, Ooi DS, Papaioaonnou A, Ste-Marie LG 2009 Bone turnover markers in the management of postmenopausal osteoporosis. Clinical biochemistry **42**(10-11)**:**929-942.
241. Reszka AA, Rodan GA 2003 Bisphosphonate mechanism of action. Curr Rheumatol Rep **5**(1)**:**65-74.
242. Russell RG, Watts NB, Ebetino FH, Rogers MJ 2008 Mechanisms of action of bisphosphonates: similarities and differences and their potential influence on clinical efficacy. Osteoporos Int **19**(6)**:**733-759.
243. Phan TC, Xu J, Zheng MH 2004 Interaction between osteoblast and osteoclast: impact in bone disease. Histology and histopathology **19**(4)**:**1325-1344.
244. Recker RR, Delmas PD, Halse J, Reid IR, Boonen S, Garcia-Hernandez PA, Supronik J, Lewiecki EM, Ochoa L, Miller P, Hu H, Mesenbrink P, Hartl F,

Gasser J, Eriksen EF 2008 Effects of intravenous zoledronic acid once yearly on bone remodeling and bone structure. J Bone Miner Res **23**(1)**:**6-16.
245. Baecker N, Boese A, Schoenau E, Gerzer R, Heer M 2005 L-arginine, the natural precursor of NO, is not effective for preventing bone loss in postmenopausal women. J Bone Miner Res **20**(3)**:**471-479.
246. Courter BJ 1994 Pseudofractures of the mandible secondary to motion artifact. The American journal of emergency medicine **12**(1)**:**88-89.
247. Sugimoto Y, Ito Y, Shiozaki Y, Shimokawa T, Mazaki T 2012 Motion Induced Artifact Mimicking Cervical Dens Fracture on the CT Scan: A Case Report. Asian spine journal **6**(3)**:**216-218.
248. Verheij LF, Blokland JA, Papapoulos SE, Zwinderman AH, Pauwels EK 1992 Optimization of follow-up measurements of bone mass. Journal of nuclear medicine : official publication, Society of Nuclear Medicine **33**(7)**:**1406-1410.
249. Valkema R, Verheij LF, Blokland JA, Zwinderman AH, Bijvoet OL, Papapoulos SE, Pauwels EK 1990 Limited precision of lumbar spine dual-photon absorptiometry by variations in the soft-tissue background. Journal of nuclear medicine : official publication, Society of Nuclear Medicine **31**(11)**:**1774-1781.
250. Khoo BC, Brown K, Cann C, Zhu K, Henzell S, Low V, Gustafsson S, Price RI, Prince RL 2009 Comparison of QCT-derived and DXA-derived areal bone mineral density and T scores. Osteoporos Int **20**(9)**:**1539-1545.
251. Leslie WD 2008 Factors affecting short-term bone density precision assessment and the effect on patient monitoring. J Bone Miner Res **23**(2)**:**199-204.
252. Rinaldi G, Wisniewski CA, Setty NG, Leboff MS 2011 Peripheral quantitative computed tomography: optimization of reproducibility measures of bone density, geometry, and strength at the radius and tibia. J Clin Densitom **14**(3)**:**367-373.
253. Laib A, Barou O, Vico L, Lafage-Proust MH, Alexandre C, Rugsegger P 2000 3D micro-computed tomography of trabecular and cortical bone architecture with application to a rat model of immobilisation osteoporosis. Medical & biological engineering & computing **38**(3)**:**326-332.
254. Horikoshi T, Endo N, Uchiyama T, Tanizawa T, Takahashi HE 1999 Peripheral quantitative computed tomography of the femoral neck in 60 Japanese women. Calcif Tissue Int **65**(6)**:**447-453.
255. Faulkner K, Moores BM 1984 Analysis of x-ray computed tomography images using the noise power spectrum and autocorrelation function. Phys Med Biol **29**(11)**:**1343-1352.
256. Blake GM 1996 Replacing DXA scanners: cross-calibration with phantoms may be misleading. Calcif Tissue Int **59**(1)**:**1-5.
257. Genant HK, Grampp S, Gluer CC, Faulkner KG, Jergas M, Engelke K, Hagiwara S, Van Kuijk C 1994 Universal standardization for dual x-ray absorptiometry: patient and phantom cross-calibration results. J Bone Miner Res **9**(10)**:**1503-1514.
258. Guglielmi G, Cammisa M, De Serio A, Giannatempo GM, Bagni B, Orlandi G, Russo CR 1997 Long-term in vitro precision of single slice peripheral Quantitative Computed Tomography (pQCT): multicenter comparison. Technol Health Care **5**(5)**:**375-381.

259. Szulc P, Boutroy S, Vilayphiou N, Chaitou A, Delmas PD, Chapurlat R 2011 Cross-sectional analysis of the association between fragility fractures and bone microarchitecture in older men: the STRAMBO study. J Bone Miner Res **26**(6)**:**1358-1367.
260. Melton LJ, 3rd, Riggs BL, van Lenthe GH, Achenbach SJ, Muller R, Bouxsein ML, Amin S, Atkinson EJ, Khosla S 2007 Contribution of in vivo structural measurements and load/strength ratios to the determination of forearm fracture risk in postmenopausal women. J Bone Miner Res **22**(9)**:**1442-1448.
261. Vilayphiou N, Boutroy S, Szulc P, van Rietbergen B, Munoz F, Delmas PD, Chapurlat R 2011 Finite element analysis performed on radius and tibia HR-pQCT images and fragility fractures at all sites in men. J Bone Miner Res **26**(5)**:**965-973.
262. Jamal SA, Gilbert J, Gordon C, Bauer DC 2006 Cortical pQCT measures are associated with fractures in dialysis patients. J Bone Miner Res **21**(4)**:**543-548.
263. Gorai I, Nonaka K, Kishimoto H, Sakata H, Fujii Y, Fujita T 2001 Cut-off values determined for vertebral fracture by peripheral quantitative computed tomography in Japanese women. Osteoporos Int **12**(9)**:**741-748.
264. Link TM, Majumdar S, Augat P, Lin JC, Newitt D, Lu Y, Lane NE, Genant HK 1998 In vivo high resolution MRI of the calcaneus: differences in trabecular structure in osteoporosis patients. J Bone Miner Res **13**(7)**:**1175-1182.
265. Majumdar S, Link TM, Augat P, Lin JC, Newitt D, Lane NE, Genant HK 1999 Trabecular bone architecture in the distal radius using magnetic resonance imaging in subjects with fractures of the proximal femur. Magnetic Resonance Science Center and Osteoporosis and Arthritis Research Group. Osteoporos Int **10**(3)**:**231-239.
266. Cortet B, Boutry N, Dubois P, Bourel P, Cotten A, Marchandise X 2000 In vivo comparison between computed tomography and magnetic resonance image analysis of the distal radius in the assessment of osteoporosis. J Clin Densitom **3**(1)**:**15-26.
267. de Irala J, Navajas RF-C, del Castillo AS 1997 Abnormally wide confidence intervals in logistic regression: interpretation of statistical program results. Pan Am J Public Health **2**(4)**:**268-271.
268. Looker AC, Wahner HW, Dunn WL, Calvo MS, Harris TB, Heyse SP, Johnston CC, Jr., Lindsay R 1998 Updated data on proximal femur bone mineral levels of US adults. Osteoporos Int **8**(5)**:**468-489.
269. Cauley JA, Lui LY, Stone KL, Hillier TA, Zmuda JM, Hochberg M, Beck TJ, Ensrud KE 2005 Longitudinal study of changes in hip bone mineral density in Caucasian and African-American women. Journal of the American Geriatrics Society **53**(2)**:**183-189.
270. Lochmuller EM, Matsuura M, Bauer J, Hitzl W, Link TM, Muller R, Eckstein F 2008 Site-Specific Deterioration of Trabecular Bone Architecture in Men and Women with Advancing Age. J Bone Miner Res.

271. Macdonald HM, Nishiyama KK, Kang J, Hanley DA, Boyd SK 2011 Age-related patterns of trabecular and cortical bone loss differ between sexes and skeletal sites: a population-based HR-pQCT study. J Bone Miner Res **26**(1)**:**50-62.
272. Dalzell N, Kaptoge S, Morris N, Berthier A, Koller B, Braak L, van Rietbergen B, Reeve J 2009 Bone micro-architecture and determinants of strength in the radius and tibia: age-related changes in a population-based study of normal adults measured with high-resolution pQCT. Osteoporos Int **20**(10)**:**1683-1694.
273. Katayev A, Balciza C, Seccombe DW 2010 Establishing reference intervals for clinical laboratory test results: is there a better way? American journal of clinical pathology **133**(2)**:**180-186.
274. Schneider P, Butz S, Allolio B, Borner W, Klein K, Lehmann R, Petermann K, Tysarczyk-Niemeyer G, Wuster C, Zander C, et al. 1995 Multicenter German reference data base for peripheral quantitative computer tomography. Technol Health Care **3**(2)**:**69-73.
275. Ashby RL, Ward KA, Roberts SA, Edwards L, Mughal MZ, Adams JE 2009 A reference database for the Stratec XCT-2000 peripheral quantitative computed tomography (pQCT) scanner in healthy children and young adults aged 6-19 years. Osteoporos Int **20**(8)**:**1337-1346.
276. Moyer-Mileur LJ, Quick JL, Murray MA 2008 Peripheral quantitative computed tomography of the tibia: pediatric reference values. J Clin Densitom **11**(2)**:**283-294.
277. Burrows M, Liu D, Moore S, McKay H 2009 Bone Microstructure at the Distal Tibia Provides a Strength Advantage to Males in Late Puberty: A HR-pQCT Study. J Bone Miner Res.
278. Eckstein F, Matsuura M, Kuhn V, Priemel M, Muller R, Link TM, Lochmuller EM 2007 Sex differences of human trabecular bone microstructure in aging are site-dependent. J Bone Miner Res **22**(6)**:**817-824.
279. Muller R, Ruegsegger P 1995 Three-dimensional finite element modelling of non-invasively assessed trabecular bone structures. Medical engineering & physics **17**(2)**:**126-133.
280. Pistoia W, van Rietbergen B, Laib A, Ruegsegger P 2001 High-resolution three-dimensional-pQCT images can be an adequate basis for in-vivo microFE analysis of bone. Journal of biomechanical engineering **123**(2)**:**176-183.
281. Lammentausta E, Hakulinen MA, Jurvelin JS, Nieminen MT 2006 Prediction of mechanical properties of trabecular bone using quantitative MRI. Phys Med Biol **51**(23)**:**6187-6198.

9 Appendices

Form 1

REQUEST FOR ORTHONE MRI SCAN FOR RESEARCH

Study Title: "On the development of bone structural & mechanical outcomes for assessing osteoporosis on non-invasive imaging modalities"

MRI system ownership:
CAMRIS
612-25 Charlton Ave. E.
Hamilton, ON L8N 1Y2

Principal Investigators:
Dr. Rick Adachi
Dr. Alexandra Papaioannou
Andy Kin On Wong
Dr. Karen Beattie
Dr. Colin Webber
Dr. Dean Inglis

Date: _____/_____/_____ (d/m/y)

Study ID: _____

Year of birth: _____ Month of birth:_____

Weight: _____ (kg) Height: _____ (m)

**** the year and month of birth are necessary for software operation**

Is there any possibility that you may be pregnant? **YES** □ **NO** □
Have you ever worked with metal (hobby/occupation)? **YES** □ **NO** □

Please check if you <u>have</u> any of the following:

Pacemaker, defibrillator, pace wires	Yes □	No □
Prosthetic heart valve	Yes □	No □
Electrodes, shunts, plates, aneurysm clips	Yes □	No □
Vascular access port or catheter	Yes □	No □
Intravascular coils, filters or stents	Yes □	No □
Insulin pump or infusion pump	Yes □	No □
Cochlear, stapes or orbit/ear implants	Yes □	No □
Bone growth/fusion stimulator	Yes □	No □
Implanted neurostimulator	Yes □	No □
Metal or wire mesh implants	Yes □	No □
Artificial limb or joint	Yes □	No □
Metal rods, pins or plates in a joint or bone	Yes □	No □
Bullets or shrapnel in your body	Yes □	No □
Metal fragments in your eye(s)	Yes □	No □
Tattoos, tattooed makeup, body piercing	Yes □	No □
Any other implanted device	Yes □	No □

Please check if you <u>have ever had</u> any of the following:

Brain, ear, eye or head surgery	Yes □	No □
Vascular (vein) surgery	Yes □	No □
Bone or joint surgery	Yes □	No □

Before your MRI, please REMOVE shoes and ALL metal objects, including:

-hearing aid	-barrettes/hair pins	-safety pins/clips	-jewelry/keys
-credit cards	-pocket knife	-coins/change	-pens/pencils
-watch	-cellular phone/pager	-clothing/undergarments containing metal	

St. Joseph's Healthcare Hamilton | CaMos Canadian Multicentre Osteoporosis Study

Form 2A

Hamilton CaMos Bone Quality Study: Case Report Form Baseline

Participant HA#/Respondent ID: ____

Interview Date: _____ / _____ / _____ Day Month Year

Time Began (24h00) _____ HRS _____ MINS

Time Ended (24h00) _____ HRS _____ MINS

Provided Consent: ☐ **Will participate in:** CAMOS1108a: ☐ CAMOS1108b: ☐

Copy of consent given to participant: ☐

Satisfied all inclusion criteria: Yes ☐ No ☐

Did not meet any exclusion criteria: Yes ☐ No ☐

Completed MRI Requisition form: Yes ☐ No ☐

Contraindicating metal devices present: Yes ☐ No ☐

Current Bone Health-Related Medications:

Name	Frequency	Dose	Duration

Timed 'up and go' Test

Time to get up from arm chair, walk 3 meters, turn around, walk back and sit down

Completed: Yes ☐ No ☐ **If No, Reason:** _____

Participant Time: _____ seconds

Grip Strength Test

Force recorded on dynamometer after sustained clenching:

Trial 1: _____ **Trial 2:** _____ **Trial 3:** _____

Sustained a fracture since the last CaMos questionnaire? Yes ☐ No ☐

Type of fracture: _____ **Location of fracture:** _____

Bone Structure Image Acquisition: 1.0 Tesla pMRI Scan:

Completed: Yes ☐ No ☐ **If No, Reason:** _____

Wrist scanned : Left ☐ Right ☐ **Is it non-dominant?** Yes ☐ No ☐

Scan filename: _____

Participant requested a copy of bone scan: Yes ☐ No ☐

Date of image segmentation: Append bone structure report
_____ / _____ / _____
Day Month Year

Bone Structure Image Acquisition: hr-pQCT Scan:
(Only those participating in CAMOS1108b)

Remind participant of their appointment with Alice Demaras

Distal Radius: Completed: Yes ☐ No ☐ **If No, Reason:** _____

Wrist scanned : Left ☐ Right ☐

Distal Tibia: Completed: Yes ☐ No ☐ **If No, Reason:** _____

Ankle scanned : Left ☐ Right ☐

Scan filename: _____

Participant requested a copy of bone scan: Yes ☐ No ☐

Append bone structure report

Bone Structure Image Acquisition: pQCT Scan:
(Only those participating in CAMOS1108b)

Remind participant of their appointment

11.5 mm Distal Radius: Completed: Yes ☐ No ☐ **If No, Reason:**

Wrist scanned : Left ☐ Right ☐

33% Distal Radius: Completed: Yes ☐ No ☐ **If No, Reason:**

11.5 mm Distal Tibia: Completed: Yes ☐ No ☐ **If No, Reason:**

Ankle scanned : Left ☐ Right ☐

66% Distal Tibia: Completed: Yes ☐ No ☐ **If No, Reason:**

Scan filename: _____

Participant requested a copy of bone scan: Yes ☐ No ☐

Append bone structure report

St. Joseph's Healthcare Hamilton | CaMos Canadian Multicentre Osteoporosis Study

Form 2B

Hamilton CaMos Bone Quality Study: Case Report Form
Year 1 Follow-up

Participant HA#/Respondent ID: ____

Interview Date: _____ / _____ / _____ (Day Month Year)

Time Began (24h00) _____ HRS _____ MINS

Time Ended (24h00) _____ HRS _____ MINS

Provided Consent: ☐ **Will participate in:** CAMOS1108A: ☐ B: ☐ C: ☐

Copy of consent given to participant: ☐

Satisfied all inclusion criteria: Yes ☐ No ☐

Did not meet any exclusion criteria: Yes ☐ No ☐

Completed MRI Requisition form: Yes ☐ No ☐

Contraindicating metal devices present: Yes ☐ No ☐

Current Bone Health-Related Medications:

Name	Frequency	Dose	Duration

Timed 'up and go' Test

Time to get up from arm chair, walk 3 meters, turn around, walk back and sit down

Completed: Yes ☐ No ☐ **If No, Reason:** _____

Participant Time: _____ seconds

Grip Strength Test

Force recorded on dynamometer after sustained clenching:

Trial 1: _____ **Trial 2:** _____ **Trial 3:** _____

Sustained a fracture since the last CaMos questionnaire? Yes ☐ No ☐

Type of fracture: _____ **Location of fracture:** _____

Bone Structure Image Acquisition: 1.0 Tesla pMRI Scan:

Completed: Yes ☐ No ☐ **If No, Reason:** _____

Wrist scanned : Left ☐ Right ☐ **Is it non-dominant?** Yes ☐ No ☐

Calf scanned : Left ☐ Right ☐ **Is it non-dominant?** Yes ☐ No ☐

Scan filename: _____

Participant requested a copy of bone scan: Yes ☐ No ☐

Date of image segmentation: Append bone structure report
_____ / _____ / _____
Day Month Year

Bone Structure Image Acquisition: hr-pQCT Scan:
(Only those participating in CAMOS1108b)

Remind participant of their appointment with Farrah Ahmed

Distal Radius: Completed: Yes ☐ No ☐ **If No, Reason:** _____

Wrist scanned : Left ☐ Right ☐

Distal Tibia: Completed: Yes ☐ No ☐ **If No, Reason:** _____

Ankle scanned : Left ☐ Right ☐

Scan filename: _____

Participant requested a copy of bone scan: Yes ☐ No ☐

Append bone structure report

Bone Structure Image Acquisition: pQCT Scan:

Remind participant of their appointment

11.5 & 26.5 mm Distal Radius: Completed: Yes ☐ No ☐ **If No, Reason:** _____

Wrist scanned : Left ☐ Right ☐

Scan filename: _____(PATNO,CTNO)

Reference distance:_____

24.5 & 29.5 mm Distal Tibia: Completed: Yes ☐ No ☐ **If No, Reason:** _____

Ankle scanned : Left ☐ Right ☐

Scan filename: _____(PATNO,CTNO)

Reference distance:_____

66% Calf: Completed: Yes ☐ No ☐ **If No, Reason:** _____

Scan filename: _____(PATNO,CTNO)

Participant requested a copy of bone scan: Yes ☐ No ☐

Append bone structure report

RESPONDENT I.D.# _____

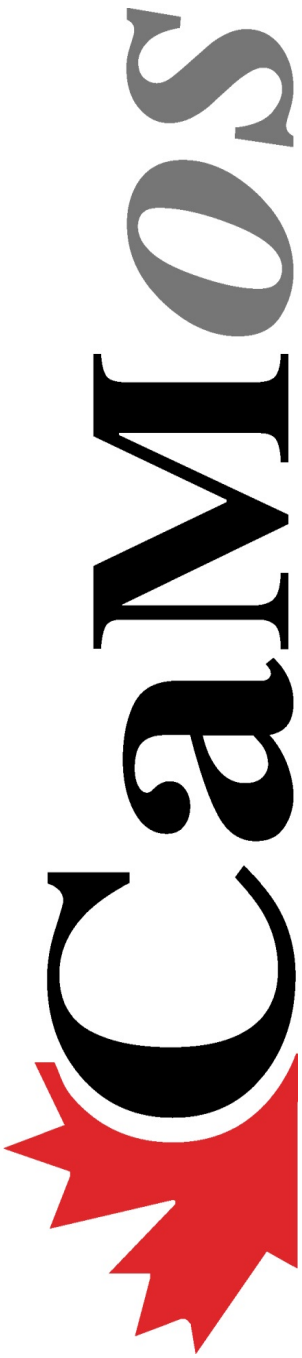

YEAR 16 FOLLOW-UP QUESTIONNAIRE

2011.10.18

CaM*os*
Canadian Multicentre Osteoporosis Study

Year 16

RESPONDENT

PROVINCIAL HEALTH # * _____

NAME _____ (Last (Maiden in Quebec)) _____ (First)

_____ * ETHNIC NAME (Last) (First)

ADDRESS _____ (No.) _____ (Street) _____ (Apt. #)

_____ (City) _____ (Province) |_|_|_| |_|_|_| (Postal Code)

TELEPHONE ( ) _____ (Area Code) WORK/OTHER ( ) _____ (Area Code)

CELL PHONE ( ) _____ E-MAIL ADDRESS : _____

DO YOU PLAN TO MOVE IN THE NEXT YEAR? ☐ YES ☐ NO

WHEN? _____

NEW ADDRESS _____

_____

FAMILY PHYSICIAN

NAME _____

ADDRESS _____

CONTACT PERSON *

NAME _____ (Last (Maiden in Quebec)) _____ (First)

ADDRESS _____ (No.) _____ (Street) _____ (Apt. #)

_____ (City) _____ (Province) |_|_|_| |_|_|_| (Postal Code)

TELEPHONE ( ) _____ (Home) ( ) _____ (Work)

RELATION TO RESPONDENT:* _____

* See note in manual

RESPONDENT I.D. #_____

* *Age at last interview* _____

Number of months since last interview _____

Date of last interview _____ / _____ / _____
Day Month Year

CaM*os*
Canadian Multicentre Osteoporosis Study

Year 16

CENTRE IDENTIFICATION ☐☐

INTERVIEWER I.D. _____ NAME _____

LOCATION OF INTERVIEW ☐ 1 HOSPITAL ☐ 2 HOME ☐ 3 OTHER ⋯➤ *(specify)* _____

DATE OF YEAR 16 INTERVIEW _____ / _____ / _____
Day Month Year

TIME BEGAN ☐☐ HRS ☐☐ MIN

TIME ENDED ☐☐ HRS ☐☐ MIN

CLINICAL ASSESSMENT *

DEXA	☐ 1 Yes	☐ 2 No	
X-RAY	☐ 1 Yes	☐ 2 No	
BLOOD	☐ 1 Yes	☐ 2 No	
p-QCT	☐ 1 Yes	☐ 2 No	☐ 3 N/A
hr-pQCT	☐ 1 Yes	☐ 2 No	☐ 3 N/A

HEARING IMPAIRMENT ☐ 1 Yes ☐ 2 No

VISUAL IMPAIRMENT ☐ 1 Yes ☐ 2 No

RESULTS TO BE SENT TO PHYSICIAN ☐ 1 Yes ☐ 2 No

RESULTS TO BE SENT TO PARTICIPANT ☐ 1 Yes ☐ 2 No

CAMOS DATA ENTRY DATE _____ / _____ / _____ _____
Day Month Year Initials

COMMENTS _____

* See note in manual

I would like to ask you general questions about yourself.

1. SOCIO-DEMOGRAPHIC INFORMATION

1.1 Sex: *(Answer by observation)*. . . . . ☐ 1 Male ☐ 2 Female

1.2 What is your date of birth?. . . . . _____ / _____ / _____
Day Month Year

1.3 Have you moved **SINCE YOUR LAST INTERVIEW**?. . . . . ☐ 1 Yes ☐ 2 No

→ How many times have you moved? . . . . . _____

→ For your most recent move, where have you moved ?

- ☐ 1 Single family home
- ☐ 2 Apartment/Condominium
- ☐ 3 Retirement community complex
- ☐ 4 Nursing home/Long term care hospital
- ☐ 5 Other: *(specify)* _____

1.4 What is your current marital status? *(Indicate only one)*

- ☐ 1 Married or living with a partner
- ☐ 2 Single
- ☐ 3 Separated
- ☐ 4 Divorced
- ☐ 5 Widowed

1.5 With whom do you currently live?

(Check all that apply)

- ☐ 1 Spouse / partner
- ☐ 2 Sibling
- ☐ 3 Children
- ☐ 4 Parents
- ☐ 5 Lives alone
- ☐ 6 Other *(specify)* _____

Go to quest 1.7

2 * See note in manual

1.6* If living with spouse or partner *(answered in question 1.5)*, which best describes your partner's current or most recent occupation?

Show the list to the respondent. Help interpret if necessary. Mark only one.

- ☐ 1 Executive, administrative and or managerial
- ☐ 2 Professional specialty occupation
- ☐ 3 Technician and or related support occupation
- ☐ 4 Marketing and or sales occupation
- ☐ 5 Administrative support occupation
- ☐ 6 Service occupation
- ☐ 7 Agriculture, forestry, fishing and/or related work
- ☐ 8 Precision production, crafts and/or repair occupation
- ☐ 9 Operator, fabricator and/or laborer
- ☐ 10 Partner does not work

1.7* What is your current employment status?

- ☐ 1 Employed full time
- ☐ 2 Employed part time *(or semi-retired)*
- ☐ 3 Retired
  - Since your last interview?
    - ☐ 1 Yes ☐ 2 No
      - How old were you? _____ years
- ☐ 4 Unemployed
- ☐ 5 Homemaker *(full time)*
- ☐ 6 Student
- ☐ 7 Disability

1.8* Which best describes your current or most recent occupation, if currently employed or retired?

Show the list to the respondent. Help interpret if necessary. Mark only one.

- ☐ 1 Executive, administrative and or managerial
- ☐ 2 Professional specialty occupation
- ☐ 3 Technician and or related support occupation
- ☐ 4 Marketing and or sales occupation
- ☐ 5 Administrative support occupation
- ☐ 6 Service occupation
- ☐ 7 Agricultural, forestry, fishing and/or related work
- ☐ 8 Precision production, crafts and/or repair occupation
- ☐ 9 Operator, fabricator and/or laborer

1.9 Do you have a particular doctor or clinic that you would call your regular doctor or clinic?. . . . . ☐ 1 Yes ☐ 2 No

* See note in manual

Do not ask question 1.10 if subject did not have a DXA at the last interview ⟶ *Check N/A*

1.10 What were the results of your bone density test, at your last interview?. . . . . ☐ 1 Don't know, I am unsure
☐ 2 High or normal bone density
☐ 3 Low without osteoporosis *(borderline "osteopenia")*
☐ 4 Low or "osteoporosis"
☐ 5 N/A *(none at last interview)*

1.11 **SINCE YOUR LAST INTERVIEW**, have you had a bone density measurement other than for this study?. . . . . ☐ 1 Yes ☐ 2 No

1.12 **SINCE YOUR LAST INTERVIEW**, have you sought information on osteoporosis:

- from the Osteoporosis Society of Canada?. . . . . ☐ 1 Yes ☐ 2 No
- from a local public health resource? *(e.g. women's health centre)*. . . . . ☐ 1 Yes ☐ 2 No
- from a health care professional: Nutritionist. . . . . ☐ 1 Yes ☐ 2 No
  Physiotherapist or exercise specialist. . . . ☐ 1 Yes ☐ 2 No
  Nurse. . . . . ☐ 1 Yes ☐ 2 No
  Physician. . . . . ☐ 1 Yes ☐ 2 No
  Other . . . . . ☐ 1 Yes ☐ 2 No
  (specify) _____
- from another source? . . . . . ☐ 1 Yes ☐ 2 No
  (specify) _____

Now we'll review your past health.

2. MEDICAL HISTORY

2.1 * **SINCE YOUR LAST INTERVIEW**, have you been told by a doctor that you have any of the following conditions?

If YES, at what age was the diagnosis made? Have you started a treatment for this condition?

	DIAGNOSIS				TREATMENT			
	Yes	No	DK	Age	Yes	No	DK	N/A
Osteoporosis								
Rheumatoid arthritis								
Osteoarthritis *(hands, feet, knees, hips, neck)*								
Lupus *(SLE)*								
Thyroid disease: 1 = Hyperthyroidism 2 = Hypothyroidism ____								
Liver disease								
Scoliosis								
Eating disorder *(bulimia, anorexia)*								
Cancer:								
Prostate *(for men)*								
Breast *(for all)*								
Uterine *(for women)*								
Multiple myeloma *(bone)*								
Other *(specify)* _____								
Inflammatory bowel disease *(Crohn's disease , ulcerative colitis)*								
Celiac disease *(Malabsorption syndrome)*								
Kidney stones								
Kidney disease								
Hypertension *(high blood pressure)*								
Heart attack								
Stroke, TIA *(Transient Ischemic attack)*								
Neuromuscular disease:								
Parkinson's								
Multiple sclerosis								
Other *(specify)* _____								
Non insulin dependent diabetes *(Type 2)*								
Insulin dependent diabetes *(Type I)*								
Phlebitis, Thrombophlebitis								
Paget's disease of bone								
Lung disease:								
Asthma								
Emphysema								
Bronchitis *(chronic)*								
Other (*specify)* _____								

* See note in manual

2.2 **IN THE PAST YEAR**, have you had a hospital admission which required an overnight stay, other than for surgery?. . . . . ☐ 1 Yes ☐ 2 No
(*Not in emergency)*

For what reason? *(Check all that apply)*

- ☐ 1 Heart disease
- ☐ 2 Breast cancer
- ☐ 3 Cancer of the uterus
- ☐ 4 Other cancer *(specify)* _____
- ☐ 5 Other hospital admission *(specify)* _____

MALE RESPONDENT → *Go to question 2.5*

2.3 **SINCE YOUR LAST INTERVIEW**,
have you had your uterus removed *(hysterectomy)*?. . . . . ☐ 1 Yes ☐ 2 No

At what age? _____ years

2.4* **SINCE YOUR LAST INTERVIEW**,
have you had one or both ovaries removed?. . . . . ☐ 1 Yes ☐ 2 No

- ☐ 1 Yes, one ovary removed.. . . . . at what age? _____ years
- ☐ 2 Yes, both ovaries removed.. . . . . at what age? _____ years
  (If ovaries were removed on separate occasions, write the age at which the second ovary ws removed)
- ☐ 3 Yes, do not know how many. . . . . at what age? _____ years

2.5 **SINCE YOUR LAST INTERVIEW**, have you had any of the following surgeries?. . . . . ☐ 1 Yes ☐ 2 No

(Check all that apply and indicate Age and Specify where applicable)

☐ 1 Gall bladder. . . . . at what age? _____ years

☐ 2 Intestine. . . . . at what age? _____ years

☐ 3 Parathyroid. . . . . at what age? _____ years

☐ 4 Thyroid. . . . . at what age? _____ years

☐ 5 Stomach. . . . . at what age? _____ years

☐ 6 Organ transplant. . . . . at what age? _____ years

(specify) _____

☐ 7 Back. . . . . at what age? _____ years

Was it due to back pain?. . . . . ☐ 1 Yes ☐ 2 No

2.6* **SINCE YOUR LAST INTERVIEW**, have you had any other surgeries?. . . . . ☐ 1 Yes ☐ 2 No

How many surgeries? ____

1. Specify _____ at what age? _____ years
2. Specify _____ at what age? _____ years
3. Specify _____ at what age? _____ years
4. Specify _____ at what age? _____ years
5. Specify _____ at what age? _____ years

2.7 **SINCE YOUR LAST INTERVIEW**, have you been confined to a bed, a wheelchair or by a cast for more than one month at a time?. . . . . ☐ 1 Yes ☐ 2 No

* See note in manual

2.8 **SINCE YOUR LAST INTERVIEW,**
have you had back pain ?. . . . . ☐ 1 Yes ☐ 2 No

Go to question 2.12

Has the back pain lasted continuously for:
☐ 1 more than 1 year
☐ 2 less than 1 year, more than 3 months
☐ 3 less than 3 months, more than 1 month
☐ 4 none of the above

2.9* **SINCE YOUR LAST INTERVIEW,**
have you been bedridden because of back pain
for more than 4 continuous hours in a day?. . . . . ☐ 1 Yes ☐ 2 No

→ For how long ?. . . . . ☐ 1 from 1 to 7 days
☐ 2 from 8 to 14 days
☐ 3 more than 14 days

→ Were you restricted to bed
on the order of a physician?. . . . . ☐ 1 Yes ☐ 2 No

2.10* **SINCE YOUR LAST INTERVIEW,**
have you had to limit your activity
or miss work because of back pain?. . . . . ☐ 1 Yes ☐ 2 No

For how long? (1)_____ days - or - (2)_____months - or - (3)_____ years

2.11 **SINCE YOUR LAST INTERVIEW,**
have you received or are you receiving disability income
or worker's compensation for back pain?. . . . . ☐ 1 Yes ☐ 2 No

Are you on permanent disability
because of back pain?. . . . . ☐ 1 Yes ☐ 2 No

8 * See note in manual

Question 2.12 Specify that the following question asks about falls and does not include falls from a sporting or motor vehicle accident.

2.12* Have you fallen **IN THE PAST 12 MONTHS**?. . . . . ☐ 1 Yes ☐ 2 No

How many times ? _____

Go to question 3.1

Which of the following was the most important reason for your most serious fall in the last year? *(apart from a sporting or a motor vehicle accident)*

☐ 1 I felt dizzy or almost fainted, had a balance problem or a feeling I was spinning
☐ 2 I was climbing up onto something *(ladder, chair, stool, etc)* and slipped
☐ 3 The footing indoors was slippery
☐ 4 The footing outdoors was slippery
☐ 5 Didn't see an obstruction
☐ 6 I wasn't paying close attention because of alcohol or other substance use or pain tranquilizer or sleeping pill medications
☐ 7 I was very ill and felt weak
☐ 8 Other *(specify)* _____

Now I will ask you about the medicines you may have taken SINCE YOUR LAST INTERVIEW.

3. DRUGS AND MEDICATIONS

3.1* **SINCE YOUR LAST INTERVIEW**, have you taken any of the following medications regularly or daily?

If YES, for approximately how many months total have you taken it?

		Total # of months taken	
Cortisone / Prednisone :			
Inhaled.	☐ 1 Yes ➤	_____	☐ 2 No
Oral.	☐ 1 Yes ➤	_____	☐ 2 No
Injection:		*# of Injection*	
Intravenous.	☐ 1 Yes ➤	_____	☐ 2 No
Intramuscular, subcutaneous.	☐ 1 Yes ➤	_____	☐ 2 No
Denosumab *(Prolia)*.	☐ 1 Yes ➤	_____	☐ 2 No
Aclasta *(Zoledronic Acid)*.	☐ 1 Yes ➤	_____	☐ 2 No

3.2* List the current medications and/or supplements taken on a regular basis

Also - include antacids such as Tums and Rolaids
- list medication or supplement taken only a portion of the year

					Since last interview
COMPANY NAME *(for vitamins and minerals, herbal and homeopathic products)*	**MEDICATION NAME**	**COMPONENT** *Calcium Vit. D*	**DOSE**	**FREQUENCY**	**TOTAL # OF MONTHS TAKEN**

Now I would like to know about any broken bone you may have had in the past year (since the last follow-up).

4. FRACTURES

4.1* **IN THE PAST YEAR**, have you fractured any bones? ☐ 1 Yes ☐ 2 No

IN THE LAST YEAR,
how many times have you fractured a bone?. . . . . _____

Complete a fracture questionnaire for each incident and each bone fractured.

MALE RESPONDENT → *Go to questions 5.2*

5.a FEMALE PARTICIPANT

FEMALE RESPONDENT 65 YEARS OLD AND OVER AT TIME OF INTERVIEW → *Go to question 6.1*

5.1* **SINCE YOUR LAST INTERVIEW**, have your menstrual periods stopped for more than one year?. . . . . ☐ 1 Yes ☐ 2 No

At what age ? _____ years

FEMALE RESPONDENT → *Go to question 6.1*

The following questions are related to the level of androgen in men. These questions are self-administered.

5.b MALE PARTICIPANT

5.2* **SINCE YOUR LAST INTERVIEW**, which of the following is your usual experience regarding spontaneous erections not related to sex?

- ☐ 1 One or more times a day *(for example, first thing when I wake up)*
- ☐ 2 Most days
- ☐ 3 Some days
- ☐ 4 Occasionally
- ☐ 5 Rarely
- ☐ 6 Never
- ☐ 7 Refuse to answer

5.3* **IN THE PAST YEAR**, have you experienced a decrease in or loss of desire for sexual activity?

☐ 1 Yes ☐ 2 No ☐ 3 Refuse to answer

5.4* **IN THE PAST YEAR**, have you had any episodes of an inability to develop or maintain an **erection** while performing sex?

☐ 1 Yes ☐ 2 No ☐ 3 Refuse to answer

In this section, we are interested in knowing about your sleep history.

6. SLEEPING HISTORY

6.1 **SINCE YOUR LAST INTERVIEW,** have you had repeated *(many times)* episodes of the following:

Waking early.	☐ 1 Yes	☐ 2 No
Nighttime wakening..	☐ 1 Yes	☐ 2 No
Problems falling asleep.	☐ 1 Yes	☐ 2 No
Daytime sleepiness..	☐ 1 Yes	☐ 2 No

6.2* **IN THE PAST 3 MONTHS**, have you noticed any changes in sleep patterns such as waking early, nighttime wakening or problems falling asleep?

☐ 1 No changes
☐ 2 Decreasing
☐ 3 Increasing
☐ 4 Never or rarely experience *(no sleep problem)*

6.3 *Night sweats are hot flushes which occur during sleep*

IN THE LAST 2 WEEKS, how often have you experienced hot flushes during the time when you were sleeping?

☐ 1 Never ➤ *Go to question 7.1*
☐ 2 Once or twice
☐ 3 Three to six times
☐ 4 Once a night
☐ 5 More than once, most nights

6.4 If you have experienced any night sweats or night time hot flushes **IN THE LAST 2 WEEKS**, please grade their usual severity: *(mark only one)*

☐ 1 Mild warm feeling
☐ 2 Moderate hot feeling with sweating or flushing
☐ 3 Moderately severe hot feeling often with sweating on part of your body
☐ 4 A major hot feeling often with sweating on most of your body

* See note in manual

Now I am going to ask you about your biological relatives (not those related to you by marriage or adoption).

7. FAMILY HISTORY

7.1 Was at least one of your biological parents still living at the time of **YOUR LAST INTERVIEW** ?. . . . ☐ 1 Yes ☐ 2 No ☐ 3 Don't know *(If adopted)*

Go to question 7.3

7.2* **SINCE YOUR LAST INTERVIEW**, did the following occur in your biological parents?
(Circle appropriate answer for each. If yes, please check the boxes for whom the condition applies)

	Yes	No	DK			
Height Loss.	1	2	3	. . . . .	☐ 1 Father	☐ 2 Mother ☐ 3 Both
Stooping.	1	2	3	. . . . .	☐ 1 Father	☐ 2 Mother ☐ 3 Both
Hip Fracture.	1	2	3	. . . . .	☐ 1 Father	☐ 2 Mother ☐ 3 Both
Wrist Fracture.	1	2	3	. . . . .	☐ 1 Father	☐ 2 Mother ☐ 3 Both
Shoulder Fracture *(upper arm)*.	1	2	3	. . . . .	☐ 1 Father	☐ 2 Mother ☐ 3 Both
Pelvic Fracture.	1	2	3	. . . . .	☐ 1 Father	☐ 2 Mother ☐ 3 Both
Ankle Fracture *(lower leg)*.	1	2	3	. . . . .	☐ 1 Father	☐ 2 Mother ☐ 3 Both

7.3* **SINCE YOUR LAST INTERVIEW**,
have any parents, siblings or children related by blood been diagnosed with the following?
If YES, please indicate which biological (blood related) parent, sibling or child.

NOTE: If no children lived beyond birth then questions relating to children are N/A
If no parents living at time of last interview then questions relating to parents are N/A (refer to 7.1)

***For fractures**, if no blood related siblings or children then indicate N/A*

		Yes	No	DK	N/A			
Fractures								
Parents.		1	2	3	4	. . . . .	☐ 1 Father	☐ 2 Mother ☐ 3 Both
Siblings ≥ 40 ☐ 1 Yes ☐ 2 No ☐ 3 N/A		1	2	3		. . . . .	☐ 1 Brother	☐ 2 Sister ☐ 3 Both
Children ≥ 40 ☐ 1 Yes ☐ 2 No ☐ 3 N/A		1	2	3		. . . . .	☐ 1 Son	☐ 2 Daughter ☐ 3 Both
Osteoporosis	Parents.	1	2	3	4	. . . . .	☐ 1 Father	☐ 2 Mother ☐ 3 Both
	Siblings.	1	2	3	4	. . . . .	☐ 1 Brother	☐ 2 Sister ☐ 3 Both
	Children.	1	2	3	4	. . . . .	☐ 1 Son	☐ 2 Daughter ☐ 3 Both
Osteoarthritis	Parents.	1	2	3	4	. . . . .	☐ 1 Father	☐ 2 Mother ☐ 3 Both
	Siblings.	1	2	3	4	. . . . .	☐ 1 Brother	☐ 2 Sister ☐ 3 Both
	Children.	1	2	3	4	. . . . .	☐ 1 Son	☐ 2 Daughter ☐ 3 Both

		Yes	No	DK	N/A	
Paget's disease	Parents.	1	2	3	4	. . . . . ☐ 1 Father ☐ 2 Mother ☐ 3 Both
	Siblings.	1	2	3	4	. . . . . ☐ 1 Brother ☐ 2 Sister ☐ 3 Both
	Children.	1	2	3	4	. . . . . ☐ 1 Son ☐ 2 Daughter ☐ 3 Both
Scoliosis	Parents.	1	2	3	4	. . . . . ☐ 1 Father ☐ 2 Mother ☐ 3 Both
	Siblings.	1	2	3	4	. . . . . ☐ 1 Brother ☐ 2 Sister ☐ 3 Both
	Children.	1	2	3	4	. . . . . ☐ 1 Son ☐ 2 Daughter ☐ 3 Both
CVD, stroke, aneurysm, hypertension	Parents.	1	2	3	4	. . . . . ☐ 1 Father ☐ 2 Mother ☐ 3 Both
	Siblings.	1	2	3	4	. . . . . ☐ 1 Brother ☐ 2 Sister ☐ 3 Both
	Children.	1	2	3	4	. . . . . ☐ 1 Son ☐ 2 Daughter ☐ 3 Both
Diabetes	Parents.	1	2	3	4	. . . . . ☐ 1 Father ☐ 2 Mother ☐ 3 Both
	Siblings.	1	2	3	4	. . . . . ☐ 1 Brother ☐ 2 Sister ☐ 3 Both
	Children.	1	2	3	4	. . . . . ☐ 1 Son ☐ 2 Daughter ☐ 3 Both
Prostate Cancer	Father.	1	2	3	4	
	Brother(s).	1	2	3	4	
	Son(s).	1	2	3	4	
Breast Cancer	Parents.	1	2	3	4	. . . . . ☐ 1 Father ☐ 2 Mother ☐ 3 Both
	Siblings.	1	2	3	4	. . . . . ☐ 1 Brother ☐ 2 Sister ☐ 3 Both
	Children.	1	2	3	4	. . . . . ☐ 1 Son ☐ 2 Daughter ☐ 3 Both
Uterine Cancer	Mother.	1	2	3	4	
	Sister(s).	1	2	3	4	
	Daughter(s).	1	2	3	4	
Ovarian Cancer	Mother.	1	2	3	4	
	Sister(s).	1	2	3	4	
	Daughter(s).	1	2	3	4	
Colon Cancer	Parents.	1	2	3	4	. . . . . ☐ 1 Father ☐ 2 Mother ☐ 3 Both
	Siblings.	1	2	3	4	. . . . . ☐ 1 Brother ☐ 2 Sister ☐ 3 Both
	Children.	1	2	3	4	. . . . . ☐ 1 Son ☐ 2 Daughter ☐ 3 Both
Multiple Myeloma	Parents.	1	2	3	4	. . . . . ☐ 1 Father ☐ 2 Mother ☐ 3 Both
	Siblings.	1	2	3	4	. . . . . ☐ 1 Brother ☐ 2 Sister ☐ 3 Both
	Children.	1	2	3	4	. . . . . ☐ 1 Son ☐ 2 Daughter ☐ 3 Both

In this section, I will ask you about your physical characteristics.

8. PHYSICAL CHARACTERISTICS

8.1* Current measured height. . . . . _____ feet _____ inches - OR - _____ cm
☐ Unable to measure

8.2* Current measured weight. . . . . _____ lbs - OR - _____ kg ☐ Unable to weigh

8.3* Waist measurement . . . . . _____ inches - OR - _____ cm ☐ Unable to measure
☐ Refuses

8.4* Hip measurement. . . . . _____ inches - OR - _____ cm ☐ Unable to measure
☐ Refuses

8.5 **SINCE YOUR LAST INTERVIEW**
have you lost any height?. . . . . ☐ 1 Yes ☐ 2 No ☐ 3 Don't know

8.6 **SINCE YOUR LAST INTERVIEW**,
what has been your **GREATEST** weight?. . . . . _____ lbs - OR - _____ kg ☐ Don't know

8.7 **SINCE YOUR LAST INTERVIEW**,
what has been your **LOWEST** weight?. . . . . _____ lbs - OR - _____ kg ☐ Don't know

8.8* **SINCE YOUR LAST INTERVIEW**, have you lost more than 10 pounds (*4.5 kg*) ?

☐ 1 Yes ☐ 2 No

Did you regain the lost weight?
☐ 1 Yes ☐ 2 No
How much did you lose ? _____ lbs -OR- _____ kg

How many times have you lost
and regained 10 pounds (*4.5 kg*) or more? _____

8.9 **SINCE YOUR LAST INTERVIEW**,
did you lose more than 10 pounds (*4.5 kg)*
intentionally by changing your diet and or your exercise?. . . . . ☐ 1 Yes ☐ 2 No

Now we would like to measure your mobility by doing a simple test of getting up from a chair and walking.

Interviewer: *Timing begins when the person starts to rise from the chair and ends when he or she returns to the chair and sits down with back and hip against the back of the chair.*

The person should be given 1 practice run and then 3 actual trials.
Note the time for each trial below.

8.10* • You will need to sit with back and hips against the back of the chair.
- On the word "GO" you will stand up without using the arm rest of the chair *(if possible)*.
- Walk to the line on the floor, turn around, walk back to the chair and sit down with your back and hips against the back of the chair.
- Walk at a regular pace, this is not a race.
- We would need you to repeat this exercise 3 times.

Total seconds.	Trial 1	Trial 2	Trial 3	Unable to perform
	_____sec.	_____sec.	_____sec.	☐

Did the participant require:

a. the use of the arm rest of the chair to rise ☐ 1 Yes ☐ 2 No

b. the use of an aid device (*cane, walker)* ☐ 1 Yes ☐ 2 No

This next test is to measure your grip strength using a dynamometer.

8.11* Do you consider yourself to be:. . . . . ☐ 1 Right handed ☐ 2 Left handed ☐ 3 Ambidextrous

- You will need to sit with back and hips fully pressed against the back of the chair with upperarm resting loosely against the body
- Hold the grip device in your hand with elbow at a 90 degree angle *(not resting elbow on arm chair rest or arms tucked into body too much).*
- You will squeeze to a maximum force for at least 3 seconds, then relax for 15 seconds.
- Repeat 3 times with each hand.

RIGHT hand measurement.	Trial 1	Trial 2	Trial 3	Unable to perform
	_____kg	_____kg	_____kg	☐

LEFT hand measurement.	Trial 1	Trial 2	Trial 3	Unable to perform
	_____kg	_____kg	_____kg	☐

* See note in manual

Now the questions I will ask will relate to the use of tobacco.

9. TOBACCO

9.1 **SINCE YOUR LAST INTERVIEW**, have you smoked cigarettes **DAILY** for at least 6 months?. . . . . ☐ 1 Yes ☐ 2 No

→ *Go to question 9.6*

9.2* **SINCE YOUR LAST INTERVIEW**, did you start smoking for the first time?. . . . . ☐ 1 Yes ☐ 2 No

→ At what age did you begin to smoke cigarettes daily ? *(for at least 6 months)* ____ years

9.3 Are you currently smoking?.. . . . . ☐ 1 Yes ☐ 2 No

→ At what age did you stop? _____ years

9.4 Approximately how many cigarettes do/did you smoke every day?. . . . . _____

9.5* **SINCE YOUR LAST INTERVIEW**, have you temporarily stopped smoking cigarettes and started again ?. . . . . ☐ 1 Yes ☐ 2 No

→ If you total up the periods, **SINCE YOUR LAST INTERVIEW**, for how many months have you stopped.. . . . . ____ months

9.6 On average, **OVER THE LAST MONTH**, have you been exposed to the tobacco smoke of others?. . . . . ☐ 1 Not at all
(i.e. environmental tobacco smoke (ETS))
☐ 2 < 3 hours/day
☐ 3 3-8 hours/day
☐ 4 9 or more hours/day

9.7 **SINCE YOUR LAST INTERVIEW**, have you been exposed to ETS for more than 6 months?. . . . . ☐ 1 Yes ☐ 2 No

→ ☐ 1 < 3 hours/day ☐ 2 3-8 hours/day ☐ 3 9 or more hours/day

→ Number of months of exposure **SINCE YOUR LAST INTERVIEW**? _____

Now I will ask you in detail about the foods you eat and drink.

10. FOOD INTAKE

10.1* How often *(on the average)* have you eaten the following items **DURING THE PAST 12 MONTHS?**

Food		Never	Servings per month	Servings per week	Servings per day	Serving size
Milk to drink * *(incl. milk flavoured with powder ex: chocolate)* * *(commercial choc. milk is not calcium fortified)*	Not fortified with calcium	☐ 1	(2)	(3)	(4)	☐ 125 ml (0.5 cup) ☐ 250 ml (1 cup) ☐ 375 ml (1.5 cups)
	Fortified with calcium	☐ 1	(2)	(3)	(4)	☐ 125 ml (0.5 cup) ☐ 250 ml (1 cup) ☐ 375 ml (1.5 cups)
Soy beverage to drink	Not fortified with calcium	☐ 1	(2)	(3)	(4)	☐ 125 ml (0.5 cup) ☐ 250 ml (1 cup) ☐ 375 ml (1.5 cups)
	Fortified with calcium	☐ 1	(2)	(3)	(4)	☐ 125 ml (0.5 cup) ☐ 250 ml (1 cup) ☐ 375 ml (1.5 cups)
Other alternative milk to drink *(Rice or Almond beverage)*		☐ 1	(2)	(3)	(4)	☐ 125 ml (0.5 cup) ☐ 250 ml (1 cup) ☐ 375 ml (1.5 cups)
Milk in cereal	Not fortified with calcium	☐ 1	(2)	(3)	(4)	☐ 60 ml (0.25 cup) ☐ 125 ml (0.5 cup) ☐ 250 ml (1 cup)
	Fortified with calcium	☐ 1	(2)	(3)	(4)	☐ 60 ml (0.25 cup) ☐ 125 ml (0.5 cup) ☐ 250 ml (1 cup)
Soy beverage in cereal	Not fortified with calcium	☐ 1	(2)	(3)	(4)	☐ 60 ml (0.25 cup) ☐ 125 ml (0.5 cup) ☐ 250 ml (1 cup)
	Fortified with calcium	☐ 1	(2)	(3)	(4)	☐ 60 ml (0.25 cup) ☐ 125 ml (0.5 cup) ☐ 250 ml (1 cup)
Other alternative milk in cereal *(Rice or Almond beverage)*		☐ 1	(2)	(3)	(4)	☐ 60 ml (0.25 cup) ☐ 125 ml (0.5 cup) ☐ 250 ml (1 cup)
Milk/Cream in tea/coffee		☐ 1	(2)	(3)	(4)	☐ 15 ml (1 tbsp) ☐ 30 ml (2 tbsp) ☐ 60 ml (4 tbsp)
Alternative beverage in tea/coffee *(Soy, Rice or Almond beverage)*		☐ 1	(2)	(3)	(4)	☐ 15 ml (1 tbsp) ☐ 30 ml (2 tbsp) ☐ 60 ml (4 tbsp)

* See note in manual

Food		Never	Servings per month	Servings per week	Servings per day	Serving size
Milk desserts * *(ex: tapioca, rice pudding)*	Not fortified with calcium	☐ 1	(2)	(3)	(4)	☐ 125 ml (0.5 cup) ☐ 250 ml (1 cup)
* *(fortified only applies for homemade desserts)*	Fortified with calcium	☐ 1	(2)	(3)	(4)	☐ 125 ml (0.5 cup) ☐ 250 ml (1 cup)
Desserts prepared with alternative milk *(Soy Rice or Almond beverage)* * *(ex: tapioca, rice pudding)* * *(homemade desserts prepared with alternative milk))*		☐ 1	(2)	(3)	(4)	☐ 125 ml (0.5 cup) ☐ 250 ml (1 cup)
Cream soups prepared with milk		☐ 1	(2)	(3)	(4)	☐ 125 ml (0.5 cup) ☐ 160 ml (2/3 cup) ☐ 250 ml (1 cup)
Cream soups prepared with alternative milk *(Soy, Rice or Almond beverage)*		☐ 1	(2)	(3)	(4)	☐ 125 ml (0.5 cup) ☐ 160 ml (2/3 cup) ☐ 250 ml (1 cup)
Ice cream, ice milk or frozen yogurt		☐ 1	(2)	(3)	(4)	☐ 125 ml (0.5 cup) ☐ 250 ml (1 cup) ☐ 375 ml (1.5 cup)
Yogurt to eat or drink	Not fortified with vitamin D	☐ 1	(2)	(3)	(4)	☐ 60 ml (0.25 cup) ☐ 125 ml (0.5 cup) ☐ 200 ml (0.75 cup) ☐ 250 ml (1 cup)
	Fortified with vitamin D *ex: Activia (not probiotic) Asana, Minigo, Silhouette, Source Drinkable (Activia, Yop)*	☐ 1	(2)	(3)	(4)	☐ 60 ml (0.25 cup) ☐ 125 ml (0.5 cup) ☐ 200 ml (0.75 cup) ☐ 250 ml (1 cup)
Hard cheese *(in sandwich or mixed dish including frozen meals)*		☐ 1	(2)	(3)	(4)	☐ 15 g (0.5 oz) ☐ 30 g (1.0 oz) ☐ 60 g (2.0 oz)
Soft cheese *(brie, camembert, goat)*		☐ 1	(2)	(3)	(4)	☐ 15 g (0.5 oz) ☐ 30 g (1.0 oz) ☐ 60 g (2.0 oz)
Orange juice	Fortified with calcium	☐ 1	(2)	(3)	(4)	☐ 125 ml (0.5 cup) ☐ 160 ml (2/3 cup) ☐ 250 ml (1 cup)
	Fortified with calcium and vitamin D	☐ 1	(2)	(3)	(4)	☐ 125 ml (0.5 cup) ☐ 160 ml (2/3 cup) ☐ 250 ml (1 cup)
Canned salmon or sardines with bones		☐ 1	(2)	(3)	(4)	☐ 30 g (1 oz) ☐ 60 g (2 oz) ☐ 90 g (3 oz)
Broccoli		☐ 1	(2)	(3)	(4)	☐ 60 ml (0.25 cup) ☐ 125 ml (0.5 cup) ☐ 250 ml (1 cup)
Dark leafy greens *(bok choy, kale, gailan (chinese broccoli), collards, dandelion greens)*		☐ 1	(2)	(3)	(4)	☐ 60 ml (0.25 cup) ☐ 125 ml (0.5 cup) ☐ 250 ml (1 cup)

Food	Never	Servings per month	Servings per week	Servings per day	Serving size
Dried beans or peas *(navy, pinto, kidney, chick peas, lentil, etc)*	☐ 1	(2).....	(3).....	(4).....	☐ 60 ml (0.25 cup) ☐ 125 ml (0.5 cup) ☐ 250 ml (1 cup)
White bread, buns, rolls, bagels, etc	☐ 1	(2).....	(3).....	(4).....	1 serving = 1 slice ½ bagel ½ pita
Whole wheat bread, buns, rolls, bagels, etc	☐ 1	(2).....	(3).....	(4).....	1 serving = 1 slice ½ bagel ½ pita
Meal replacement drink *(1serving = 235ml (8oz))* *(ex: Ensure, Boost, etc)*	☐ 1	(2).....	(3).....	(4).....	1 serving
Tofu	☐ 1	(2).....	(3).....	(4).....	☐ 60 ml (0.25 cup) ☐ 125 ml (0.5 cup) ☐ 250 ml (1 cup)

Now some questions about the beverages you might choose to drink.

BEVERAGES

10.2* How many of the following drinks did you consume **IN THE PAST 12 MONTHS**?

One serving is:

- *tea or coffee is 6 oz (180 ml)*
- *cola is 12 oz - 1 can (355 ml)*
- *energy drink - 8 oz (235 ml)*
- *1 bottle or can of beer or a glass of draft (12 oz)*
- *1 straight or mixed drink with (1-1½ oz) hard liquor*
- *1 glass of wine or a wine cooler (4-5 oz)*

Beverages		Never	Servings per month	Servings per week	Servings per day
Coffee	caffeinated	☐ 1	(2).....	(3).....	(4).....
	decaffeinated	☐ 1	(2).....	(3).....	(4).....
Tea	caffeinated	☐ 1	(2).....	(3).....	(4).....
	decaffeinated	☐ 1	(2).....	(3).....	(4).....
Colas	caffeinated	☐ 1	(2).....	(3).....	(4).....
	decaffeinated	☐ 1	(2).....	(3).....	(4).....
Energy drink *(ex: Monster, Nos, Red Bull, Rockstar)*		☐ 1	(2).....	(3).....	(4).....
Alcoholic beverages		☐ 1	(2).....	(3).....	(4).....

In this section I will ask you about your physical activities and exercise.

11. PHYSICAL ACTIVITY

11.1 During a typical week **IN THE PAST 6 MONTHS**, how much time did you usually spend walking?
(to work, school, while doing errands, for leisure)

- ☐ 1 None
- ☐ 2 Less than 1 hour
- ☐ 3 Between 1-5 hours
- ☐ 4 Between 6-10 hours
- ☐ 5 Between 11-20 hours
- ☐ 6 More than 20 hours

11.2 **SINCE YOUR LAST INTERVIEW**, which of the following describes the paid work you usually do or what you consider your job?

Or if retired *(since last interview)* or unemployed, which best describes your *(most recent)* job?

- ☐ 1 I am usually sitting during the day and do not walk around very much
- ☐ 2 I stand or walk quite a lot during the day but I do not have to lift or carry heavy objects
- ☐ 3 I usually lift or carry light loads or I often have to climb stairs or hills
- ☐ 4 I do heavy work or have to carry loads
- ☐ 5 N/A ..... *Subject retired before last interview*

11.3* Do you **CURRENTLY** participate in any regular physical activity or programme *(either on your own or in a formal class)*?. . . . . ☐ 1 Yes ☐ 2 No

➤ How many times/week? _____

➤ How long per session? _____ minutes

11.4 **SINCE YOUR LAST INTERVIEW**, have you engaged in a physical activity/sport at a competitive level?. . . . . ☐ 1 Yes ☐ 2 No

Sport/Activity	Age started competing	Age stopped competing	Level of competition *(indicate all that apply)*			
			local	provincial	national	international
			☐ 1	☐ 2	☐ 3	☐ 4
			☐ 1	☐ 2	☐ 3	☐ 4
			☐ 1	☐ 2	☐ 3	☐ 4

11.5* On the average **DURING THE LAST YEAR**,
how many hours **IN A WEEK** did you spend in the following activities?

	Never	½ - 1 hr	2 - 3 hrs	4 - 6 hrs	7 - 10 hrs	11 - 20 hrs	21 - 30 hrs	31 hrs & over
➤ Strenuous Sports. . . . . *(such as jogging, bicycling on hills, tennis, racquetball, swimming laps, aerobics)*	☐ 1	☐ 2	☐ 3	☐ 4	☐ 5	☐ 6	☐ 7	☐ 8
➤ Vigorous Work.. . . . . *(such as moving heavy furniture, loading or unloading trucks, shovelling, weight lifting or equivalent manual labour)*	☐ 1	☐ 2	☐ 3	☐ 4	☐ 5	☐ 6	☐ 7	☐ 8
➤ Moderate Activity. . . . . *(such as housework, brisk walking, golfing, bowling, bicycling on level ground, gardening)*	☐ 1	☐ 2	☐ 3	☐ 4	☐ 5	☐ 6	☐ 7	☐ 8

11.6* On the average **DURING THE LAST YEAR**,
how many hours **IN A DAY** did you spend in the following sitting activities?

	Never	<than 1 hr	1 - 2 hrs	3 - 4 hrs	5 - 6 hrs	7 - 10 hrs	11 hrs & over	N/A
➤ Sitting in a car or bus.	☐ 1	☐ 2	☐ 3	☐ 4	☐ 5	☐ 6	☐ 7	
➤ Sitting at work/school.	☐ 1	☐ 2	☐ 3	☐ 4	☐ 5	☐ 6	☐ 7	☐ 8
➤ Watching TV..	☐ 1	☐ 2	☐ 3	☐ 4	☐ 5	☐ 6	☐ 7	
➤ Sitting at meals.	☐ 1	☐ 2	☐ 3	☐ 4	☐ 5	☐ 6	☐ 7	
➤ For leisure- sitting at computer..	☐ 1	☐ 2	☐ 3	☐ 4	☐ 5	☐ 6	☐ 7	
➤ Other sitting activities.. . . . . *(such as reading, playing cards, sewing)*	☐ 1	☐ 2	☐ 3	☐ 4	☐ 5	☐ 6	☐ 7	

11.7 On the average, **DURING THE LAST YEAR**,
how many hours **IN A DAY** *(over a 24 hr period)* did you sleep *(include naps)* ?

☐ 1 5 hours or less
☐ 2 6 hours
☐ 3 7 hours
☐ 4 8 hours
☐ 5 9 hours
☐ 6 10 hours or more

11.8 Rate your overall level of physical activity compared to your peers **DURING THE LAST YEAR**.

☐ 1 A lot less active
☐ 2 Somewhat less active
☐ 3 About the same
☐ 4 Somewhat more active
☐ 5 A lot more active

* See note in manual

Now I want to ask you a question about being in the sunlight.

12. SUNLIGHT EXPOSURE

12.1* **IN THE PAST 12 MONTHS**, did you ever expose a considerable part of your body to direct sunlight?. . . . . ☐ 1 Never ☐ 3 Regularly ☐ 2 Seldom ☐ 4 Often

Considerable part of the body =	*part of the body exposed for 30 minutes or more in a socially acceptable swimsuit or equivalent*
Never	*did not expose considerable part of my body to direct sunlight for at least 30 minutes each day*
Seldom	*sometimes but less than 3 months of the year*
Regularly	*3 to 6 months of the year*
Often	*more than 6 months of the year*

12.2 **IN THE PAST 12 MONTHS**, have you used sunscreen or face cream with SPF to protect your skin against sunlight?. . . . . ☐ 1 Yes ☐ 2 No

☐ 1 Sometimes ☐ 2 Usually ☐ 3 Always

12.3* **IN THE PAST 5 YEARS**, have you spent one month or more in a Southern location? *(Outside Canada)*. . . . . ☐ 1 Yes ☐ 2 No

Some communities add fluoride to their drinking water. The following questions ask about how long you have lived in your current community in order to determine your most recent fluoride intake and your primary source of drinking water.

13. FLUORIDE

13.1* How long have you lived in the community you now live in? _____ years _____ months

13.2 What is your current primary source of drinking water?. . . . . ☐ 1 Municipal *(tap)* ☐ 2 Well ☐ 3 Bottled

The next set of questions are concerned with any limitations you may have in routine activities as well as your day to day health. Not all the questions may apply to you but please be patient in responding.

14. DISABILITY AND HEALTH STATUS *

14.1 Do you need the help of another person for personal care such as eating, bathing, dressing or getting around inside the house because of any impairment or health problem?. . . . . ☐ 1 Yes ☐ 2 No

Who provides this help?

- ☐ 1 A spouse/partner or relative living in your household
- ☐ 2 A spouse/partner or relative not living in your household
- ☐ 3 A non-relative, regardless of where he/she lives
- ☐ 4 A combination of the previous categories

14.2 Do you need the help of another person in looking after personal affairs, doing everyday household chores, going shopping or getting around outside the house, because of any impairment or health problem?. . . . . ☐ 1 Yes ☐ 2 No

Who provides this help?

- ☐ 1 A spouse/partner or relative living in your household
- ☐ 2 A spouse/partner or relative not living in your household
- ☐ 3 A non-relative, regardless of where he/she lives
- ☐ 4 A combination of the previous categories

14.3 Compared to other people of the same age in good health, are you limited in the kind or amount of activity you can do because of a long-term physical or mental condition or health problem?. . . . ☐ 1 Yes ☐ 2 No

Please administer MMSE if respondent is **currently** 65 years of age and older

Now I would like to ask you how your health has been on the average, over the past week. I will ask you about different areas of general health. For some of the questions, I want you to tell me which statement most closely describes how you felt.

15. HEALTH STATUS QUESTIONNAIRE : * TORRANCE QUESTIONNAIRE

INTERVIEWER ADMINISTERED VERSION

Interviewer: For each question that lists a number of choices, circle the letter for the one choice that the respondent feels best describes the usual level of ability over the past week.

1.1 Are you able to see well enough without glasses or contact lenses to read ordinary newsprint?

☐ Yes ⟶ Go to 2.1

☐ No

1.2 If not, which of the following describes your *usual* ability to see well enough to read ordinary newspring? Are you:

a. Able to see well enough but with glasses or contact lenses.
b. Unable to see well enough even with glasses or contact lenses.
c. Unable to see at all.

2.1 Are you able to see well enough without glasses or contact lenses to recognize a friend on the other side of street?

☐ Yes ⟶ Go to 3.1

☐ No

2.2 If not, which of the following best describes your *usual* ability to see well enough to recognize a friend on the other side of the street? Are you:

a. Able to see well enough but with glasses or contact lenses.
b. Unable to see well enough even with glasses or contact lenses.
c. Unable to see at all.

3.1 Are you able to hear what is said in a group conversation with at least three other people *without* a hearing aid?

☐ Yes ⟶ Go to 4.1

☐ No

* GW Torrance and DH Feeny, McMaster University
Questionnaire development supported through research grants funded by the Ontario Ministry of Health and US Agency for Health Care Policy and Research

3.2 If not, which statement describes your *usual* ability to hear in a group conversation with at least three other people? Are you:

a. Able to hear what is said with a hearing aid.
b. Unable to hear what is said even with a hearing aid.
c. Unable to hear what is said, but don't wear a hearing aid.
d. Unable to hear.

4.1 Are you able to hear what is said in a conversation with one other person in a quiet room without a hearing aid?

☐ Yes ⟶ Go to 5.1
☐ No

4.2 If not, which one of the following best describes your *usual* ability to hear what is said in a conversation with one other person in a quiet room? Are you:

a. Able to hear what is said with a hearing aid.
b. Unable to hear what is said even with a hearing aid.
c. Unable to hear what is said, but don't wear a hearing aid.
d. Unable to hear.

5.1 Are you able to be understood when speaking the same language with strangers?

☐ Yes ⟶ Go to 6.1
☐ No

5.2 If not, which of the following best describes your *usual* ability to be understood when speaking the same language with strangers? Are you:

a. Able to be understood partially.
b. Unable to be understood.
c. Unable to speak at all.

6.1 Are you able to be understood when speaking the same language with people who know you well?

☐ Yes ⟶ Go to 7.1
☐ No

6.2 If not, which of the following best describes your *usual* ability to be understood when speaking the same language with people who know you well? Are you:

a. Able to be understood partially.
b. Unable to be understood.
c. Unable to speak at all.

7.1 Which one of the following best describes how you usually feel? Are you:

a. Happy and interested in life.
b. Somewhat happy.
c. Somewhat unhappy.
d. Very unhappy.
e. So unhappy that life is not worthwhile.

8.1 Are you free of pain and discomfort?

☐ Yes ⟶ Go to 9.1
☐ No

8.2 If not, which one of the following best describes your level of pain? Do you have:

a. Mild to moderate pain that prevents no activities.
b. Moderate pain that prevents a few activities.
c. Moderate to severe pain that prevents some activities.
d. Severe pain that prevents most activities.

9.1 Are you able to walk around the neighbourhood **without** difficulty and **without** walking equipment, and have no health limitation in vigorous activities such as running and strenuous sports?

NOTE: Walking equipment refers to mechanical supports such as braces, a cane, crutches or a walker.

☐ Yes ⟶ Go to 10.1
☐ No

9.2 If not, which one of the following best describes your *usual* ability to walk? Are you:

a. Able to walk around the neighbourhood without difficulty and without walking equipment, and have some health limitation in vigourous activities such as running and strenuous sports
b. Able to walk around the neighbourhood with difficulty, but without walking equipment or a helper.
c. Able to walk around the neighbourhood with walking equipment, but without a helper.
d. Able to walk only short distances with walking equipment. Able to walk short distances with a helper, and require a wheelchair to get around the neighbourhood.
e. Unable to walk alone, even with walking equipment. Able to walk short distances with a helper, and require a wheelchair to get around the neighbourhood.
f. Cannot walk at all

10.1 Do you have full use of two hands and ten fingers?

☐ Yes ⟶ Go to 11.1

☐ No

10.2 If not, which one of the following best describes *usual* ability to use your hands and fingers? Do you have:

a. Limited use of hands or fingers, but do not require special tools or help from others.
b. Limited use of hands or fingers, require special tools but do not require help from others.
c. Limited use of hands or fingers, require the help of another person for some tasks.
d. Limited use of hands or fingers, require the help of another person for most tasks.
e. Limited use of hands or fingers, require the help of another person for all tasks.

11.1 Are you able to remember most things?

☐ Yes ⟶ Go to 12.1

☐ No

11.2 If not, which one of the following best describes *usual* ability to remember things?

a. Somewhat forgetful.
b. Very forgetful.
c. Unable to remember anything at all.

12.1 Are you able to think clearly and solve day to day problems?

☐ Yes ⟶ Go to 13.1

☐ No

12.2 If not, which one of the following best describes *usual* ability to think and solve day to day problems? Do you:

a. Have a little difficulty when trying to think and solve day to day problems
b. Have some difficulty when trying to think and solve day to day problems
c. Have great difficulty when trying to think and solve day to day problems

or are you:

d. Unable to think or solve day to day problems

JUST A FEW MORE QUESTIONS IN THIS SECTION

13.1 Do you eat, bathe, dress and use the toilet normally?

☐ Yes ⟶ Go to 14.1

☐ No

13.2 If not, which one of the following best describes *usual* ability to perform these basic activities?

a. Eat, bathe, dress and use the toilet **independently, with difficulty.**
b. Requires mechanical equipment to eat, bathe, dress or use the toilet independently.
c. Requires the help of another person to eat, bathe, dress or use the toilet.

14.1 Are you generally happy and free from worry?

☐ Yes ⟶ Go to 15.1

☐ No

14.2 If not, which one of the following best describes how you usually feel?

a. Occasionally fretful, angry, irritable, anxious or depressed.
b. Often fretful, angry, irritable, anxious or depressed.
c. Almost always fretful, angry, irritable, anxious or depressed.
d. Extremely fretful, angry, irritable, anxious or depressed, usually requiring hospitalization or psychiatric institutional care.

THIS IS THE LAST QUESTION IN THIS SECTION. IT IS A DIFFERENT QUESTION ABOUT PAIN. JUST TO REMIND ME:

15.1 Are you free of pain and discomfort?

☐ Yes ⟶ Go to next page

☐ No

15.2 If not, which one of the following best describes your *usual* level of pain?

a. Occasional pain. Discomfort relieved by non-prescription drugs or self-control activity without disruption of normal activities.
b. Frequent pain. Discomfort relieved by oral medicines with occasional disruption of normal activities.
c. Frequent pain. Frequent disruption of normal activities. Discomfort requires prescription narcotics for relief.
d. Severe pain. Pain not relieved by drugs and constantly disrupts normal activities.

One more question to complete the questionnaire.

16. ADDITIONAL INFORMATION

16.1 For statistical purposes only, we need to know the range of your total, gross household income last year. Now, could you please indicate from the following list, in what range your household income falls?

(If there is hesitation, tell them they may choose not to respond)

- ☐ 1 Under $20,000
- ☐ 2 $20,000 to $40,000
- ☐ 3 $41,000 to $60,000
- ☐ 4 $61,000 to $80,000
- ☐ 5 Over $80,000
- ☐ 6 Refuses to answer

THAT ENDS THE QUESTIONNAIRE.
THANK YOU VERY MUCH FOR YOUR HELP.

TIME FINISHED _____ hrs _____min.

INTERVIEWER'S ASSESSMENT

As an interviewer my assessment of the process and the respondent was:

(*Circle one number on each line*)

	Not at all	A little	Neutral	Somewhat	A great deal
a. The respondent appeared or seemed interested in the research	1	2	3	4	5
b. The respondent seemed to cooperate with me	1	2	3	4	5
c. I believe that the respondent understood the questions	1	2	3	4	5
d. I believe that the respondent listened well	1	2	3	4	5
e. I perceived that the respondent was restless or wanted to hurry the process	1	2	3	4	5
f. The respondent expressed feelings of tiredness during the interview	1	2	3	4	5

Nutrition questionnaire completed at home?. . . . ☐ 1 Yes ☐ 2 No completed at time of interview

Did the respondent require help to complete?

☐ 1 Yes ☐ 2 No

SF- 36 questionnaire completed at home?. . . . . ☐ 1 Yes ☐ 2 No completed at time of interview

Did the respondent require help to complete?

☐ 1 Yes ☐ 2 No

Consent to access Provincial Health number
Consent signed?. . . . . ☐ 1 Yes ☐ 2 No

Indicate Provincial Health number

.....

Comments :

_____

_____

_____

_____

32 * See note in manual

Fracture Questionnaire

1. INCIDENT # _____

2. Which bone was broken?

☐ 1 Back *(Specify if available)* _____			
☐ 2 Hip.	☐ 1 Left	☐ 2 Right	
☐ 3 Ribs / Sternum.	☐ 1 Left	☐ 2 Right	
☐ 4 Pelvis			
☐ 5 Shoulder (upper arm).	☐ 1 Left	☐ 2 Right	
☐ 6 Elbow.	☐ 1 Left	☐ 2 Right	
☐ 7 Forearm/wrist.	☐ 1 Left	☐ 2 Right	
☐ 8 Hand	☐ 1 Left	☐ 2 Right	
☐ 9 Finger(s).	☐ 1 Left	☐ 2 Right	
☐ 10 Upper leg.	☐ 1 Left	☐ 2 Right	
☐ 11 Knee.	☐ 1 Left	☐ 2 Right	
☐ 12 Lower leg.	☐ 1 Left	☐ 2 Right	
☐ 13 Ankle.	☐ 1 Left	☐ 2 Right	
☐ 14 Foot.	☐ 1 Left	☐ 2 Right	
☐ 15 Toe(s)	☐ 1 Left	☐ 2 Right	
☐ 16 Other *(specify)* _____	☐ 1 Left	☐ 2 Right	☐ 3 N/A

3. How did it happen?

- ☐ 1 Fell out of bed or off a chair *(from sitting position)*
- ☐ 2 Fell climbing a chair or a ladder
- ☐ 3 Fell on stairs
- ☐ 4 Motor vehicle accident
- ☐ 5 Sporting injury *(i.e. skiing, playing hockey, cycling, running or jogging, etc.)*
- ☐ 6 Slipped or tripped inside home *(on carpet, wet floor, getting in/out of bath, etc.)*
- ☐ 7 Slipped or tripped and fell outside the home rather than sporting *(on ice, on the curb, etc.)*
- ☐ 8 Heavy object fell or struck body causing the fracture
- ☐ 9 Bone(s) broke with no fall or injury
- ☐ 10 Other *(specify)* _____

4. What was the date of the fracture?. . . . . _____ / _____ ☐ Don't know
Month Year

5. When did the fracture occcur? During the ..... ☐ 1 Day *(8 a.m. to 4 p.m.)*
☐ 2 Evening *(4 p.m. to midnight)*
☐ 3 Night *(midnight. to 8 a.m.)*

6. Were X-rays of the fracture taken?. . . . . ☐ 1 Yes ☐ 2 No

→ Fracture confirmed . . . . . ☐ 1 Yes
(To be confirmed by centre staff after review of the medical report or X-ray report)
☐ 2 No
☐ 3 Missing documentation
☐ 4 Refused (to sign consent form)
☐ 5 Inconclusive

→ What was the date of the X-rays. . . . . _____ / _____ (Month / Year) ☐ Don't know

→ At what clinic/hospital were the x-rays taken?. . . . . _____ ☐ Don't know

7. Was the fracture treated?. . . . . ☐ 1 Yes ☐ 2 No → Go to question 10

Where was the fracture treated ?. . . . In: ☐ 1 Hospital ☐ 2 Physician's office ☐ 3 Home

→ Go to question 10

8. *IN HOSPITAL* - Date . . . . . _____ / _____ (Month / Year)

☐ 1 Emergency Clinic - OR - ☐ 2 In-Patient → Length of stay _____ days

Hospital Name: _____ ☐ Don't know

Treating Doctor: _____ ☐ Don't know

Treatment received : ☐ 1 Surgery ☐ 2 Cast ☐ 3 Other *specify:* _____

☐ 1 Internal and/or external fixation *(pins, nails, screws)*
☐ 2 Joint replacement

Where did you go when you left the hospital? *(Pick one from the list)*

☐ 1 Home
☐ 2 Rehabilitation centre → What was the name? _____
☐ 3 Convalescent home → How long did you stay? _____ days
☐ 4 Other : *specify* _____

9. *IN PHYSICIAN'S OFFICE* Physician's name _____

Date of first visit : _____ / _____ Total number of visits ? _____
Month Year

Treatment received : ☐ 1 Cast ☐ 2 Other *specify:* _____

10. As a consequence of your fracture,
were you treated with physiotherapy? . . . . . ☐ 1 Yes ☐ 2 No
(Check all that apply)

	TOTAL # of visits	*TOTAL # of weeks*
☐ in Hospital. . . . . ➤	_____	_____
☐ in Public Rehabilitation Centre. . . . . ➤	_____	_____
☐ in Private Convalescent Centre. . . . . ➤	_____	_____
☐ in Community Health Centre. . . . . ➤	_____	_____
☐ in Private Clinic. . . . . ➤	_____	_____
☐ at Home from a Private Clinic. . . . . ➤	_____	_____
☐ in Senior's Home . . . . . ➤	_____	_____

11 As a consequence of your fracture,
were you visited by an occupational therapist? . . . . . ☐ 1 Yes ☐ 2 No

How many visits total ? _____ How many weeks? _____

If subject has not yet returned home - go to question 17

12. As a consequence of your fracture,
were you visited at home by a nurse? . . . . . ☐ 1 Yes ☐ 2 No

How many visits total ? _____ How many weeks? _____

13. As a consequence of your fracture,
did you receive help from a homemaker? . . . . . ☐ 1 Yes ☐ 2 No
(meals on wheels, housekeeping, personal hygiene)

How many visits total ? _____ How many weeks? _____

14. As a consequence of your fracture, did you receive help from a family member or friend ?. . . . . ☐ 1 Yes ☐ 2 No

    How many days total did you receive help? . . . . . _____ days

    Did this person have a paying job? ☐ 1 Yes ☐ 2 No

    How many days off from work did this person take as a result of your fracture?. . . . . _____days

15. Since the fracture, have you given up any of your usual activities permanently?.. . . . . ☐ 1 Yes ☐ 2 No

16. Do you go out . . . . . ☐ 1 Less often ☐ 2 The same ☐ 3 More often

17. Have you been told that your fracture is osteoporosis related?. . . . . ☐ 1 Yes ☐ 2 No ☐ 3 Don't know

THANK YOU!

DATE _____/_____/_____
Day Month Year

Form 5

CaMosBQS

Canadian Multicentre Osteoporosis Bone Quality Study
Étude Canadienne multicentrique sur la qualité de l'os

pQCT Image Tracking Form

Baseline Image File & Data Collection

CENTRE:

CENTRE TECHNICIAN'S INITIALS:

DATE SENT: ____ / ____ / ____ (day / month / year)

For verification that image and data for invoiced participant scans have been received

R : received at Hamilton Image Analysis Centre

W: Wrist, **A:** Ankle, **C:** Calf

	CaMos ID#	Stratec PTID#	ROI Location W / A / C	Arm side	Leg side	Stratec CT #	DATE SUBJECT SCANNED ON POCT	Comments (ie. Motion)	Chair Stand Y/N	Hands ✓/ ✗	30 CST #	Image File R	R INIT
1			W /A/ C										
2			W /A/ C										
3			W /A/ C										
4			W /A/ C										
5			W /A/ C										
6			W /A/ C										
7			W /A/ C										
8			W /A/ C										
9			W /A/ C										
10			W /A/ C										
11			W /A/ C										
12			W /A/ C										
13			W /A/ C										
14			W /A/ C										
15			W /A/ C										
16			W /A/ C										
17			W /A/ C										
18			W /A/ C										
19			W /A/ C										
20			W /A/ C										

TOTAL : 0

TOTAL TO DATE: ____

Comments

FOR HAMILTON IMAGING CENTRE'S USE

REC'D AT COORDINATING CENTRE ____ / ____ / ____ (day / month / year)

Comments

Form 6

CaMosBQS

Canadian Multicentre Osteoporosis Bone Quality Study
Étude Canadienne multicentrique sur la qualité de l'os

hr-pQCT Image Tracking Form

Baseline Image File & Data Collection

For verification that image and data for invoiced participant scans have been received

CENTRE:

CENTRE TECHNICIAN'S INITIALS:

DATE SENT: ____ / ____ / ____ (day / month / year)

R : received at Hamilton Image Analysis Centre **W:** Wrist, **A:** Ankle

	CaMos ID#	Scanco Sample#	ROI Location W / A	Arm side	Leg side	Scanco Measurem.#	DATE SUBJECT SCANNED ON POCT	Comments (ie. Motion)	Chair Stand Y/N	Hands ✓/ ✗	30 CST #	Image File R	R INIT
1			W / A										
2			W / A										
3			W / A										
4			W / A										
5			W / A										
6			W / A										
7			W / A										
8			W / A										
9			W / A										
10			W / A										
11			W / A										
12			W / A										
13			W / A										
14			W / A										
15			W / A										
16			W / A										
17			W / A										
18			W / A										
19			W / A										
20			W / A										

TOTAL : 0

TOTAL TO DATE: ____

Comments

FOR CALGARY IMAGING CENTRE'S USE

REC'D AT X-RAY CENTRE ____ / ____ / ____ (day / month / year)

Comments